PL-TR-
97-1071

# MICRO-PARTICLE IMPACT DETECTOR EXPERIMENT ON MIGHTYSAT I

Patrick J. Serna
Gary H. Liechty
Craig L. Neslen
Renzo Del Frate
Edwin Draper

January 1998

Final Report







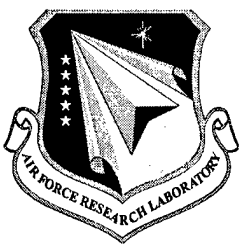


AIR FORCE RESEARCH LABORATORY
Space Vehicles Directorate
3550 Aberdeen Ave SE
AIR FORCE MATERIEL COMMAND
KIRTLAND AIR FORCE BASE, NM 87117-5776

PL-TR-97-1071

Using Government drawings, specifications, or other data included in this document for any purpose other than Government procurement does not in any way obligate the U.S. Government. The fact that the Government formulated or supplied the drawings, specifications, or other data, does not license the holder or any other person or corporation; or convey any rights or permission to manufacture, use, or sell any patented invention that may relate to them.

This report has been reviewed by the Public Affairs Office and is releasable to the National Technical Information Service (NTIS). At NTIS, it will be available to the general public, including foreign nationals.

If you change your address, wish to be removed from this mailing list, or your organization no longer employs the addressee, please notify AFRL/VSSE, 3550 Aberdeen Ave SE, Kirtland AFB, NM 87117-5776.

Do not return copies of this report unless contractual obligations or notice on a specific document requires its return.

This report has been approved for publication.

PATRICK J. SERNA
Project Manager

FOR THE COMMANDER

DAVID H. HILLAND, DR-III
Protection Technology Group Lead

BRUCE A. THIEMAN, Colonel, USAF
Deputy Director, Space Vehicles

# REPORT DOCUMENTATION PAGE

Form Approved
OMB No. 0704-0188



| 1. AGENCY USE ONLY *(Leave blank)* | 2. REPORT DATE | 3. REPORT TYPE AND DATES COVERED |
|---|---|---|
| | 30 Jan 98 | Final Report, 15 Jul 96 – 1 Oct 97 |

4. TITLE AND SUBTITLE
Micro-Particle Impact Detector Experiment on MightySat I

5. FUNDING NUMBERS
PE: 63401F
PR: 4400
TA: AB
WU: 01

6. AUTHOR(S)
Patrick J. Serna, Gary H. Liechty, Craig L. Neslen *
Renzo Del Frate and Edwin Draper **

7. PERFORMING ORGANIZATION NAME(S) AND ADDRESS(ES)
Air Force Research Laboratory/VSSE
3550 Aberdeen, SE
Kirtland AFB, NM 87117-5776

8. PERFORMING ORGANIZATION REPORT NUMBER
PL-TR-97-1071

9. SPONSORING/MONITORING AGENCY NAME(S) AND ADDRESS(ES)

10. SPONSORING/MONITORING AGENCY REPORT NUMBER

11. SUPPLEMENTARY NOTES
* Air Force Research Laboratory/VSSE, ** Science Applications Corporation, 2109 Air Park Rd, SE, Albuquerque, NM 87106

12a. DISTRIBUTION/AVAILABILITY STATEMENT
Approved For Public Release; Distribution Is Unlimited

12b. DISTRIBUTION CODE

13. ABSTRACT *(Maximum 200 Words)*

The purpose of this paper is to present an engineering design of a spaceborne Micro-Particle Impact Detector (MPID) experiment. This experiment is manifested on an Air Force Research Laboratory spacecraft called MightySat I scheduled for launch in July 1998. A follow-on report will present the resulting particle impact data.

The objective of this experiment is to measure direction and time of impact of spaceborne micron size particles with time of impact resolution of 0.1 s. The primary element in this experiment consists of two Metal-Oxide-Semiconductor (MOS) discharge capacitor detectors that discharge upon hypervelocity particle impact. These detectors were developed by Prof. J.J. Wortman from North Carolina State University. Each MOS particle detector is 3 in x 1-1/2 in and approximately 0.013 in thick. Each particle detector is bonded to a detector assembly that is in turn mechanically fastened to the external bottom plate of the MightySat I spacecraft. The detector assembly and associated electronics weigh less than 0.4 lb and have a total impact sensing area of 3.7 $in^2$. Each particle impact causes an impact event record to be stored in the spacecraft control unit for later downlink. Each impact event record will store time of impact and output from two coarse sun sensors. Data from the coarse sun sensors is used to help determine attitude of the spacecraft.

The Air Force Research Laboratory MightySat I spacecraft is a 6-sided composite structure, 20.5 in (height) by 19.0 in (diameter), 150 lb., and spin stabilized with 5 degree attitude knowledge. The MightySat I spacecraft is scheduled for orbit injection using a standard hitchhiker ejection system from space shuttle flight STS-88. Anticipated orbit for the spacecraft is 210 nmi at 51.6 degrees.

| 14. SUBJECT TERMS | 15. NUMBER OF PAGES |
|---|---|
| Micro-Particle, Hypervelocity Impact, Spaceborne Particle Detectors, MightySat I | 164 |
| | 16. PRICE CODE |

| 17. SECURITY CLASSIFICATION OF REPORT | 18. SECURITY CLASSIFICATION OF THIS PAGE | 19. SECURITY CLASSIFICATION OF ABSTRACT | 20. LIMITATION OF ABSTRACT |
|---|---|---|---|
| UNCLASSIFIED | UNCLASSIFIED | UNCLASSIFIED | UNLIMITED |

NSN 7540-01-280-5500

Standard Form 298 (Rev. 2-89)
Prescribed by ANSI Std. 239-18
28-102

CONTENTS


| Section | | | Page |
|---|---|---|---|
| 1.0 | Introduction | | 1 |
| 2.0 | Experiment Configuration | | 2 |
| | 2.1 | Overall Configuration | 2 |
| | 2.2 | Electronic Board Design | 4 |
| | 2.3 | Micro-Particle Detector Holder Assembly Design | 11 |
| | 2.4 | Attitude Determination | 16 |
| 3.0 | Thermal Cycle Testing | | 17 |
| | 3.1 | Electronic Board | 17 |
| | 3.2 | Detector Assembly | 22 |
| | 3.3 | Detector #2 and #3 Test Setup | 26 |
| | 3.4 | Detector #3 Test Execution | 27 |
| | 3.5 | Detector #2 Test Execution | 29 |
| 4.0 | Vibration Testing | | 31 |
| | 4.1 | Electronic Board | 31 |
| | 4.2 | Detector Assembly | 36 |
| | 4.3 | Detector #3, Post Thermal and Vibration Tap Test | 38 |
| 5.0 | On-Orbit Operations | | 41 |
| 6.0 | Conclusion | | 42 |
| | References | | 43 |
| | Appendixes | | |
| | A. | Electronic Board Parts List | A-1 |
| | B. | Detector Assembly Stress Calculations | B-1 |
| | C. | Detector Mounting Procedure | C-1 |
| | D. | BASIC Source Code For Monitoring of Electronic Board Output Line | D-1 |
| | E. | Thermal Analysis of MPID | E-1 |
| | F. | Thermocouple Data, Detectors #2 and #3 | F-1 |
| | G. | Vibration Accelerometer Data, Qualification Board | G-1 |
| | H. | Vibration Accelerometer Data, Flight Board | H-1 |
| | I. | Vibration Accelerometer Data, Detector Assembly #2 | I-1 |
| | J. | Vibration Accelerometer Data, Detector Assembly #3 | J-1 |

## FIGURES


| Figure | | Page |
|---|---|---|
| 1. | Electronic Board Mounted to Spacecraft and Spacecraft Coordinate System | 2 |
| 2. | Detector Locations | 3 |
| 3. | Spacecraft Orbit and Rotation Orientation | 3 |
| 4. | Electronic Board Schematic | 5 |
| 5. | Electronic Board Component Layout | 6 |
| 6. | Electronic Board Timing Diagram | 7 |
| 7. | General Instrumentation Test Configuration | 9 |
| 8. | Detailed Instrumentation Test Configuration | 10 |
| 9. | Detector Assembly | 11 |
| 10. | Top Plate | 13 |
| 11. | Bottom Plate | 14 |
| 12. | Type T Thermocouple Location | 18 |
| 13. | Qualification Board Thermal Test Profile | 18 |
| 14. | Flight Board Thermal Test Profile | 19 |
| 15. | Initial Detector Assembly Temperature Profile | 23 |
| 16. | Initial Thermocouple Locations | 23 |
| 17. | Detector Charge - Discharge Circuit | 24 |
| 18. | Detector Number 5, Test Points | 24 |
| 19. | Revised Detector Temperature Test Profile | 25 |
| 20. | Thermal Test Mounting Plates | 26 |
| 21. | Thermal Test Thermocouple Locations | 27 |
| 22. | Detector Number 3, Capacitance and Temperature Measurements | 28 |
| 23. | Detector Number 3, Current Measurements During Soak Periods | 28 |
| 24. | Detector Number 2, Capacitance and Temperature Measurements | 29 |
| 25. | Detector Number 2, Current Measurements During Soak Periods | 30 |
| 26. | Electronic Board Accelerometer Location | 32 |
| 27. | Detector Vibration Axis | 36 |
| 28. | Detector Mounted To Vibration Table With Accelerometer Locations | 37 |
| 29. | Detector Tap Test Bias Circuit | 39 |
| 30. | Capacitance Measurements After Bias and Discharge, Detector Number 3 | 40 |

# TABLES


| Table | | Page |
|---|---|---|
| 1. | MIL-P-55110 Paragraphs | 8 |
| 2. | Sample Output From Laptop Output Line Monitor | 20 |
| 3. | Thermal Performance Measurements, Qualification Board | 21 |
| 4. | Thermal Performance Measurements, Flight Board | 22 |
| 5. | Vibration Test Accelerometer Locations | 32 |
| 6. | Random Vibration Levels | 33 |
| 7. | Vibration Performance Measurements, Qualification Board | 33 |
| 8. | Vibration Performance Measurements, Flight Board | 34 |
| 9. | Vibration Data Differences, Qualification Board | 35 |
| 10. | Vibration Data Differences, Flight Board | 35 |
| 11. | Random Vibration Test Levels | 36 |
| 12. | Vibration Capacitance and Resistance Measurements, Detector Number 2 | 38 |
| 13. | Vibration Capacitance and Resistance Measurements, Detector Number 3 | 38 |

## 1.0 INTRODUCTION

The purpose of this report is to present the engineering design of a spaceborne Micro Particle Impact Detector (MPID) experiment. This experiment is manifested on an Air Force Research Laboratory spacecraft called MightySat I scheduled for launch in July 1998. A follow-on report will present the resulting particle impact data.

The objective of this experiment is to measure direction and time of impact of spaceborne micron size particles with time of impact resolution of 0.1 s. The primary element in this experiment consists of two Metal-Oxide-Semiconductor (MOS) discharge capacitor detectors that discharge upon hypervelocity particle impact. The detectors were developed by Prof. J.J. Wortman from North Carolina State University. Each MOS particle detector is 3 in x 1-1/2 in, approximately 0.013 in thick and are capable of detecting particle sizes to at least 0.4 μm. Each particle detector is bonded to a detector holder assembly that is in turn mechanically fastened to the external bottom plate of the MightySat I spacecraft. The detector assembly and associated electronics weigh less than 0.4 lb and have a total impact detection area of 3.7 $in^2$. Each particle impact causes an impact event record to be stored in the spacecraft control unit for later downlink. Each impact event record will store time of impact and output from two coarse sun sensors. Data from the coarse sun sensors is used to help determine attitude of the spacecraft.

The Air Force Research Laboratory MightySat I spacecraft, developed largely by CTA Space Systems in McLean, VA is a 6-sided composite structure, 20.5 in (height) by 19.0 in (diameter), 150 lb, and spin stabilized with 5° attitude knowledge. The MightySat I spacecraft is scheduled for orbit injection using a standard hitchhiker ejection system from space shuttle flight STS-88. Anticipated orbit for the spacecraft is 210 nmi at 51.6° (Ref. 1).

## 2.0 EXPERIMENT CONFIGURATION

### 2.1 Overall Configuration.

This experiment configuration consists of two distinct parts: the electronic board and the micro-particle detector assembly. The electronic board consists of a dc-dc converter section, detector bias section, and output conditioning section. The detector assembly consists of the micro-particle detector and an aluminum mount frame.

The electronic board was fastened to the side of the spacecraft power switching unit which is mounted to the bottom, inside surface of the spacecraft. Figure 1 shows the mounted electronic board with respect to the spacecraft coordinate system. The electronic board is not encapsulated in a separate enclosure but open to the local spacecraft environment. The detector assemblies were mounted to the bottom, outside surface of the spacecraft so that the impact detecting surface is in the -Z direction. Figure 2 shows a plan view of the locations of the two micro-particle detector assemblies.

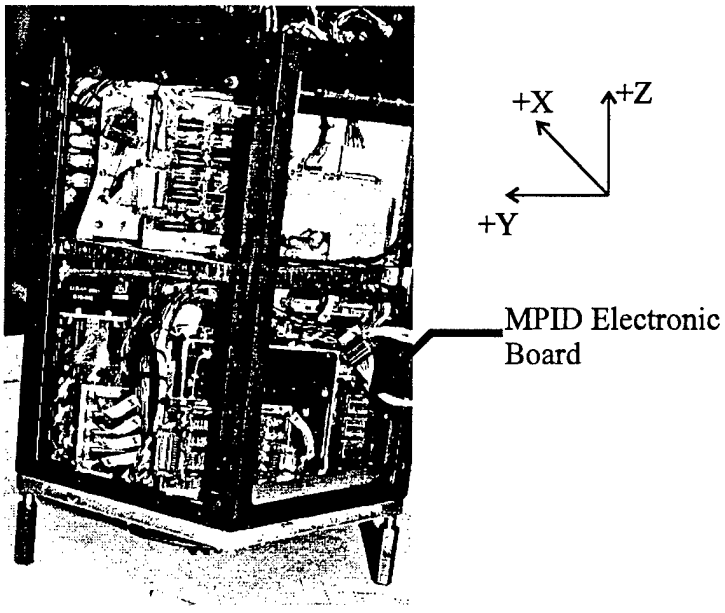


Figure 1. Electronic Board Mounted to Spacecraft and Spacecraft Coordinate System

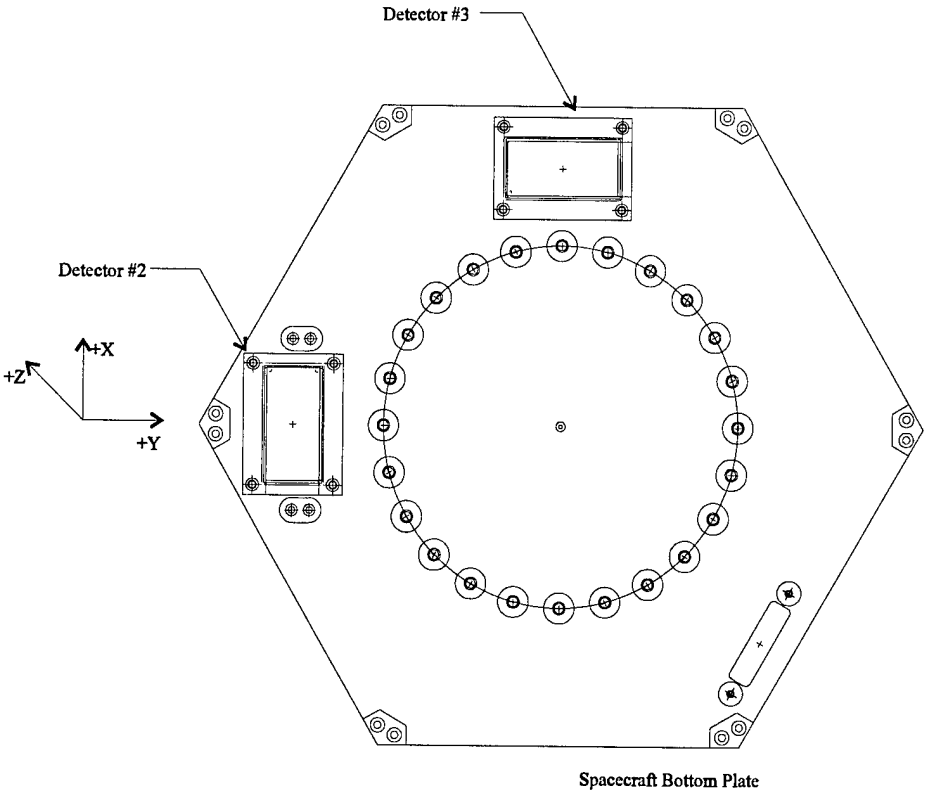


Figure 2. Detector Locations

The spacecraft will be spin stabilized and will rotate about the Y axis, see figure 3.

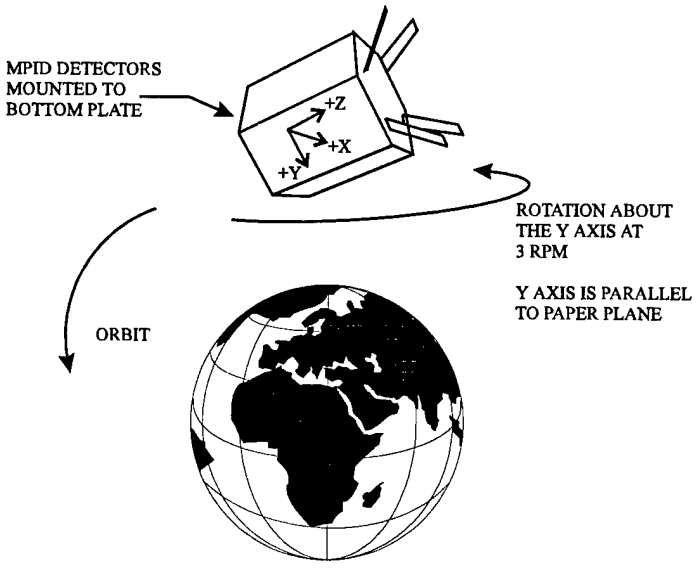


Figure 3. Spacecraft Orbit and Tumble Orientation

2.2 Electronic Board Design.

The purpose of the electronic board is to provide 60 vdc bias to each of the detectors and to provide an impact interrupt signal to the spacecraft memory I/O board. The spacecraft bus supplies the electronic board with +15 vdc and +5 vdc. The electronic board consumes 900 mW for +15 vdc and 0.2 mW for +5 vdc and with all components installed weighs 0.25 lbs. The electronic board provides a CMOS bilevel, active high, output signal to interrupt the spacecraft memory I/O board upon a particle impact. When an impact occurs and the memory I/O receives an interrupt, the current spacecraft time and the two coarse sun sensor readings are stored in the spacecraft's local memory and in one of the nine 8k spacecraft mailboxes as a 26 byte record. After storing the impact information, the spacecraft resets the electronic board. After storing 307 impact records the assigned mailbox will be full and data will be written onto existing impact records. Receiving 307 records in one day is extremely unlikely. However, the impact mailbox status will be carefully monitored and downlink times will be adjusted as appropriate. The spacecraft mailbox contents can be transmitted to the ground station on a daily basis.

A schematic of the electronic board is shown in figure 4. Figure 5 shows the board layout. Parts list for the electronic board is tabulated in appendix A.

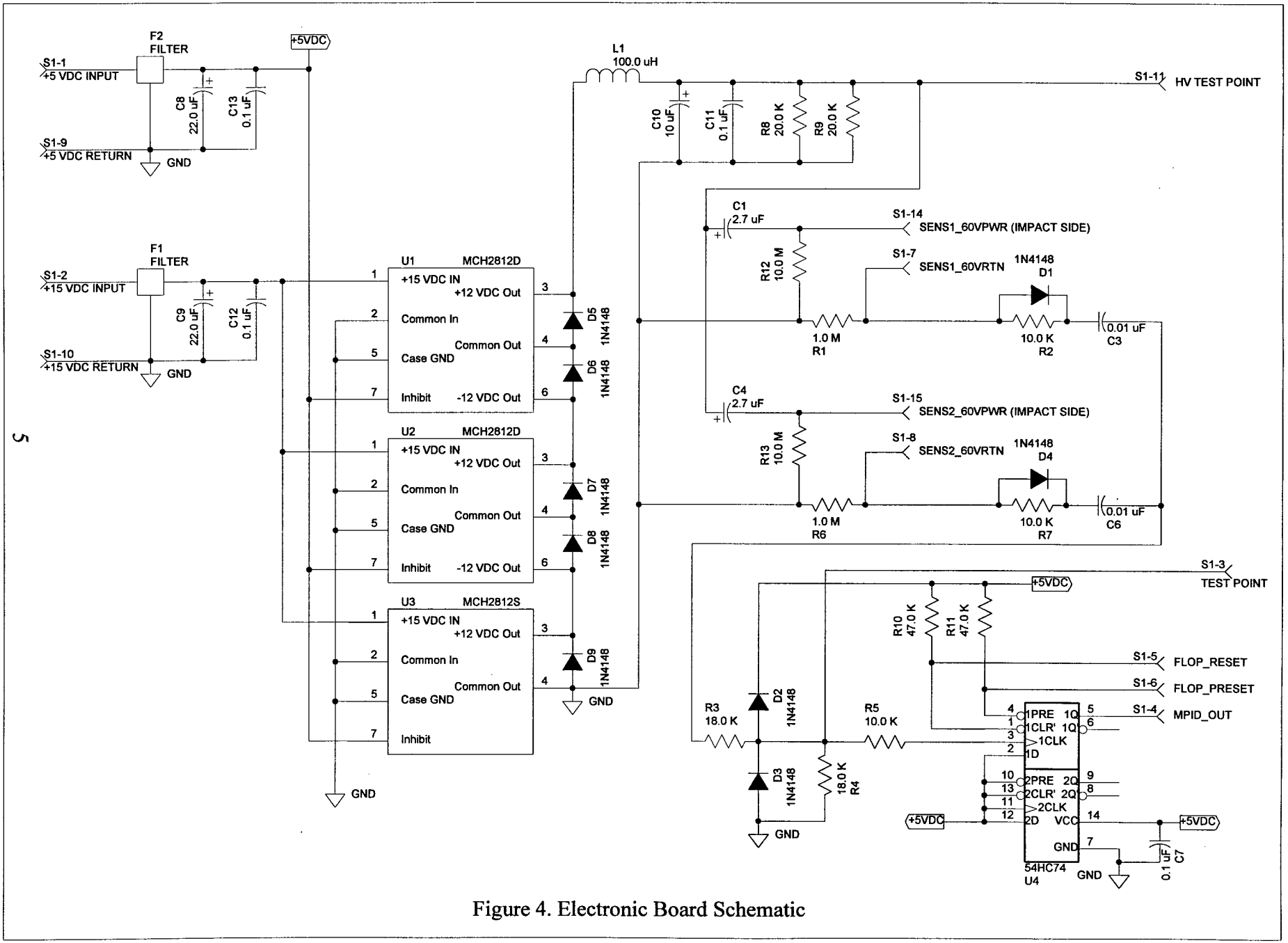


Figure 4. Electronic Board Schematic

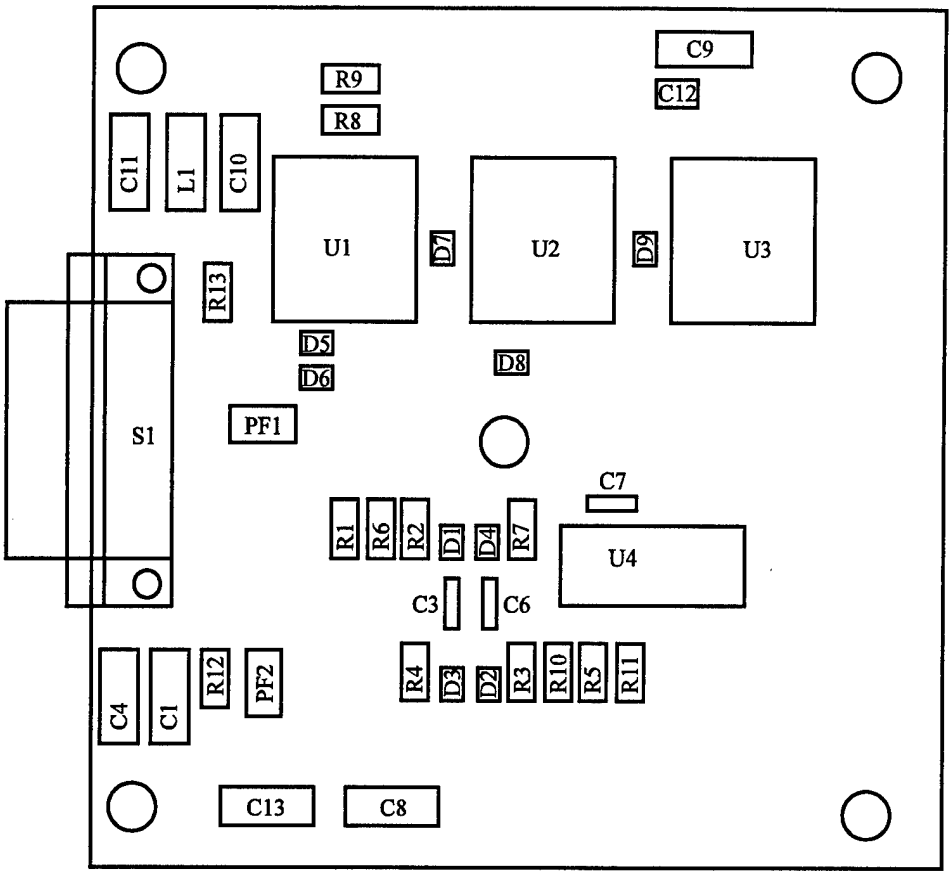


Figure 5. Electronic Board Component Layout

DC-DC converters, U1, U2, and U3 were placed in series for the purpose of generating a 60 vdc detector bias. Inductor L1 and capacitors C10 and C11 were used to form a low pass filter with a cutoff frequency of 10 kHz (Ref. 2). The low pass filter cutoff frequency, $f_c$, was determined using the following equation:

$$f_c = \frac{1}{\pi\sqrt{LC}};$$

where L = 100 μH and C = 10.1 μF.

Resistors R8 and R9 are used to load the three dc-dc converters to 90% of their maximum output load current. This loading is for the purpose of stablizing the converter's output voltage since they are not continuously loaded by capacitors C10 and C11. Upon a particle impact a positive going pulse clamped between approximately +0.6 vdc and +5.0 vdc by D2 and D3 will be seen at test point S1-3. This positive going pulse is used to clock through a +5 vdc level to the output of flip-flop U4, connector pin S1-4. Expected pulse width is approximately 100 ms. An active high on S1-4 will cause an interrupt to the spacecraft I/O board, which initiates a particle impact software service routine by the spacecraft I/O board. After the spacecraft services the impact interrupt the spacecraft will generate an active low pulse on connector S1-5 to reset flip-

flop U4. A timing diagram that shows logic relationships between key signal points on the electronic board is shown in figure 6.

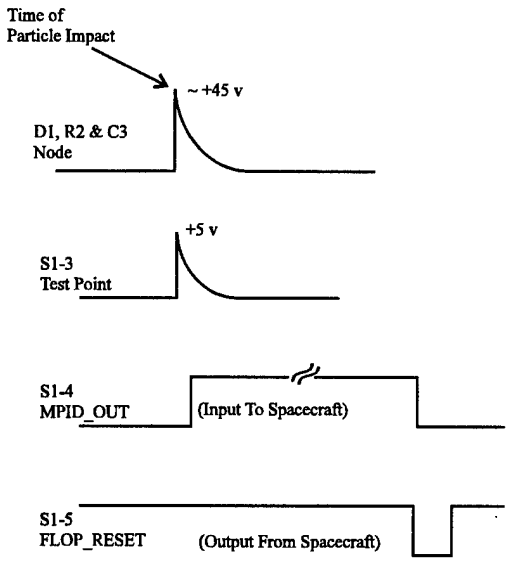


Figure 6. Electronic Board Timing Diagram

Connector pins S1-11 (HV Test Point), S1-3 (Test Point), and S1-6 (Flop_Preset) are not used by the spacecraft and were included for pre-flight diagnostic purposes only. The +15 vdc and +5vdc power returns are connected together at the board connector and are at the same potential as the spacecraft ground.

The electronic board, without components, was manufactured according to MIL-P-55110 and adhered to the military specification paragraphs tabulated in table 1 and the MightySat I Interface Control Document (Ref. 3).

Table 1. MIL-P-55110 Paragraphs

| Mil. Spec. Paragraph | Paragraph Title | | Mil. Spec. Paragraph | Paragraph Title |
|---|---|---|---|---|
| 3.4 | Material | | 3.6.1.2 | Soldermask Thickness |
| 3.6.1.1 | Visual | | 3.6.3.1 | Cleanliness |
| 3.6.1.1.1 | Annular Ring | | 3.6.4 | Cond Edge |
| 3.6.1.1.3 | Cond Spacing | | 3.6.4.2 | Bow & Twist |
| 3.6.1.1.4 | Dimensional | | 3.6.4.4 | Plating Adhes |
| 3.6.1.1.5 | Edges of PCB | | 3.6.4.6 | Solderability |
| 3.6.1.1.6 | Hole Pattern | | 3.6.4.7 | Soldermask Cu |
| 3.6.1.1.7 | Lar-Lar Regis | | 3.8 | Marking |
| 3.6.1.1.10 | Surface | | 3.8.1 | Traceability |
| 3.6.1.1.11 | Subsurface | | 3.9 | Workmanship |
| 3.6.1.1.12 | Cond Pattern | | | |

Two electronic boards were fabricated and all components installed in each board. The first electronic board fabricated was labeled qualification board and the second labeled flight board. The instrumentation test configuration used for testing both electronic boards prior to thermal and vibration testing, during thermal testing, and after vibration testing is shown in figures 7 and 8. Figure 7 shows a general test configuration and figure 8 shows a detailed configuration of the test break-out box and the test output isolation circuit. The instrumentation test configuration was used independent of the spacecraft.

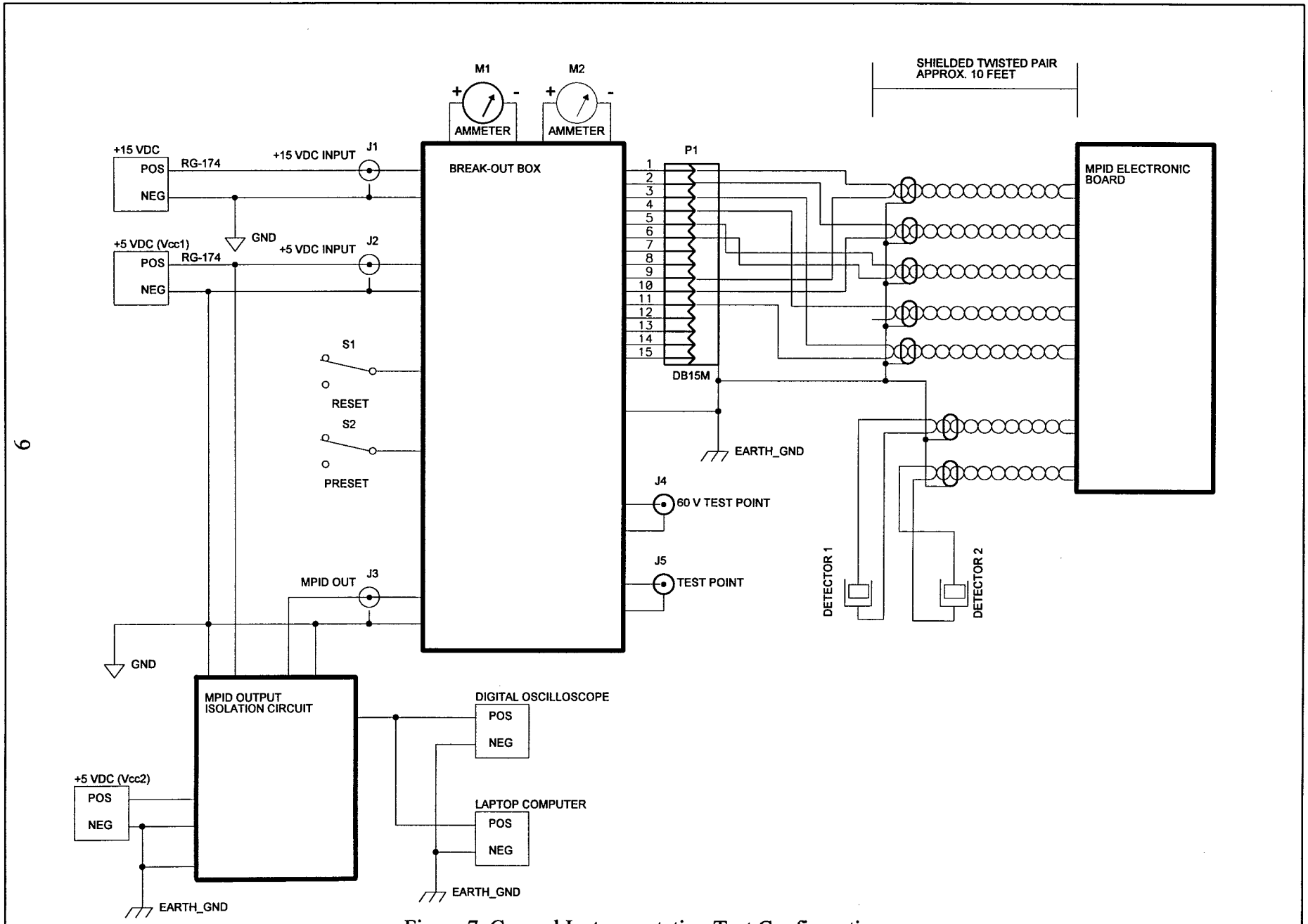


Figure 7. General Instrumentation Test Configuration

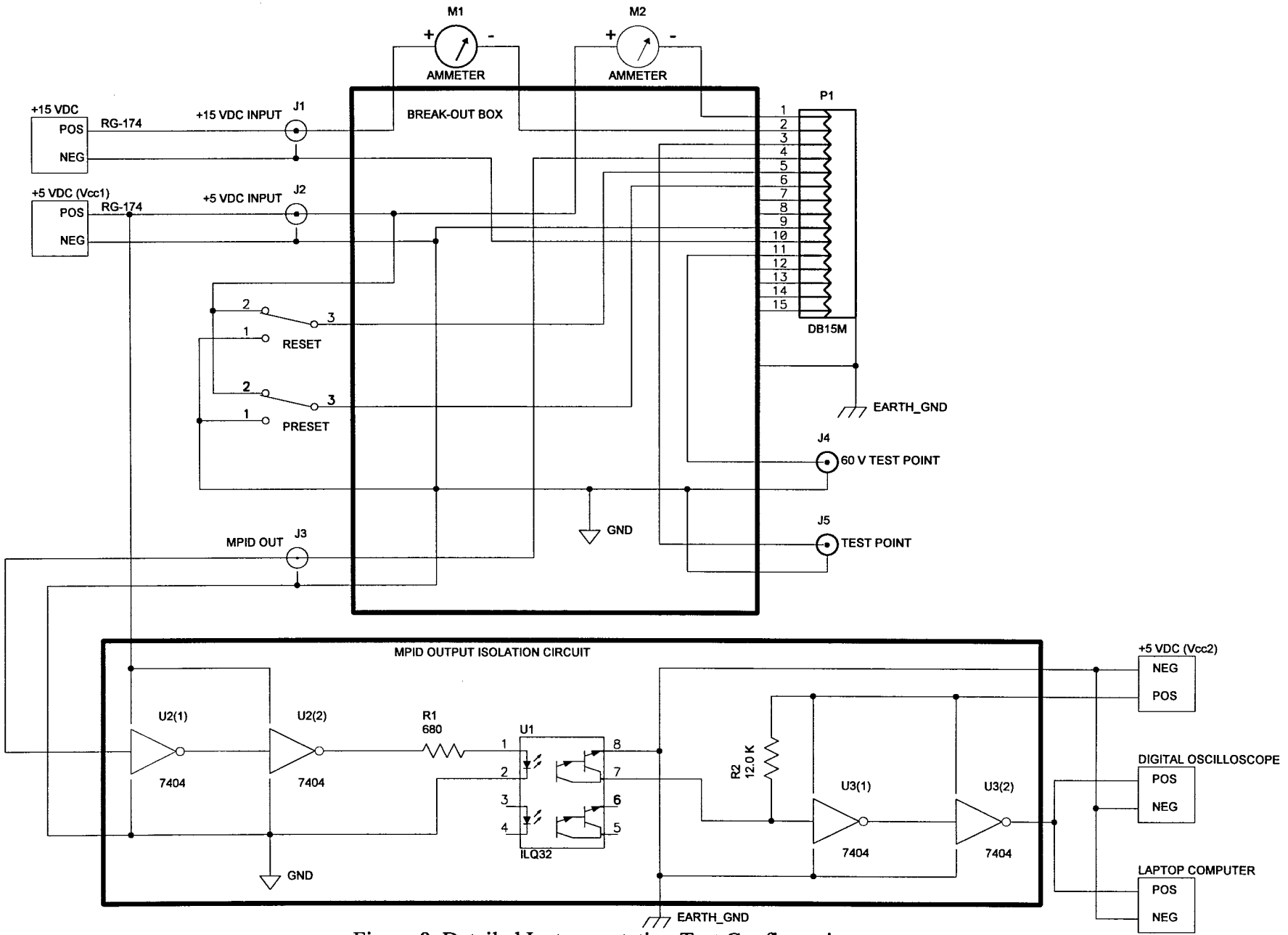


Figure 8. Detailed Instrumentation Test Configuration

2.3 Detector Assembly.

The detector assembly consisted of three elements: top plate, MPID detector, and bottom plate. An assembly drawing of the detector assembly configuration is shown in figure 9 (Ref. 4).

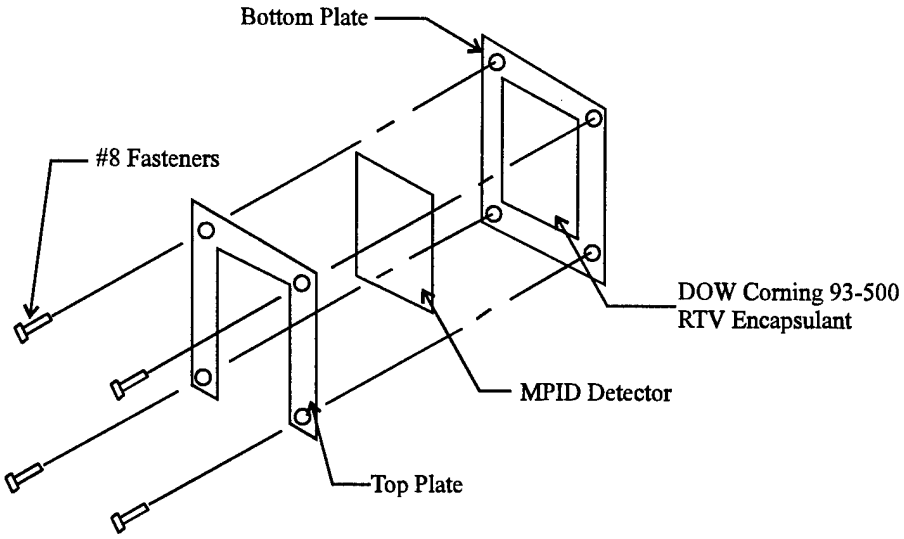


Figure 9. Detector Assembly

The micro-particle detectors are metal-oxide-semiconductor capacitor impact detectors manufactured by North Carolina State University (Ref. 5). Two detectors were supplied by North Carolina State University and two backup detectors were supplied by NASA Langley Research Center. Specifics of the detectors, other than a general overview, will not be discussed in this report. A complete description can be found in reports authored by Kassel and Wortman (Ref. 5 and 6).

The detectors consist of a parallel plate capacitor with a dielectric thickness of 1.0 μm and a top surface thickness of 0.1 μm. A 60 vdc bias voltage is applied across the capacitor, resulting in a charged capacitor. When particles impact the top surface of the detector, a discharge occurs. This discharge is monitored and recorded. The detectors used in this experiment are identical to the detectors flown on the Clementine Spacecraft Mission.[1]

Initial detector mounting plans were to bond the detectors directly to the satellite using GE RTV 566. However, at the request of NASA, a mechanical holder assembly was used to mount the detectors to the bottom plate of the spacecraft.[2] Detector assembly design was required to meet static loading of 25g and a random vibration profile discussed in section 4 of this report.

---

[1] Wortman J.J., Electrical and Computer Engineering Department, North Carolina State University.
Jones J.J., Kinard W., NASA Langley Research Center, Hampton, VA, private communication, 1996

[2] Davis R.J., Aerospace Corporation, Albququerque, NM.
Payne E., Air Force Research Laboratory/VS, Kirtland AFB, NM, private communication, 1996

A static load analysis was used to design the detector assemblies using assumed temperature extremes of -60°C and 100°C. Operational temperature profiles were unknown at the time of detector assembly design. The random vibration profile was used to qualify the design for space flight by experimentation.

Due to their mounting locations on the satellite, the holders were restricted to a total thickness of 0.125 inches and dimensions not to exceed 2.6 inches x 3.6 inches. Figures 10 and 11 show the mechanical design of the detector assembly top and bottom plates. Both plates were gold anodized. The mechanical fasteners selected for these holders were # 8-32 x ½ inch stainless steel countersunk screws (20 in-lbs torque / $s_y$ = 30 Kpsi ), MS24693-C50.

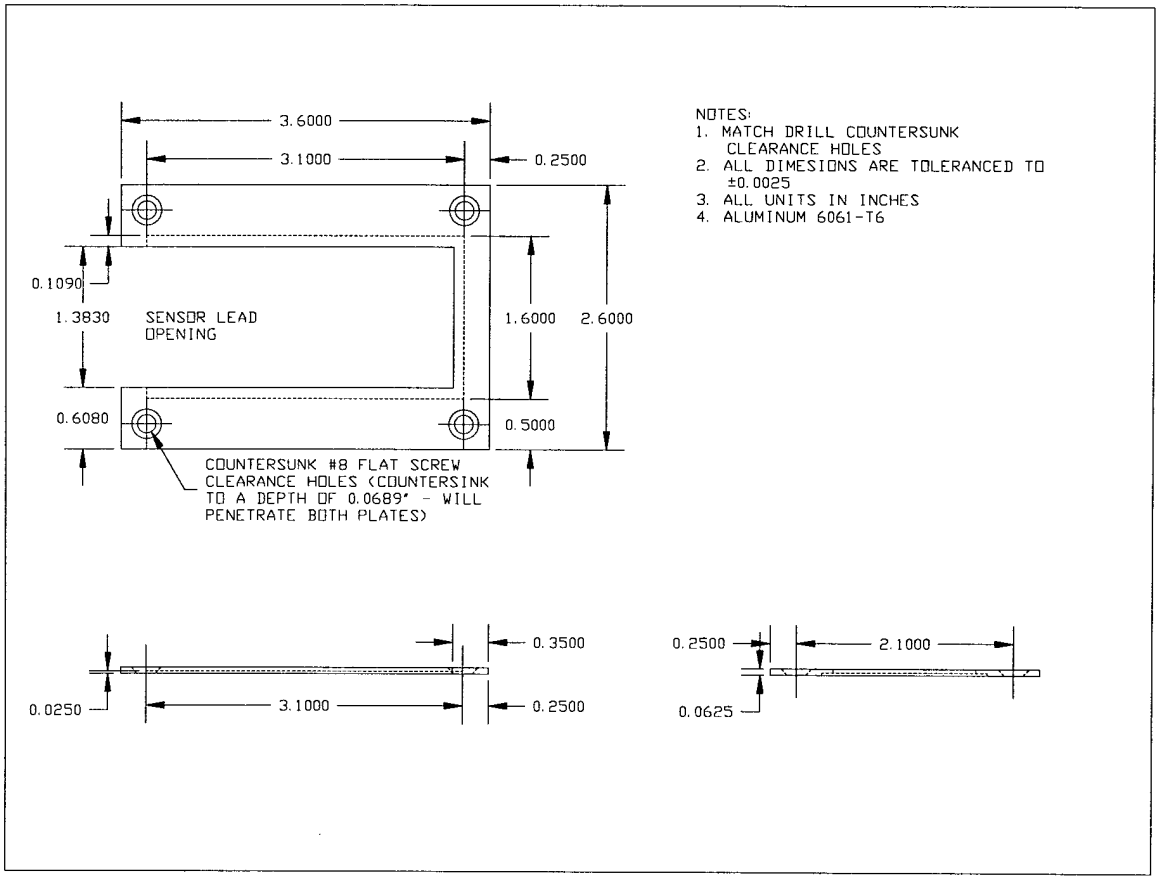


Figure 10. Top Plate

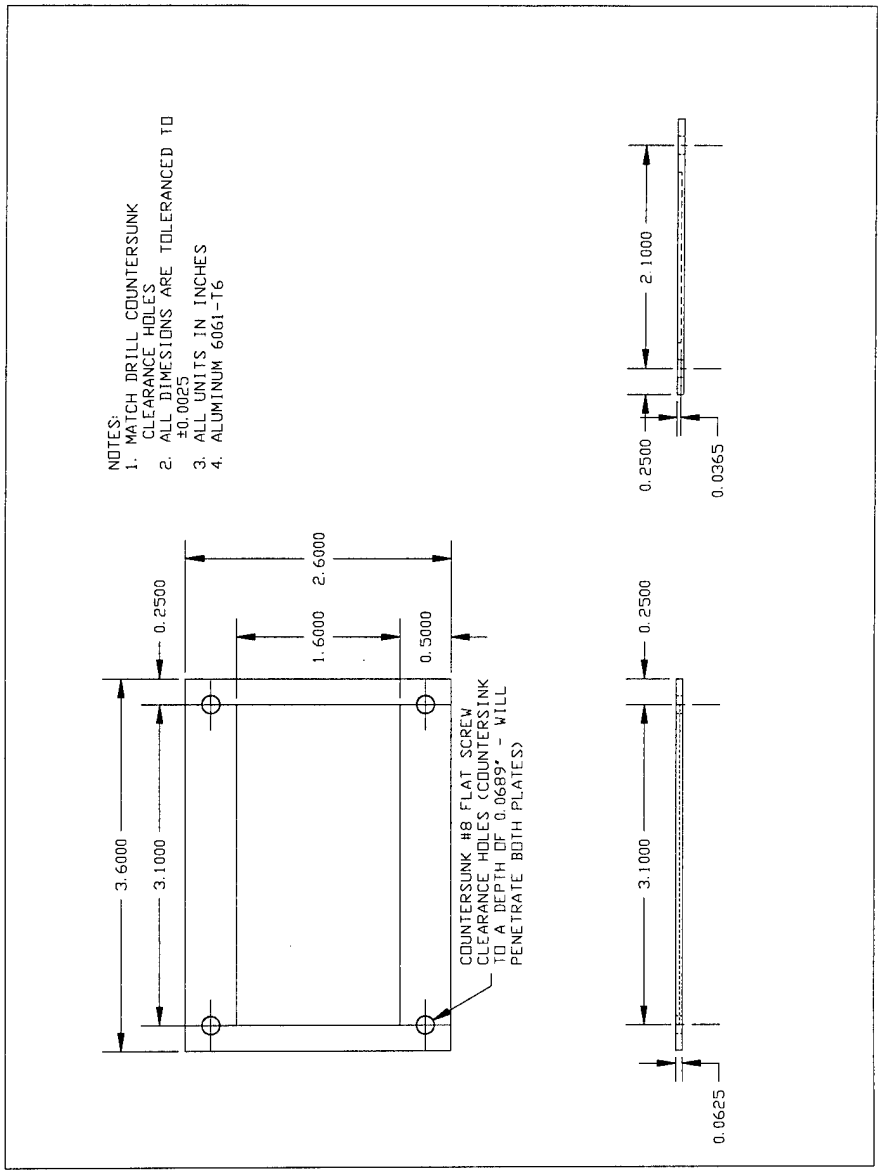


Figure 11. Bottom Plate

The force loads of the fasteners and the compressed members were determined using the following relationships:

$$F_b = \frac{k_b}{k_b + k_m} P + F_i;$$

$$F_m = \frac{k_m}{k_b + k_m} P - F_i;$$

where

$F_b$ ≡ bolt/fastener load
$F_m$ ≡ fastened member load
$F_i$ ≡ bolt/fastener preload
P ≡ external load
$k_b$ ≡ bolt/fastener stiffness
$k_m$ ≡ fastened member stiffness.

The stresses of these design elements (fasteners and members) were calculated with the following equations:

$$\sigma_b = \frac{F_b}{A_c};$$

$$\sigma_m = \frac{F_m}{A_c};$$

where

$\sigma_b$ ≡ bolt/fastener stress
$\sigma_m$ ≡ fastened member stress
$A_c$ ≡ area of contact between fasteners and members.

Using a maximum external load of 25g and a fastener torque of 20 in-lb, it was determined that the operational stresses occurring at each of the four fasteners were $\sigma_b$=1.8kpsi and $\sigma_m$=-1.8kpsi. Appendix B contains complete stress and force calculations. Comparing these operational stresses to their respective material yield strengths, the design elements were predicted to be operating well below their failure levels.

DOW Corning 93-500 RTV was selected as the bonding adhesive to mount the detectors to the assemblies based on a number of its mechanical properties. These include the adhesive's operating temperature range of -115°C to 200°C and proven space qualification. DOW 93-500 was used on the Long Duration Exposure Facility (LDEF), to secure experiment M0003-5 to the

spacecraft. LDEF post flight evaluation of 93-500 concluded that all bonds survived the mision intact (Ref. 7). In addition the 93-500 low viscosity allowed easy application, self-leveling, and complete degassing. Mounting procedures for the detectors are documented in Appendix C along with the adhesive specifications.

2.4 Attitude Determination and Control Subsystems.

The spacecraft attitude determination and control subsystem consists of a three-axis magnetometer sensor, torque coil actuators in each axis, software to control the spacecraft attitude, and two coarse sun sensors. The controller is a Bdot rate controller that will spin the spacecraft up to 3 RPM and then precess the spin axis (+Y) to be parallel to the orbit normal. The Mission Planning Computer has an attitude estimator software routine to process downlinked three-axis magnetometer sensor data through a Kalman filter to estimate the spin axis pointing vector to an accuracy of 5°. At the time the measurements are taken on orbit, attitude knowledge will be accurate to 2.5°, because the nutation about the spin axis will be included in the measurements. However, in attempting to extrapolate the attitude after that time, the spacecraft nutation must be added in and is on the order of 2°. This then yields an attitude knowledge error of less than 3°. In addition to the three-axis magnetometer sensor system, the seven solar panels and two coarse sun sensors can be used to resolve the instantaneous spacecraft attitude relative to the sun line. This will be done through post processing of the data on the ground by Air Force Research Laboratory and the Aerospace Corporation using a triad method to achieve a more accurate attitude estimate than could be obtained by the Kalman filter alone (Ref. 8).

The coarse sun sensors consist of Gallium-Indium-Phosphate on Gallium cascade solar cells. These two cells were covered with fused-silica coverglass, with an ultra-violet reflective coating. One sun sensor is located on the center of the marman adapter ring on the underside of the spacecraft bottom plate, while the second sensor is located on the -X and -Y corner of the spacecraft top plate. The two sun sensors were built by Air Force Research Laboratory/VS from 2 x 2 cm cascade cells. The analog output of the sun sensors will be collected and converted to a digital signal by status I/O line number 2 (Ref. 8).

Use of the three-axis magnetometer sensor system and post processing of solar panel and sun sensor data, will permit an attitude knowledge at time of a particle impact to be known to an accuracy of 5°.

## 3.0 THERMAL CYCLE TESTING

The purpose of conducting thermal cycle testing was to demonstrate that the electronic board and detector assembly could operate properly and survive in the predicted thermal environment.

### 3.1 Electronic Board.

The qualification electronic board was tested in a Cincinnati Sub Z-32 environmental chamber and the flight electronic board was tested in a Thermotron S-1.2C environmental chamber. Type T thermocouples were fastened to various components on each electronic board using thermally conductive grid tape at locations shown in figure 12. Shown in figure 13 is the air temperature profile inside the chamber and thermal test data collected from thermocouples mounted in locations A, B, and C for the qualification board. Shown in figure 14 is the air temperature profile inside the chamber, thermal test data collected from thermocouples mounted in locations A, B, and C, and the desired thermal profile for the flight board. Unfortunately, the thermocouple data recording system did not record thermocouple data for the flight board between 17:30 and 07:00, as shown in figure 14. The desired thermal profile consisted of eight cycles with extreme electronic board temperature setpoints of +55 °C and -25 °C. The intent of the thermal test was to ensure the board, not the components of the board, reached the extreme test temperatures (Ref. 9 and 10).

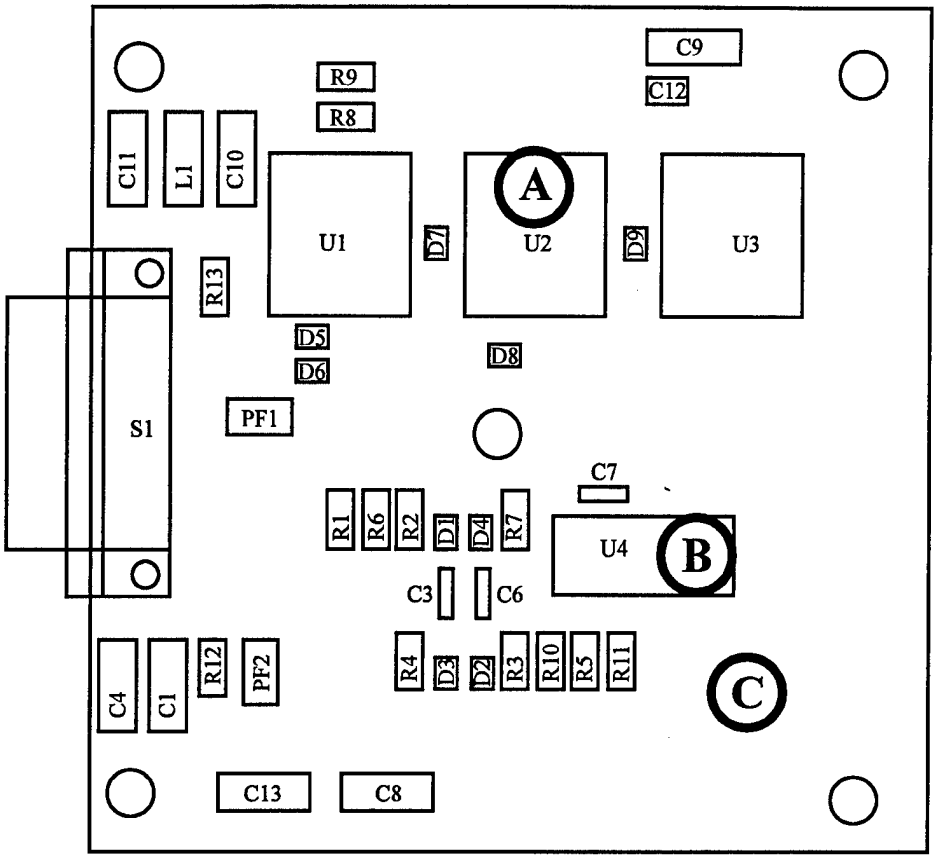


Figure 12. Type T Thermocouple Location

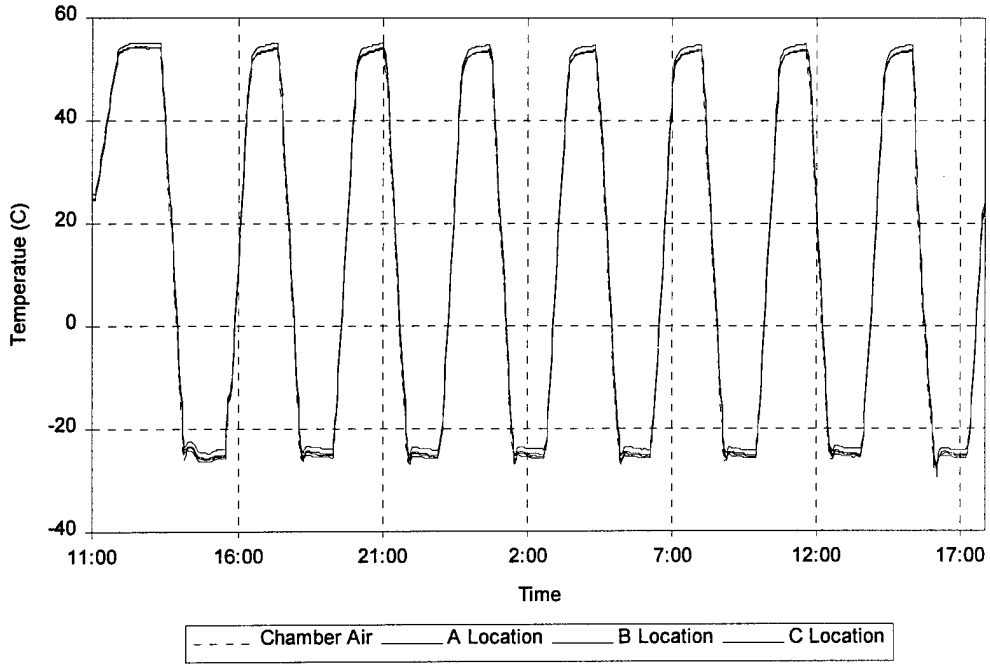


Figure 13. Qualification Board Thermal Test Profile

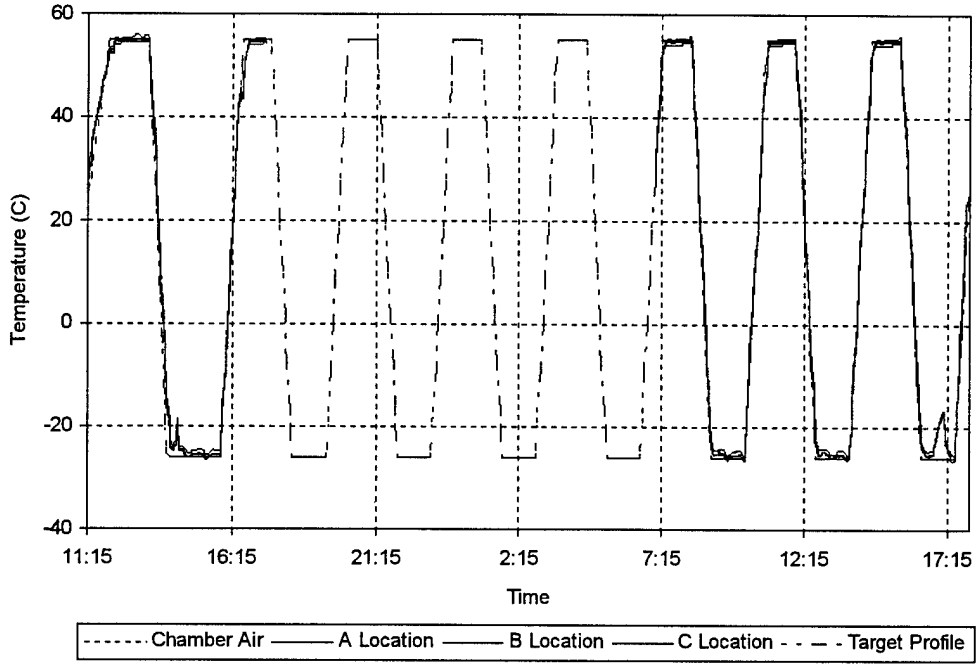


Figure 14. Flight Board Thermal Test Profile

During the thermal test, each board was electrically powered using the instrumentation test circuit shown in figures 7 and 8. The digital oscilloscope, shown in figures 7 and 8, was configured to trigger on a positive going edge of the electronic board output line, MPID_OUT, pin S1-4. A BASIC software program was run on the laptop computer, shown in figures 7 and 8, to sample and record the electronic board output line, MPID_OUT, every minute using LPT1 port, pin 13, as an input to the LPT1 port. The purpose of the oscilloscope and laptop computer configurations was to measure and record any transition of the electronic board output line from a high to low state or a low to high state during the thermal test and pre- and post- vibration testing. The source code used on the laptop computer is listed in appendix D. A sample output from the laptop computer output line monitor routine is tabulated in table 2. As seen in table 2 a state change in the MPID_OUT line occured at sample numbers 11, 9, and 7 and was caused by manually depressing switch S1 or S2 of figures 7 and 8. Decimal number 88 read on LPT1 port represents a high state of the MPID_OUT line and a decimal number 72 represents a low state of MPID_OUT line.

Table 2. Sample Output From Laptop Output Line Monitor

| Sample Number | LPT1 Port Status (decimal) | Date | Time | Bit 4 Status |
|---|---|---|---|---|
| 13 | 88 | 11-06-1996 | 10:34:36 | high |
| 12 | 88 | 11-06-1996 | 10:35:36 | high |
| 11 | 72 | 11-06-1996 | 10:36:36 | low |
| 10 | 72 | 11-06-1996 | 10:37:36 | low |
| 9 | 88 | 11-06-1996 | 10:38:36 | high |
| 8 | 88 | 11-06-1996 | 10:39:37 | high |
| 7 | 72 | 11-06-1996 | 10:40:37 | low |
| 6 | 72 | 11-06-1996 | 10:41:37 | low |
| 5 | 72 | 11-06-1996 | 10:42:37 | low |
| 4 | 72 | 11-06-1996 | 10:43:37 | low |
| 3 | 72 | 11-06-1996 | 10:44:38 | low |
| 2 | 72 | 11-06-1996 | 10:45:39 | low |
| 1 | 72 | 11-06-1996 | 10:46:39 | low |
| 0 | 72 | 11-06-1996 | 10:47:39 | low |

Note: 88D = 59H = 0101 1001
72D = 49H = 0100 1001

In addition to the oscilloscope and laptop computer measurements, several electronic board performance measurements were manually measured and recorded. Nominal and measured performance values are tabulated in tables 3 and 4.

Operation of both the qualification and flight electronic boards was nominal before, during and after thermal testing.

Table 3. Thermal Performance Measurements, Qualification Board

| Time (hour) | Temp. On U2, DC-DC Conv. (°C) | +5 v Current (μA) | +15 v Current (A) | High Voltage Test Point (v) | Manual Reset and Preset (y/n) | +5 v Noise Level at Supply (mv) | +15 v Noise Level at Supply (mv) |
|---|---|---|---|---|---|---|---|
| Nom. | N/A | 35 | 0.05 | 64.3 | yes | 20 | 30 |
| | | | | | | | |
| 10:30 | 24.45 | 35 | 0.05 | 64.2 | yes | 20 | 30 |
| 11:05 | 24.48 | 35 | 0.05 | 64.3 | yes | 20 | 30 |
| 12:00 | 53.37 | 35 | 0.05 | 64.2 | yes | 20 | 30 |
| 13:30 | 38.48 | 35 | 0.05 | 64.1 | yes | 20 | 30 |
| 14:45 | -26.27 | 36 | 0.06 | 64.2 | yes | 20 | 30 |
| 15:50 | -4.64 | 36 | 0.06 | 64.3 | yes | 20 | 30 |
| 17:00 | 53.49 | 35 | 0.05 | 64.1 | yes | 20 | 30 |
| 17:45 | 14.77 | 35 | 0.06 | 64.4 | yes | 20 | 30 |
| 08:35 | -3.66 | 35 | 0.06 | 64.5 | yes | 20 | 30 |
| 09:45 | -25.7 | 36 | 0.06 | 64.4 | yes | 20 | 30 |
| 11:00 | 52.87 | 36 | 0.05 | 64.5 | yes | 20 | 30 |
| 12:30 | -26.08 | 35 | 0.06 | 64.5 | yes | 20 | 30 |
| 14:00 | 12.89 | 35 | 0.06 | 64.7 | yes | 20 | 30 |
| 15:30 | 23.94 | 35 | 0.06 | 65.1 | yes | 20 | 30 |
| 17:00 | -25.64 | 35 | 0.06 | 64.6 | yes | 20 | 30 |
| 17:45 | 20.55 | 35 | 0.05 | 64.3 | yes | 20 | 30 |
| 17:55 | - | 35 | 0.05 | 64.1 | yes | 20 | 30 |

Table 4. Thermal Performance Measurements, Flight Board

| Time (hour) | Temp. On U2, DC-DC Conv. (°C) | +5 v Current (μA) | +15 v Current (A) | High Voltage Test Point (v) | Manual Reset and Preset (y/n) | +5 v Noise Level at Supply (mv) | +15 v Noise Level at Supply (mv) |
|---|---|---|---|---|---|---|---|
| Nom. | N/A | 35 | 0.05 | 64.2 | yes | 20 | 30 |
| | | | | | | | |
| 11:00 | 24.11 | 35 | 0.06 | 64.1 | yes | 20 | 3 0 |
| 11:15 | 24.11 | 35 | 0.06 | 64.1 | yes | 20 | 30 |
| 12:30 | 54.50 | 35 | 0.05 | 64.3 | yes | 20 | 30 |
| 13:45 | 11.36 | 36 | 0.05 | 64.2 | yes | 20 | 30 |
| 14:30 | -24.60 | 35 | 0.05 | 64.1 | yes | 20 | 30 |
| 15:15 | -25.81 | 35 | 0.05 | 64.1 | yes | 20 | 30 |
| 16:00 | -9.41 | 35 | 0.06 | 64.2 | yes | 20 | 30 |
| 16:45 | 53.79 | 35 | 0.06 | 64.3 | yes | 20 | 30 |
| 17:15 | 54.32 | 35 | 0.06 | 64.2 | yes | 20 | 30 |
| 08:30 | 30.76 | 35 | 0.06 | 64.1 | yes | 20 | 30 |
| 09:45 | -25.35 | 35 | 0.06 | 64.3 | yes | 20 | 30 |
| 11:00 | 53.86 | 35 | 0.06 | 64.3 | yes | 20 | 30 |
| 12:45 | -25.26 | 35 | 0.06 | 64.4 | yes | 20 | 30 |
| 14:15 | 17.73 | 35 | 0.05 | 64.3 | yes | 20 | 30 |
| 15:40 | 46.61 | 36 | 0.05 | 64.1 | yes | 20 | 30 |
| 17:00 | -18.83 | 35 | 0.05 | 64.2 | yes | 20 | 30 |
| 18:00 | 25.54 | 35 | 0.05 | 64.1 | yes | 20 | 30 |

3.2 Detector Assembly.

Particle detector assembly numbers 3 and 5, including detectors, were initially tested in a Thermotron S-1.2C environmental chamber using the temperature profile shown in figure 15. For this initial thermal test, type T thermocouples were placed at locations shown in figure 16. Also, shown in figure 15 is the thermocouple data for the initial thermal test. Prior to test initiation, capacitance measurements for detector numbers 3 and 5 were 79.0 ηF and 82.0 ηF, respectively. Thermal cycling was initiated by ramping up to +136 °C, followed by a ramp down to -50 °C. Approximately 12 minutes into the -50 °C cold soak the temperature chamber fan and compressor stopped operating and the chamber temperature began to rise. Four minutes after chamber malfunction, ice crystals and fog began forming on the detector surface. The chamber was reprogrammed and a slow ramp up to ambient temperature was initialized. All fog and ice crystals disappeared from the detector surfaces as the experiment temperatures increased to ambient levels, +20°C (Ref.11).

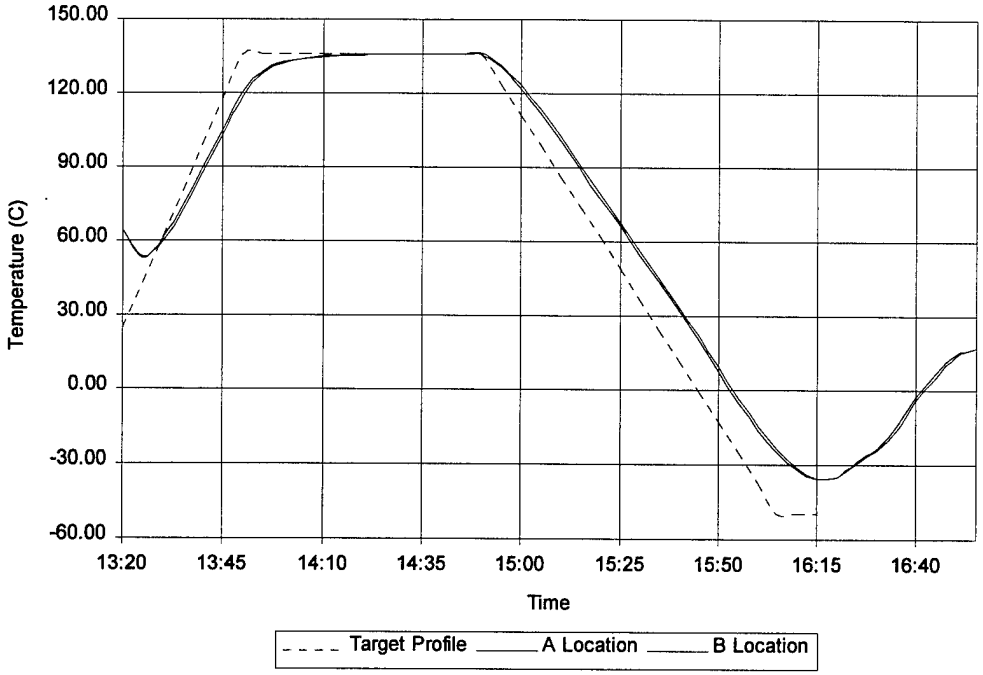


Figure 15. Initial Detector Assembly Temperature Profile

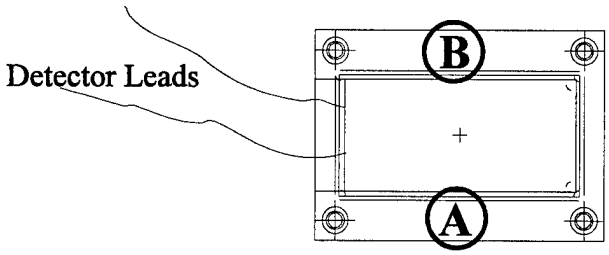


Figure 16. Initial Thermocouple Locations

Approximately eight hours after the chamber malfunctioned, the capacitance of each detector measured 0.0 ηF. An attempt was made to "revive" detector numbers 3 and 5 using the electronic circuit shown in figure 17. Each detector was allowed to charge to 80 vdc for approximately 5 minutes and then was discharged through C1, C2, and R2 by depressing switch S1 for approximately 2 minutes. After several cycles of charging and discharging each detector, capacitance measurement for detector number 3 was 78.0 ηF and for detector number 5 was 0.0 ηF.

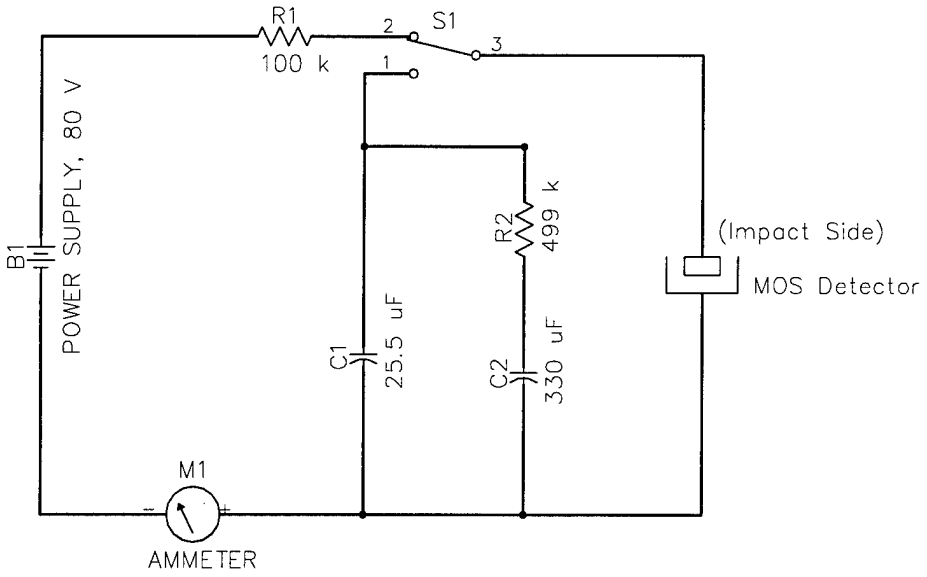


Figure 17. Detector Charge - Discharge Circuit

Additional charge and discharge cycles to detector number 5 had no effect on the capacitance measurement of 0.0 ηF. A continuity measurement was made between points B and C, shown in figure 18, for detector number 5 and was discovered to be electrically open. After a 24 gauge wire was attached to point C using conductive epoxy, a capacitance measurement was then taken between points A and C in figure 18 and was 81.9 ηF. The conclusion is that the electrical connection of detector number 5 between points B and C became electrically open either during or after the initial temperature cycle.

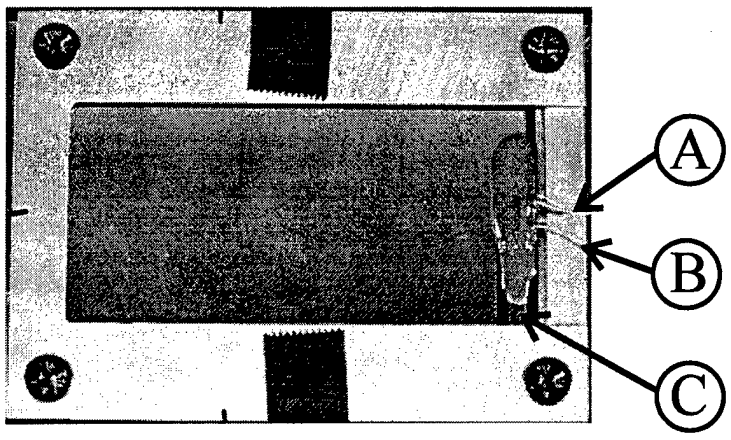


Figure 18. Detector Number 5, Test Points

Due to complications that arose during the first thermal cycle test and the uncertain cause of capacitance variation for detectors 3 and 5, the Aerospace Corporation was tasked to perform a new temperature prediction, appendix E. Based on the new temperature prediction conducted by the Aerospace Corporation a new temperature profile was developed and is shown in figure 19 with new temperature limits of +62 °C and -50 °C. The particle detector assembly underwent two cycles at the test levels illustrated in figure 19 using a 1 °C/min. ramp rate with 15 minute soak periods at +62 °C, +32 °C, -50 °C, and -2°C. Although it is desirable to test space experiments at test levels 11°C above and below the predicted high and low temperatures, this procedure was not executed on the particle detectors. It was determined that the -50°C thermal prediction from the Aerospace Corporation was very conservative and that it would be unwise to subject the detectors to their predicted operational lower limit temperature.[3]

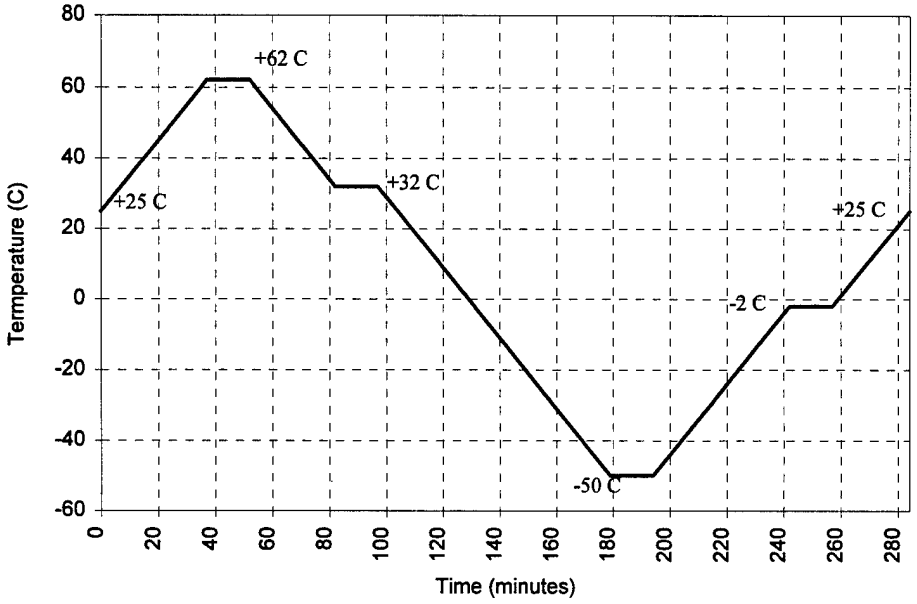


Figure 19. Revised Detector Temperature Test Profile

The detectors were unpowered during the temperature profile except for 15 minute soak periods of +32 °C and -2 °C. During the 15 minute powered intervals the current draw was monitored and recorded. When the detector was unpowered, capacitance measurements were recorded every minute.

To avoid a recurrence of ice crystals forming on the detector surface, it was decided to perform the detector thermal cycle profile in the Shrader 24" thermal vacuum.

[3] Serna P.J., Liechty G.H., Lamkin T., Air Force Research Laboratory, Kirtland AFB, NM.
Mirate C., Perez J., Nagao L., Stottlemyer D., Jackson and Tull, Albuquerque, NM, private communication 1996

3.3 Detector Assembly #2 and #3 Test Setup.

Detectors number 2 and 3 were fastened to the center of a 0.25 inches thick trapezoidal G10 plate, figure 20, using four #8-32 x 3/8 inch screws. The intent of using the G10 plate was to isolate the detector from the large thermal mass and thermal variations that exist throughout the thermal chamber.

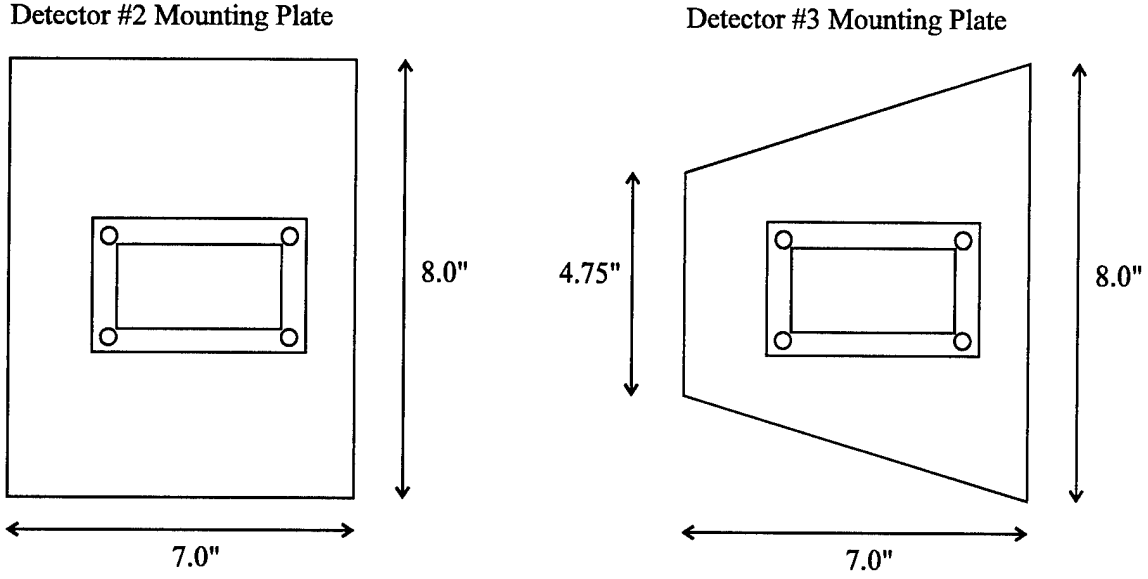


Figure 20. Thermal Test Mounting Plates

The lengths of the two detector leads were lengthened by soldering a 28 gauge unshielded, twisted, wire to the detector leads. A male pin was attached at the end of each 28 gauge wire that would allow detector plug-in to the chamber 15 pin connector.

The G10 plate and the detector were placed in the middle of the thermal vacuum chamber and instrumented with type K thermocouples as shown in figure 21. Letters A through F indicate thermocouple locations and correspond to thermocouple channels 0 through 5. The thermocouples were fastened to the chamber plate and the detector assembly with kapton tape. The chamber pressure was allowed to reach at least $9.9 \times 10^{-4}$ Torr before proceeding with the thermal profile (Ref. 11).

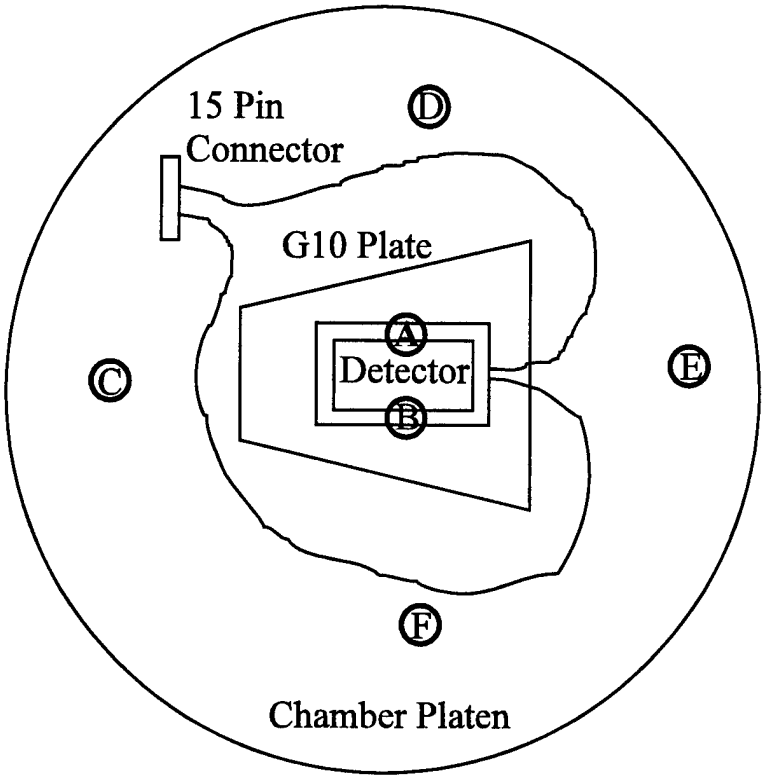


Figure 21. Thermal Test Thermocouple Locations

3.4 Detector #3 Test Execution.

The first cycle was completed at the close of business on 17 December 1996. All chamber power was removed and detector 3 was allowed to remain in the chamber under vacuum overnight. The second and final thermal cycle was executed on 18 December 1996 following additional chamber pump down for 5 minutes. After cycle completion, the chamber and detector were allowed to stabilize at ambient temperatures (20-25°C) before venting the chamber and removing the detector assembly.

The capacitance readings were somewhat sporadic at various intervals during detector 3 thermal cycle test. Fluctuations in the range of 54.0 to 97.0 ηF and 36.0 to 57.0 ηF occurred frequently during the test. Nominal capacitance measurement for detector number 3 is 76.7 ηF. Fluctuation levels and frequency diminished during the second cycle as compared to the first cycle.

Detector number 3 capacitance measurements and corresponding temperature measurements for thermocouple location A are shown in figure 22. Temperature data for thermocouple locations A through F are contained in appendix F.

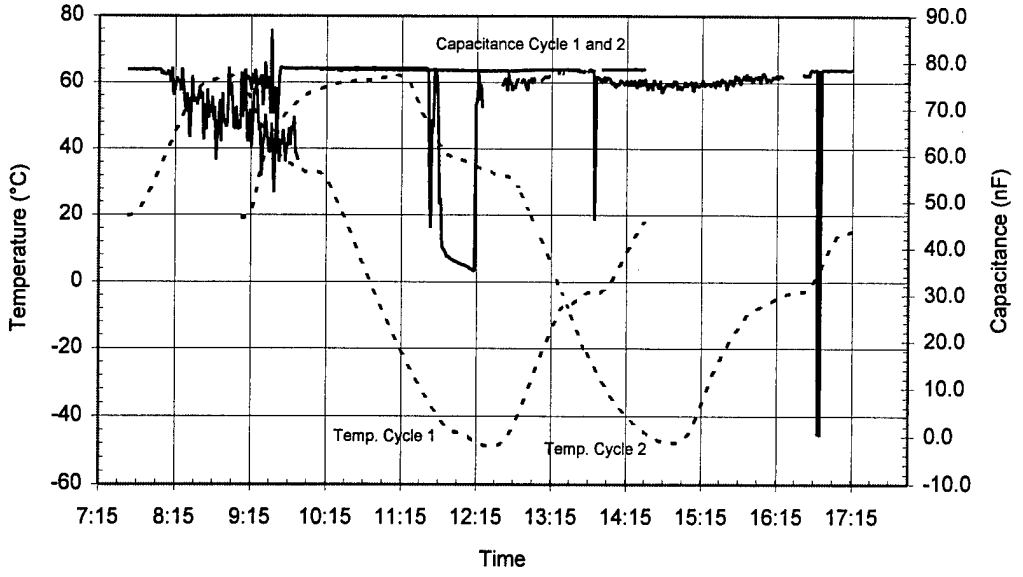


Figure 22. Detector Number 3, Capacitance and Temperature Measurements

Detector number 3 current measurements taken during 15 minute soak periods at temperatures of +32°C and -2°C are shown in figure 23. Nominal current measurements for detector number 3 range between 1 and 20 ηA.

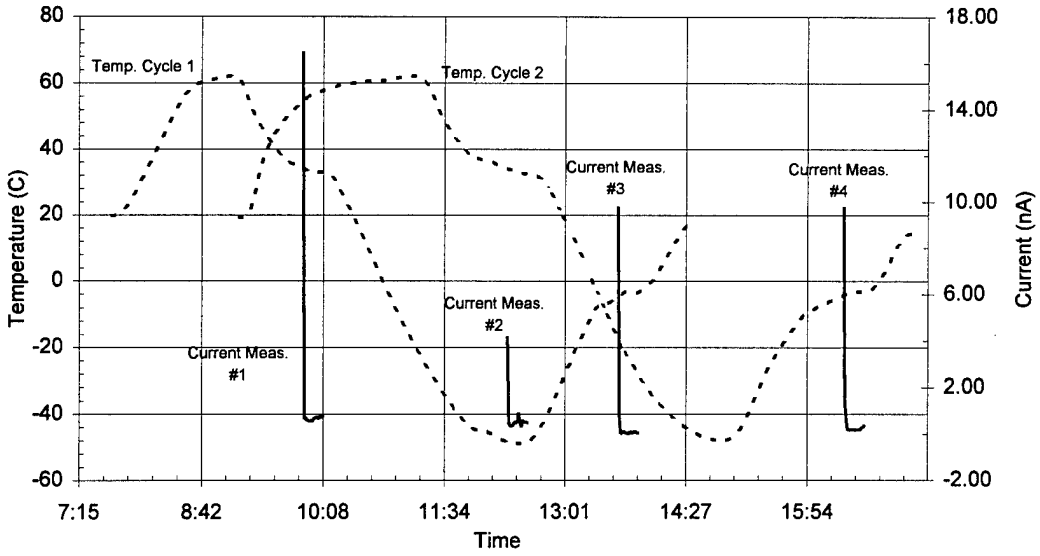


Figure 23. Detector Number 3, Current Measurements During Soak Periods

3.5 Detector #2 Test Execution.

The first cycle was completed on Friday, 19 December 1996. All chamber power was removed and detector number 2 was allowed to remain in the chamber under vacuum over the weekend. The second and final thermal cycle was executed on 23 December 1996 following additional chamber pump down for several minutes. After cycle completion, the chamber and detector were allowed to approach ambient temperatures (20-25°C) before venting the chamber and removing the detector assembly.

The capacitance readings of detector 2 were very stable for almost the entire test duration. Fluctuations between 0 and 78.5 ηF were observed for 2-3 minutes just prior to the 15 minute hot soak at 62°C of the first cycle. Nominal capacitance measurement for detector number 2 is 78.8 ηF. This was the only occurrence of capacitance fluctuations during test execution of detector 2.

Detector number 2 capacitance measurements and corresponding temperature measurements for thermocouple location A are shown in figure 24. Temperature data for thermocouple locations A through F are contained in appendix F.

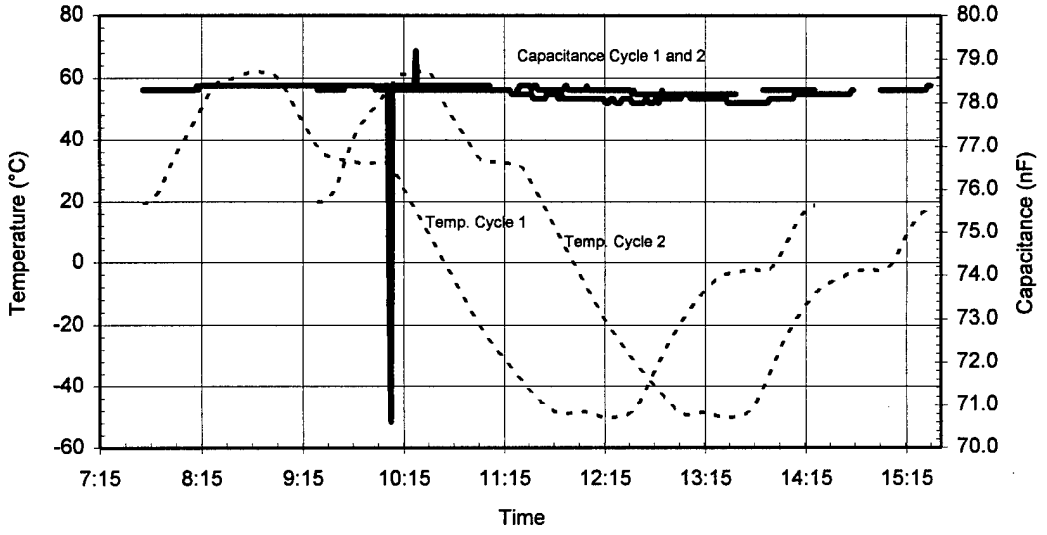


Figure 24. Detector Number 2, Capacitance and Temperature Measurements

Detector number 2 current measurements taken during 15 minute soak periods at temperatures of +32°C and -2°C are shown in figure 25. Nominal current measurements for detector number 3 range between 1 and 20 ηA.

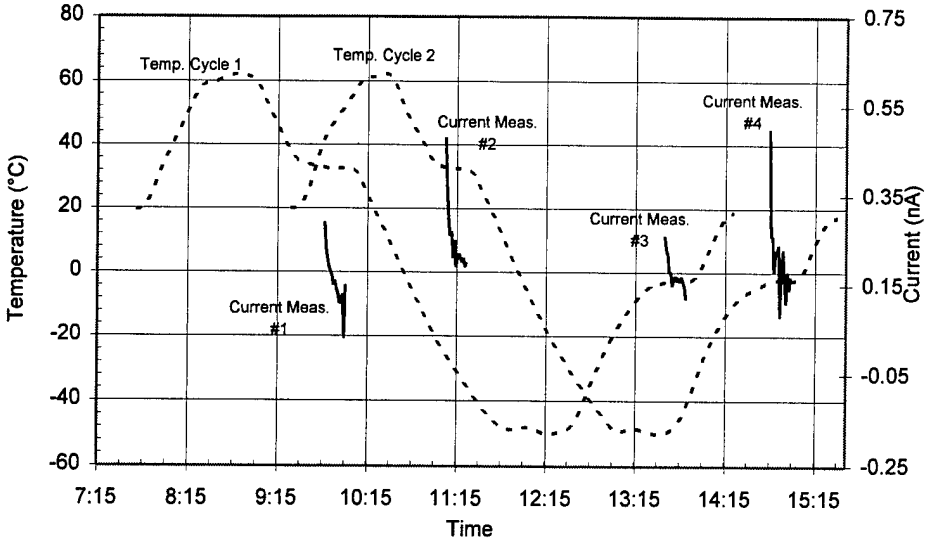


Figure 25. Detector Number 2, Current Measurements During Soak Periods

## 4.0 VIBRATION TESTING

The purpose of conducting vibration testing was to demonstrate that the electronic board and detector assembly could properly operate and survive in the predicted vibration environment.

### 4.1 Electronic Board.

The qualification and flight electronic boards underwent vibration testing using vibration recommendations found in 1992 Goddard SFC Hitchhiker Customer Accomodations and Requirements Specifications for payloads less than 50 lb (Ref. 14). Each electronic board underwent vibration testing in the X, Y, and Z axes. In addition, each test axis underwent three vibration patterns in order: 1) pre-sine sweep; 2) random; and 3) post-sine sweep. The purpose of conducting the three vibration patterns in order was to allow comparison of the pre-sine sweep with the post-sine sweep to determine if the random vibration caused damage to the electronic board. Ideally, the pre and post sine sweeps would be identical if no damage occured during the random vibration.

Note: The axis used for vibration testing of the electronic board are not the same axis as the spacecraft axis. The axis used for vibration testing were used only for vibration testing of the electronic board.

Five #6-32 x 3/8 in electronic board mounting standoffs were attached to the vibration table interface plate and torqued to 12 in-lb. Each electronic board was fastened to the mounting standoffs using 5 #6-32 x 3/8 in screws with washers. The screws were initially torqued to 5 in-lb beginning with screw number 1 and proceeding in order to screw number 5, see figure 26. After securing screws 1 through 5 to 5 in-lb. each screw was torqued to 10 in-lb beginning with screw number 1 and proceeding to number 5. A PCB model 355A53 accelerometer was fastened to the vibration interface plate in the axis of vibration using kapton tape and wax and was used as the control accelerometer. Two PCB model 352B22 accelerometers were used to gather data on the electronic board. One accelerometer was placed in location D and remained in this location for X, Y, and Z axes tests. The second accelerometer was moved from positions A, B, and C according to table 5 (Ref. 12 and 13).

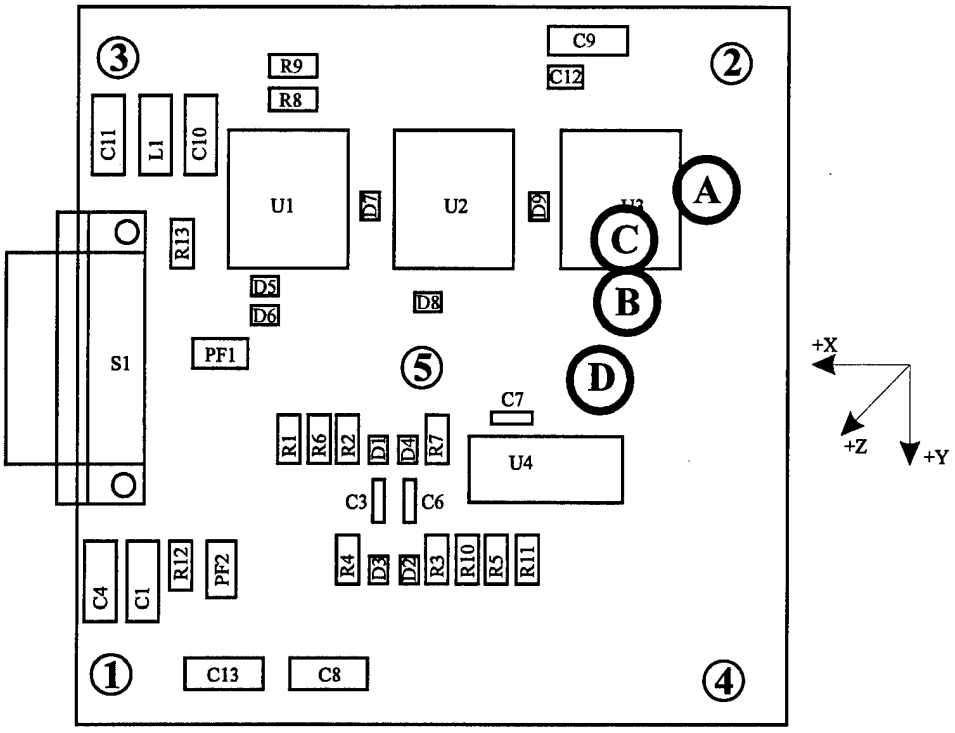


Figure 26. Electronic Board Accelerometer Location

Table 5. Vibration Test Accelerometer Locations

| Vibration Axis | Accelerometer Locations |
|---|---|
| X | A & D |
| Y | B & D |
| Z | C & D |

Table 6 presents the vibration levels to which the electronic board was exposed to. The vibration level for random vibration was 12.9 Grms. Both the pre and post sine sweep vibration tests were performed between 20 and 2,000 Hz at 0.5 g's.

Table 6. Random Vibration Levels

| Frequency (Hz) | Level ($G^2$/Hz) |
|---|---|
| 20 | 0.025 |
| 50 | 0.15 |
| 600 | 0.15 |
| 2000 | 0.025 |

Accelerometer data plots for each accelerometer measurement is contained in appendix G for the qualification board and appendix H for the flight board.

Prior to the start of each axis (X, Y, and Z) vibration test and at the end of all vibration tests, electronic board performance measurements were manually recorded. Nominal and measured electronic board vibration performance values are tabulated in tables 7 and 8.

Table 7. Vibration Performance Measurements, Qualification Board

| | +5 v Current (μA) | +15 v Current (A) | High Voltage Test Point (v) | Manual Reset and Preset (y/n) | +5 v Noise Level at Supply (mv) | +15 v Noise Level at Supply (mv) |
|---|---|---|---|---|---|---|
| Nominal | 35 | 0.05 | 64.3 | yes | 20 | 30 |
| | | | | | | |
| Pre-Z | 35 | 0.05 | 64.3 | yes | 30 | 20 |
| Pre-X | 35 | 0.05 | 64.3 | yes | 25 | 30 |
| Pre-Y | 35 | 0.05 | 64.3 | yes | 30 | 35 |
| Post Vib | 35 | 0.05 | 64.3 | yes | 30 | 30 |

Table 8. Vibration Performance Measurements, Flight Board

| | +5 v Current (μA) | +15 v Current (A) | High Voltage Test Point (v) | Manual Reset and Preset (y/n) | +5 v Noise Level at Supply (mv) | +15 v Noise Level at Supply (mv) |
|---|---|---|---|---|---|---|
| Nominal | 35 | 0.05 | 64.2 | yes | 20 | 30 |
| | | | | | | |
| Pre-Z | 35 | 0.05 | 64.1 | yes | 20 | 30 |
| Pre-X | 35 | 0.05 | 64.1 | yes | 25 | 20 |
| Pre-Y | 35 | 0.05 | 64.2 | yes | 20 | 20 |
| Post Vib | 35 | 0.05 | 64.2 | yes | 20 | 20 |

Following completion of the vibration tests, QA/QC personnel from Jackson and Tull inspected the qualification and flight boards for any visible signs of material fatigue or failure. No signs of material fatigue or failure were found on either the qualification board or the flight board.

Electronic operation of both the qualification and flight electronic boards were nominal before and after each vibration test.

Examination of the sine sweep vibration accelerometer data revealed differences between the post and pre sine sweep vibration results in the Z axis for the qualification and flight board. Data associated with the vibration data differences is tabulated in tables 9 and 10. Based on the data tabulated in tables 9 and 10, the qualification board was selected to fly on the MightySat I spacecraft. The decision to fly the qualification board was based on the acceleration levels seen at accelereometer location D, Z axis, for the flight board.

Table 9. Vibration Data Differences, Qualification Board

| | | g Level at Accelerometer Location (g) | | Mathematical g Level Difference (pre-post) | |
|---|---|---|---|---|---|
| Axis | Frequency (Hz) | D (Channel 2) | A, B, or C (Channel 3) | D (Channel 2) | A, B, or C (Channel 3) |
| Z | 600 (pre-sine) | -- | 2.0 | -- | 1.8 |
| Z | 600 (post-sine) | -- | 0.2 | -- | |
| | | | | | |
| X | 590 (pre-sine) | -- | 0.0 | -- | -0.32 |
| X | 590 (post-sine) | -- | 0.32 | -- | |
| X | 1,000 (pre-sine) | -- | 0.1 | -- | -0.15 |
| X | 1,000 (post-sine) | -- | 0.32 | -- | |
| | | | | | |
| Y | 550 (pre-sine) | -- | 0.3 | -- | 0.1 |
| Y | 550 (post-sine) | -- | 0.2 | -- | |
| Y | 1,500 (pre-sine) | -- | 0.7 | -- | -1.1 |
| Y | 1,500 (post-sine) | -- | 1.8 | -- | |

Table 10. Vibration Data Differences, Flight Board

| | | g Level at Accelerometer Location (g) | | Mathematical g Level Difference (pre-post) | |
|---|---|---|---|---|---|
| Axis | Frequency (Hz) | D (Channel 2) | A, B, or C (Channel 3) | D (Channel 2) | A, B, or C (Channel 3) |
| Z | 200 (pre-sine) | 0.7 | 0.8 | -1.3 | -1.2 |
| Z | 200 (post-sine) | 2.0 | 2.0 | | |
| Z | 600 (pre-sine) | -- | 1.8 | -- | 1.45 |
| Z | 600 (post-sine) | -- | 0.35 | | |
| Z | 1,100 (pre-sine) | -- | 0.22 | -- | 0.1 |
| Z | 1,100 (post-sine) | -- | 0.12 | | |
| | | | | | |
| X | 550 (pre-sine) | -- | 0.35 | -- | -0.15 |
| X | 550 (post-sine) | -- | 0.5 | | |
| | | | | | |
| Y | 590 (pre-sine) | -- | 0.75 | -- | 0.2 |
| Y | 590 (post-sine) | -- | 0.55 | | |
| Y | 600 (pre-sine) | -- | 0.3 | -- | -0.1 |
| Y | 600 (post-sine) | -- | 0.4 | | |

4.2 Detector Assembly.

Detector assemblies number 2 and 3 underwent vibration testing using vibration recommendations found in 1992 Goddard SFC Hitchhiker Customer Accomodations and Requirements Specifications for payloads less than 50 lb (Ref. 14). Each detector assembly underwent vibration testing in the X, Y, and Z axes. In addition, each test axis underwent three vibration patterns in order: 1) pre-sine sweep; 2) random; and 3) post-sine sweep. The purpose of conducting the three vibration patterns in order was to allow comparison of the pre-sine sweep with the post-sine sweep to determine if the random vibration caused damage to the detector assembly. Ideally, the pre and post sine sweeps would be identical if no damage occured during the random vibration.

Note: The axis used for vibration testing of the detector holder assembly are not the same axis as the spacecraft axis. The axis used for vibration testing were used only for vibration testing.

Detector assembly vibration axis are shown in figure 27.

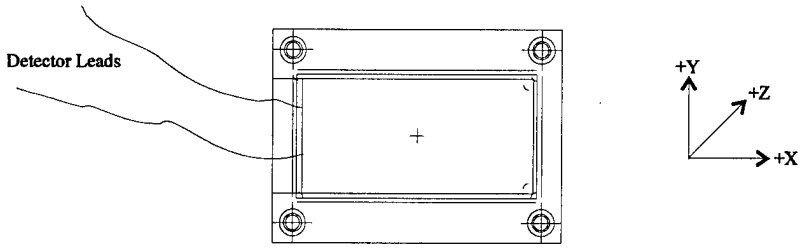


Figure 27. Detector Vibration Axis

Test parameters used for the sine sweep vibration tests were a 0.5 impulse over a frequency range of 20 to 2,000 Hz. Frequency ramp rate was 4 octaves per minute over the frequency range. Table 11 presents the random vibration test levels.

Table 11. Random Vibration Test Levels

| Frequency (Hz) | ASD Test Level ($G^2$/Hz) |
|---|---|
| 20 | 0.025 |
| 50 | 0.15 |
| 600 | 0.15 |
| 2000 | 0.025 |

Four #8-32 x 3/8 inch countersunk screws were used to fasten the detector to the vibration table interface plate. The mounting screws were tightened to a final 20 in-lb torque setting at 5 in-lb increments. After tightening each screw, a strip of kapton tape was placed over each detector screw to prevent fastener back-out during the vibration test. The two detector leads were attached to the vibration table interface plate using kapton tape.

The vibration table interface plate was instrumented with a PCB model 355A53 accelerometer and was used as the vibration control accelerometer. Two PCB model 352B22 accelerometers were mounted on the top edge of the detector assembly to gather data regarding the response of the detector assembly. Figure 28 shows the location of these three accelerometers. The two detector accelerometers were mounted to the detector assembly in the same location for all vibration tests and had a sensing axis in the Z direction only. This was due to the 1/8 inch thickness of the detector assembly. As a result, only the Z axis detector assembly vibration accelerometer data is included in this report. However, the vibration control accelerometer data is included in this report for the X, Y, and Z axes in appendixes I and J (Ref. 15).

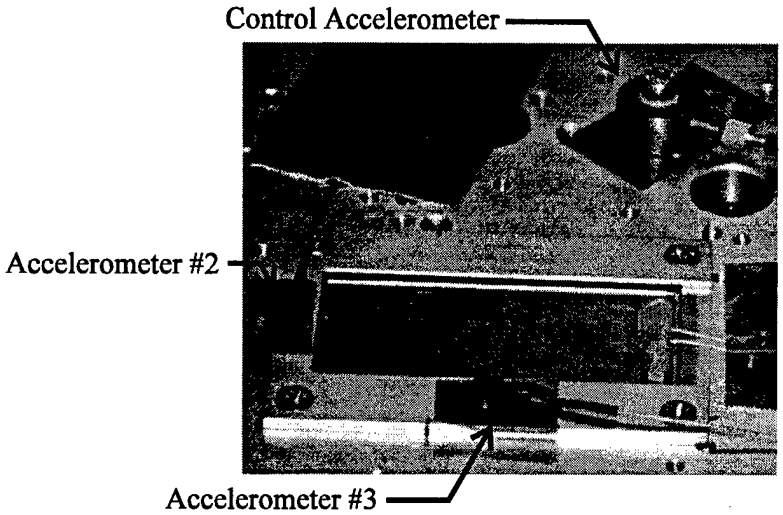


Figure 28. Detector Mounted To Vibration Table With Accelerometer Locations

Prior to and after each axis vibration test, capacitance and resistance measurements were taken for each detector assembly. Nominal and measured capacitance and resistance values are presented in tables 12 and 13.

Table 12. Vibration Capacitance and Resistance Measurements, Detector Number 2

| Vibration Axis | Pre/Post Test | Capacitance (ηF) | Impact Lead to Mounting Plate (open/short) | Bottom Lead to Mounting Plate (open/short) |
|---|---|---|---|---|
| Nominal | N/A | 78.8 | open | open |
| | | | | |
| Z | Pre | 78.8 | open | open |
| Z | Post | 79.0 | open | open |
| X | Pre | 78.8 | open | open |
| X | Post | 78.8 | open | open |
| Y | Pre | 78.9 | open | open |
| Y | Post | 78.9 | open | open |

Table 13. Vibration Capacitance and Resistance Measurements, Detector Number 3

| Vibration Axis | Pre/Post Test | Capacitance (ηF) | Impact Lead to Mounting Plate (open/short) | Bottom Lead to Mounting Plate (open/short) |
|---|---|---|---|---|
| Nominal | N/A | 76.7 | open | open |
| | | | | |
| Z | Pre | 65 - 69 | open | open |
| Z | Post | 64 - 69 | open | open |
| X | Pre | 64 - 67 | open | open |
| X | Post | 65 - 68 | open | open |
| Y | Pre | 65 - 68 | open | open |
| Y | Post | 65 - 69 | open | open |

4.3 Detector Number 3, Post Thermal and Vibration Tap Test.

After thermal and vibration testing for detector assembly number 3, a gentle tap test was conducted to confirm that this detector would respond to an impact. The circuit shown in figure 29 was used to bias the detector during the tap tests. After the detector's current reached approximately 5 ηA, a small eyeglass type screwdriver was used to gently tap detector number 3 several times to cause a detector discharge.

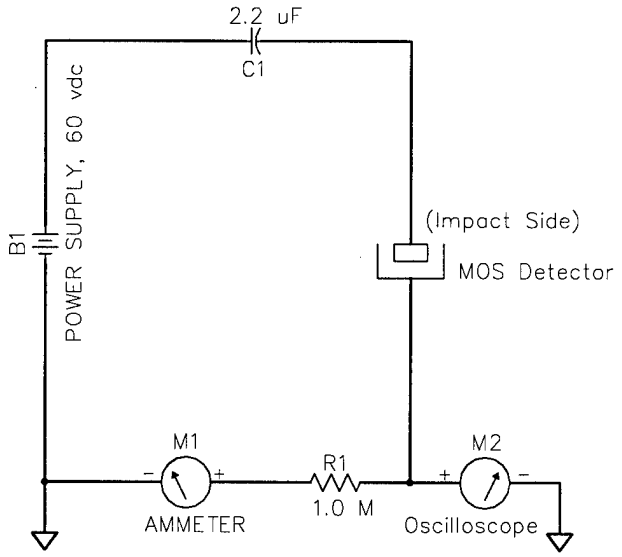


Figure 29. Detector Tap Test Bias Circuit

Although this type of tap test does not simulate an actual hypervelocity particle impact, it does however, provide some confidence that detector number 3 will respond to a hypervelocity particle impact.

After detector number 3 was biased and gently tapped several times with an eyeglass type screwdriver, capacitance measurements were taken every minute for 44 min. The resulting capacitance measurements are presented in figure 30. As seen in figure 30, capacitance measurement fluctuations for detector number 3, decreased after the detector was biased and discharged with a gentle tap.

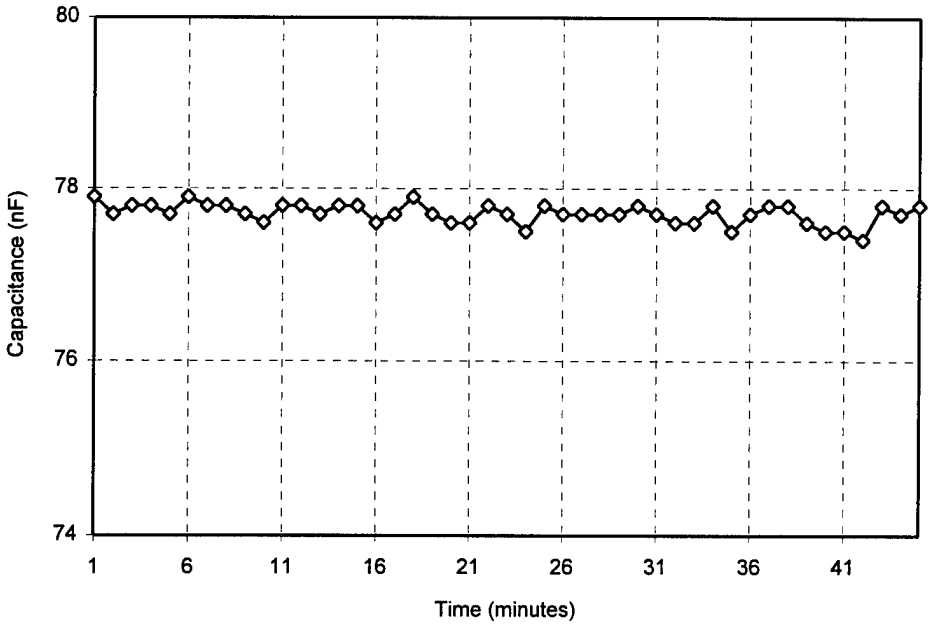


Figure 30. Capacitance Measurements After Bias and Discharge, Detector #3

## 5.0 ON-ORBIT OPERATIONS

Ground station operations of this experiment consists of powering the electronic board and dowlinking mailbox data once a week. The spacecraft impact mailbox is cleared once a week after data is downlinked. Enabling or dissembling power to the electronic board is the only command for this experiment. There are no other control commands for this experiment.

The downlink data format is 26 bytes (hexadecimal) long and is filled with some filler bytes. The first 4 bytes are header information (0C 0C 0C 0C) and identifies this mailbox as micro-particle impact data. The 5th byte indicates the cumulative number of impacts. The 6th and 7th bytes are course sun sensor readings, followed by an 8 byte time stamp (yr, mo, day, hr, min, sec, n1, n2). N1 and n2 are 1/224th and 1/255 of a second per count. The remaining 11 bytes are filler bytes (Ref. 16).

A sample data string follows:

0C0C0C0C 0CFFFF97 02142208 1ECE3400 00000000 00000000

where;

| | |
|---|---|
| 0C0C0C0C | = header information |
| 0C | = number of impacts |
| FFFF | = course sun sensor data |
| 97 | = year |
| 02 | = month |
| 14 | = day |
| 22 | = hour |
| 08 | = minutes |
| 1E | = seconds |
| CE | = 1/224th of a second per count |
| 34 | = 1/255th of a second per count |
| 00 | = filler byte |
| 00000000 | = filler bytes |
| 00000000 | = filler bytes |

## 6.0 CONCLUSION

This report presented the engineering design of a space borne micro-particle detector experiment. This experiment is manifested on a Air Force Research Laboratory spacecraft called MightySat I scheduled for launch in July 1998. Because this experiment had not yet flown at the time this report was prepared, particle impact data was unavailable. However, a follow-on report will present the resulting particle impact data. This report also presented thermal and vibration test data that was used to qualify this experiment for flight on the space shuttle.

## REFERENCES


1. Davis, R.J., Monahan, J.F., Itchkawich T.J., *"Mighty Sat I: Technology In Space For About A Nickel ($M)"*, American Institute of Aeronautics and Astronautics, Tenth Annual AIAA/USA Conference on Small Satellite, 16-19 Sep 96, Logan, Utah

2. Buchsbaum, W.H., *"Buchsbaum's Complete Handbook Of Practical Electronic Reference Data"*, Second Edition, 1978, Prentice-Hall, Inc., Englewood Cliffs, N.J., ISBN 0-13-084624-4, TK7825.B8 1978

3. Itchkawich T.J., et al, *"MightySat I Interface Control Document"*, ICD-SC-EXP-004, 23 Sep 96, CTA Space Systems, 1521 West Branch Dr, McLean, VA, 22102, 703-883-2684

4. Santiago, J.G., *"A Thermal Analysis Of The Micro-Particle Impact Detector (MPID)"*, Aerospace Technical Memorandum, ATM Number 97 (1212-02)-1, The Aerospace Corporation, P.O. Box 92957, Los Angeles, CA 90009-2957, 310-336-6707

5. Wortman J.J., Kassel P.C., *"Metal-Oxide-Silicon Capacitor Detectors for Measuring Micrometeoroid and Space Debris Flux"*, Journal of Spacecraft and Rockets, 1994, Electrical and Computer Engineering Department, North Carolina State University, Raleigh, NC 27695

6. Kassel P.C., *"Characteristics of Capacitor-Type Micrometeoroid Flux Detectors When Impacted With Simulated Micrometeoroids"*, Langley Research Center, National Aeronautics and Space Administration, Hampton, VA 23665, NASA TN D-7359

7. Dursch H.W., et.al., *"Evaluation of Adhesive Materials Used on the Long Duration Exposure Facility"*, Langley Research Center, National Aeronautics and Space Administration, NASA Report N95-22918, NASA-CR-4646, March 1995, Hampton, VA 23665

8. Itchkawich T.J., et al, *"Orbital Operations Handbook"*, MSAT-00H-001, 27 Dec 96, page 68, CTA Space Systems, 1521 West Branch Dr, McLean, VA, 22102, 703-883-2684

9. Neslen C.L., *"MPID Qualification Electronic Board Thermal Cycle Test Report"*, 29-30 Oct 96, Phillips Laboratory/SXE, Aerospace Engineering Facility, 3550 Aberdeen, Ave, SE, Kirtland AFB, NM 87117, Document Number 96-009-290-003

10. Neslen C.L., *"MPID Flight Electronic Board Thermal Cycle Test Report"*, 29-30 Oct 96, Phillips Laboratory/SXE, Aerospace Engineering Facility, 3550 Aberdeen, Ave, SE, Kirtland AFB, NM 87117, Document Number 96-009-290-002

11. Neslen C.L., *"MPID Program Detector Thermal Cycle Test, Test Report"*, 16-23 Dec 96, Phillips Laboratory/SXE, Aerospace Engineering Facility, 3550 Aberdeen, Ave, SE, Kirtland AFB, NM 87117, Document Number 97-009-290-006

12. Neslen C.L., "*MPID Flight Electronic Board Vibration Test Report*", 13 Nov 96, Phillips Laboratory/SXE, Aerospace Engineering Facility, 3550 Aberdeen, Ave, SE, Kirtland AFB, NM 87117, Document Number 96-009-290-004

13. Neslen C.L., "*MPID Qualification Electronic Board Vibration Test Report*", 12 Nov 96, Phillips Laboratory/SXE, Aerospace Engineering Facility, 3550 Aberdeen, Ave, SE, Kirtland AFB, NM 87117, Document Number 96-009-290-005

14. "*1992 Goddard SFC Hitchhiker Customer Accomodations and Requirements Specifications*", Document Number HHG-730-1503-06, Goddard Space Flight Center, Greenbelt, MD 20771

15. Neslen C.L., "*MPID Program Detector Vibration Test*", 8 Jan 97, Phillips Laboratory/SXE, Aerospace Engineering Facility, 3550 Aberdeen, Ave, SE, Kirtland AFB, NM 87117, Document Number 96-009-290-007

16. Itchkawich T.J., et al, "*Orbital Operations Handbook*", MSAT-00H-001, 27 Dec 96, page 171, CTA Space Systems, 1521 West Branch Dr, McLean, VA, 22102, 703-883-2684

# APPENDIX A

## Electronic Board Parts List

| Part | Value | Rating | Package | Manufacturer | Part # | Notes |
|---|---|---|---|---|---|---|
| R1 | 1.0M | 5%, 1/4 W | Axial | Dale | RLR07C1004FS | Carbon Film |
| R2 | 10k | 5%, 1/4 W | Axial | Dale | FLR07C1002FS | Carbon Film |
| R3 | 19.1K | 5%, 1/4 W | Axial | Dale | RLR07C1912FS | Carbon Film |
| R4 | 19.1k | 5%, 1/4 W | Axial | Dale | RLR07C1912FS | Carbon Film |
| R5 | 10k | 5%, 1/4 W | Axial | Dale | RLR07C1002FS | Carbon Film |
| R6 | 1.0M | 5%, 1/4 W | Axial | Dale | RLR07C1004FS | Carbon Film |
| R7 | 10k | 5%, 1/4 W | Axial | Dale | RLR07C1002FS | Carbon Film |
| R8 | 20k | 5%, 1/4 W | Axial | Dale | RLR07C2002GS | Carbon Film |
| R9 | 20k | 5%, 1/4 W | Axial | Dale | RLR07C2002FS | Carbon Film |
| R10 | 49.9k | 5%, 1/4 W | Axial | Dale | RLR07C4992FS | Carbon Film |
| R11 | 49.9k | 5%, 1/4 W | Axial | Dale | RLR07C4992FS | Carbon Film |
| R12 | 10M | 5%, 1/4 W | Axial | Dale | RLR07C1005FS | Carbon Film |
| R13 | 10M | 5%, 1/4 W | Axial | Dale | RLR07C1005FS | Carbon Film |
| C1 | 2.7µF | | Axial Leads 0.130" Dia, 0.335" L, 0.020" Leads | | M39003-01-3003J | Polarized Tantalum |
| C3 | 0.01µF | 100v | CK05 | Kemet | M39014-01-1575 | Ceramic |
| C4 | 2.7µF | | Axial Leads, 0.130" Dia, 0.335" L, 0.020" Leads | | M39003-01-3003J | Polarized Tantalum |
| C6 | 0.01µF | 100v | CK05 | Kemet | M39014-01-1575 | Ceramic |
| C7 | 0.1µF | 100v | CK05 | Kemet | M39014-02-1270 | Ceramic |
| C8 | 22.0µF | 75v | Axial Leads 0.325"Dia, 0.686"L, 0.025" Leads | Sprague | M39003-01-3138J | Polarized tantalum |

| Part | Value | Rating | Package | Manufacturer | Part # | Notes |
|---|---|---|---|---|---|---|
| C9 | 22.0µF | 75v | Axial | Sprague | M39006-22-6490 | Polarized tantalum |
| C10 | 10.0µF | 75v | Axial | Sprague | M39003-01-3138J | Polarized tantalum |
| C11 | 0.1µF | 75v | CK05 | Kemet | M39014-01-1575 | Ceramic |
| C12 | 0.1µF | 75v | CK05 | Kemet | M39014-02-1270 | Ceramic |
| C13 | 0.1µF | 75v | CK05 | Kemet | M39014-02-1270 | Ceramic |
| L1 | 100µH | | Axial Leads 0.162" Dia, 0.410"L, 0.025" Leads | Dale | IMS-5-100 | EM Shielded |
| D1 | 1N4148 | DO35 | Axial | | JANTX1N4148-1 | Signal Diode |
| D2 | 1N4148 | DO35 | Axial | | JANTX1N4148-1 | Signal Diode |
| D3 | 1N4148 | DO35 | Axial | | JANTX1N4148-1 | Signal Diode |
| D4 | 1N4148 | DO35 | Axial | | JANTX1N4148-1 | Signal Diode |
| D5 | 1N4148 | DO35 | Axial | | JANTX1N4148-1 | Signal Diode |
| D6 | 1N4148 | DO35 | Axial | | JANTX1N4148-1 | Signal Diode |
| D8 | 1N4148 | DO35 | Axial | | JANTX1N4148-1 | Signal Diode |
| D9 | 1N4148 | DO35 | Axial | | JANTX1N4148-1 | Signal Diode |

| Part | Value | Rating | Package | Manufacturer | Part # | Notes |
|---|---|---|---|---|---|---|
| U1 | | | | Interpoint | MCH2812D | +15vdc to ±12 vdc DC/DC Converter |
| U2 | | | | Interpoint | MCH2812D | +15vdc to ±12vdc DC/DC Converter |
| U3 | | | | Interpoint | MCH2812S | +15vdc to +12 vdc DC/DC Converter |
| U4 | 54HC74 | | 14-Pin Dip | Motorola | MC54HC74NJ | Dual D Flip-Flops |
| S1 | | | | Positronics | SND15F42B30T2G | 15 Pin Female D Subminiature |
| F1 | | 70v | Axial | Spectrum Control | M15733/64-0001 | Input Power Filter |
| F2 | | 70v | Axial | Spectrum Control | M15733/64-0001 | Input Power Filter |

# APPENDIX B

# DETECTOR ASSEMBLY STRESS CALCULATIONS

Force Relations for Bolt and Members:

Force on bolt:

$$F_b = \frac{k_b}{k_b + k_m} P + F_i \qquad \text{(B-1)}^*$$

Force on member:

$$F_m = \frac{k_m}{k_b + k_m} P - F_i \qquad \text{(B-2)}^*$$

where:

Stiffness of bolt:

$$k_b = \frac{A_t A_u E_b}{A_t l_u + A_u l_t} \qquad \text{(B-3)}$$

$A_t$ = threaded surface area
$A_u$ = unthreaded surface area
$l_t$ = threaded length of fasteners
$l_u$ = unthreaded fastener length
$E_b$ = modulus of elasticity

Stiffness of each member:

$$k_x = \frac{\pi E_x d \tan(x)}{\ln\left[\frac{(2t_x \tan x + D - d)(D + d)}{(2t_x \tan x + D + d)(D - d)}\right]} \qquad \text{(B-4)}$$

$E_x$ = modulus of elasticity
d = nominal fastener diameter
x = frustam apex angle (~30°)
D = contacting surface diameter
$t_x$ = thickness of each member
$k_x$ = stiffness of each memeber

* Discussed in section 2.3 of the main report text

Total stiffness of all fastened members :

$$k_m = \frac{1}{\sum_x 1/k_x} \qquad \text{(B-5)}$$

Numerical Calculations:

$A_t = \pi\, d_t\, l_t = \pi\,(0.164)\,(0.428)$

$\underline{A_t = 0.221\ in^2}$

$l_t = 0.428$ in

$A_u = \pi\,(r_1 l_1 - r_2 l_2) = \pi\,[(0.166 * 0.212) - (0.082 * 0.107)]$

$\underline{A_u = 0.086\ in^2}$

$l_u = 0.072$ in

$E_b = 27.6$ Mpsi

$$\therefore\ k_b = \frac{(0.221)(0.086)(27.6*10^6)}{(0.221)(0.072)+(0.086)(0.428)}$$

$\underline{k_b = 9.95 \times 10^6\ lb/in}$

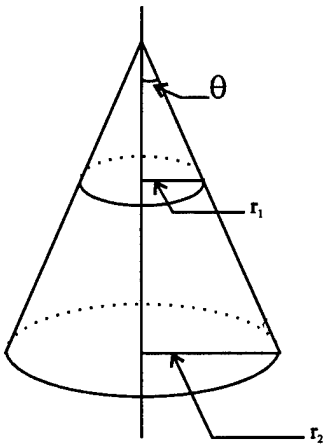


$r_1 = 0.166$ inches

$r_2 = 0.082$ inches

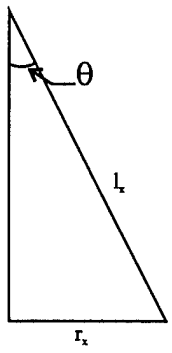


$\sin\theta_x = r_x / l_x$

$l_1 = r_1 / (\sin 50) = 0.212$

$l_2 = r_2 / (\sin 50) = 0.107$

$E_x = E_1 = E_2$ and $t_x = t_1 = t_2$

$\Rightarrow k_1 = k_2 = k_x$

$\therefore k_m = k_1 / k_2$ (B-6)

where:

$E_1 = 10.3$ Mpsi

$D = 0.332$ in

$d = 0.164$ in

$t_1 = 1/16$ in

$$k_m = \frac{\pi(10.3*10^6)(0.164)(\tan 30)}{2\ln\left[\frac{((2)(1/16)(\tan 30)+0.332-0.164)(0.332+0.164)}{((2)(1/16)(\tan 30)+0.332-0.164)(0.332-0.164)}\right]} \quad \text{(B-7)}$$

$\underline{k_m = 6.92 * 10^6 \text{ lb/in}}$

$T = k F_i d$ (B-8)

where:

T = preload torque
k = friction coefficent of fatener and members (~0.20)

$$F_i = \frac{T}{kd} = \frac{20}{(0.20)(0.164)}$$

$\underline{F_i = 609.8 \text{ lb}}$

$$P = 25\ g\ m_d \qquad \text{(B-9)}$$

where:

$g$ = gravitational acceleration
$m_d$ = mass of detector assembly (~0.0047 slugs)

$P = 25\ (32.2)\ (0.0047)$

$\underline{P = 3.78\ lb}$

$$F_b = \left(\frac{9.95}{9.95 + 6.92}\right) 3.78 + 609.8$$

$\underline{F_b = 612.0\ lb}$

$$F_m = \left(\frac{6.92}{9.95 + 6.92}\right) 3.78 + 609.8$$

$\underline{F_m = -608.2\ lb}$

$A_c = A_u = 0.086\ in^2$

$\therefore \sigma_b = (612.0) / [4\ (0.086)]$

$\underline{\sigma_b = 1779\ psi}$ $(\sigma_{yb} = 30\ kpsi)$

$\sigma_m = (-608.2) / [4\ (0.086)]$

$\underline{\sigma_m = -1768\ psi}$ $(\sigma_{yb} = 30\ kpsi)$

Form Approved
OMB No. 0704-0188

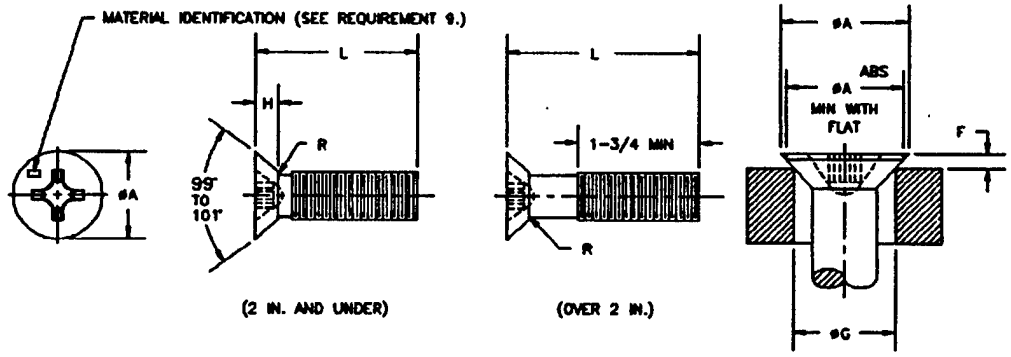


TABLE I

| THREAD SIZE | | .0600 (#0) | .0860 (#2) | .1120 (#4) | | .1380 (#6) | | .1640 (#8) | | .1900 (#10) | | .2500 | | .3125 | | .3750 | |
|---|---|---|---|---|---|---|---|---|---|---|---|---|---|---|---|---|---|
| THREADS PER INCH | | 80 UNF | 56 UNC | 40 UNC | 48 UNF | 32 UNC | 40 UNF | 32 UNC | 36 UNF | 24 UNC | 32 UNF | 20 UNC | 28 UNF | 18 UNC | 24 UNF | 16 UNC | 24 UNF |
| ØA HEAD DIAMETER | MAX SHARP | .119 | .172 | .225 | | .279 | | .332 | | .385 | | .507 | | .635 | | .762 | |
| | MIN SHARP | .104 | .156 | .207 | | .257 | | .308 | | .359 | | .477 | | .600 | | .722 | |
| | ABS. MIN | .096 | .143 | .191 | | .238 | | .285 | | .333 | | .442 | | .556 | | .670 | |
| F PROTRUSION ABOVE GAGING DIAMETER | MAX | .020 | .022 | .025 | | .028 | | .031 | | .034 | | .040 | | .047 | | .053 | |
| | MIN | .012 | .014 | .016 | | .017 | | .019 | | .021 | | .025 | | .030 | | .034 | |
| ØG GAGING DIAMETER | | .074 | .121 | .167 | | .214 | | .261 | | .307 | | .415 | | .528 | | .638 | |
| H HEAD HEIGHT | REF | .026 | .037 | .049 | | .060 | | .072 | | .083 | | .110 | | .136 | | .165 | |
| R FILLET RADIUS | MAX | .007 | .008 | .015 | | .015 | | .020 | | .020 | | .020 | | .025 | | .030 | |
| | MIN | .003 | .004 | .010 | | .010 | | .010 | | .010 | | .010 | | .010 | | .015 | |

REQUIREMENTS:

1. MATERIAL:
ALUMINUM ALLOY PER QQ-A-225/6, BRASS PER ASTM B16, ASTM B36, ASTM B134 OR ASTM B206, COPPER-SILICON ALLOY PER ASTM B98 OR ASTM B99, UNS C65100, UNS C65500 OR UNS C66100, NICKLE-COPPER ALLOY PER QQ-N-281, TYPE A (UNS N04400), CARBON STEEL PER FED-STD-66, CORROSION RESISTANT STEEL PER FED-STD-66, COMPOSITION 302, 303, 304, 305 OR 316 OR EQUAL TO OR INTERCHANGEABLE WITH 16-18 OR 18-8 CHROMIUM-NICKLE ALLOY STEEL (DEVELOPED FOR COLD HEADING).

2. PROTECTIVE COATING, PLATING OR TREATMENT:
ANODIZE IN ACCORDANCE WITH MIL-A-8625, TYPE I OR II, CLASS 1. BLACK CHEMICAL FINISH IN ACCORDANCE WITH MIL-F-495. BLACK OXIDE COATING IN ACCORDANCE WITH MIL-C-13924. CADMIUM PLATE IN ACCORDANCE WITH QQ-P-416, TYPE II, CLASS 3. NICKLE PLATE IN ACCORDANCE WITH QQ-N-290, CLASS 1, GRADE E. CLEAN AND DESCALE IN ACCORDANCE WITH ASTM A380.

3. MAGNETIC PERMEABILITY:
CORROSION RESISTANT STEEL SCREWS SHALL HAVE A MAGNETIC PERMEABILITY IN ACCORDANCE WITH THE PROCUREMENT SPECIFICATION.

4. HEAT TREATMENT:
ALUMINUM ALLOY SCREWS, 62 KSI MINIMUM ULTIMATE TENSILE STRENGTH IN ACCORDANCE WITH MIL-H-6088.

5. RECESS:
THE RECESS SHALL BE IN ACCORDANCE WITH MS9006.

6. THREADS:
THREADS SHALL BE CLASS 2A IN ACCORDANCE WITH FED-STD-H28/2. ACCEPTABILITY OF SCREW THREADS SHALL BE IN ACCORDANCE WITH FED-STD-H28/20, SYSTEM 21.

7. THREAD LENGTH:
FOR SCREWS UP TO AND INCLUDING 2.000 INCHES IN LENGTH, THE COMPLETE THREADS SHALL EXTEND TO WITHIN TWO (2) THREADS OF THE BEARING SURFACE OF THE HEAD, OR CLOSER IF PRACTICABLE. SCREWS OF LONGER LENGTH SHALL HAVE A MINIMUM COMPLETE THREAD LENGTH OF 1.750 INCHES.

(K) DENOTES CHANGE(S)

INCH-POUND

| | | |
|---|---|---|
| PREPARING ACTIVITY: IS<br>CUSTODIANS: ARMY- AR NAVY- AS<br>AIR FORCE- 99<br>REVIEW: AT, AV, EA, MC, ME, MI, NS, SH<br>USER:<br>PROJECT NUMBER: 5305-2079 | MILITARY SPECIFICATION SHEET<br>TITLE<br>SCREW, MACHINE, FLAT COUNTERSUNK HEAD, 100°, CROSS RECESSED, UNC-2A AND UNF-2A | SPECIFICATION SHEET NUMBER<br>MS24693 28 MAR 95<br>REV K<br>SUPERSEDING MS24693J 14 FEB 95 AND AN501 21 APR 67<br>AMSC- N/A FSC 5305 |
| DISTRIBUTION STATEMENT<br>A. Approved for public release; distribution is unlimited. | | Page 1 of 5 |

DD Form 672, MAY 88 PREVIOUS EDITIONS ARE OBSOLETE

# APPENDIX C

## Detector Mounting Procedure

Procedure for Attaching MPID Sensor to Mounting Plate:

NOTE: Before handling sensor, review information on handling procedures.
Before using Dow Corning 93-500 RTV review technical data sheet and MSDS.

1. Prior to beginning bonding procedure, perform resistance check of sensor. Cut 1.6 x 3.1 inch polyethylene sheet and line recess in detector tray. Place detector on top of polyethylene sheet. Check with meter between each lead and the detector tray. The reading should be "Open". This check will be repeated (with the adhesive in place instead of the polyethylene) once the detector is placed in the tray and the final vacuum outgassing is done prior to initial 2 hour cure.

2. Preheat oven to 150 °F, ±5 °F. Allow oven temperature to stabilize overnight. Install leveling tray, and adjust using a precision level. This will prevent an uneven adhesive layer from forming or the detector from moving in the holder recess during the curing process.

3. To prevent contamination of Dow Corning RTV 93-500 all tools which may come in contact with adhesive or surfaces where adhesive will be placed must be cleaned with acetone prior to use. (Sterile packaged syringes are an exception) Clean all surfaces to be bonded with Acetone, blow dry with dry Nitrogen at 5 psi. An exception is the sensor itself which can only be cleaned with dry nitrogen. Of particular concern is latex contamination, use only cotton gloves when handling tools and parts, and once they have been acetone cleaned, never touch any surface which will contact the adhesive.

4. Mix Dow Corning 93-500 Space Grade Encapsulant 10 parts Base to 1 part Curing Agent by Weight in a cleaned aluminum mixing cup. Prior to cleaning the cup, crimp the edge to form a pouring spout. 93-500 Base can be poured from its container into the mixing cup, and appropriate amount being approximately 5-6 grams. As the Curing Agent represents only one-tenth of the weight of the Base, more precision is necessary. Draw Curing Agent from the container with a sterile syringe with 22 bore needle, set the scale to reflect the appropriate weight. Too much or too little curing Agent can contribute o an improper cure or inaccurate curing times. Discard this syringe after emptying excess Curing Agent back into container.

5. Place mixing cup in bell jar and degas as follows: When gauge pressure begins to fall, wait until it is approximately 1200 microns and shut valve. 93-500 should be foaming at this point. Wait until all, or nearly all bubbles have disappeared and bring back up to atmosphere. This should take no more than 2-3 minutes. Do not expose the 93-500 to vacuum for extended periods prior to curing or to higher vacuum than given, this can interfere with the curing rate.

6. Load 93-500 into syringe by pouring into a sterile syringe. This will both lessen the chance of contamination by and decrease the amount of entrapped air.

7. Apply to detector holder recess in a thin layer by moving the nozzle of the syringe over the surface. One half CC is sufficient to form a layer which, when cured, will be 0.007 to 0.009 inches in thickness beneath the detector. Apply 93-500 to a cleaned glass slide to serve as a control sample. Cap the syringe and set it aside.

8. Repeat the degassing procedure listed in Step 5 for both the detector holder and control sample. There will be fewer bubbles than during the initial degassing procedure.

9. Place the detector holder and control sample in the oven on the leveling tray for 15 minutes at 150 °F. Brief exposure to heat (150 °F) at this point will not appreciably accelerate the cure, it will thin the 93-500 and produce a more level layer in the tray.

10. Remove the detector tray and mount the detector, placing it full surface on the area covered by the 93-500. Move it slightly using the leads to drive out as much trapped air as possible. Handle detector only by the edges at the corners with plastic tweezers. Do not contact the upper surface of the detector with anything, and insofar as possible, minimize contact with any part of the detector.

11. Degas the detector and control sample by following the procedure in Step 5. Air trapped under detector will not be visible. After three minutes, let the bell jar back up to atmosphere relatively quickly. Tests with transparent samples have shown that nearly all bubbles under the detector will disappear at this point. Any remaining will be small and low pressure.

12. Place the detector holder and detector on the leveling tray and bolt it down, using moderate but even torque on the corner screws.

13. Place the assembly in the oven at 150 °F until desired tackiness of 93-500 is achieved. This will be judged by the control sample. This will require 2 hours. The remaining 93-500 in the syringe should stay at room temperature.

14. Cut the point off a 22 Bore needle, making sure it has as close to a circular opening as possible, and attach this to the syringe. Elevate the tip of the syringe and squeeze out the air trapped inside, if this is not done, air at 1 ATM may be entrapped in the covering bead applied to the edges of the detector.

15. Remove the leveling tray and control sample. Add beads of 93-500 to the control sample, removing any remaining air in the syringe. Use 93-500 in syringe to apply a thin bead around the edge of the detector and to fill and gaps between the sides and the detector. The 93-500 is slightly tacky at this point, and "glue strings" can be formed when the syringe is lifted away from the point of application. Never move the syringe across the detector, always away from it when it is being lifted. In this manner, if a "glue string" forms, it will be on the tray. With caution, the syringe may be lifted cleanly.

16. Return leveling tray and control sample to oven and cure for an additional two hours at 150 °F. At the end of this time period, turn off oven and let cool overnight with door shut and detector and sample inside.

CATEGORY: ADHESIVE
TYPE: Silicone

IDENTIFICATION: DC 93-500

DESCRIPTION: This product is colorless to a light straw color and it is transparent.

APPLICATION: Used as a solar cell and a cover glass adhesive. It is frequently used for encapsulation (potting) and conformal coating.

MANUFACTURER: Dow Corning Corporation
Midland, MI 48640

TREATMENT:
Mix ratio: 10 parts by weight A/1 part B by weight
Cure: Room temperature for 24 hours allows handling
Room temperature for 7 days for a full cure

OUTGASSING: (GSFC No. 10158)
TML = 0.20%
CVCM = 0.02%

PROPERTIES: (Dow Corning Data Form No. 10-102-82)

| | |
|---|---|
| Hardness, Shore A | |
| Service temperature range, °C (°F) | -65 to 200 (-85 to 392) |
| Specific gravity | 1.08 |
| Brittle Point, °C (°F) | -65 (-85) |
| Shelf life, months | 6 |
| Tensile strength, MPa ($lb/in^2$) | 5.5 (790) |
| Elongation, % | 110 |
| Pot life, hours | ~ 1 |

PRECAUTIONS:
* The curing of this product can be inhibited by materials such as plasticizers, other silicones, organic sulfur, nitrogen containing compounds, various rubbers, and tapes.

* The cleanliness of the contracting surface is of prime importance.

NOTES:
* Substrate surfaces must be primed.

* Shelf life is based on shipping date.

* Glass Transition Temperature = -108 °C.

# APPENDIX D

## BASIC Source Code For Monitoring of Electronic Board Output Line

```
REM data port lpt1:3BC, lpt2:378, lpt3:278
REM status ports lpt1:3BD, lpt2:379, lpt3:279
REM control ports lpt1:3BE, lpt2:27A, lpt3:27A
REM
REM use 378 for lap top
REM use 3BC for p.c.
REM
REM select => pin 13; bit 4
REM pe => pin 12; bit 5
REM
REM 88D = 58H = 0101 1000
REM 72D = 48H = 0100 1000
REM
REM reset => pin 4;      preset => pin 3
REM use lower case for instructions
REM
intcon# = 1583#
startt# = 60#
jinter# = startt# * intcon#
usernum% = 5
WHILE usernum% <= 10
CLS
PRINT
PRINT
PRINT
PRINT "SELECT An Option:"
PRINT "  1) Create a new data file"
PRINT "  2) Collect data and append to data file"
PRINT "  3) Display data"
PRINT "  4) Print data"
PRINT "  5) Change Interval"
PRINT "  6) Exit"
PRINT
INPUT "Enter 1, 2, 3, 4, 5, or 6: ", num%
PRINT
SELECT CASE num%
CASE 1
   CLS
   FOR i% = 1 TO 5
     PRINT
   NEXT i%
   INPUT "Enter new file name:   ", filename$
   OPEN filename$ FOR OUTPUT AS #1
   INPUT "Enter date  ", today$
   INPUT "Enter time  ", xtime$
```

```
    PRINT "Interval time is:  "; startt#; " (sec)", "Interval:"; jinter#
    PRINT #1, filename$, today$, xtime$, startt#; " (sec)", jinter#
    PRINT #1, "  "
    INPUT "Enter any key to continue"; temp$
    CLOSE #1
CASE 2
    CLS
    FOR i% = 1 TO 5
      PRINT
    NEXT i%
    INPUT "Enter file name to append data to:   ", filename$
    OPEN filename$ FOR APPEND AS #1
    INPUT "Enter date  ", today$
    INPUT "Enter time  ", atime$
    PRINT #1, filename$, today$, atime$, startt#, jinter#
    INPUT "Enter total time for data taking (mins)  ", rtime%
    timex% = (60 / startt#) * rtime%
    j = 0
    inter# = jinter#
    WHILE timex% <> 0
     timex% = timex% - 1
      FOR i# = 1 TO inter#
       j = j + 0
      NEXT i#
     status% = INP(&H379)
     PRINT #1, timex%; "     "; status%, DATE$, TIME$
     PRINT timex%; "     "; status%, DATE$, TIME$
    WEND
    INPUT "Press any key to continue:  "; temp
    PRINT #1, "  "
    CLOSE #1
CASE 3
    CLS
    FOR i% = 1 TO 5
      PRINT
    NEXT i%
    INPUT "Enter file name to display data:   ", filename$
    OPEN filename$ FOR INPUT AS #1
    INPUT #1, filename$, today$, timey$, astar#, ajinte#
    PRINT filename$, today$, timey$, astar#, ajinte#
    DO WHILE (NOT EOF(1))
      INPUT #1, cntr%, stat%, bdate$, btime$
      PRINT cntr%, stat%, bdate$, btime$
    LOOP
    INPUT "Press any key to continue:  "; temp$
```

```
    CLOSE #1
 CASE 4
    CLS
    FOR i% = 1 TO 5
      PRINT
    NEXT i%
    INPUT "Enter file name to print data   ", filename$
    OPEN filename$ FOR INPUT AS #1
    INPUT #1, filename$, today$, timer$, bstart#, bjinte#
    LPRINT filename$, today$, timer$, bstart#, bjinte#
    DO WHILE (NOT EOF(1))
      INPUT #1, cntr%, stat%, cdate$, ctime$
      LPRINT cntr%, stat%, cdate$, ctime$
    LOOP
    CLOSE #1
 CASE 5
    CLS
    FOR i% = 1 TO 5
      PRINT
    NEXT i%
    PRINT "The current interval setting is:  "; startt#; " (sec)"
    INPUT "Enter new interval setting (sec):   "; startt#
    jinter# = startt# * intcon#
 CASE 6
    CLS
    FOR i% = 1 TO 5
      PRINT
    NEXT i%
    PRINT "Program stopped"
    STOP
 END SELECT
 WEND
```

# APPENDIX E

## Thermal Analysis of MPID

## Conducted by

The Aerospace Corporation
Attn: J.G. Santiago (310-336-6707)
P.O. Box 92957
Los Angeles, CA 90009-2957

THE AEROSPACE CORPORATION

ALWAYS SEND ONE COPY TO THE LIBRARY

AEROSPACE TECHNICAL MEMORANDUM

ATM NO.: 97(1212-02)-1

TO: R. J. Davis

FROM: Spacecraft Thermal Dept.

TITLE: A Thermal Analysis of the Micro-Particle Impact Detector (MPID)

DATE: 9 December 1996

AUTHOR(S): J. G. Santiago

DIVISION: Vehicle Systems Division

FILING SUBJECT(S): 97.5445.44-16

CCC: 5445

PROJECT OR PROGRAM: MightySat I

PAGES: 9


ABSTRACT/SUMMARY

A thermal analysis of the Micro-particle impact detector (MPID) experiment is presented. This experiment, which is to be flown on the MightySat I spacecraft, detects micro-meteoroid impacts by measuring impact force. The present analysis calculates a worst-case, maximum expected on-orbit temperature for MPID. To this end, a geometric math model of the spacecraft, a thermal math model of the spacecraft, and a heat balance calculation on MPID was used. In addition, the report presents measurements of the MPID's optical properties. The MPID is expected to have a strong conductive coupling to the bottom shelf and the MPID-to-bottom shelf temperature difference is unlikely to be significant. That is, the temperature of the MPID is driven by the temperature of the satellite. The estimated worst-case temperature of MPID was 52 °C.



Prepared by:

Juan G. Santiago, Senior MTS
Satellite Heat Transfer Section
Spacecraft Thermal Department

Approved by:

Tung T. Lam, Manager
Satellite Heat Transfer Section
Spacecraft Thermal Department


**DISTRIBUTION:**
M. Bello
R. F. Johnson
D. G. Gilmore

## Introduction

This report presents a thermal analysis of the Micro-particle impact detector (MPID) experiment to be flown on the MightySat I spacecraft. MPID detects micro-meteoroid impacts by measuring impact force with an electronic plate lined with a piezoelectric array. MPID consists of a roughly palm-sized, thin metallic plate (with a piezoelectric element), a retaining cover, and a frame attached to the "bottom shelf" of MightySat.

The thermal analysis presented here calculates the maximum expected, on-orbit temperature of MPID. The method of the analysis consists of a geometric math model (GMM) used to calculate heat fluxes incident on MightySat I, a thermal math model (TMM) used to calculate on-orbit spacecraft component temperatures and internal heat transfer rates, and a heat balance calculation on MPID. The following sections describe these phases of the analysis as well as relevant assumptions. A discussion of the results is then presented.

## Geometric Math Model of MightySat I

A GMM of MightySat I developed by the Spacecraft Thermal Department (Gilmore, 1996) was used here. Figure 1 shows an illustration of the GMM model which uses 13 surfaces to model the exterior surfaces of MightySat I. Since the present analysis is concerned with a worst-case maximum temperature of MPID, a sun angle (i.e., a Beta angle) of 90° was assumed so that the spacecraft was exposed to sunlight at all times. Furthermore, as a worst-case condition, the spacecraft was assumed to have an inertial attitude which kept the bottom shelf pointed toward the sun at all times. The incident heat fluxes due to the solar flux, earth emission, and earth albedo were calculated using Aerospace's ATRIUM code. Since the assumed attitude and Beta angle result in constant values for all three environmental fluxes, a relatively large orbit increment of 30° was used to obtain obit-average fluxes. The Monte-Carlo calculations were achieved using 5000 emitted rays per surface.

As an extension of the GMM, the author created a program which re-arranges ATRIUM's output into a list of 30 heat-flux tables that correspond to 30 nodes on the TMM and can be read by SINDA. This extension facilitates parametric investigations of the effect of attitude and Beta angle on spacecraft component temperatures.

## Thermal Math Model of MightySat I

As in the case of the GMM, a previously developed TMM of MightySat I (Gilmore, 1996) was used here. This TMM was developed to predict on-orbit temperatures of the spacecraft's battery pack but was well suited to the present effort. The TMM uses over 216

nodes to model the MightySat I's composite structure, exterior panels, the three shelves within the spacecraft, and various spacecraft components including the battery pack, antennas, transmitter, receiver, card cages, and SMARD devices. The TMM models both conductive heat transfer and radiative heat transfer within the spacecraft. Again, this model was slightly modified for the current effort. In addition, as a worst-case condition, a constant battery heater power of 6 W was assumed. Also note that the present analysis assumes that the environmental heat absorbed by the bottom deck (without the MPID) was assumed to be the same as the heat absorbed by the bottom deck/MPID assembly. This assumption is reasonable because the exterior surface area of MPID is only about 2% of the area of the bottom deck.

Selected calculated component temperatures given the calculated environmental heat fluxes are presented in Table 1.

Table 1: Selected Calculated Component Temperatures

| *Spacecraft Component* | *Calculated Temperature for 90° Beta (°C)* |
|---|---|
| Top Shelf | -49 |
| Middle Shelf | -14 |
| Battery Pack | 39 |
| Bottom Shelf | 51 |
| Marmon ring | 51 |

The overall temperature gradient across the length of the spacecraft from the shade side (top shelf) to the spacecraft's Marmon ring (on the bottom shelf) for this assumed, worst-case condition attitude and Beta angle is approximately 100 °C. Also, note that temperature difference between the bottom shelf and the middle shelf (65 °C) is much greater than the temperature difference between the middle shelf and the top shelf (35 °C). This is due to the highly non-linear temperature dependence of the thermal heat radiated by the sides of the spacecraft.

For the present analysis, the parameter of importance is the calculated temperature of the bottom shelf (51 °C) to which the MPID is attached and which has a much higher thermal mass than the MPID.

Measurements of MPID Plate Surface Properties

An accurate estimate of the maximum expected MPID temperature requires knowledge of the component's surface properties (particular the highly specular sun-facing, exterior surface). Consequently, a prototype of the MPID assembly was obtained (Davis, 1996) and used to measure the exterior surface properties of the MPID plate.

These room-temperature surfaces property measurements were assumed to be valid for on-obit temperature predictions.

A solar spectrum reflectometer manufactured by Devices and Services Co. was used to measure the solar reflectivity of the exterior surface of the prototype at room temperature. This device illuminates the sample using a tungsten-halogen lamp and measures the intensity of reflected light using four detectors tuned to four spectral ranges. As per the recommendation of the manufacturer, the device was calibrated using both a blackbody cavity and a specular surface standard. The measured solar reflectivity was 0.76 (accordingly, the solar absorptivity measurement is 0.24). The manufacturer lists the precision of the device as approximately ±0.02% of the reflectivity measurement (Devices and Services Co., 1982). The resolution and repeatability of the measurements were observed by the author to be within about ±0.005 reflectivity units.

Next, an Emissometer Model AE also manufactured by Devices and Services Co. was used to measure the infra-red emissivity of the exterior surface of the prototype at room temperature. The emissometer makes a thermal measurement of emissivity using a detector head (heated to 180 °F) which houses a differential thermopile with low and high emittance sensors. The sample and standards are kept at room temperature during measurements and calibrations, respectively, by mounting them on a fin-cooled heat sink. A few drops of water were used to provide good thermal contact between the prototype/sample and the heat sink. The device was properly calibrated and the measured infra-red emissivity of the prototype's exterior surface was 0.10. The manufacturer lists the precision of the device as approximately ±0.01 emissivity units (Devices and Services Co., 1984). However, note that the measurements performed by the author were slightly off-design. That is, since the sample was large enough to cover only about 9/10th of the detector head, small strips of material were used around the edges of the detector head in order to form a complete enclosure. The edge effects produced by such substitutions was assumed to be negligible. This assumption was verified by using both high and low emissivity surfaces to complete the enclosure. In fact, the measured emissivity varied only to within ±0.01 emissivity units for edge materials with emissivities ranging from 0.05 to 0.9 emissivity units. For an edge material of emissivity similar to that of the sample, the resolution and repeatability of the emissivity measurements were within about ±0.01 emissivity units.

MPID Heat Balance

The MPID aluminum plate is adhered to an aluminum frame by a one micron layer of Dow Corning 93-500 Space Encapsulant as shown in Figure 2. The plate has a detector

area of about 4.1 by 8.1 cm and is roughly 0.5 mm thick. The frame area is 9.2 by 6.6 cm and roughly 1.1 mm thick with a recessed portion to which the plate is adhered that is milled to about the depth of the plate. An aluminum retaining cover serves as a mechanical fastener. The thin encapsulant layer results in a rather large MPID plate-to-frame conduction coupling of about 400 W/°C. In series with this conduction coupling, the MPID's frame is attached to the bottom shelf using four #8 bolts (0.16 inch diameter) torqued to 18 in-lb. Note that the maximum recommended torque for these bolts is 19.8 in-lb (Marks et al., 1987).

The MPID temperature was determined using a simple, steady-state heat balance calculation. The input and output heat rates on MPID can be expressed as follows:

$$q_s - q_e - q_{rad} - q_{cond} = 0 \qquad (1)$$

where $q_s$ = absorbed solar radiation (W)

$q_e$ = thermal radiation emitted by MPID to space (W)

$q_{rad}$ = net heat rate from the MPID's back surface to the bottom shelf (W)

$q_{cond}$ = heat conduction from MPID to the bottom shelf (W)

Equation (1) can be re-written as follows:

$$\alpha S A_p - \varepsilon \sigma T_{MPID}^4 A_p = 4C_b(T_{MPID} - T_{S/C}) + \varepsilon_{eff}\sigma(T_{MPID}^4 - T_{S/C}^4)A_p \qquad (2)$$

where

$\varepsilon$ = infra-red emissivity of the MPID outer surface (measured)

$\varepsilon_{eff}$ = effective emissivity of MPID/bottom shelf enclosure (assumed to equal 0.5)

$\alpha$ = solar absorptivity of the MPID outer surface (measured)

$T_{MPID}$ = temperature of MPID

$T_{S/C}$ = temperature of spacecraft (calculated using TMM and GMM models)

$A_p$ = outer (or inner) surface area of MPID (measured)

$S$ = solar flux (assumed to be 1400 W/m$^2$)

$C_b$ = conductance of each bolted joint (assumed to be 0.3 W/°C)

$\sigma$ = Boltzman's constant

The terms on the left-hand side of Eq. (2) represent the radiative heat transfer at the exterior surface and the terms on the right-hand side represent the heat transfer at the MPID-to-

bottom shelf interface. Given the expected contact conductance of the bolted joints, the problem is weakly dependent on the assumption for $\varepsilon_{eff}$. Also, note that the bottom shelf is able to absorb the heat of MPID with negligible bottom shelf, in-plane temperature gradients.

The key parameter in the problem is the magnitude of the conduction coupling between MPID plate and the bottom shelf. The conductance of bolted joints in a vacuum is difficult to characterize and empirically derived guidelines are commonly used. For example, the TRW design guideline for individual, #8 bolted joints of "small stiff surfaces" is 0.8 W/°C (Gilmore, 1994). On the other hand, Bratkovich (1991) suggests that the main parameter in such joints is the surface roughness of the bolted surfaces and lists values between 2.6 and 0.4 W/°C for surfaces roughness characterized by elements between 8 to 50 microinches (for #8 bolts and plates between 0.125 and 0.5 inches). Despite the difference in approaches and the scatter in experimental data of such studies, it is encouraging that the recommended conduction couplings for the bolted joints investigated here are all in the same order of magnitude! Therefore, the present analysis will assume a worst-case conductance of about 0.3 W/°C. This conservative assumption corresponds to a contact conductance coefficient between the frame and the bottom shelf of approximately 200 W/m$^2$-°C (35 Btu/hr-ft$^2$-°F).

Given the parameters described above, the measured MPID surface properties, an assumed effective emissivity between the bottom shelf and MPID of 0.5, a bottom shelf temperature of 51 °C, and geometry, the calculated MPID temperature was 51.7 °C. The heat rates are:

$q_s = 1.1$ W
$q_e = 0.21$ W
$q_{rad} = 0.00$ W
$q_{cond} = 0.89$ W

Note that the actual, on-orbit frame-to-bottom shelf conduction coupling would have to be 19 times lower than the worst-case value assumed here (0.3 W/°C per bolt) before the calculated MPID-to-bottom shelf temperature difference exceeds 10 °C. Such an error is unlikely. Further, given a conduction coupling on the order of 0.3 W/°C, the radiative coupling between the MPID and the bottom deck is negligible. Also, slots machined in the retaining cover prevent the cover from pressing down on the MPID plate (in fact, the cover will probably not touch the plate). Therefore, the plate has a poor conduction coupling to the retaining cover and heat transfer between these components was assumed negligible.

Conclusion and Recommendation

In brief, the MPID is expected to have a strong conductive coupling to the bottom shelf and the MPID-to-bottom shelf temperature difference is unlikely to be significant. The temperature of the MPID is driven by the temperature of the bottom shelf of the spacecraft. Consequently, the major source of error in the present analysis is probably the calculation of the expected, on-orbit temperature of the bottom shelf. In order to account for such errors, the MPID should be thermal vacuum tested to about 63 °C (about 11 °C higher than the maximum estimated temperature as a design margin).

References

Bratkovich, T. F. (1991), "Correlation for Contact Region Bolted Joint Conductance in Vacuum," The Aerospace Corporation, ATM No. 91(9975)-15, 10 April, 1991.

Davis, Robert (1996), Personal and written communication.

Gilmore, David (1996), Personal and written communication.

Gilmore, D. (1994), Satellite Thermal Control Handbook, The Aeropace Corporation Press, El Segundo, California.

Devices and Services Co. (1982), Technical Note 82-1, Solar Spectrum Reflectometer Operating Manual.

Devices and Services Co. (1984), Technical Note 84-3, Emissometer Model AE Operating Manual.

Marks, L. S., Baumeister, T., and Avallone, E. A. (1987), Mark's Handbook for Mechanical Engineers, McGraw-Hill Book Co, New York.

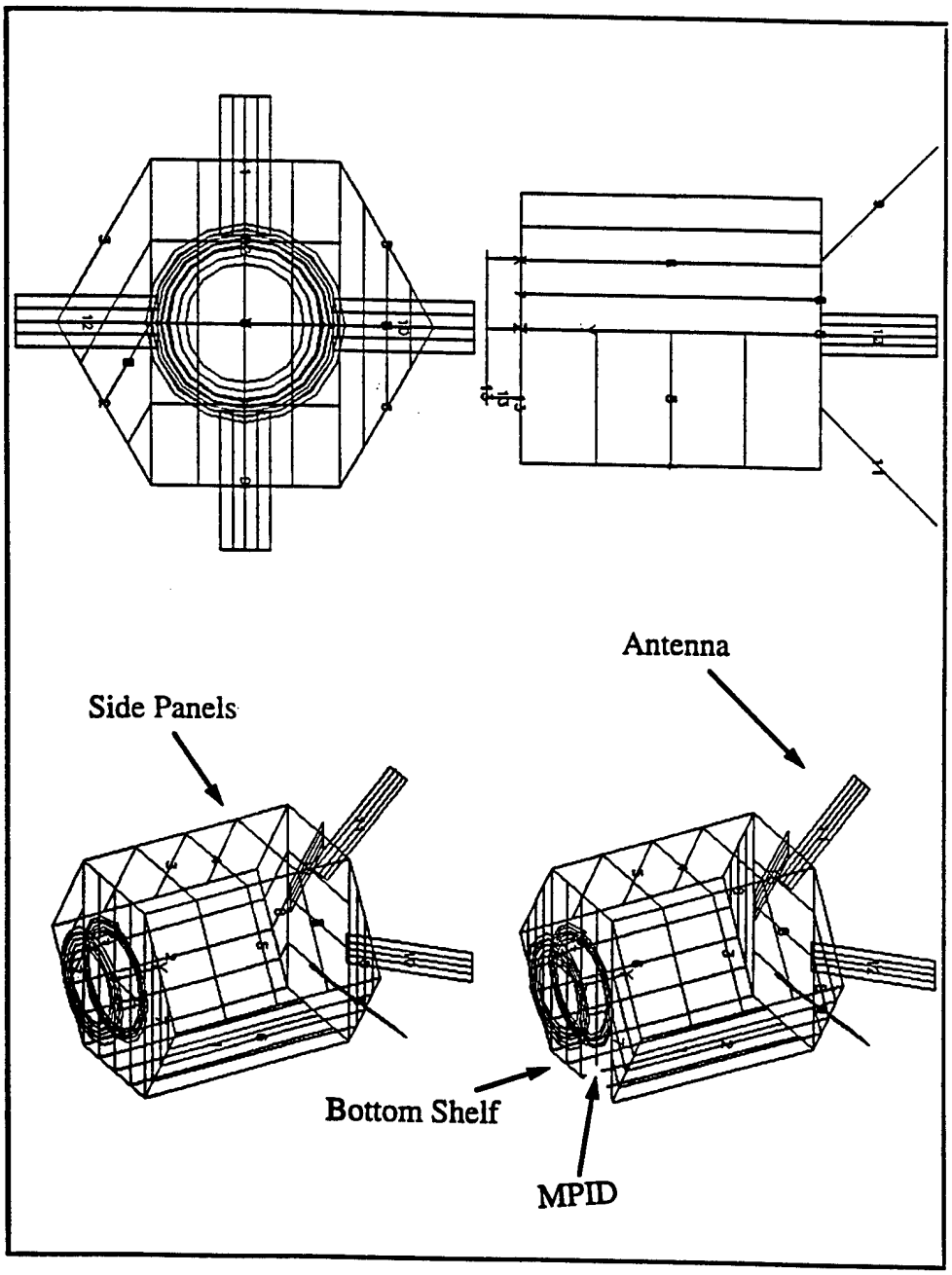


Figure 1: Geometric math model of MightySat I spacecraft

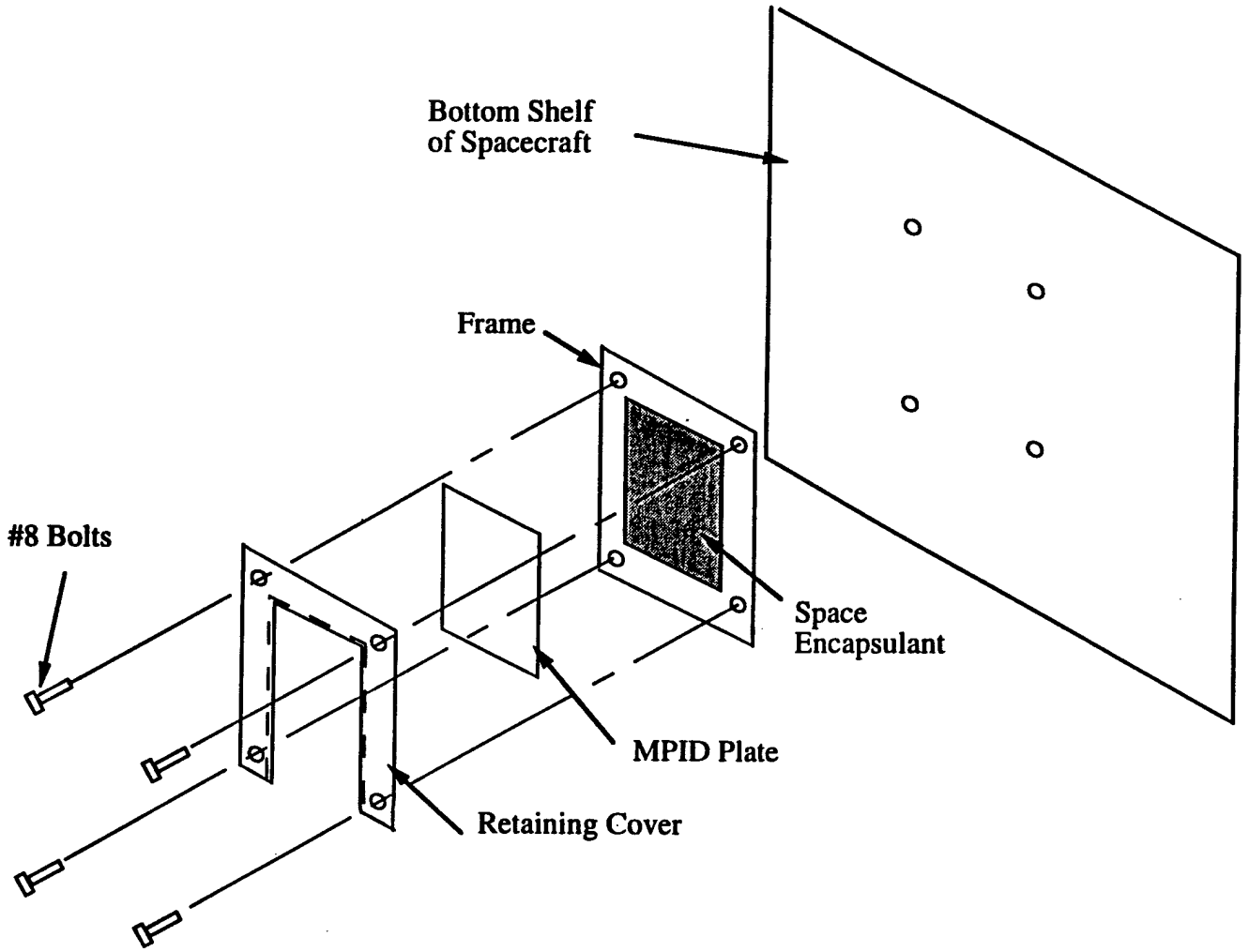


Figure 2: Schematic of MPID plate assembly

# APPENDIX F

# THERMOCOUPLE DATA, DETECTORS #2 AND #3

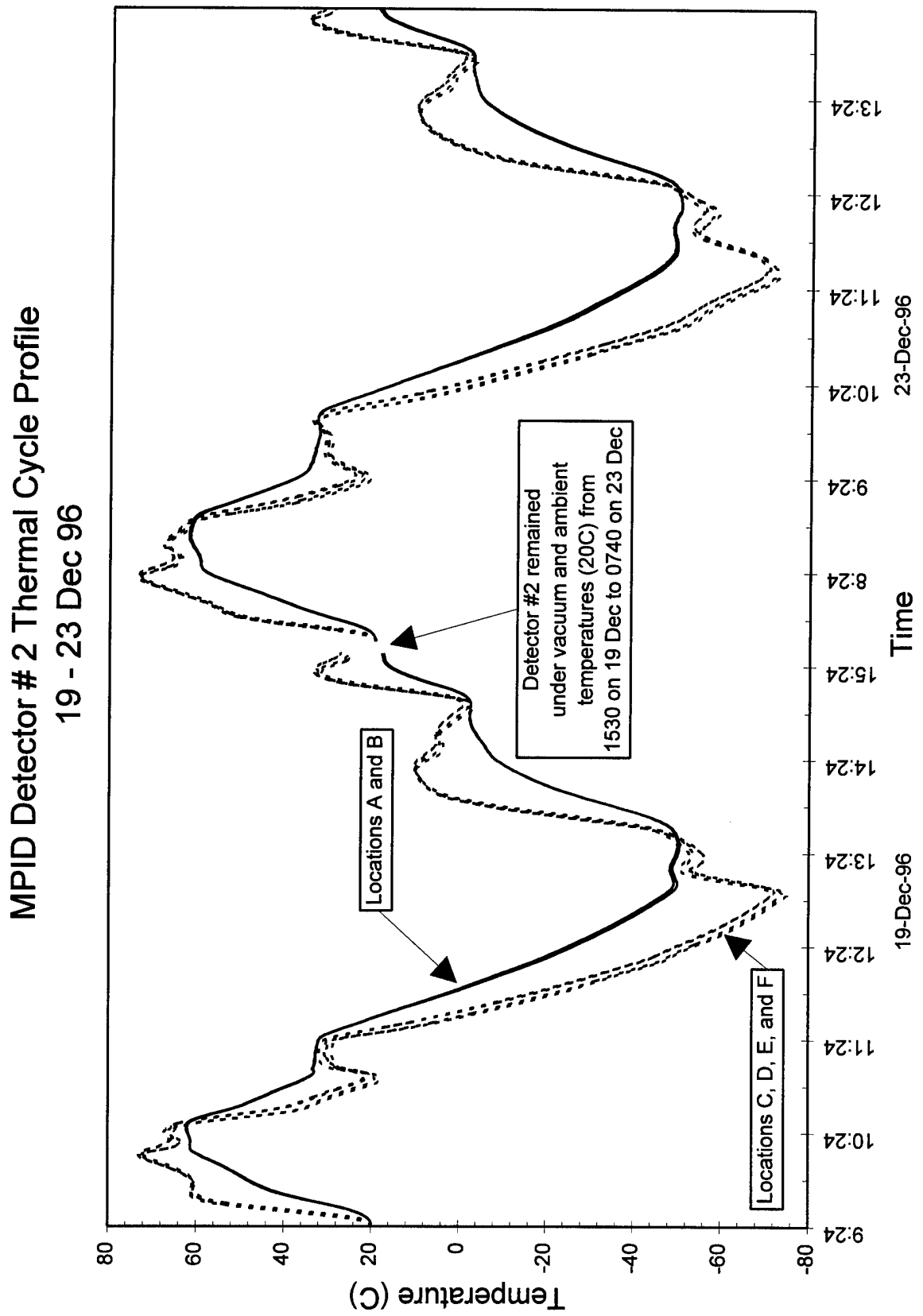
MPID Detector # 2 Thermal Cycle Profile
19 - 23 Dec 96
Temperature (C)
80
60
40
20
0
-20
-40
-60
-80
Time
9:24
10:24
11:24
12:24
13:24
14:24
15:24
8:24
9:24
10:24
11:24
12:24
13:24
19-Dec-96
23-Dec-96
Locations A and B
Locations C, D, E, and F
Detector #2 remained
under vacuum and ambient
temperatures (20C) from
1530 on 19 Dec to 0740 on 23 Dec

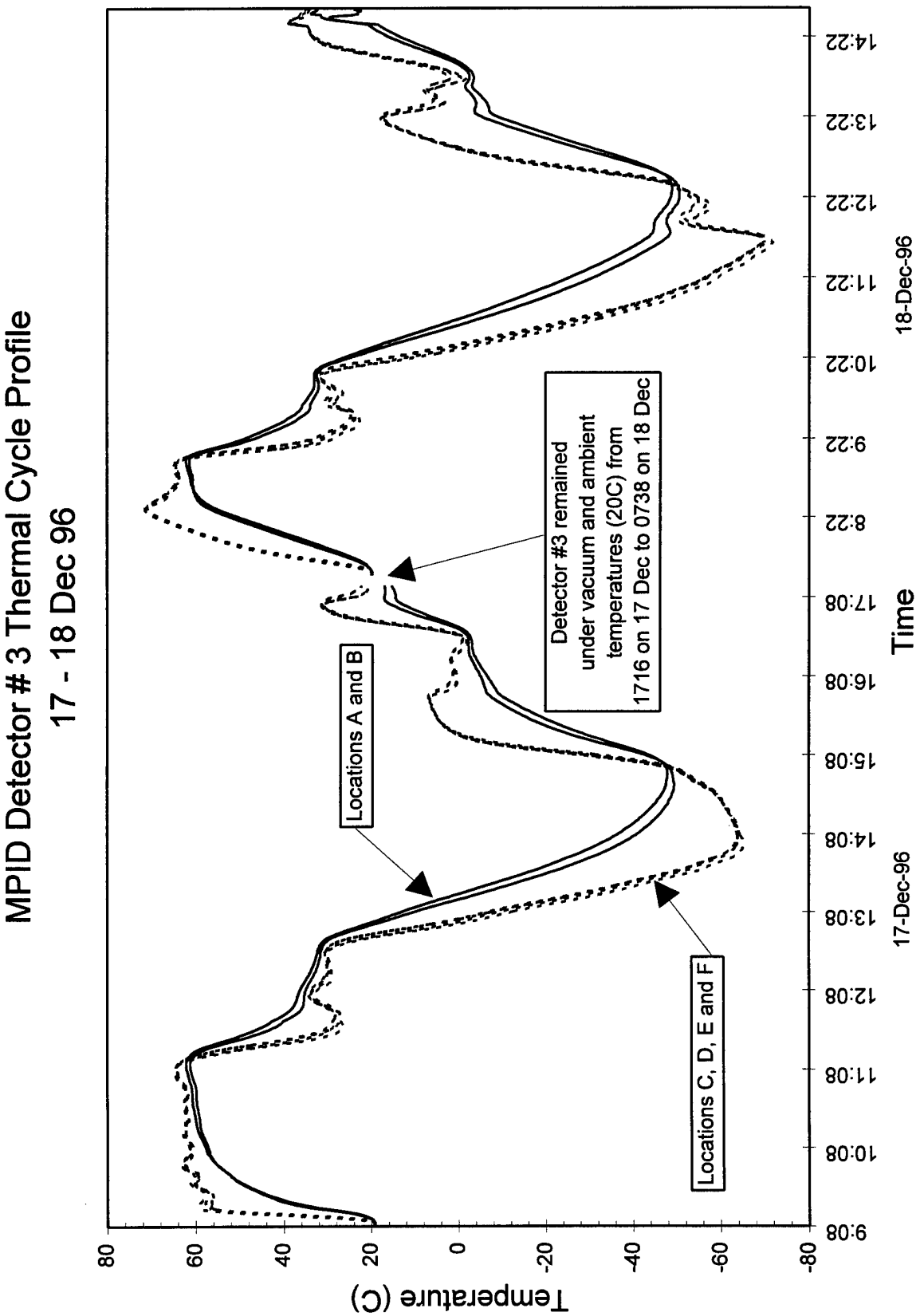
MPID Detector # 3 Thermal Cycle Profile
17 - 18 Dec 96
Temperature (C)
80
60
40
20
0
-20
-40
-60
-80
Time
9:08
10:08
11:08
12:08
13:08
14:08
15:08
16:08
17:08
8:22
9:22
10:22
11:22
12:22
13:22
14:22
17-Dec-96
18-Dec-96
Locations A and B
Locations C, D, E and F
Detector #3 remained
under vacuum and ambient
temperatures (20C) from
1716 on 17 Dec to 0738 on 18 Dec

# APPENDIX G

## Vibration Accelerometer Data, Qualification Board

Vibration Acceleromenter Data, Qualification Board

| Appendix Page Number | Figure Number | Time of Test | Vibration Axis | Accelerometer Location | Vibration Type |
|---|---|---|---|---|---|
| G-3 | G-1 | 12:24 | Z | D (ch 2) | Calibrate, 1/2 G Sine Sweep |
| G-4 | G-2 | 12:24 | Z | C (ch 3) | Calibrate, 1/2 G Sine Sweep |
| G-5 | G-3 | 12:27 | Z | D (ch 2) | Calibrate, Random |
| G-6 | G-4 | 12:27 | Z | C (ch 3) | Calibrate, Random |
| G-7 | G-5 | 13:39 | Z | D (ch 2) | Pre-Sine Sweep, 1/2 G |
| G-8 | G-6 | 13:39 | Z | C (ch 3) | Pre-Sine Sweep, 1/2 G |
| G-9 | G-7 | 13:43 | Z | D (ch 2) | Random |
| G-10 | G-8 | 13:43 | Z | C (ch 3) | Random |
| G-11 | G-9 | 13:48 | Z | D (ch 2) | Post-Sine Sweep, 1/2 G |
| G-12 | G-10 | 13:48 | Z | C (ch 3) | Post-Sine Sweep, 1/2 G |
| G-13 | G-11 | 14:51 | X | D (ch 2) | Pre-Sine Sweep, 1/2 G |
| G-14 | G-12 | 14:51 | X | A (ch 3) | Pre-Sine Sweep, 1/2 G |
| G-15 | G-13 | 14:54 | X | D (ch 2) | Random |
| G-16 | G-14 | 14:54 | X | A (ch 3) | Random |
| G-17 | G-15 | 14:58 | X | D (ch 2) | Post-Sine Sweep, 1/2 G |
| G-18 | G-16 | 14:58 | X | A (ch 3) | Post-Sine Sweep, 1/2 G |
| G-19 | G-17 | 15:20 | Y | D (ch 2) | Pre-Sine Sweep, 1/2 G |
| G-20 | G-18 | 15:20 | Y | B (ch 3) | Pre-Sine Sweep, 1/2 G |
| G-21 | G-19 | 15:23 | Y | D (ch 2) | Random |
| G-22 | G-20 | 15:23 | Y | B (ch 3) | Random |
| G-23 | G-21 | 15:27 | Y | D (ch 2) | Post-Sine Sweep, 1/2 G |
| G-24 | G-22 | 15:27 | Y | B (ch 3) | Post-Sine Sweep, 1/2 G |

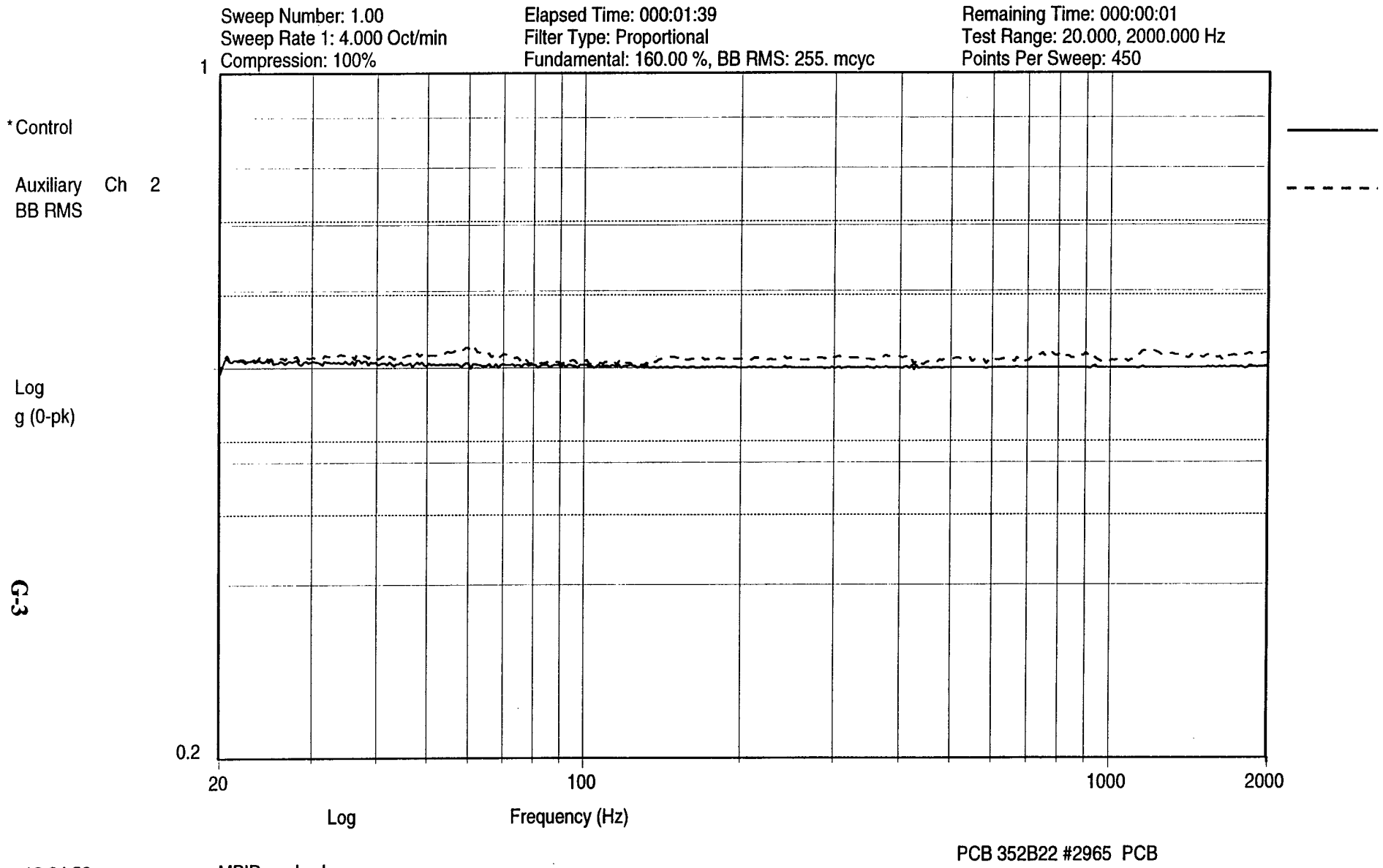


**Figure G1. Calibrate, 1/2 g Sine Sweep**

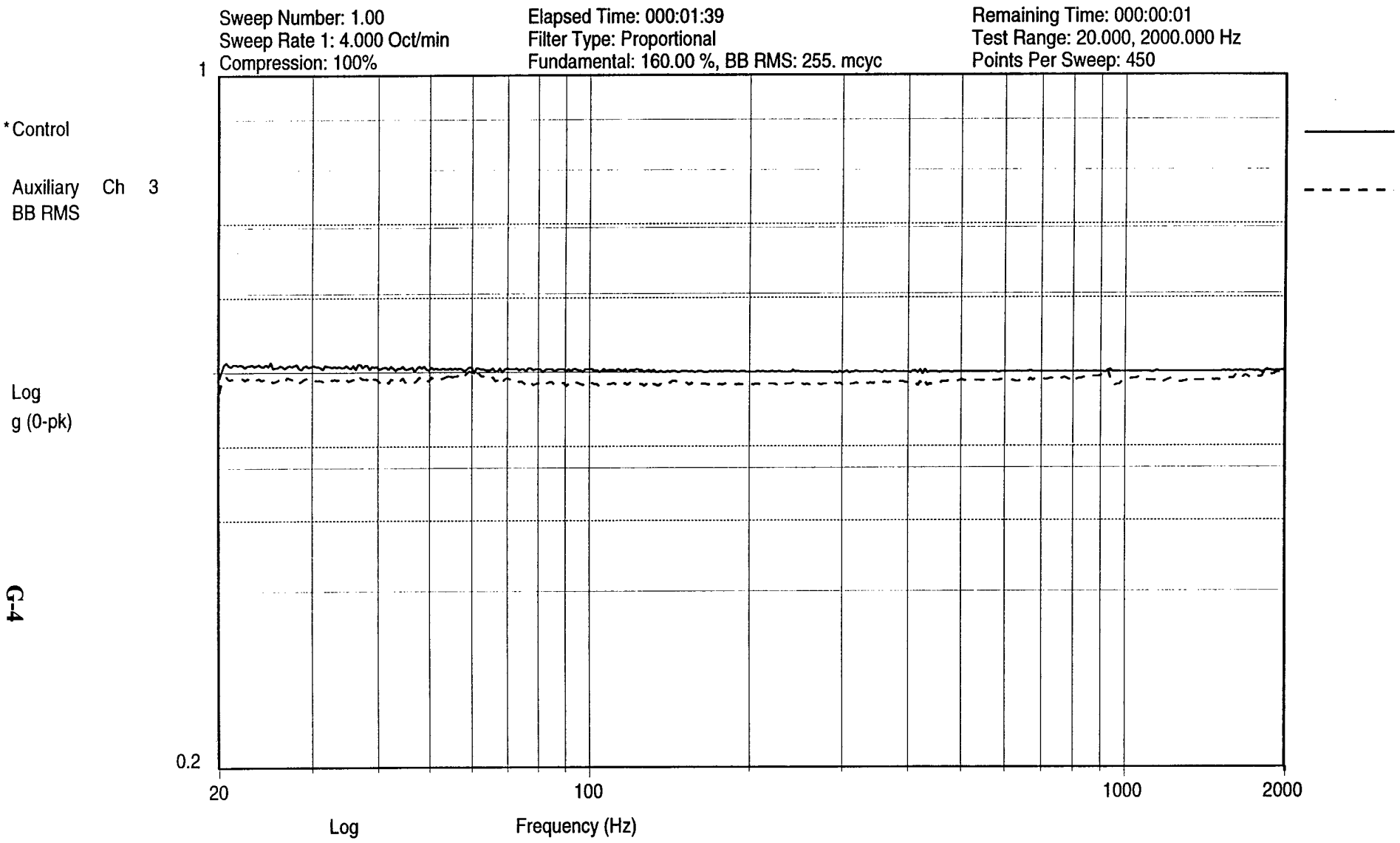


**Figure G2. Calibrate, 1/2 g Sine Sweep**

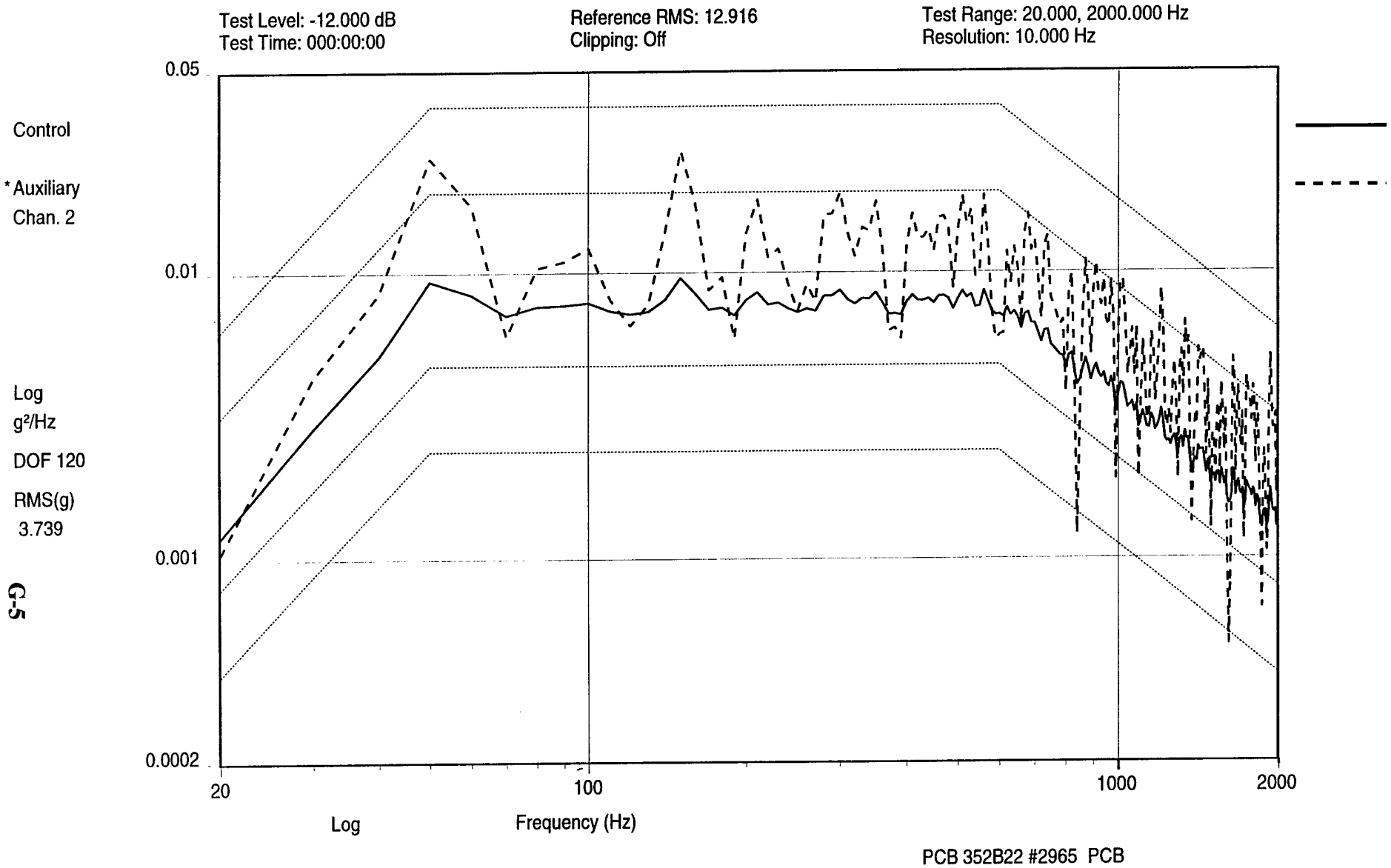


**Figure G3. Calibrate, Random**

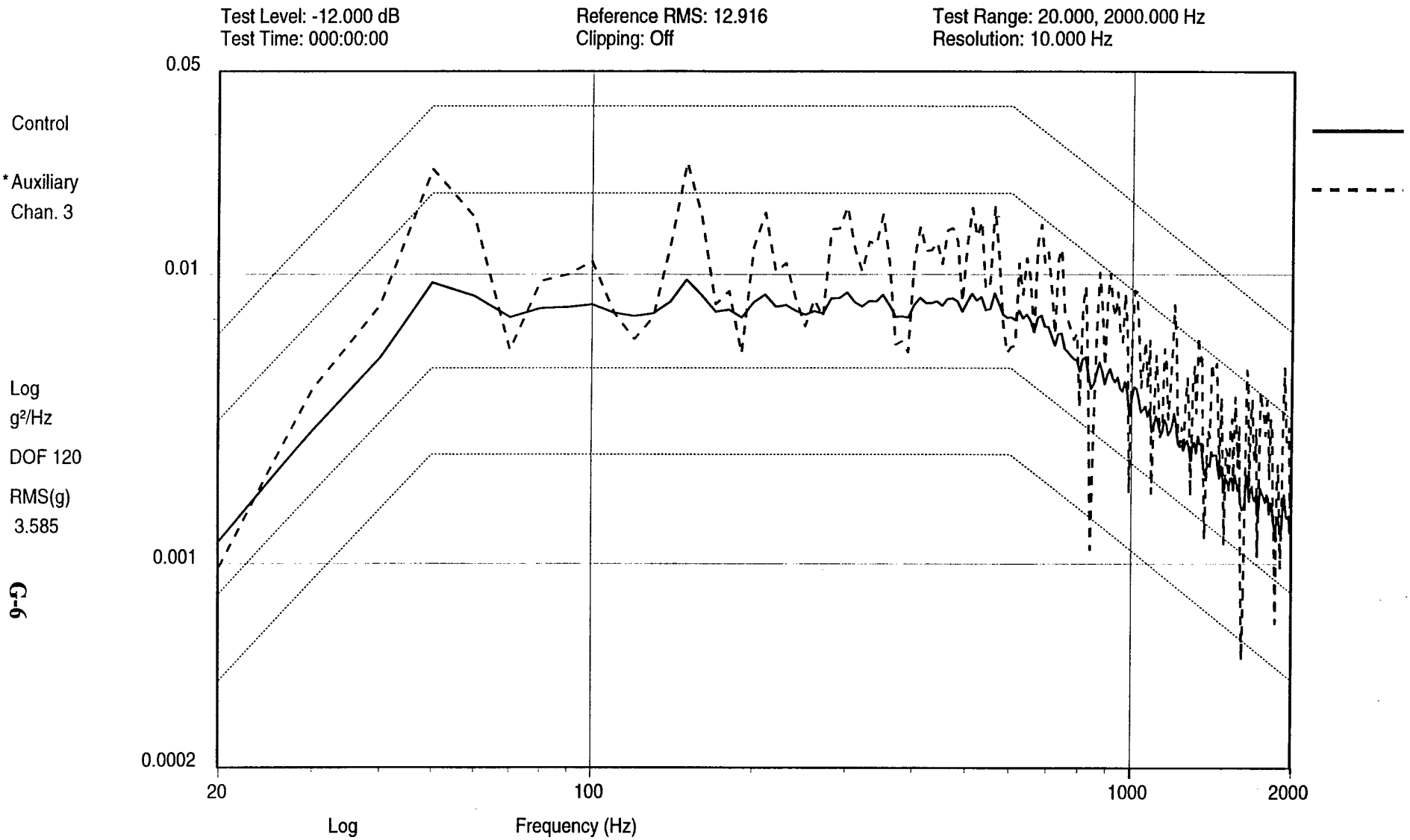


**Figure G4. Calibrate, Random**

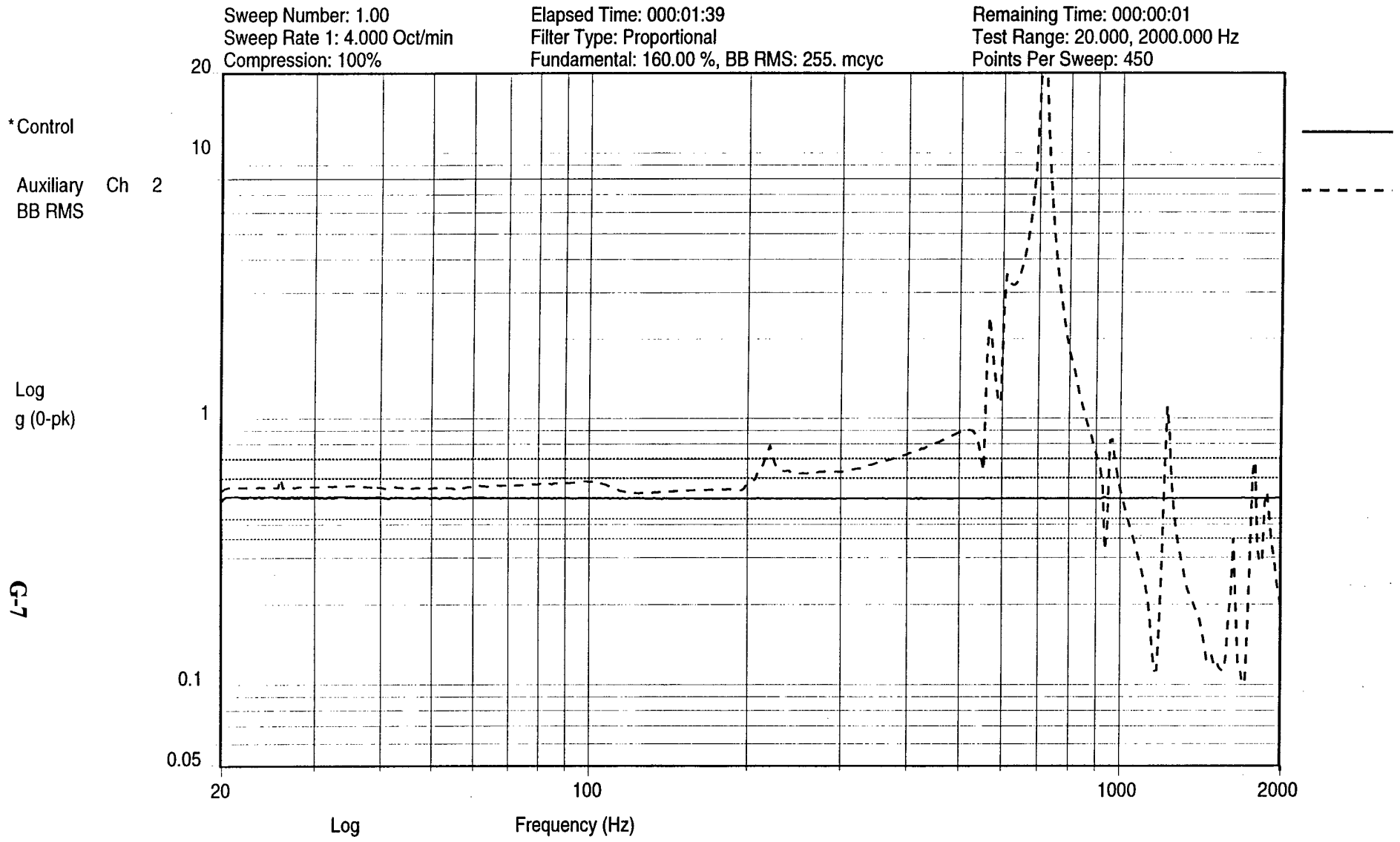


**Figure G5. Pre-Sine Sweep, 1/2 g**

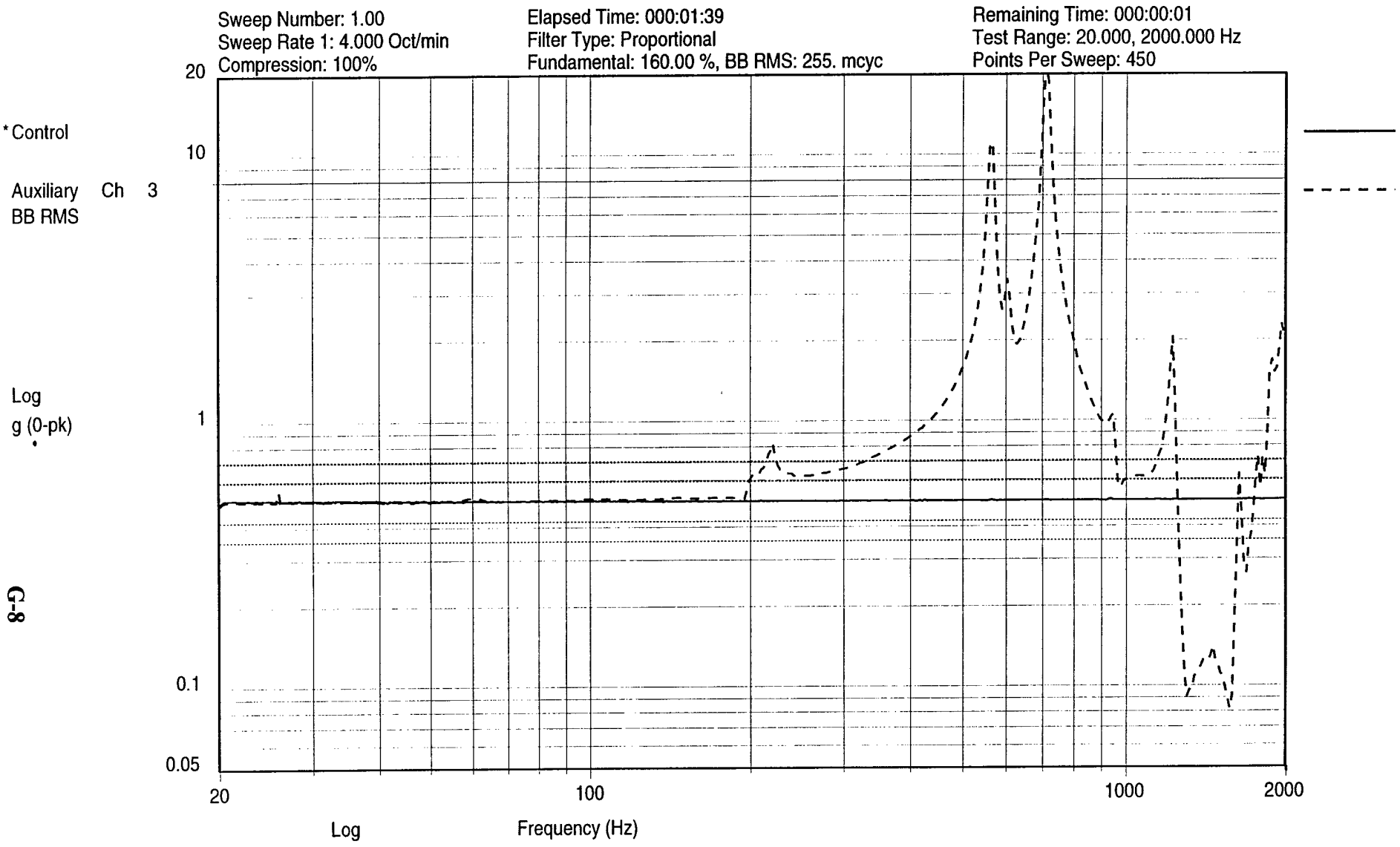


**Figure G6. Pre-Sine Sweep, 1/2 g**

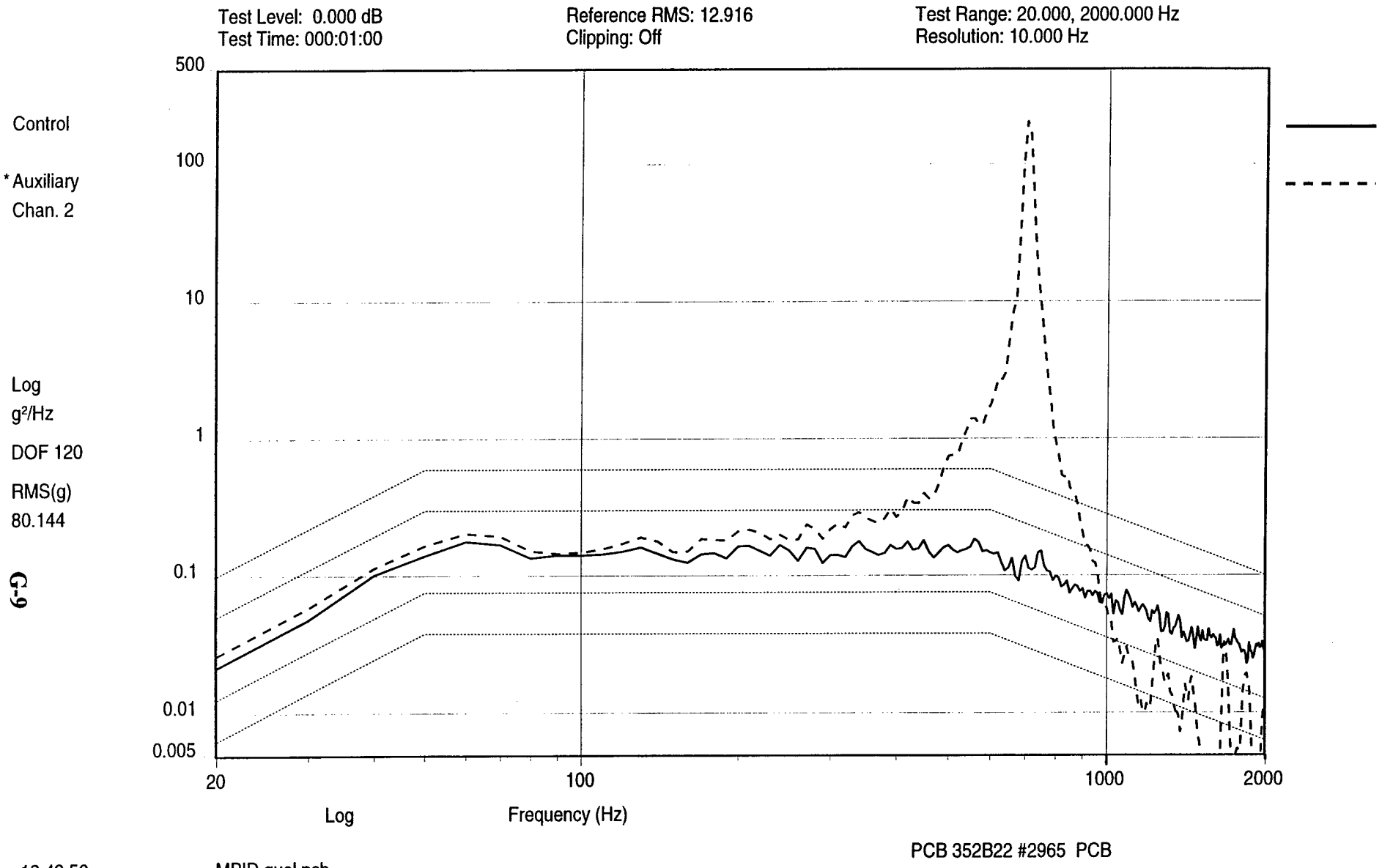


**Figure G7. Random**

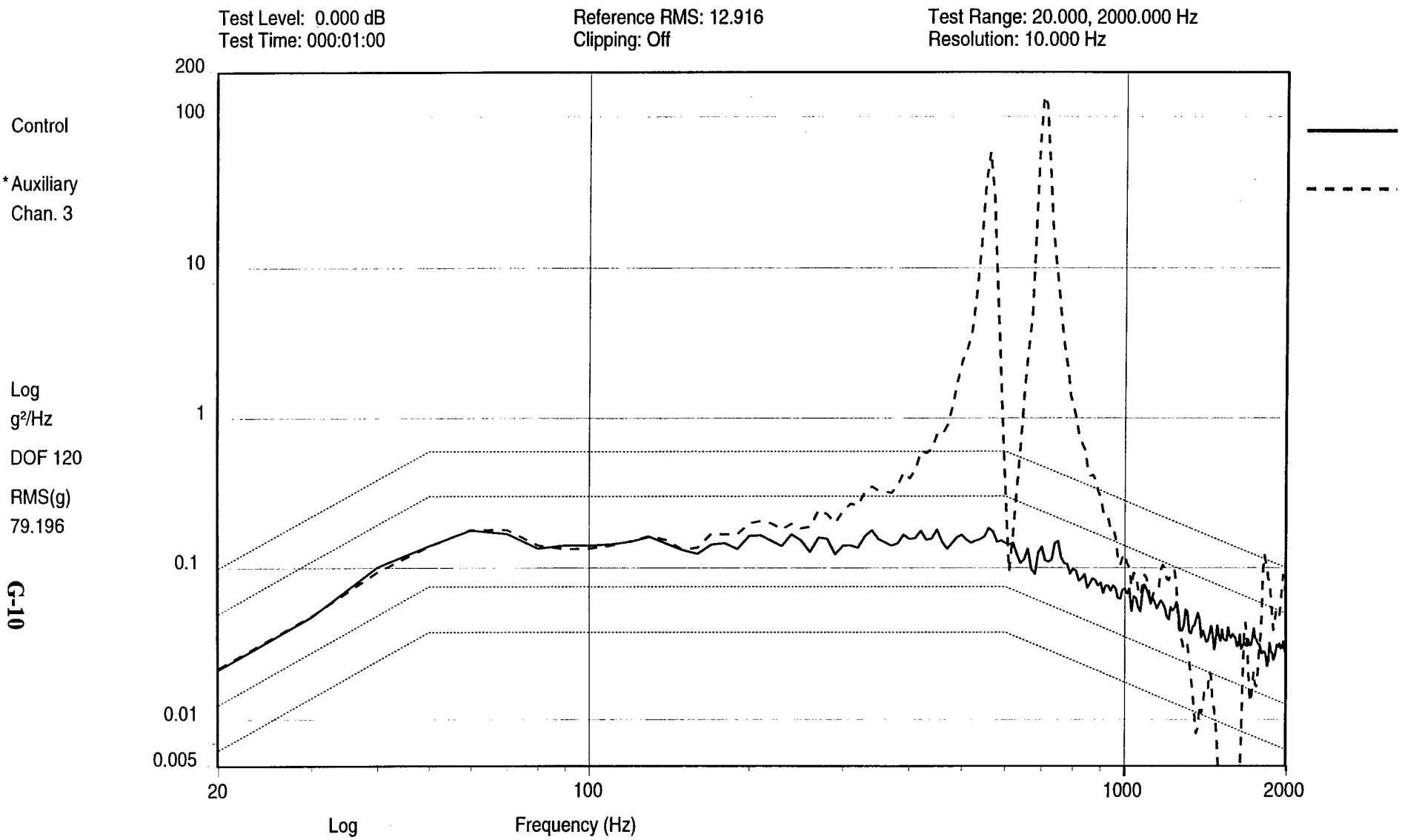


**Figure G8. Random**

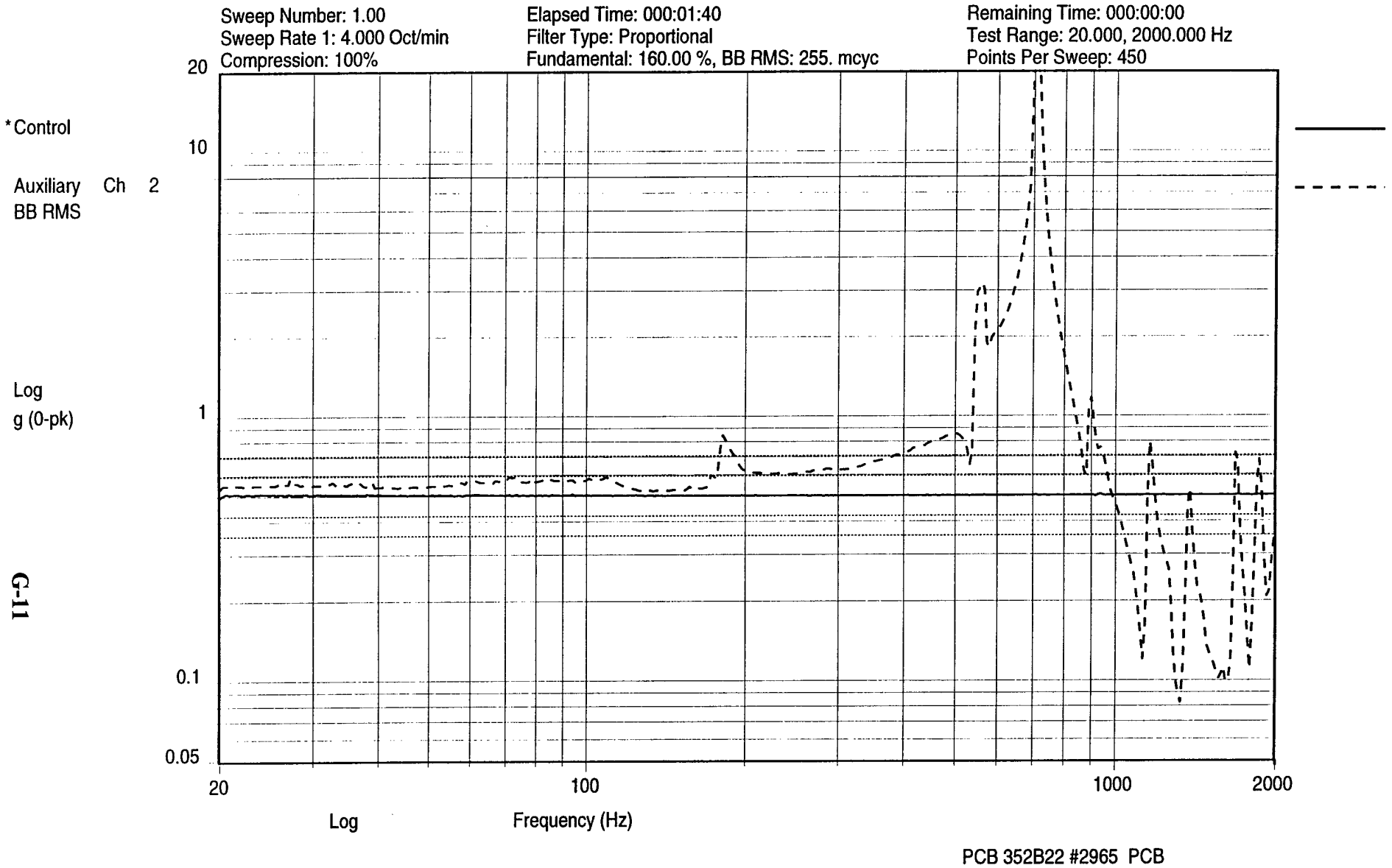


**Figure G9. Post-Sine Sweep, 1/2 g**

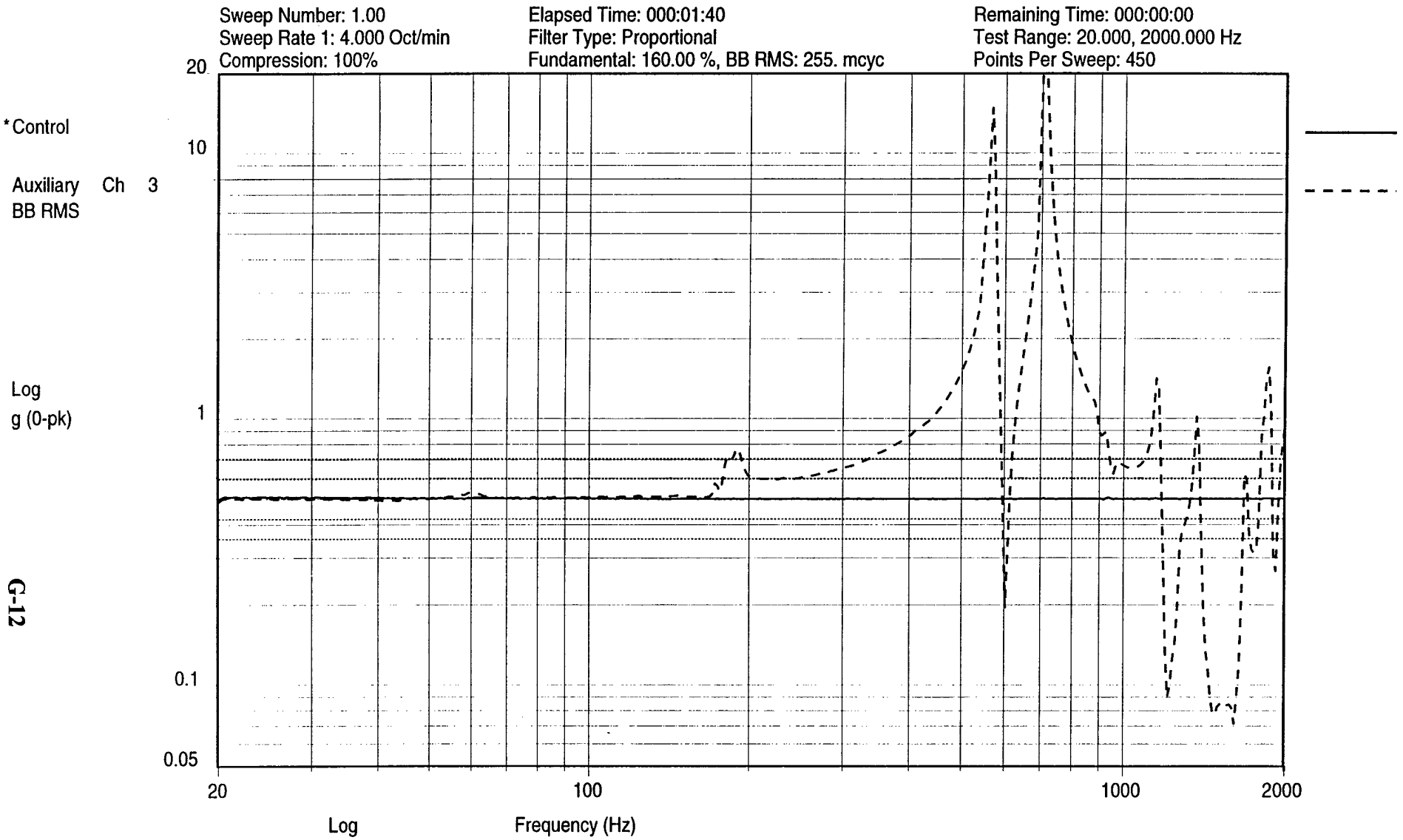


**Figure G10. Post-Sine Sweep, 1/2 g**

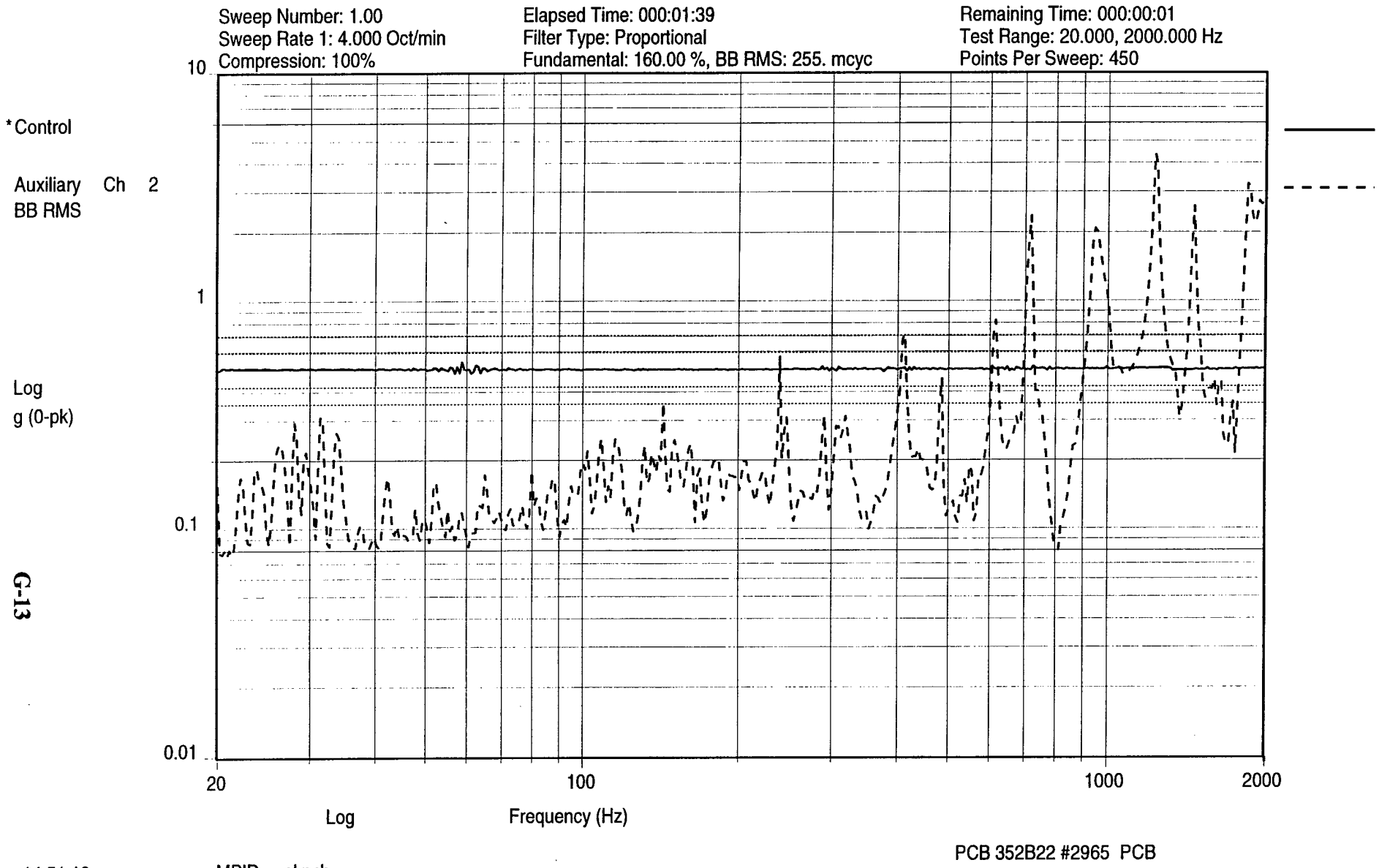


**Figure G11. Pre-Sine Sweep, 1/2 g**

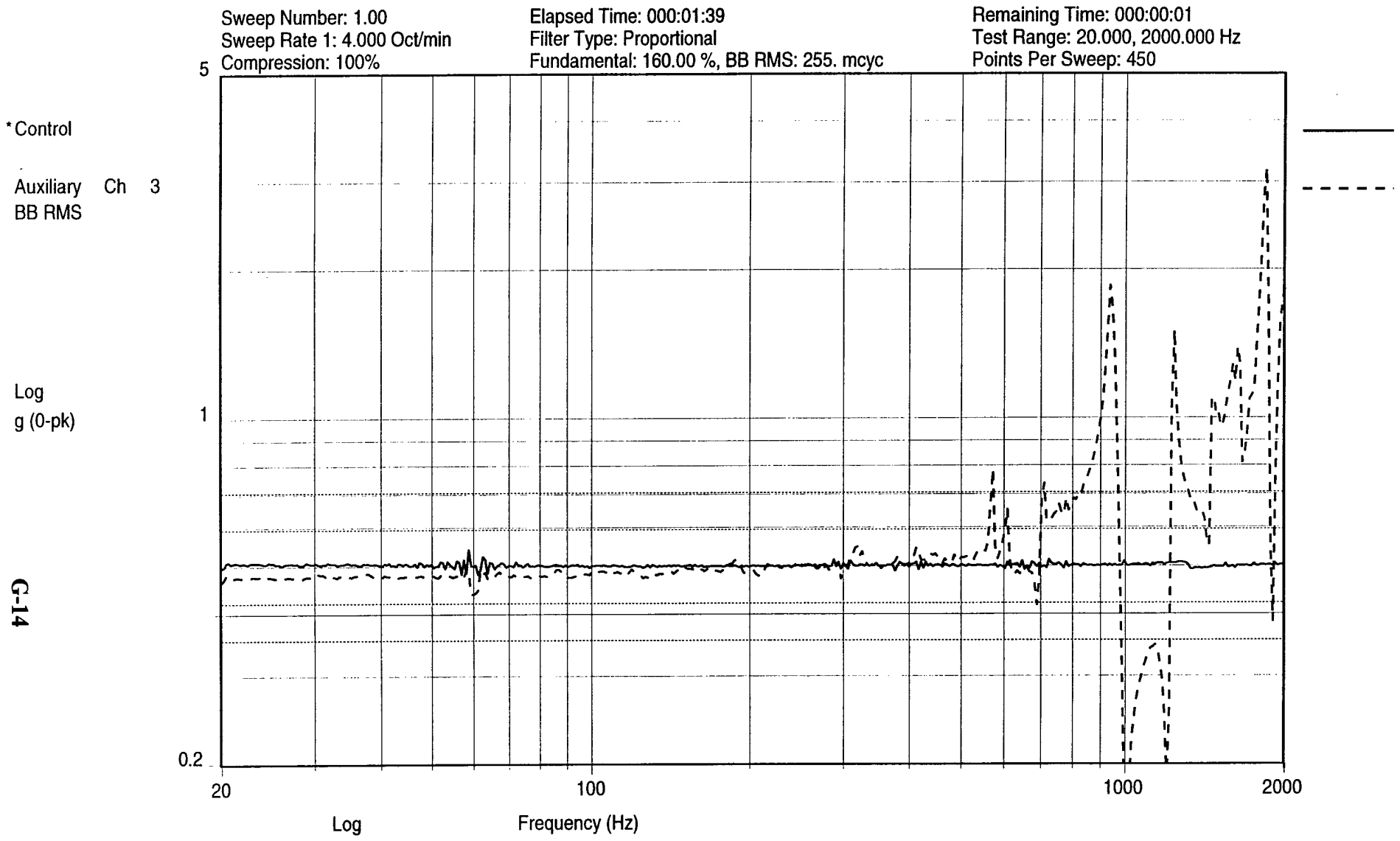


**Figure G12. Pre-Sine Sweep, 1/2 g**

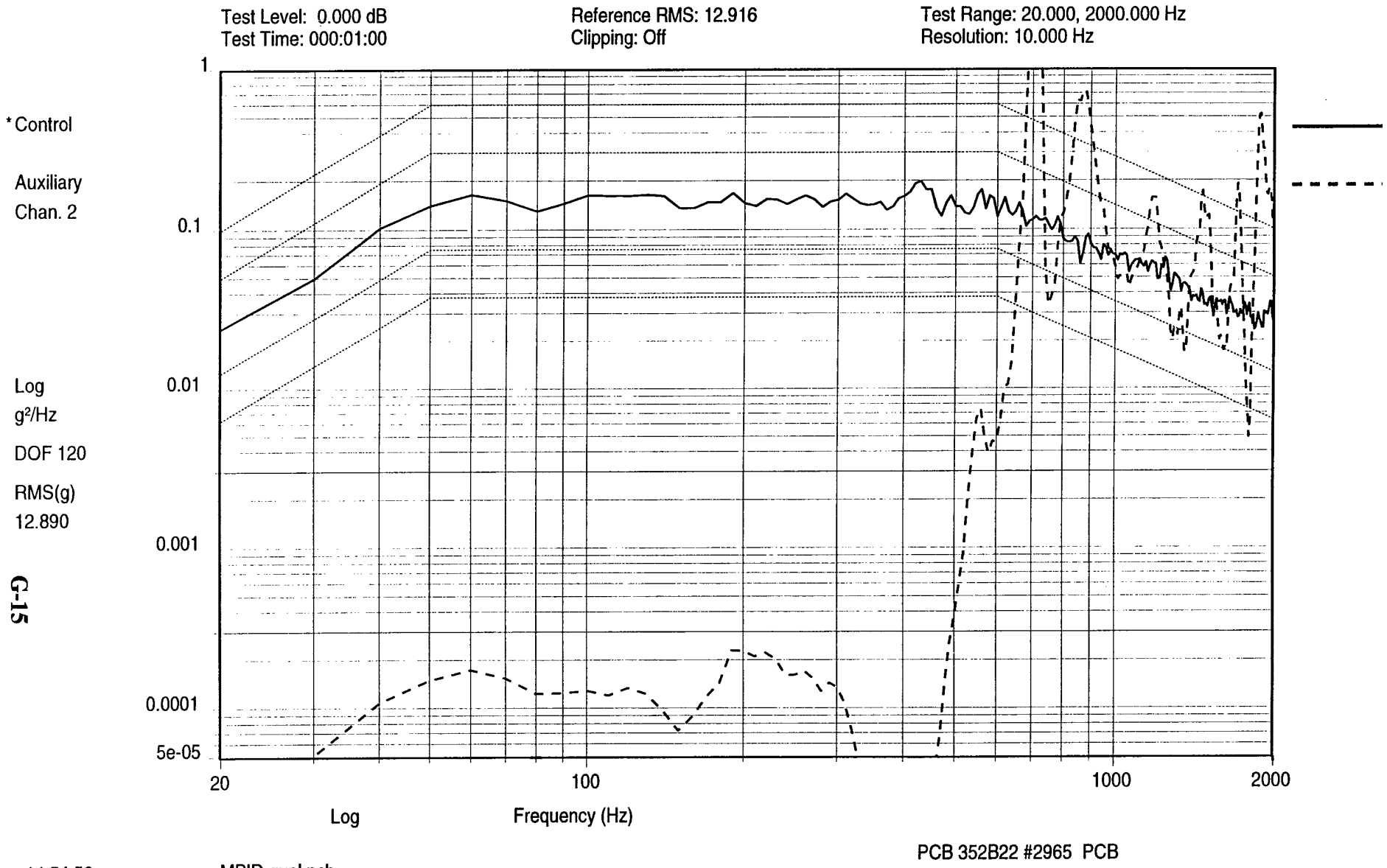


**Figure G13. Random**

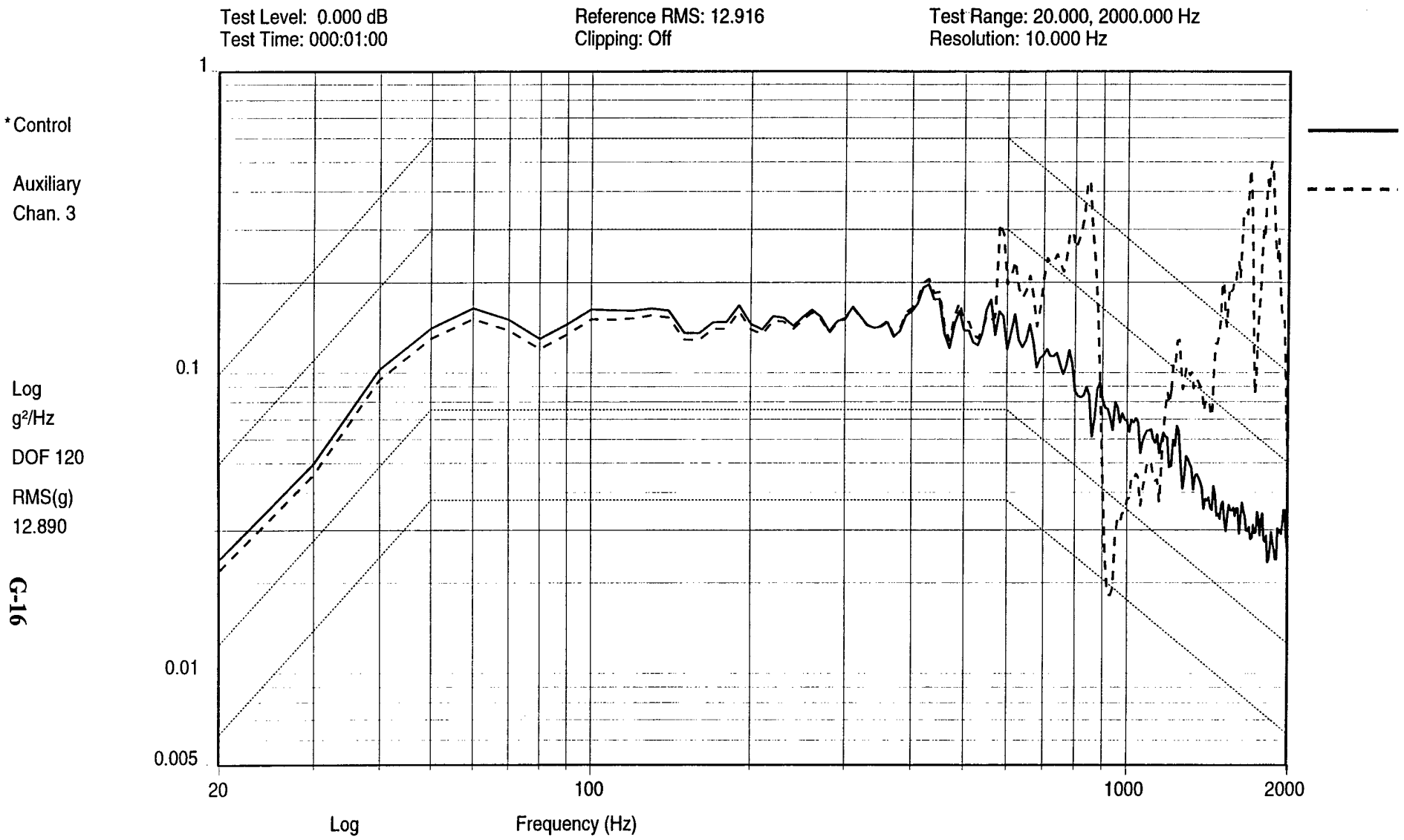


**Figure G14. Random**

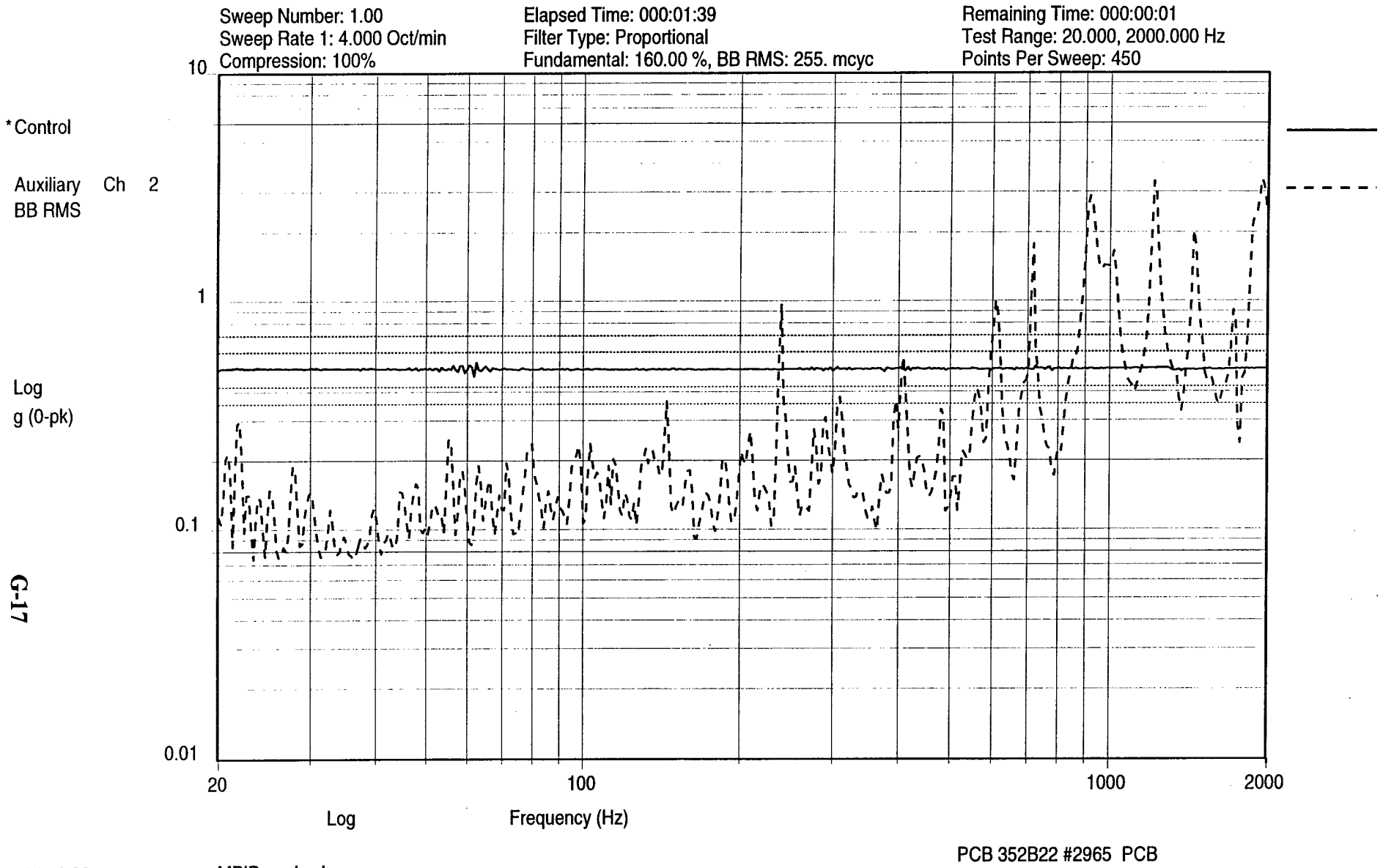


14:58:32
Tue Nov 12 1996

MPID qual pcb
1/2 g Sine Sweep x post

Data Review Name: mpid_11_12_96.007

**Figure G15. Post-Sine Sweep, 1/2 g**

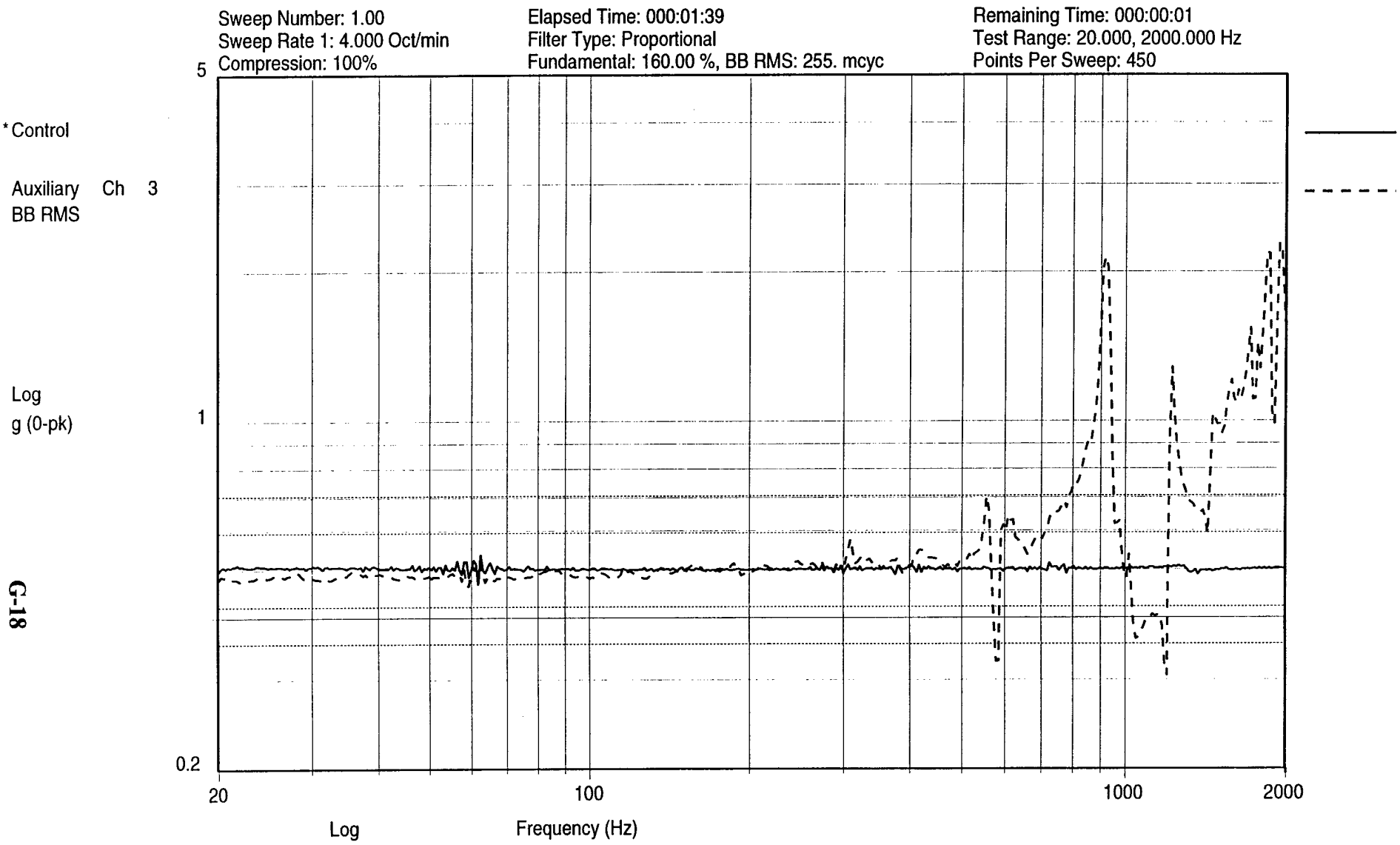


**Figure G16. Post-Sine Sweep, 1/2 g**

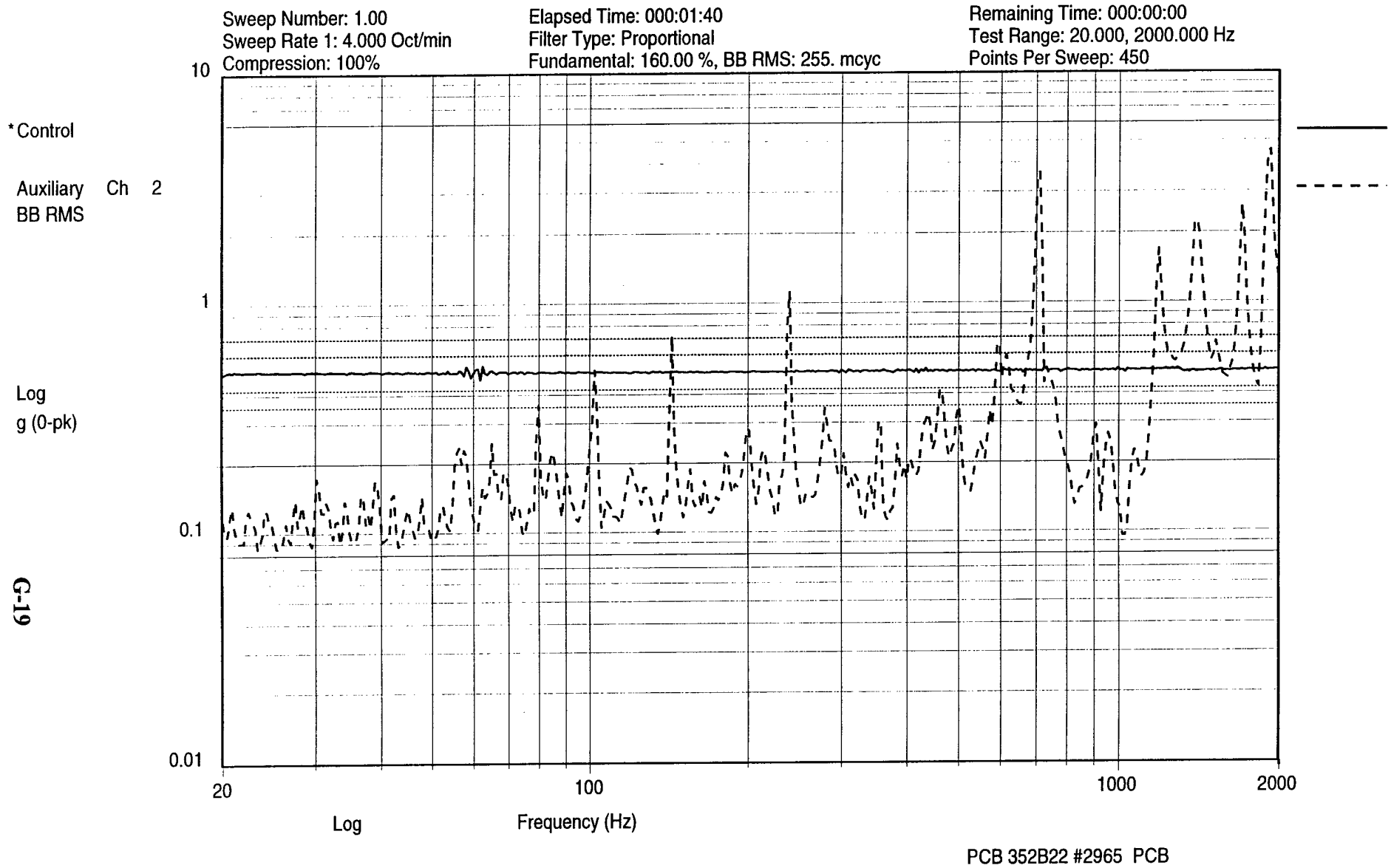


**Figure G17. Pre-Sine Sweep, 1/2 g**

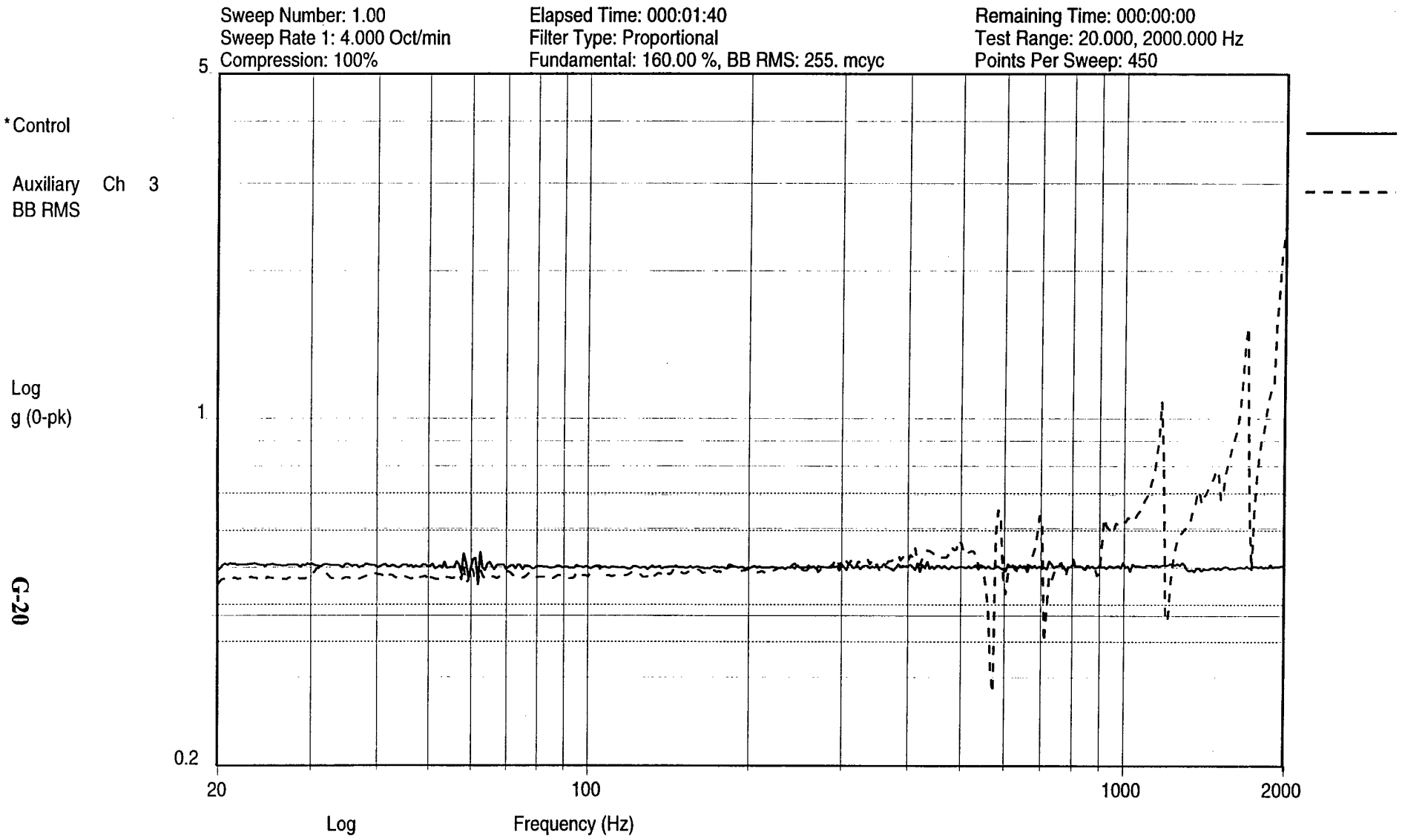


**Figure G18. Pre-Sine Sweep, 1/2 g**

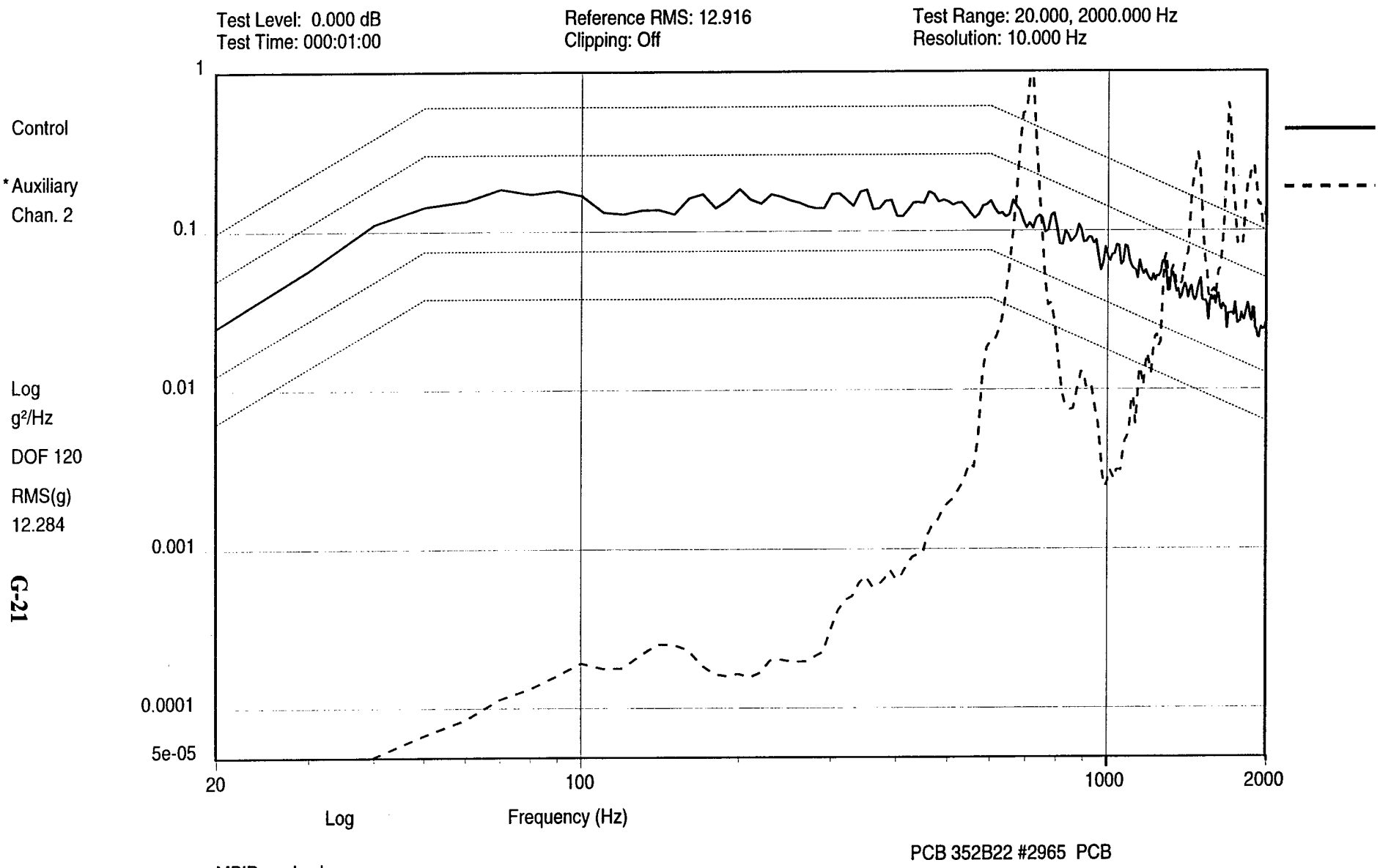


15:23:53
Tue Nov 12 1996

MPID qual pcb
Y axis

Data Review Name: mpid_11_12_96.004

**Figure G19. Random**

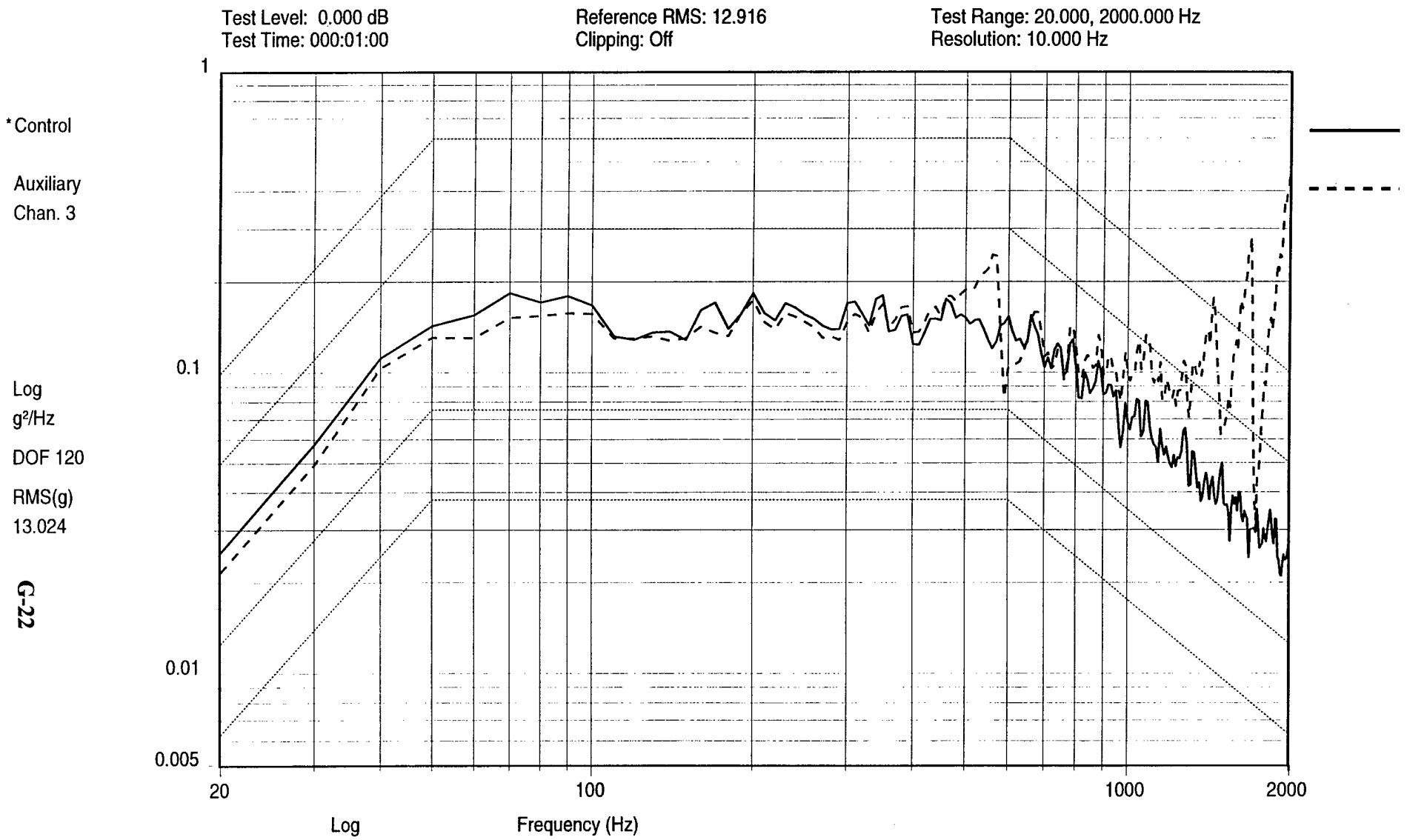


**Figure G20. Random**

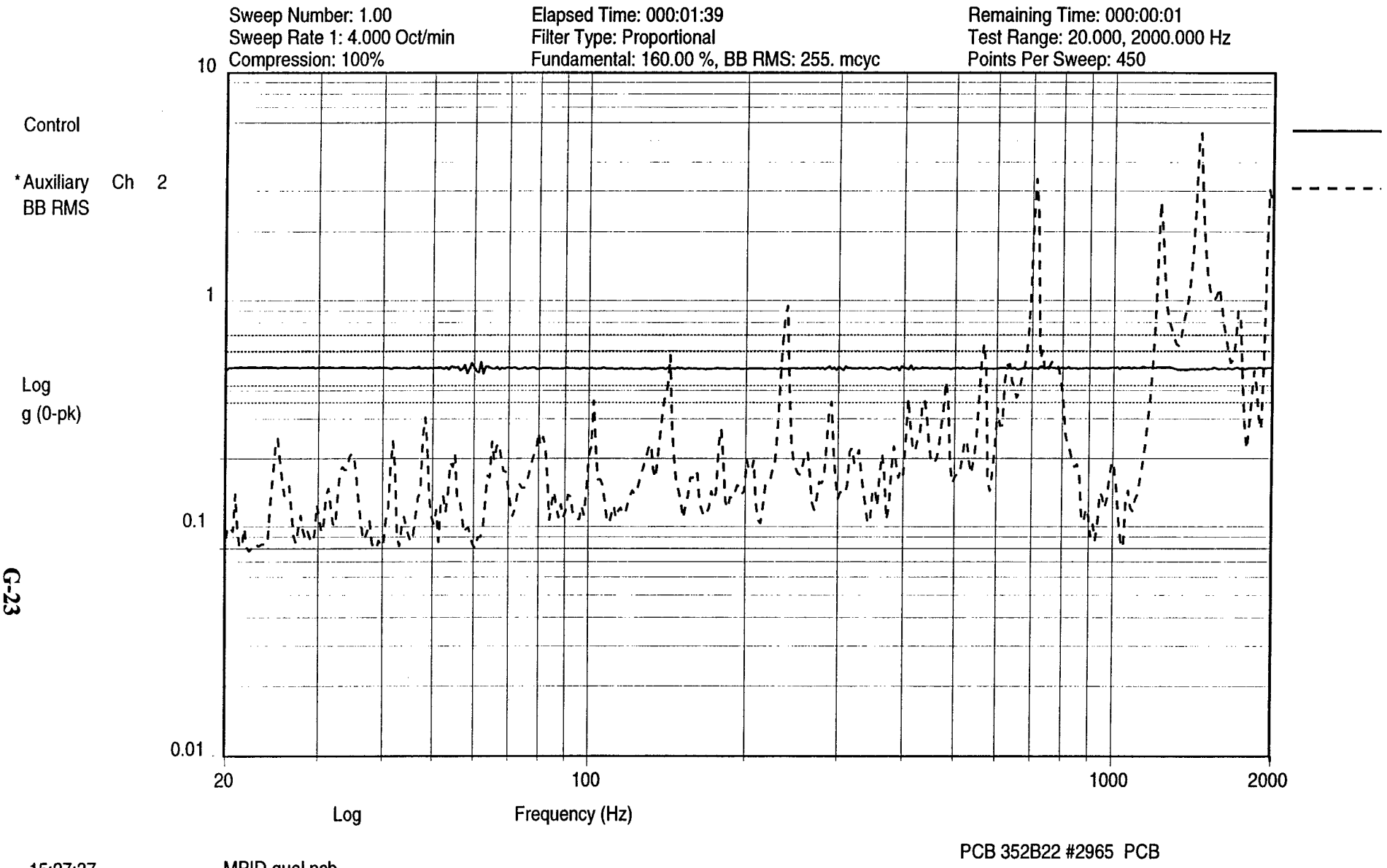


**Figure G21. Post-Sine Sweep, 1/2 g**

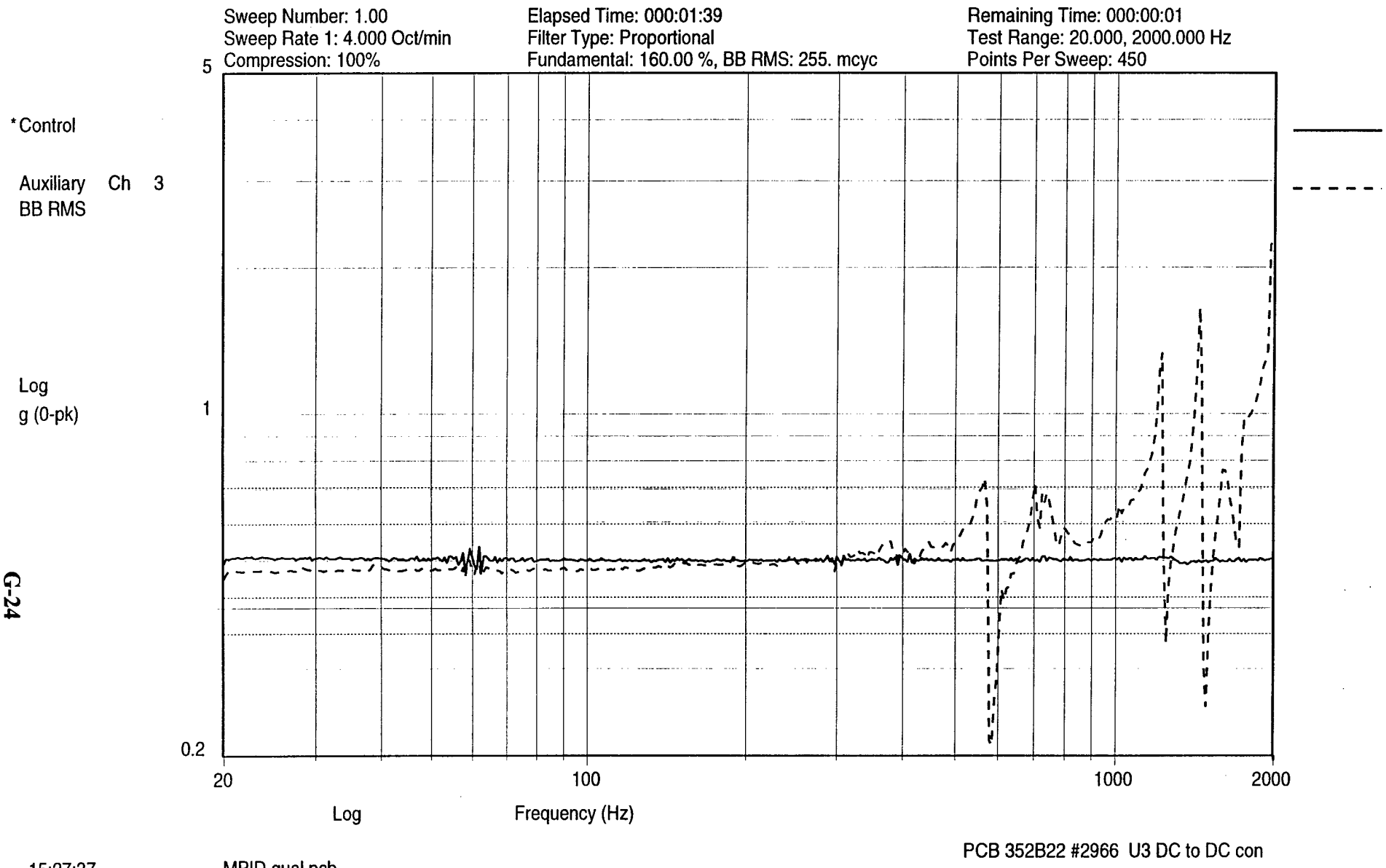


**Figure G22. Post-Sine Sweep, 1/2 g**

# APPENDIX H

## Vibration Accelerometer Data, Flight Board

Vibration Acceleromenter Data, Flight Board

| Appendix Page Number | Figure Number | Time of Test | Vibration Axis | Accelerometer Location | Vibration Type |
|---|---|---|---|---|---|
| H-3 | H-1 | 9:09 | Z | D (ch 2) | Calibrate, 1/2 G Sine Sweep |
| H-4 | H-2 | 9:09 | Z | C (ch 3) | Calibrate, 1/2 G Sine Sweep |
| H-5 | H-3 | 9:13 | Z | D (ch 2) | Calibrate, Random |
| H-6 | H-4 | 9:13 | Z | C (ch 3) | Calibrate, Random |
| H-7 | H-5 | 9:51 | X | D (ch 2) | Pre-Sine Sweep, 1/2 G |
| H-8 | H-6 | 9:51 | X | C (ch 3) | Pre-Sine Sweep, 1/2 G |
| H-9 | H-7 | 9:56 | X | D (ch 2) | Random |
| H-10 | H-8 | 9:55 | X | C (ch 3) | Random |
| H-11 | H-9 | 10:02 | X | D (ch 2) | Post-Sine Sweep, 1/2 G |
| H-12 | H-10 | 10:03 | X | C (ch 3) | Post-Sine Sweep, 1/2 G |
| H-13 | H-11 | 10:27 | Y | D (ch 2) | Pre-Sine Sweep, 1/2 G |
| H-14 | H-12 | 10:27 | Y | A (ch 3) | Pre-Sine Sweep, 1/2 G |
| H-15 | H-13 | 10:34 | Y | D (ch 2) | Random |
| H-16 | H-14 | 10:34 | Y | A (ch 3) | Random |
| H-17 | H-15 | 10:40 | Y | D (ch 2) | Post-Sine Sweep, 1/2 G |
| H-18 | H-16 | 10:41 | Y | A (ch 3) | Post-Sine Sweep, 1/2 G |
| H-19 | H-17 | 11:18 | Z | D (ch 2) | Pre-Sine Sweep, 1/2 G |
| H-20 | H-18 | 11:18 | Z | B (ch 3) | Pre-Sine Sweep, 1/2 G |
| H-21 | H-19 | 11:22 | Z | D (ch 2) | Random |
| H-22 | H-20 | 11:22 | Z | B (ch 3) | Random |
| H-23 | H-21 | 11:27 | Z | D (ch 2) | Post-Sine Sweep, 1/2 G |
| H-24 | H-22 | 11:27 | Z | B (ch 3) | Post-Sine Sweep, 1/2 G |

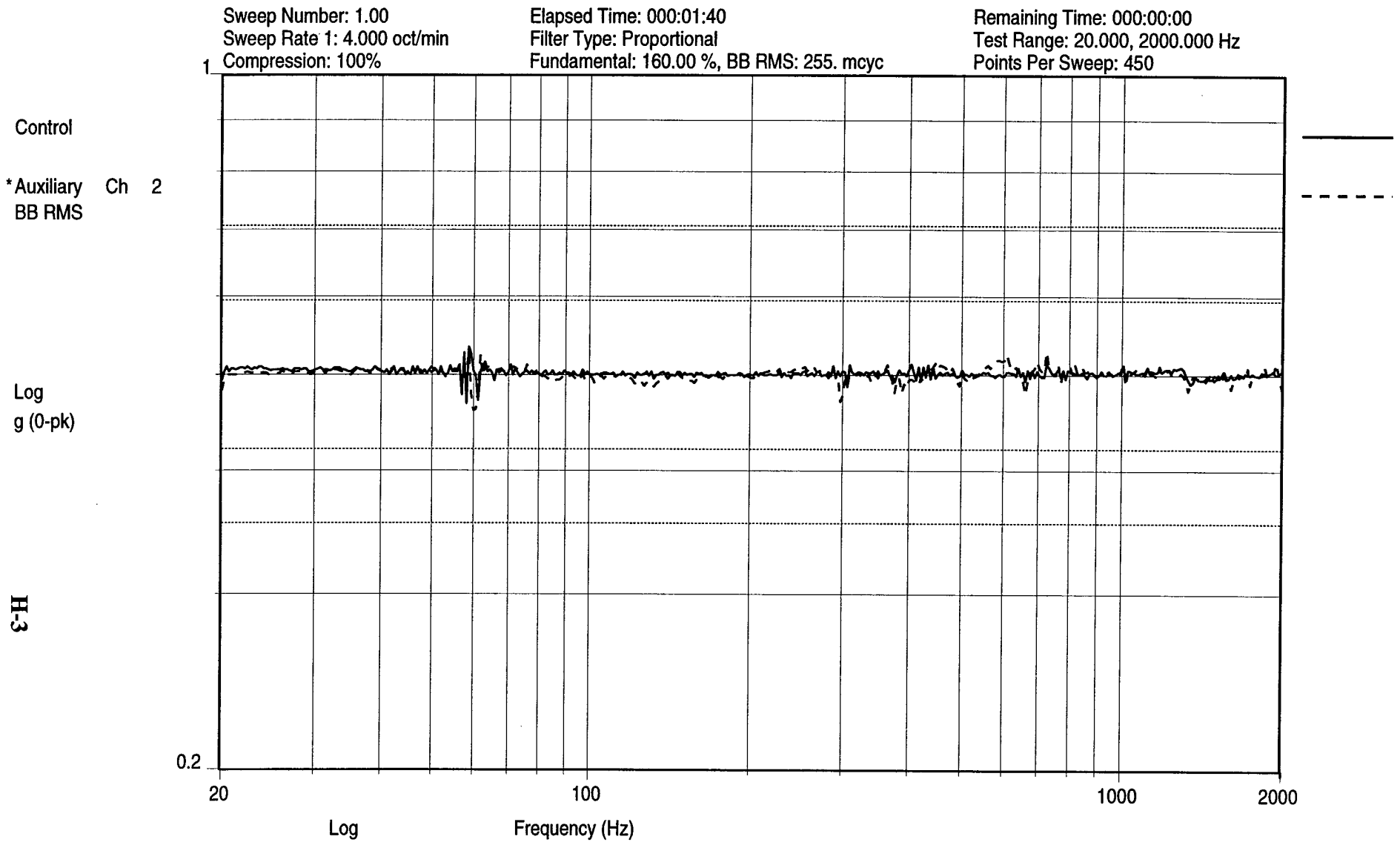


**Figure H-1. Calibrate, 1/2 G Sine Sweep**

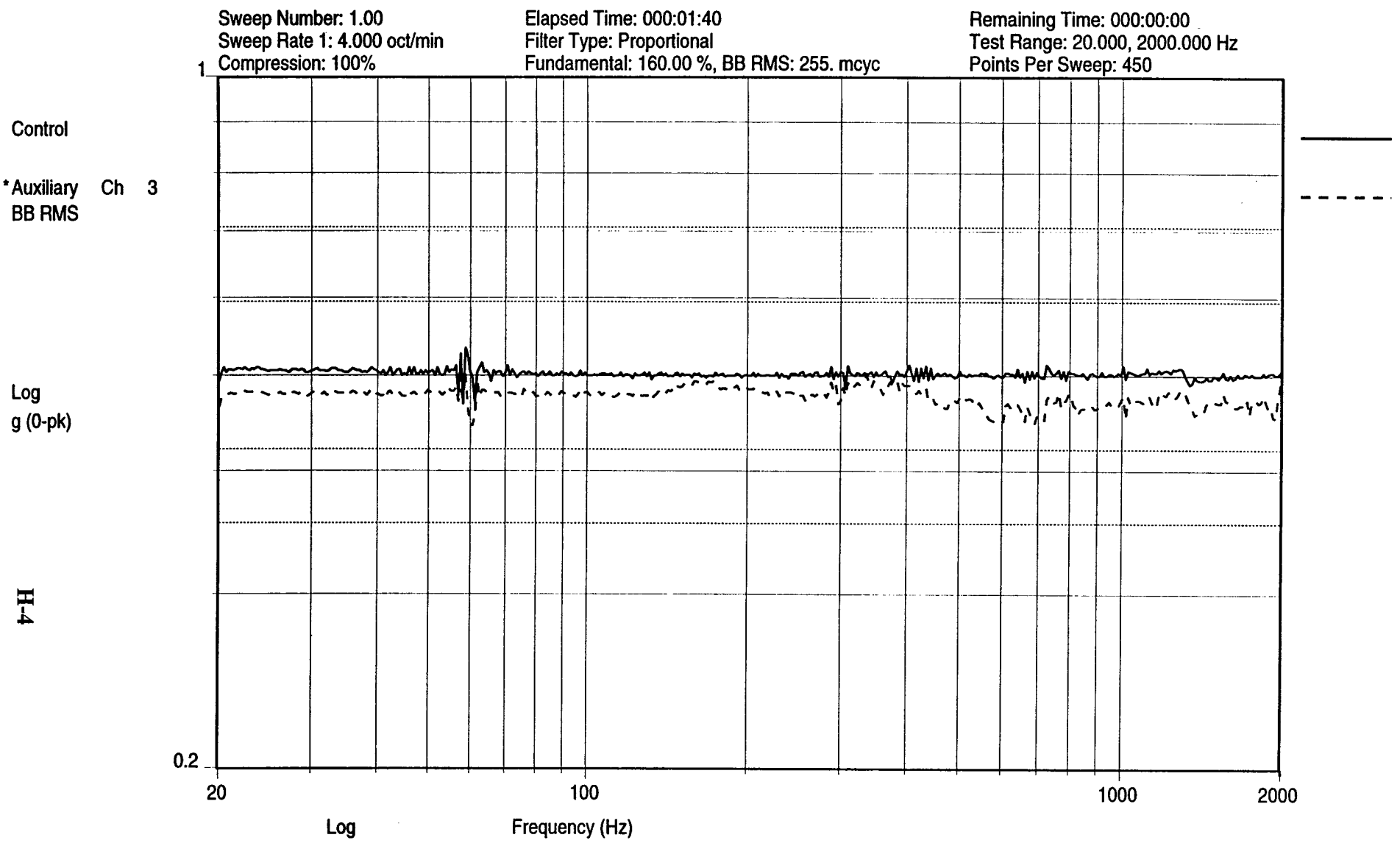


**Figure H-2. Calibrate, 1/2 G Sine Sweep**

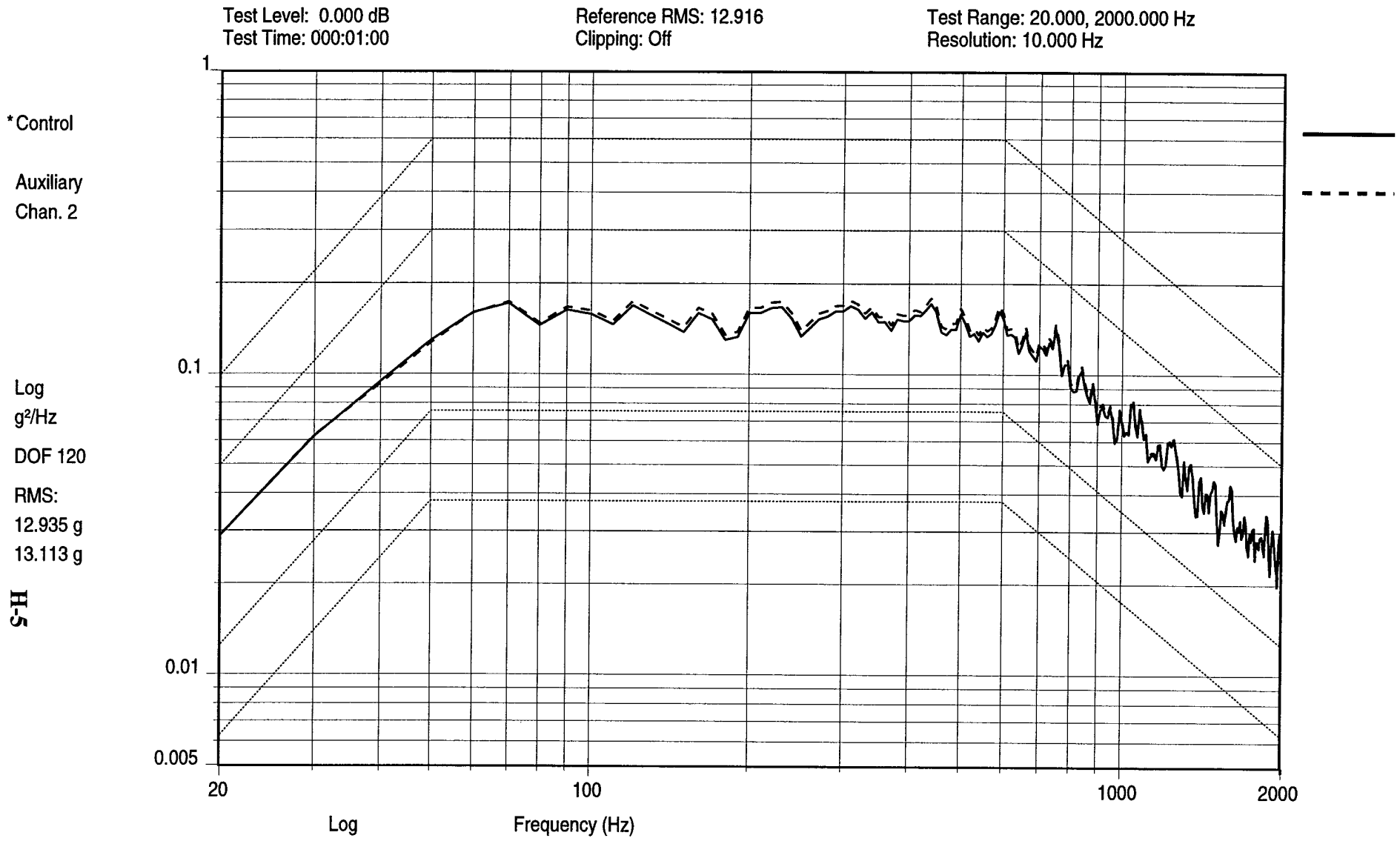


**Figure H-3. Calibrate, Random**

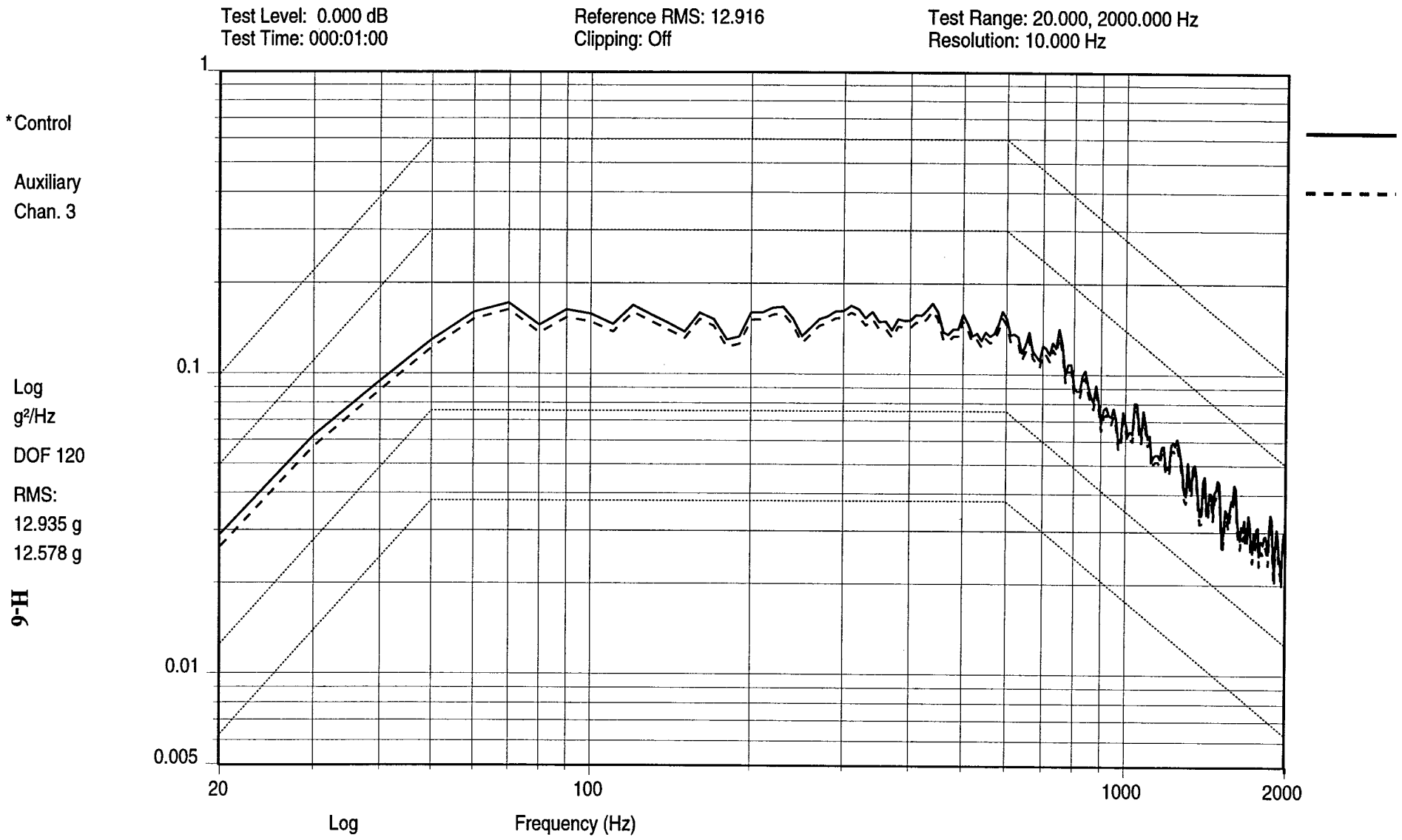


**Figure H-4. Calibrate, Random**

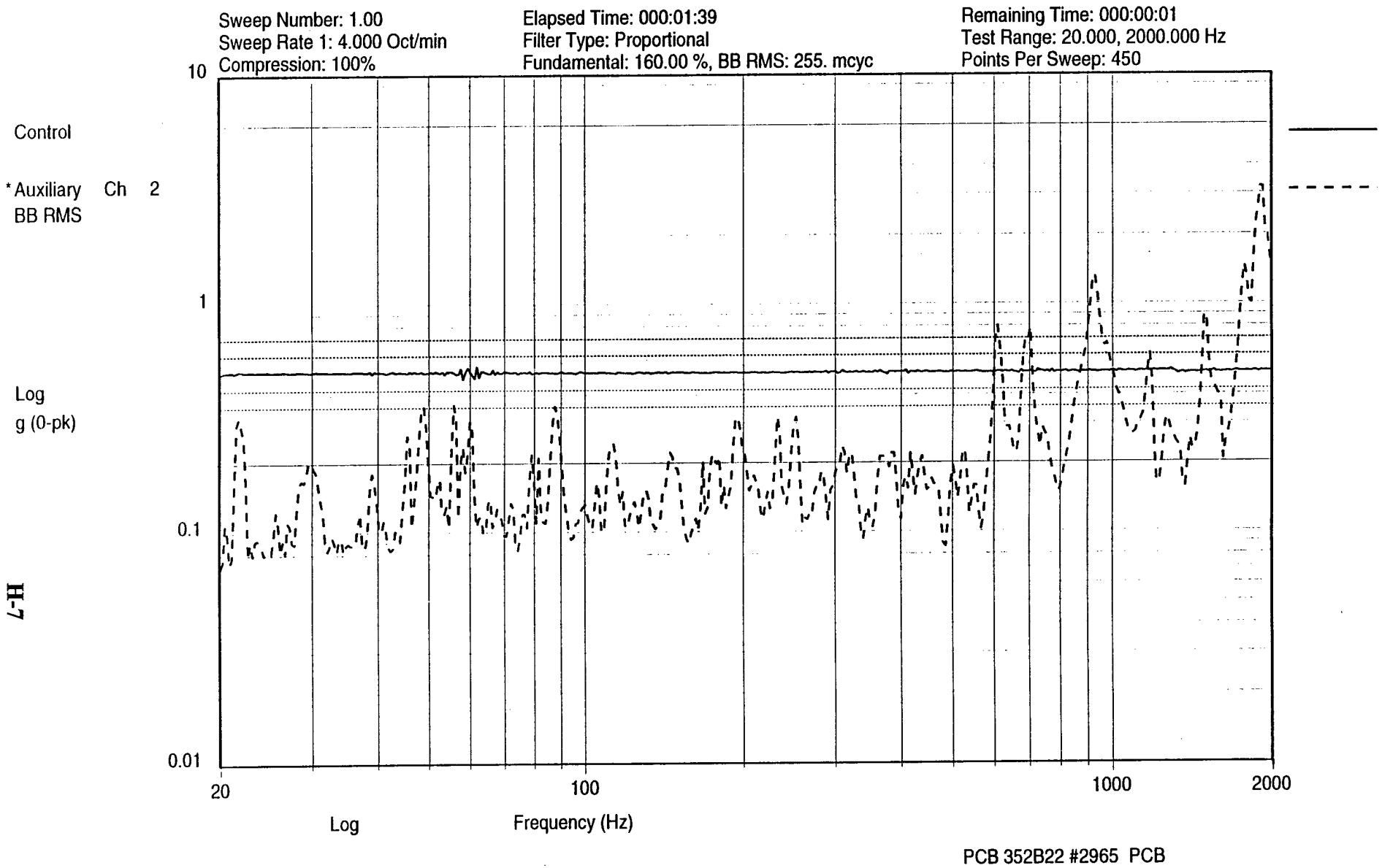


**Figure H-5. Pre-Sine Sweep, 1/2 G**

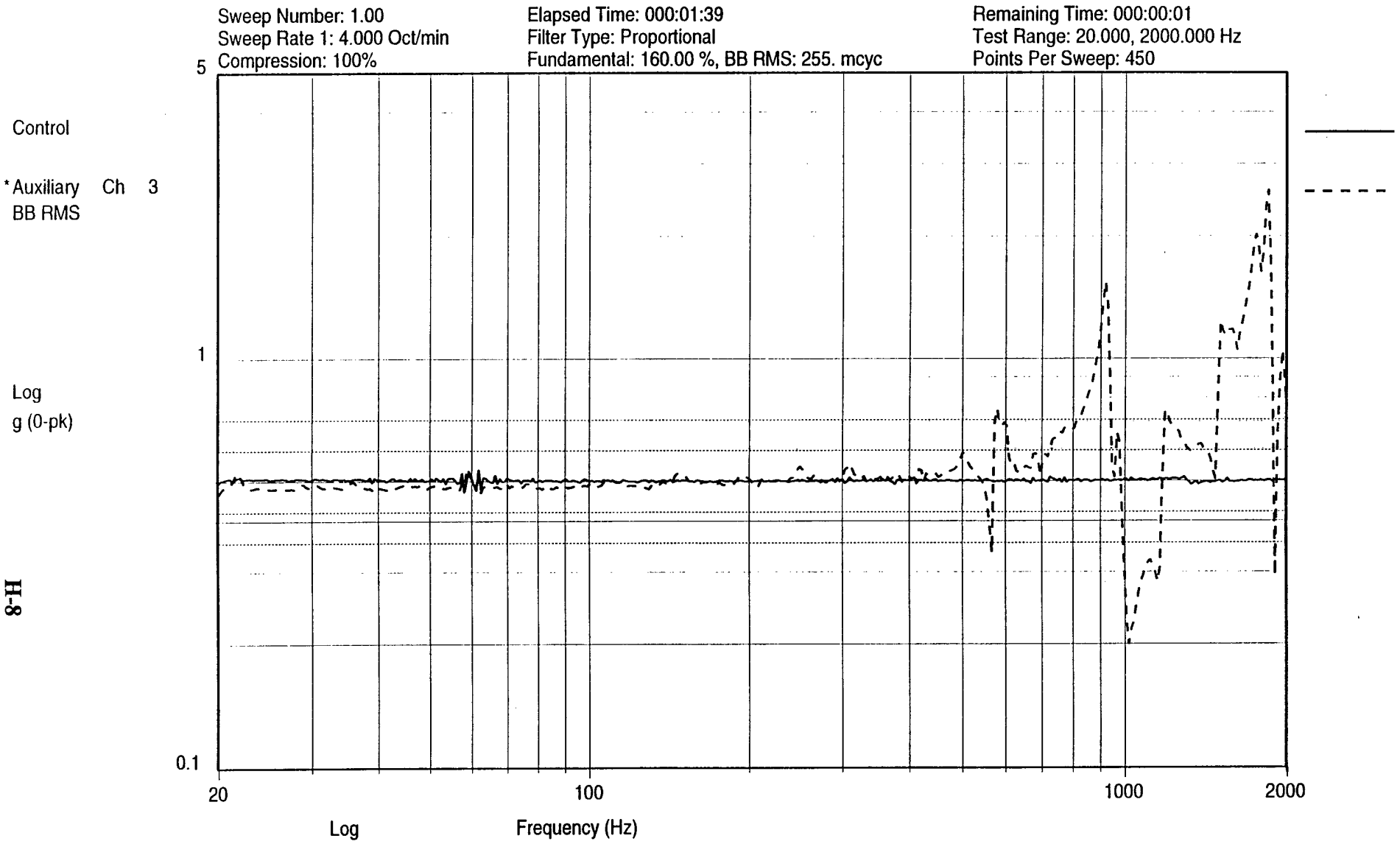


**Figure H-6. Pre-Sine Sweep, 1/2 G**

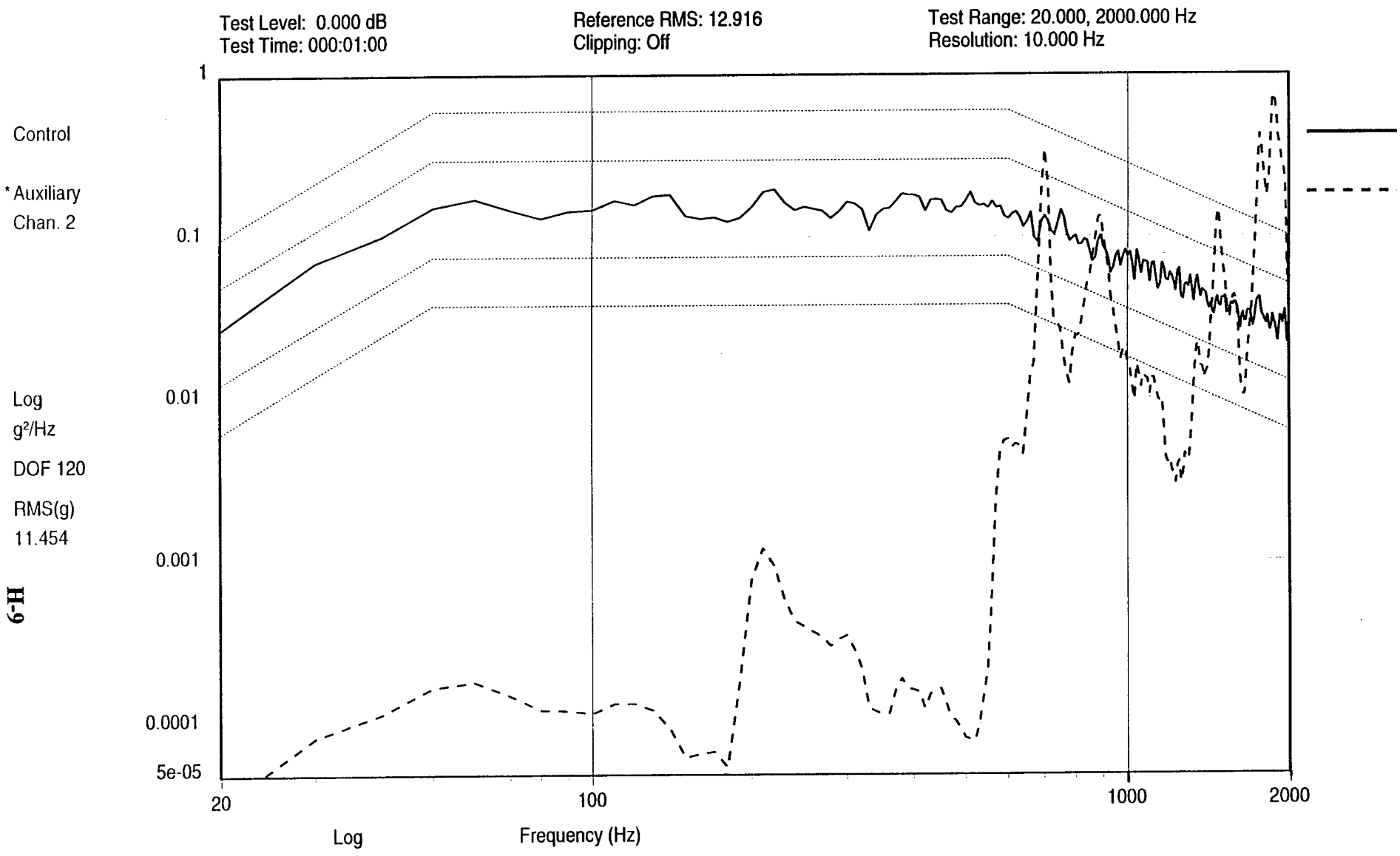


**Figure H-7. Random**

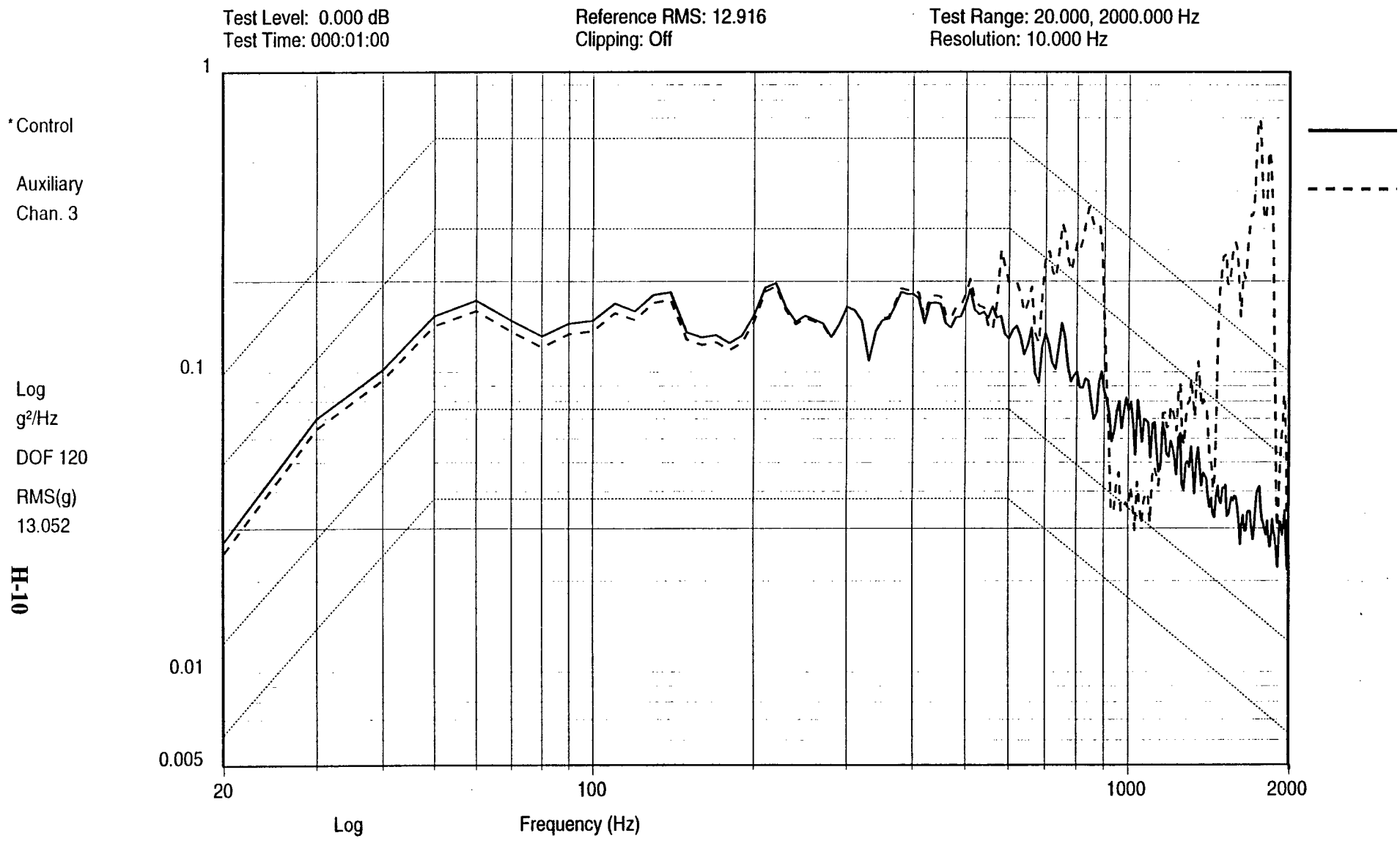


**Figure H-8. Random**

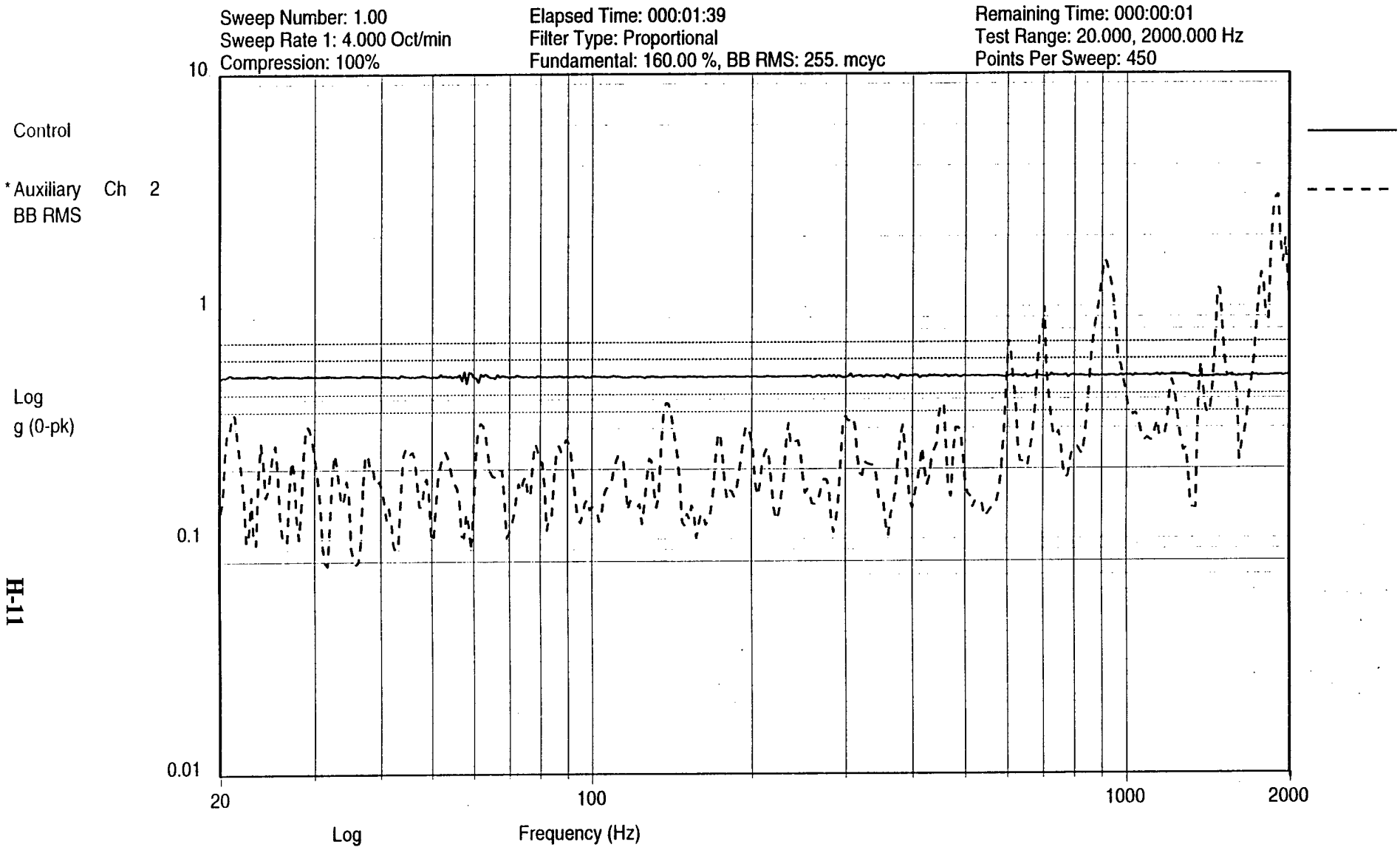


**Figure H-9. Post-Sine Sweep, 1/2 G**

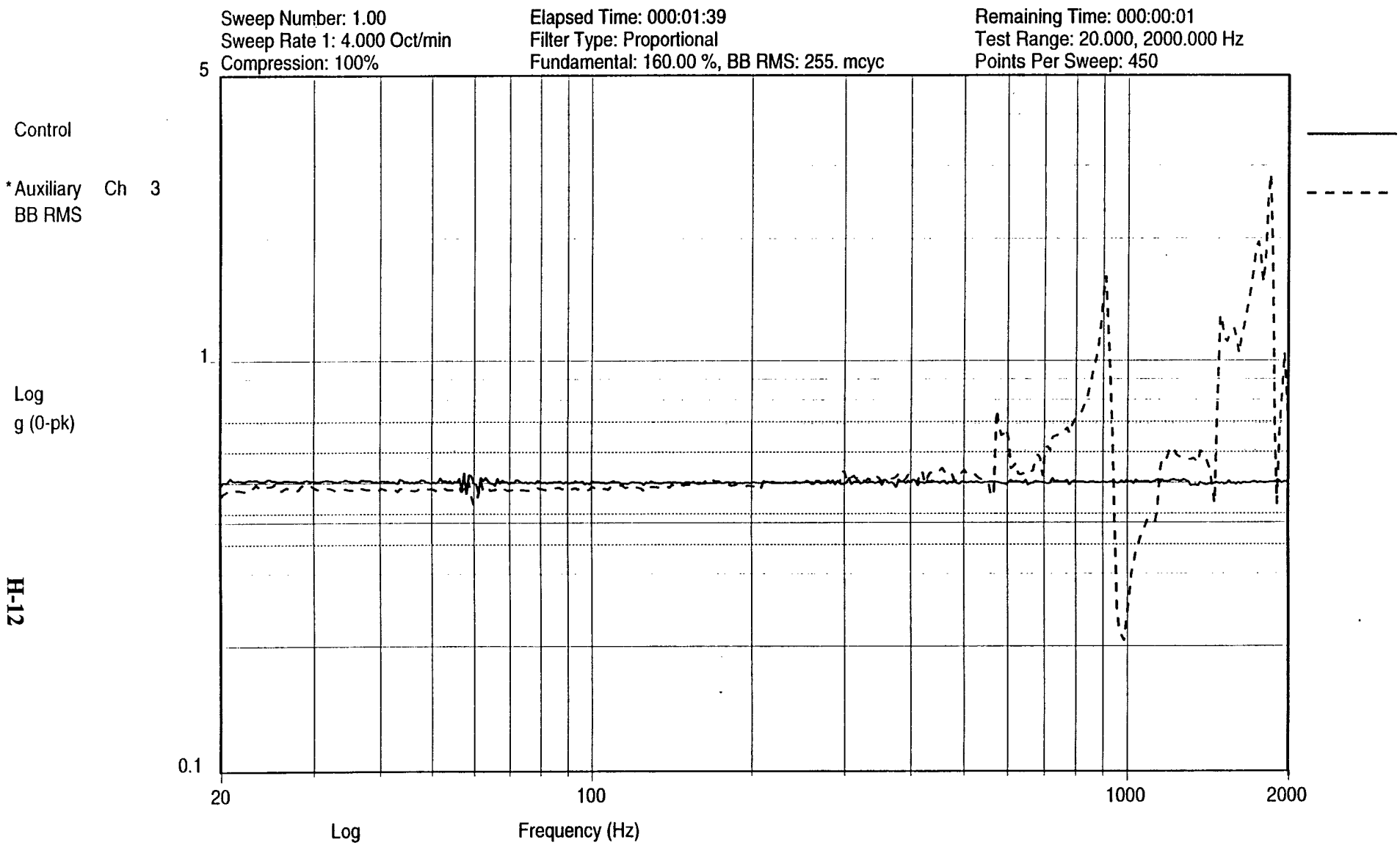


**Figure H-10. Post-Sine Sweep, 1/2 G**

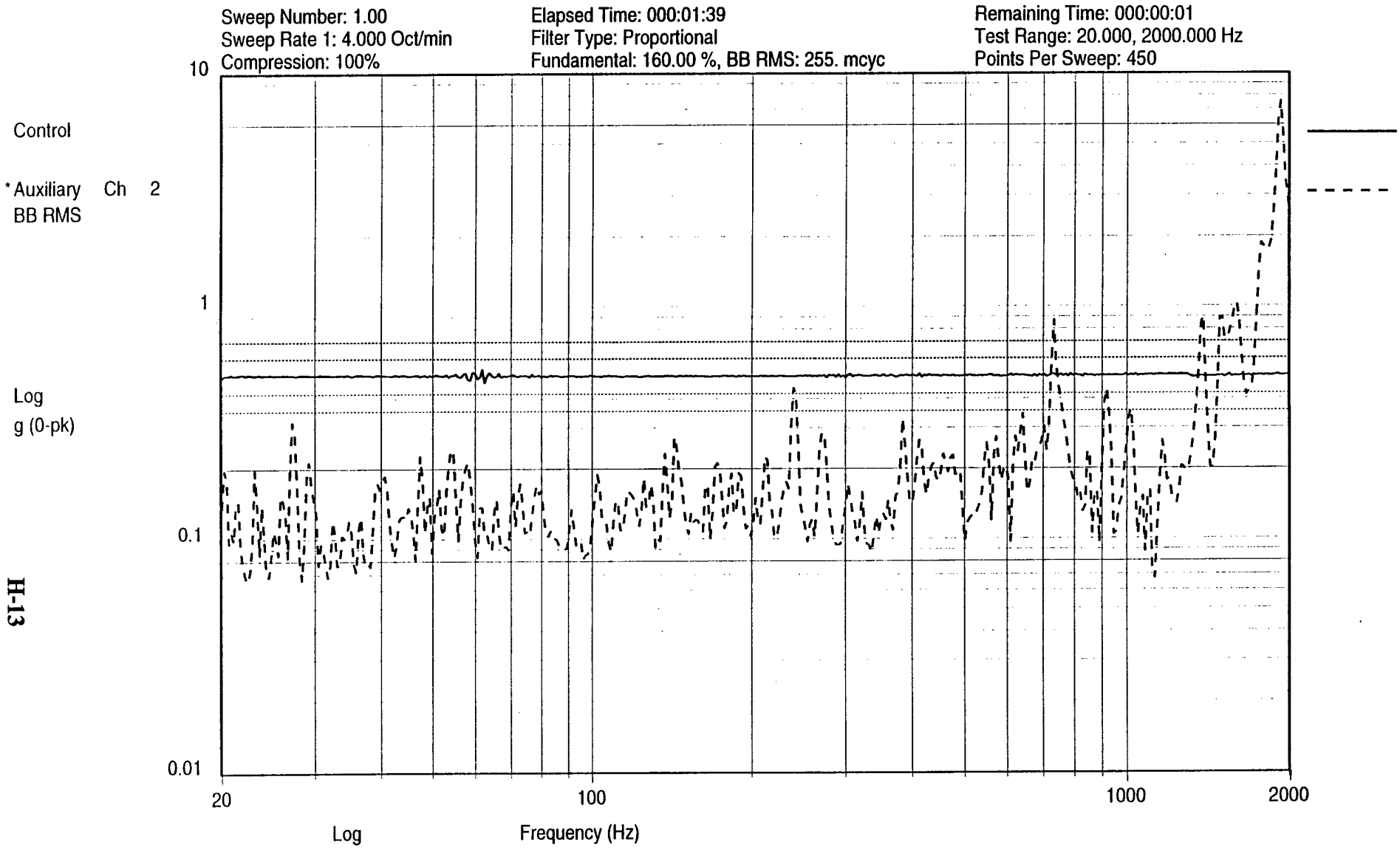


**Figure H-11 Pre-Sine Sweep, 1/2 G**

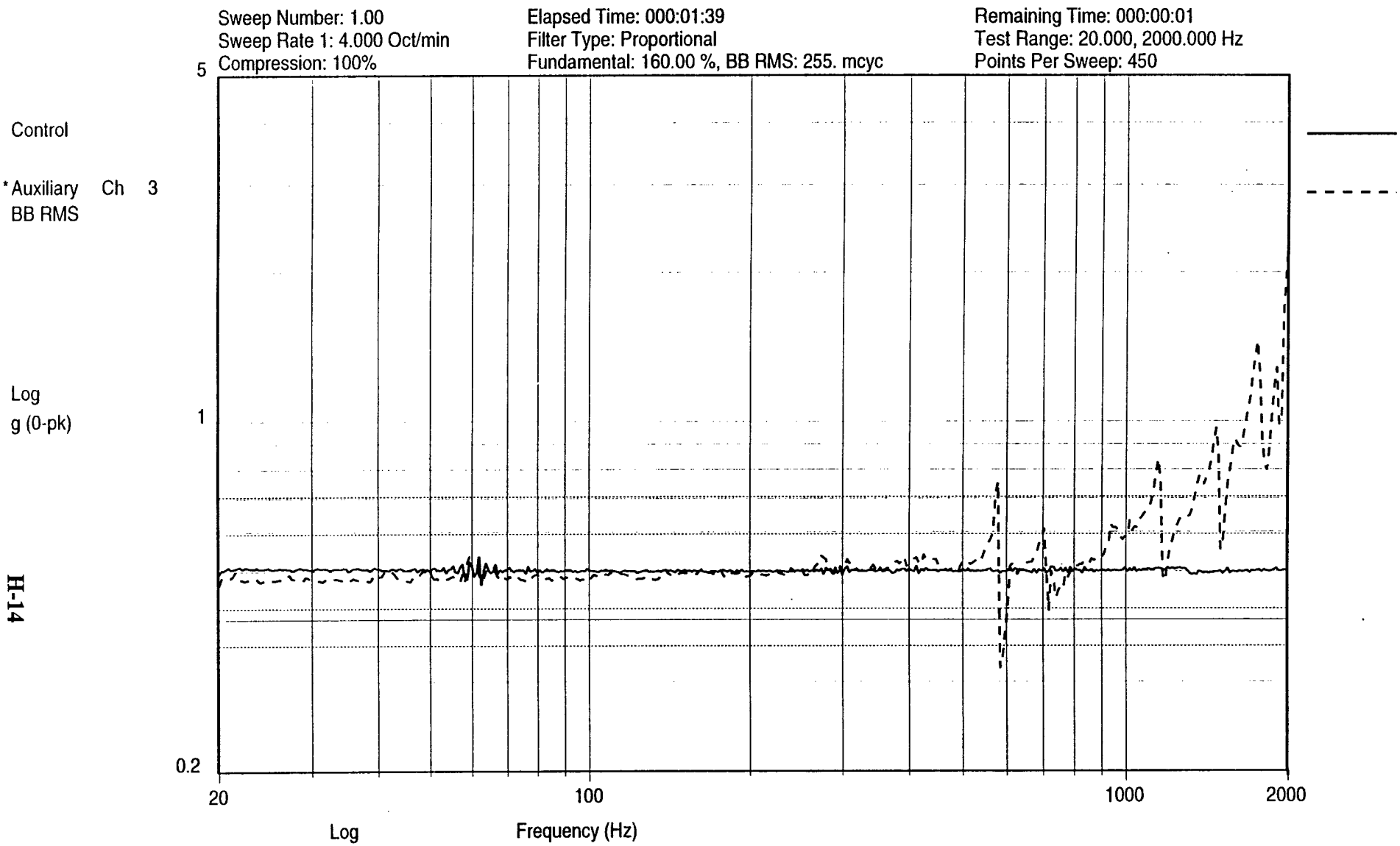


**Figure H-12. Pre-Sine Sweep, 1/2 G**

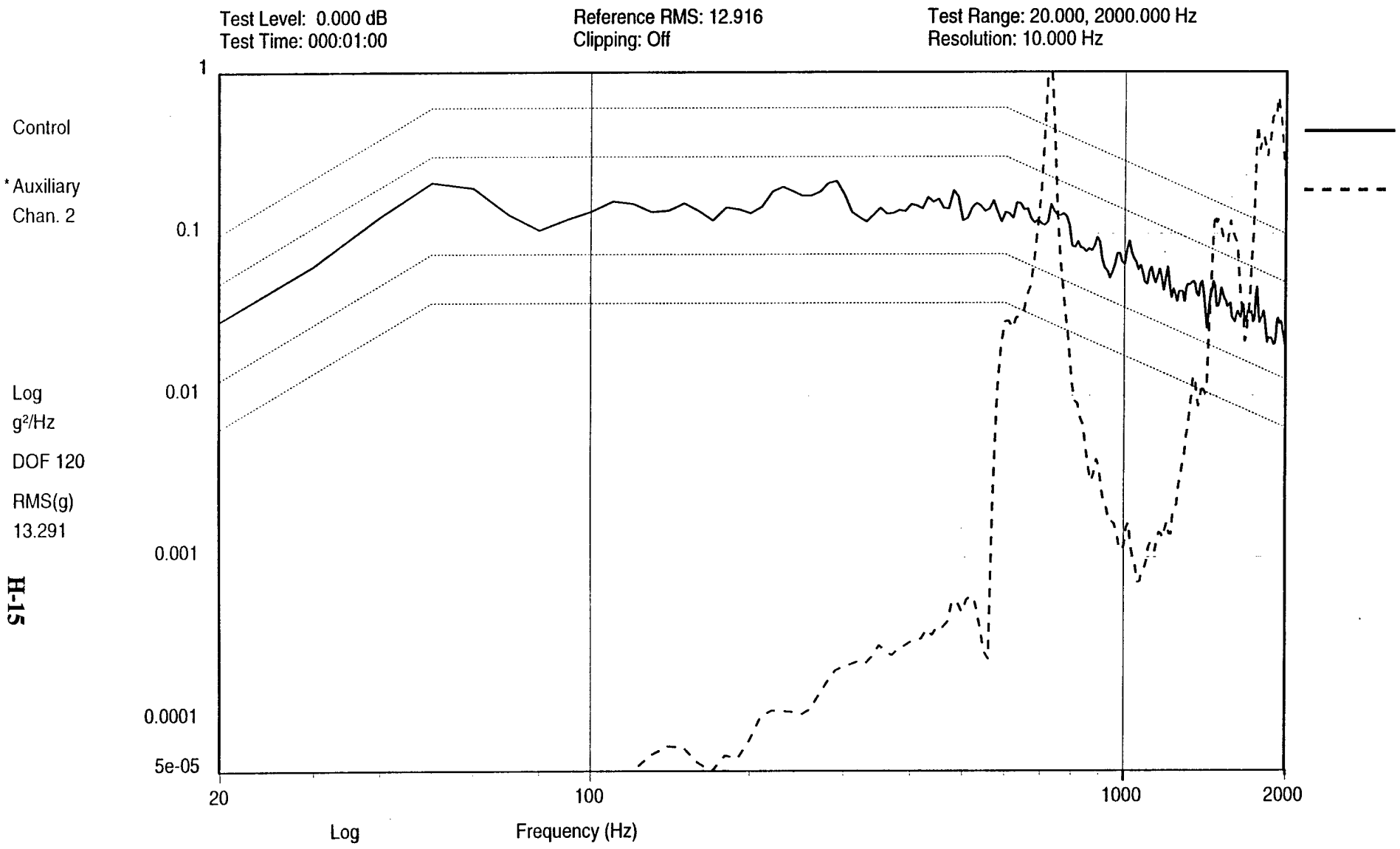


**Figure H-13. Random**

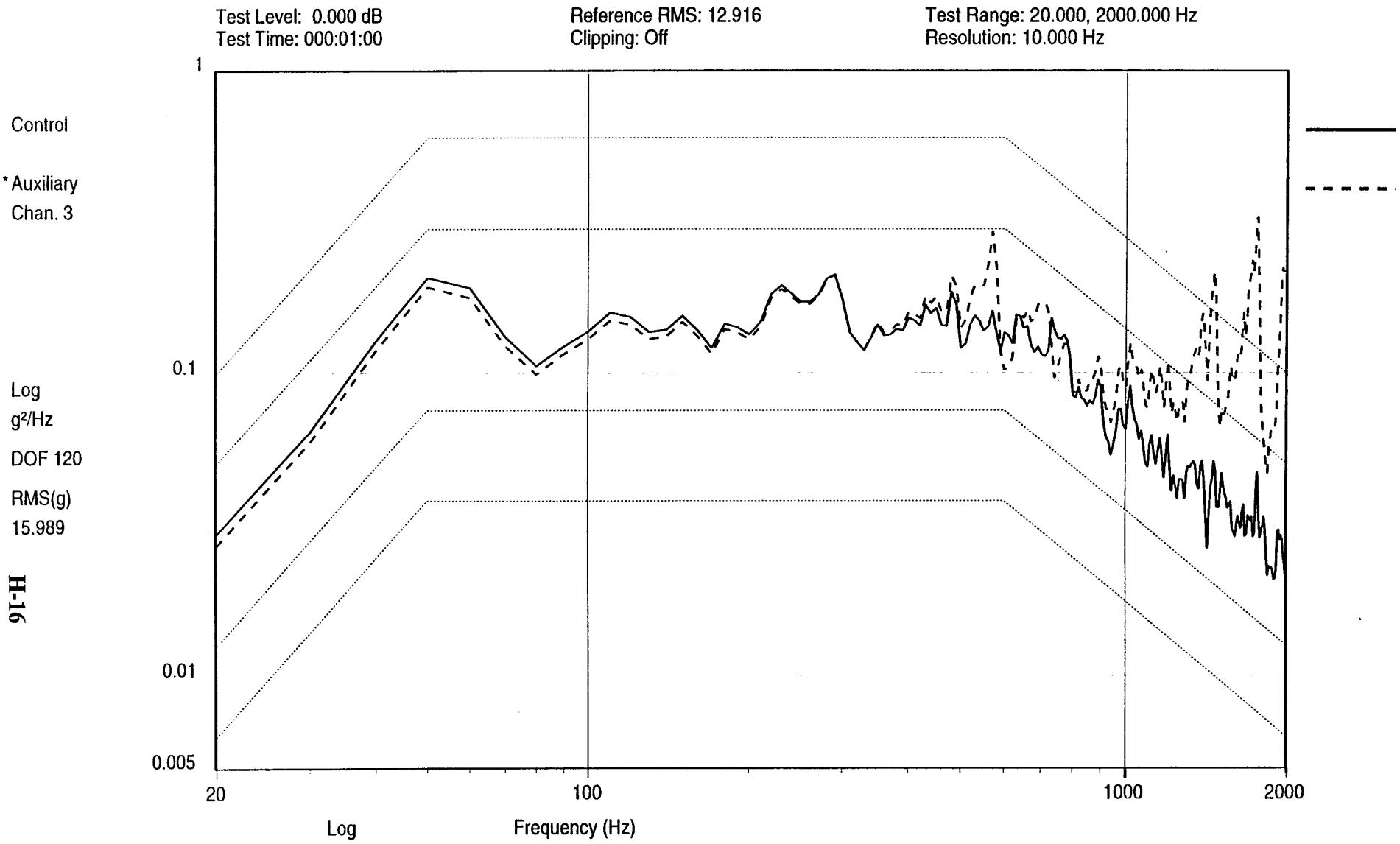


**Figure H-14. Random**

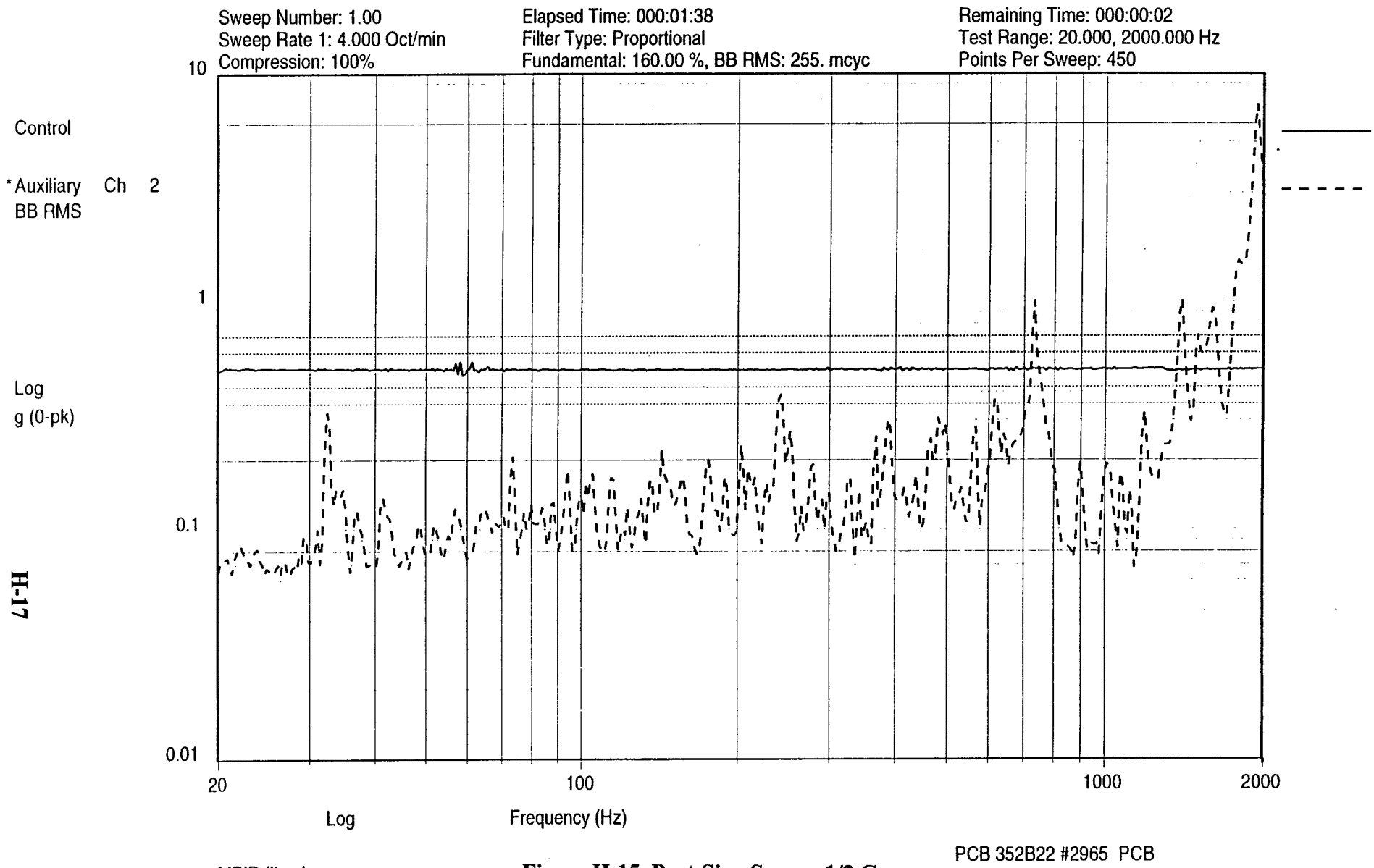


**Figure H-15. Post-Sine Sweep, 1/2 G**

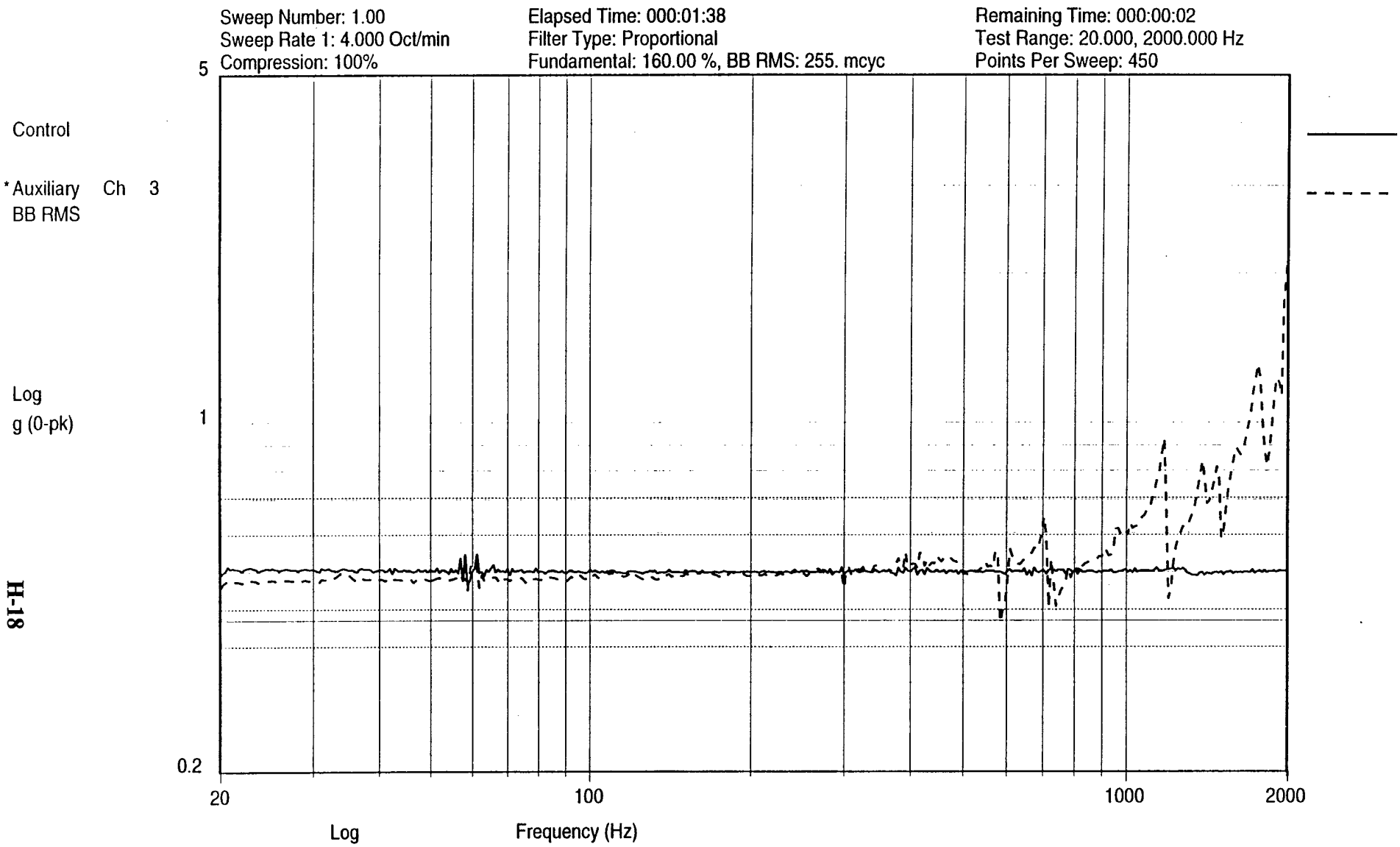


**Figure H-16. Post-Sine Sweep, 1/2 G**

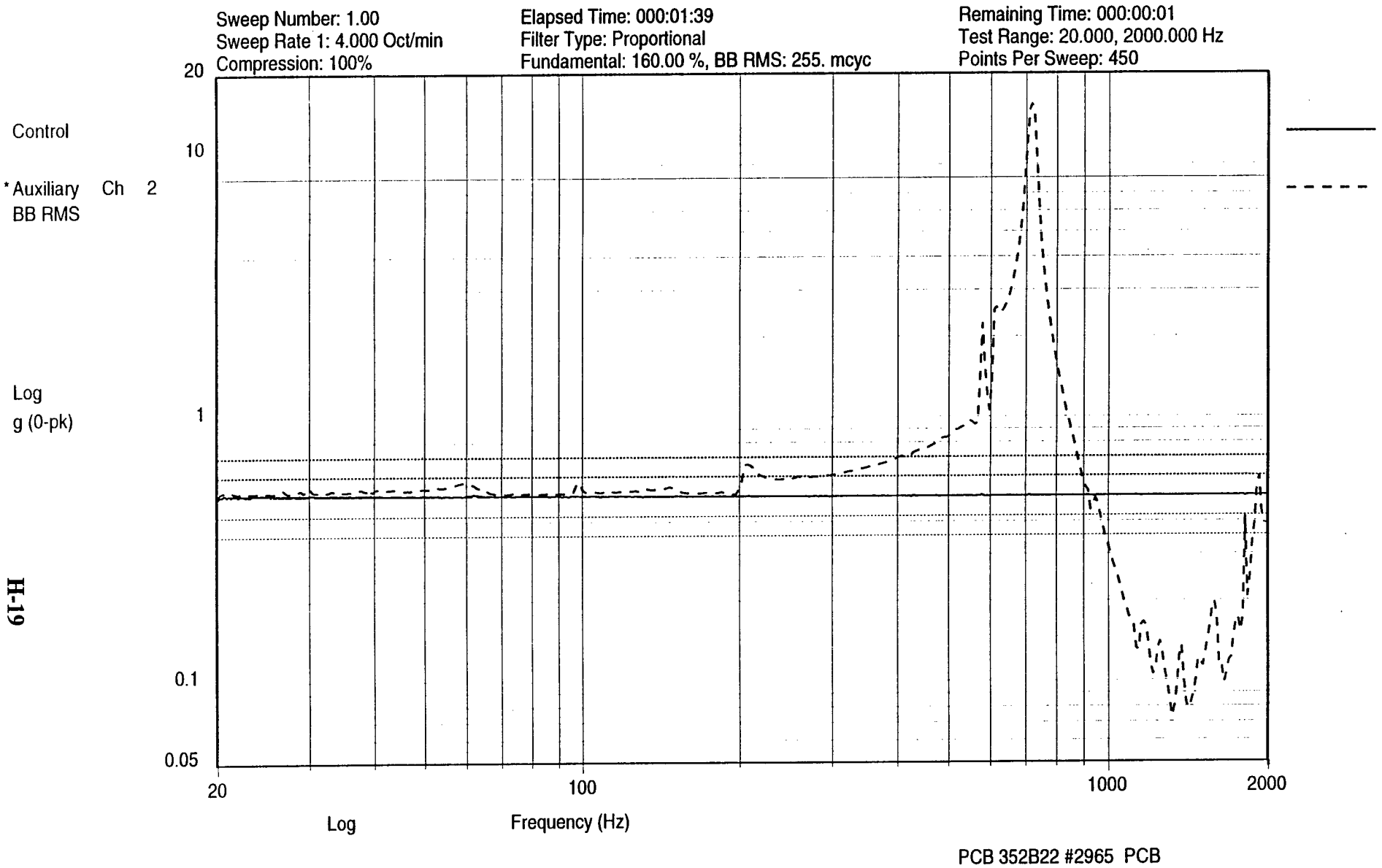


11:18:30
13-Nov-1996

MPID flt pcb
1/2 g Sine Sweep z pre
Test Name: mpid_11_13_96.006

**Figure H-17. Pre-Sine Sweep, 1/2 G**

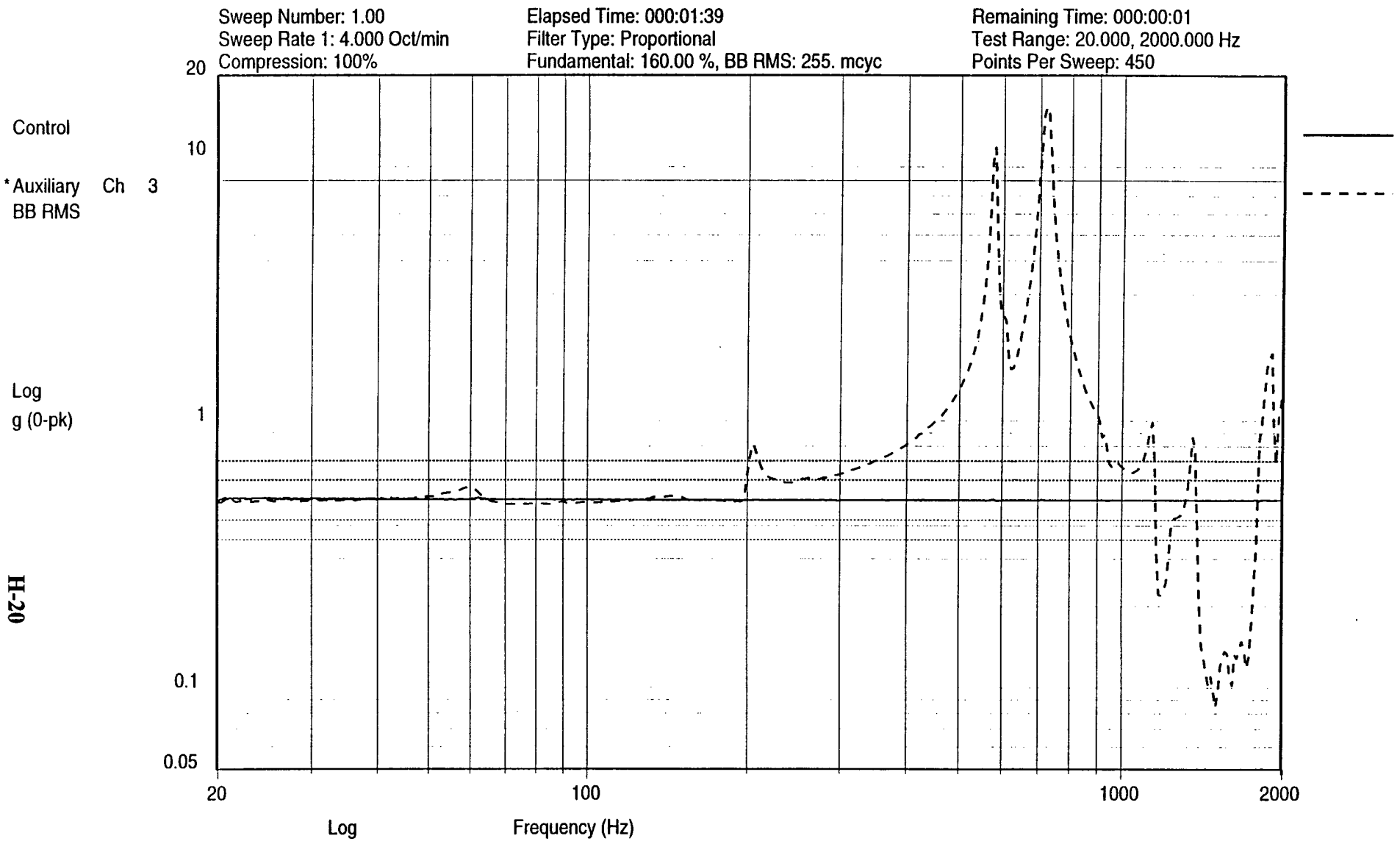


**Figure H-18. Pre-Sine Sweep, 1/2 G**

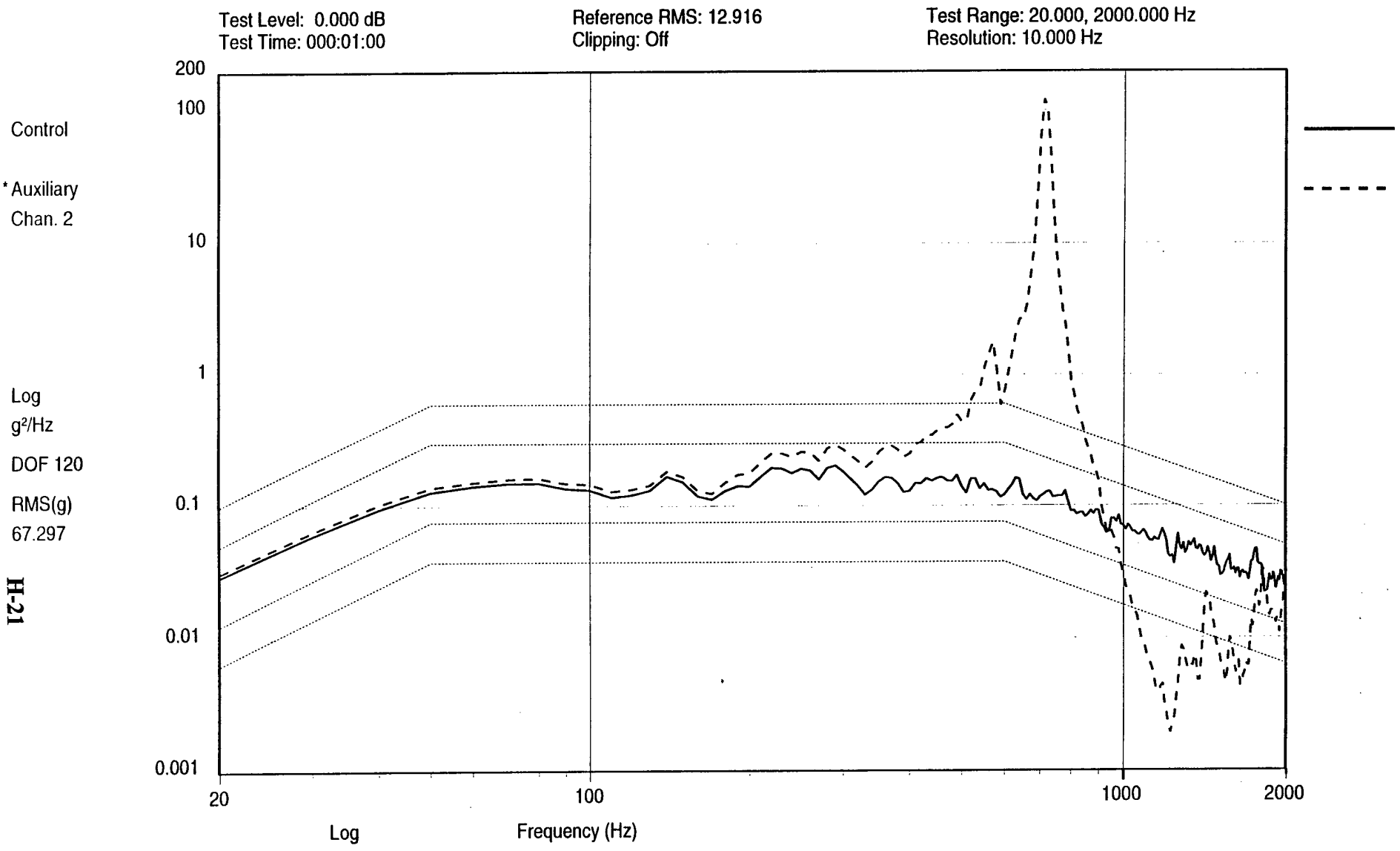


**Figure H-19. Random**

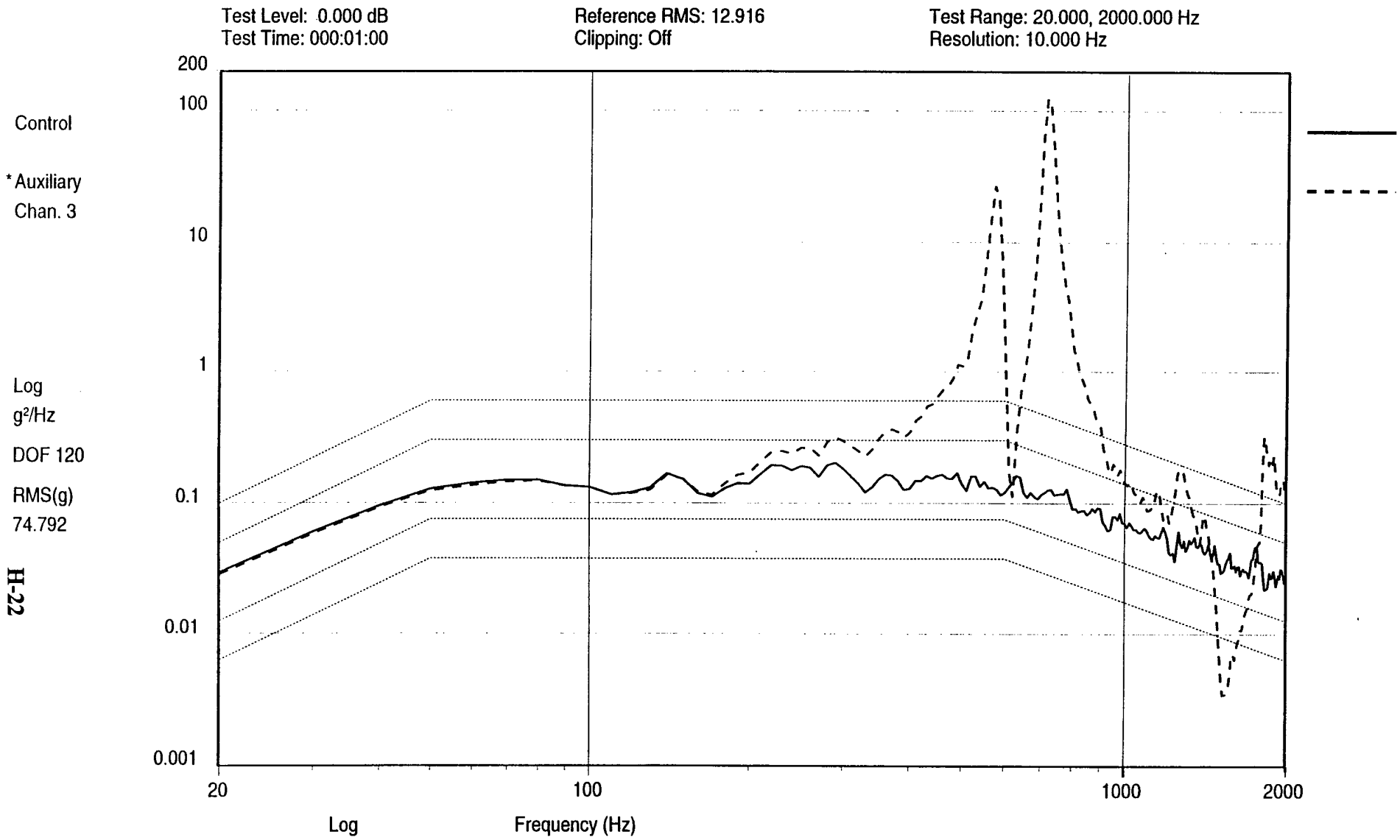


**Figure H-20. Random**

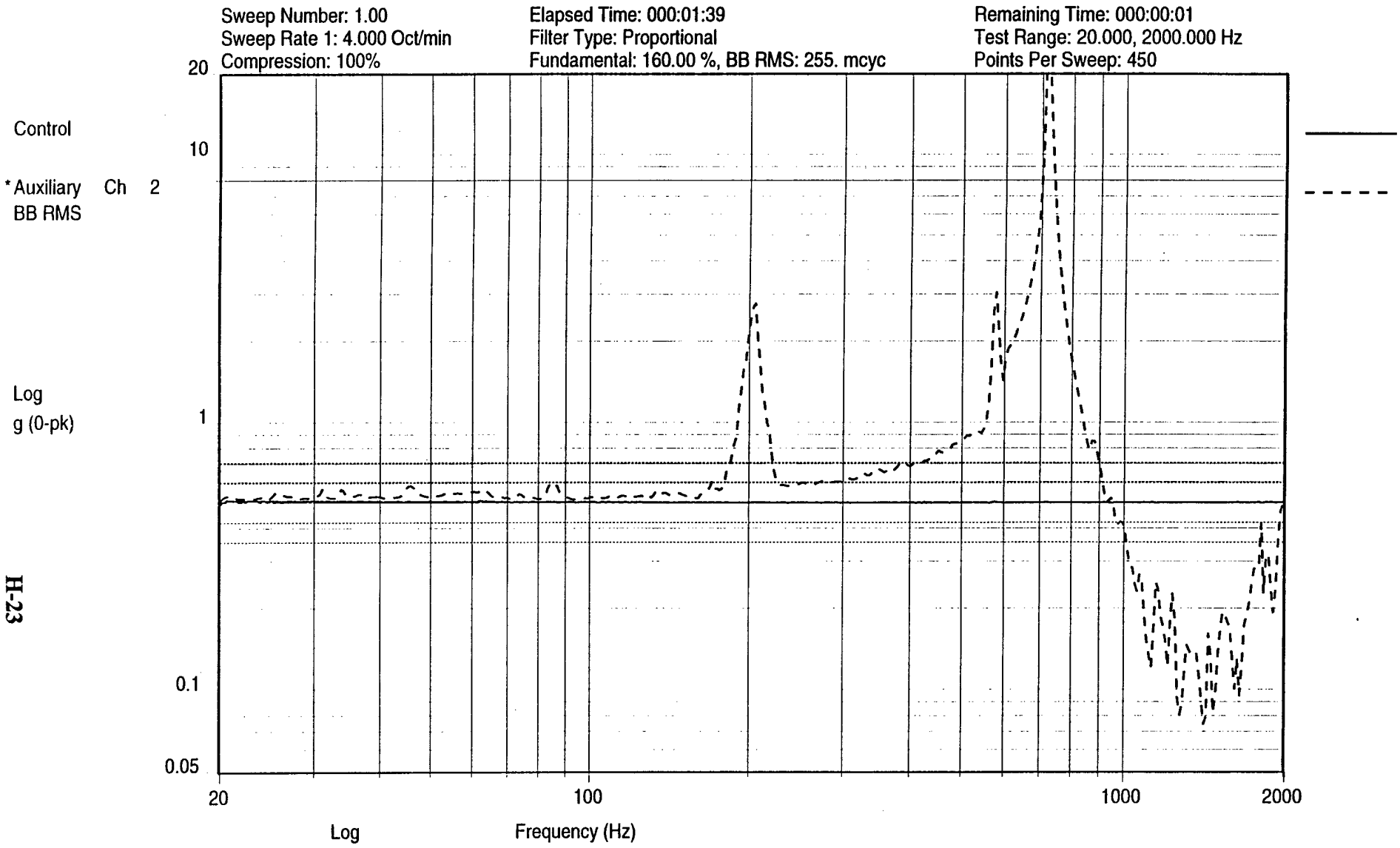




11:27:45
13-Nov-1996

MPID flt pcb
1/2 g Sine Sweep z post
Test Name: mpid_11_13_96.007

**Figure H-21. Post-Sine Sweep, 1/2 G**

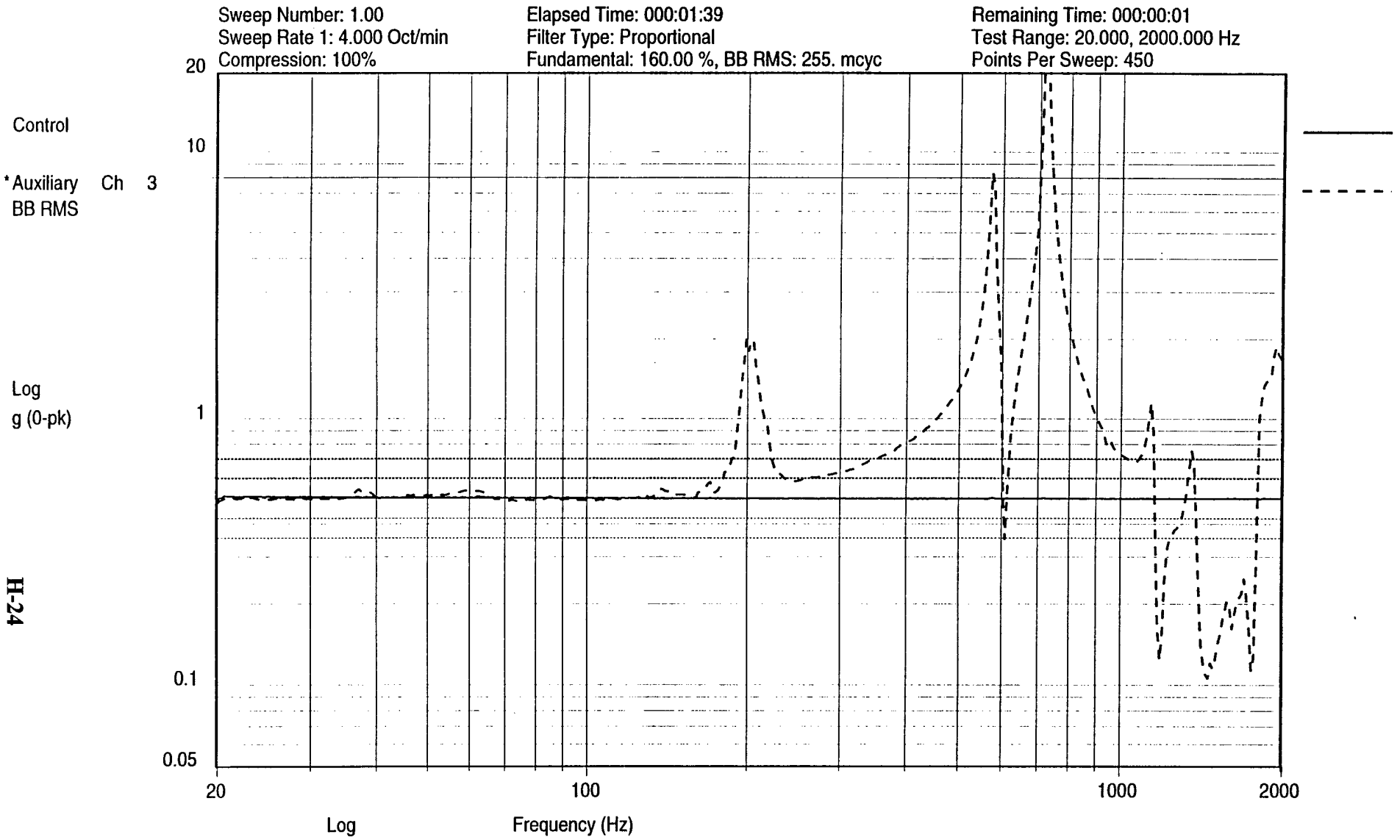


**Figure H-22. Post-Sine Sweep, 1/2 G**

# APPENDIX I

## Vibration Accelerometer Data, Detector #2

Vibration Acceleromenter Data, Detector #2

| Appendix Page Number | Figure Number | Time of Test | Vibration Axis | Accelerometer Location | Vibration Type |
|---|---|---|---|---|---|
| I-3 | I-1 | 10:48 | Z | A | Pre-Sine Sweep, 1/2 g |
| I-4 | I-2 | 10:48 | Z | B | Pre-Sine Sweep, 1/2 g |
| I-5 | I-3 | 10:54 | Z | A | Random |
| I-6 | I-4 | 10:54 | Z | B | Random |
| I-7 | I-5 | 10:59 | Z | A | Post-Sine Sweep, 1/2 g |
| I-8 | I-6 | 10:59 | Z | B | Post-Sine Sweep, 1/2 g |
| I-9 | I-7 | 15:25 | X | Control | Pre-Sine Sweep, 1/2 G |
| I-10 | I-8 | 15:29 | X | Control | Random |
| I-11 | I-9 | 15:34 | X | Control | Post-Sine Sweep, 1/2 G |
| I-12 | I-10 | 16:03 | Y | Control | Pre-Sine Sweep, 1/2 G |
| I-13 | I-11 | 16:07 | Y | Control | Random |
| I-14 | I-12 | 16:11 | Y | Control | Post-Sine Sweep, 1/2 G |

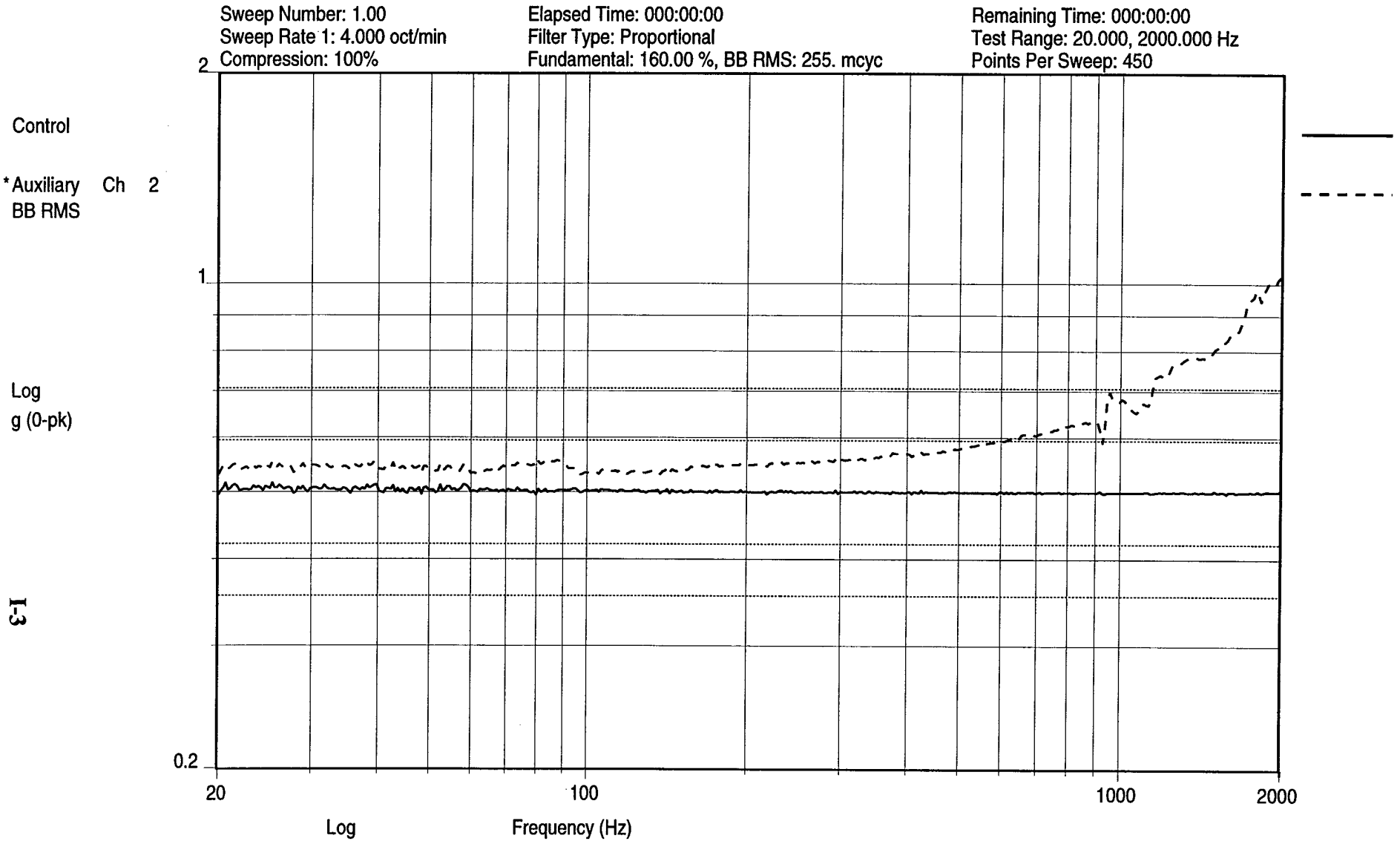


**Figure I-1. Pre-Sine Sweep, 1/2 g**

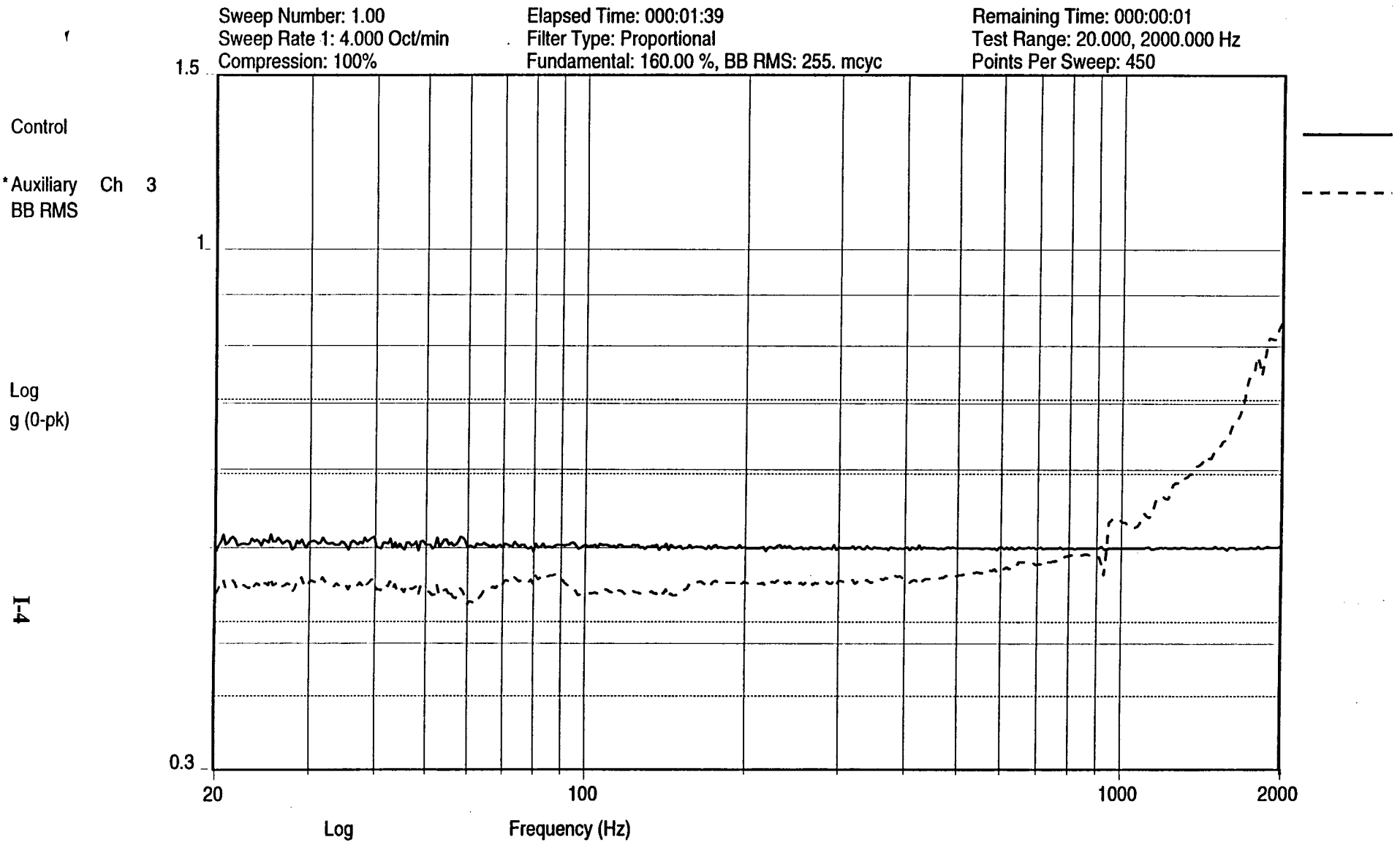


**Figure I-2. Pre-Sine Sweep, 1/2 g**

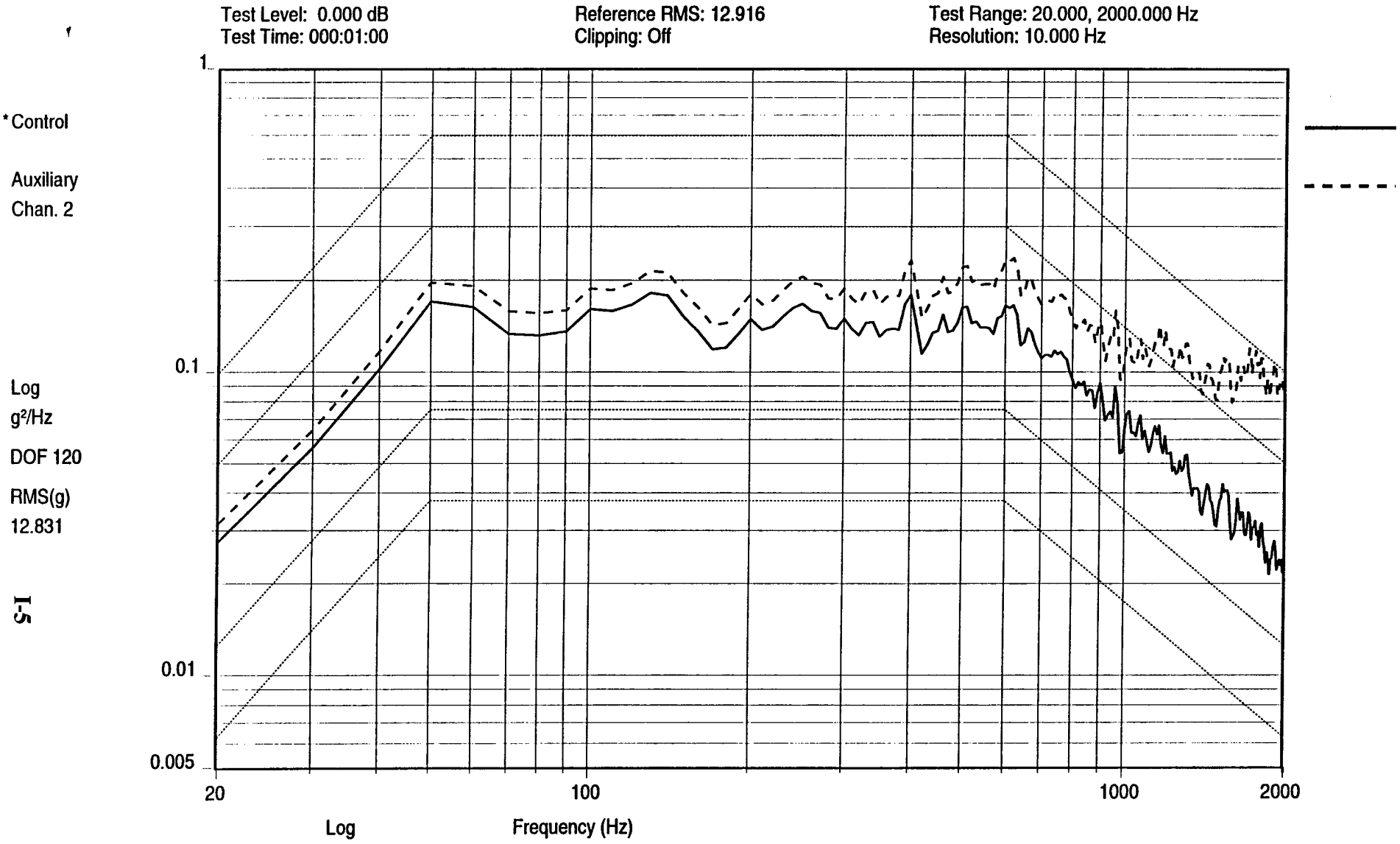


**Figure I-3. Random**

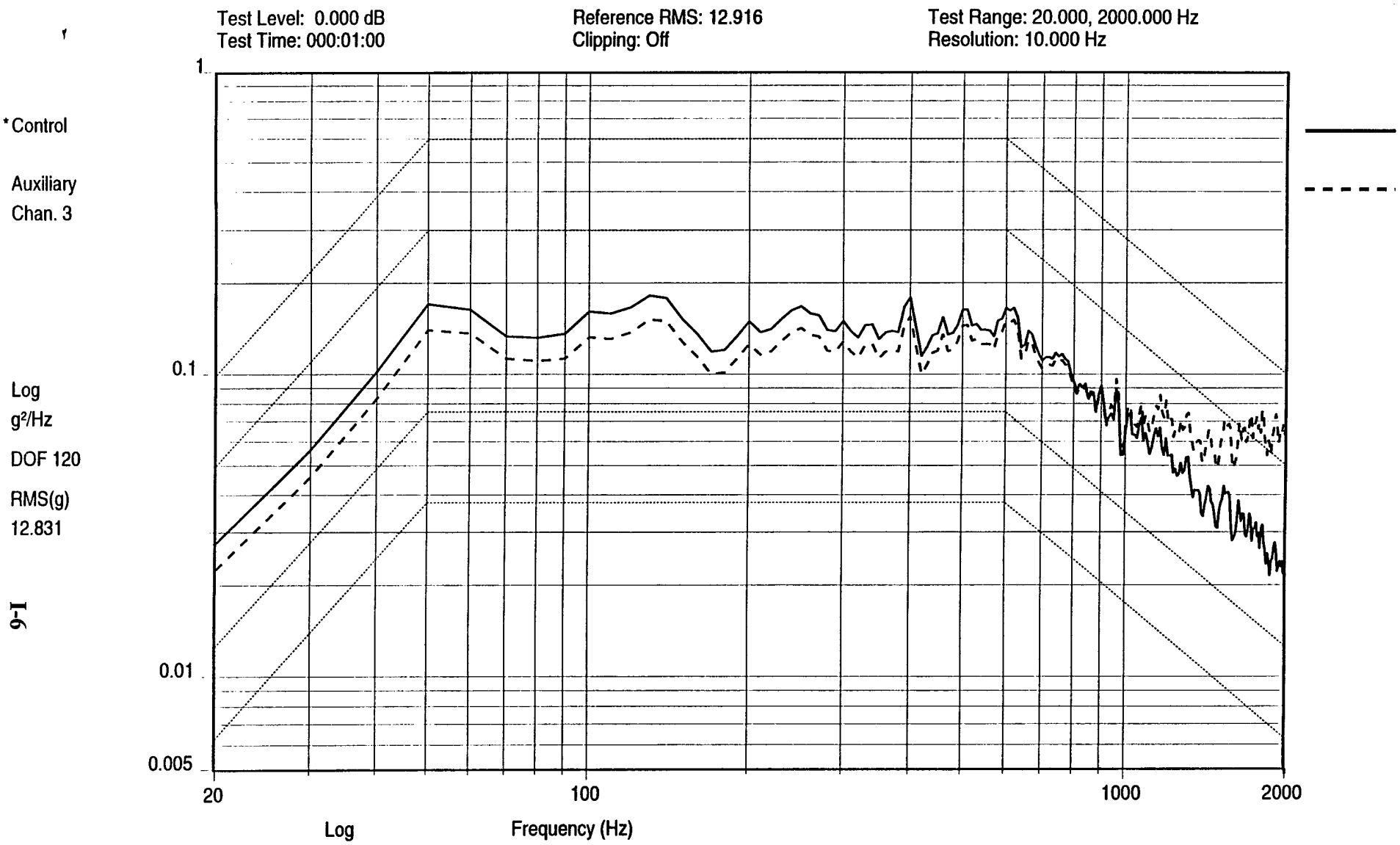


**Figure I-4. Random**

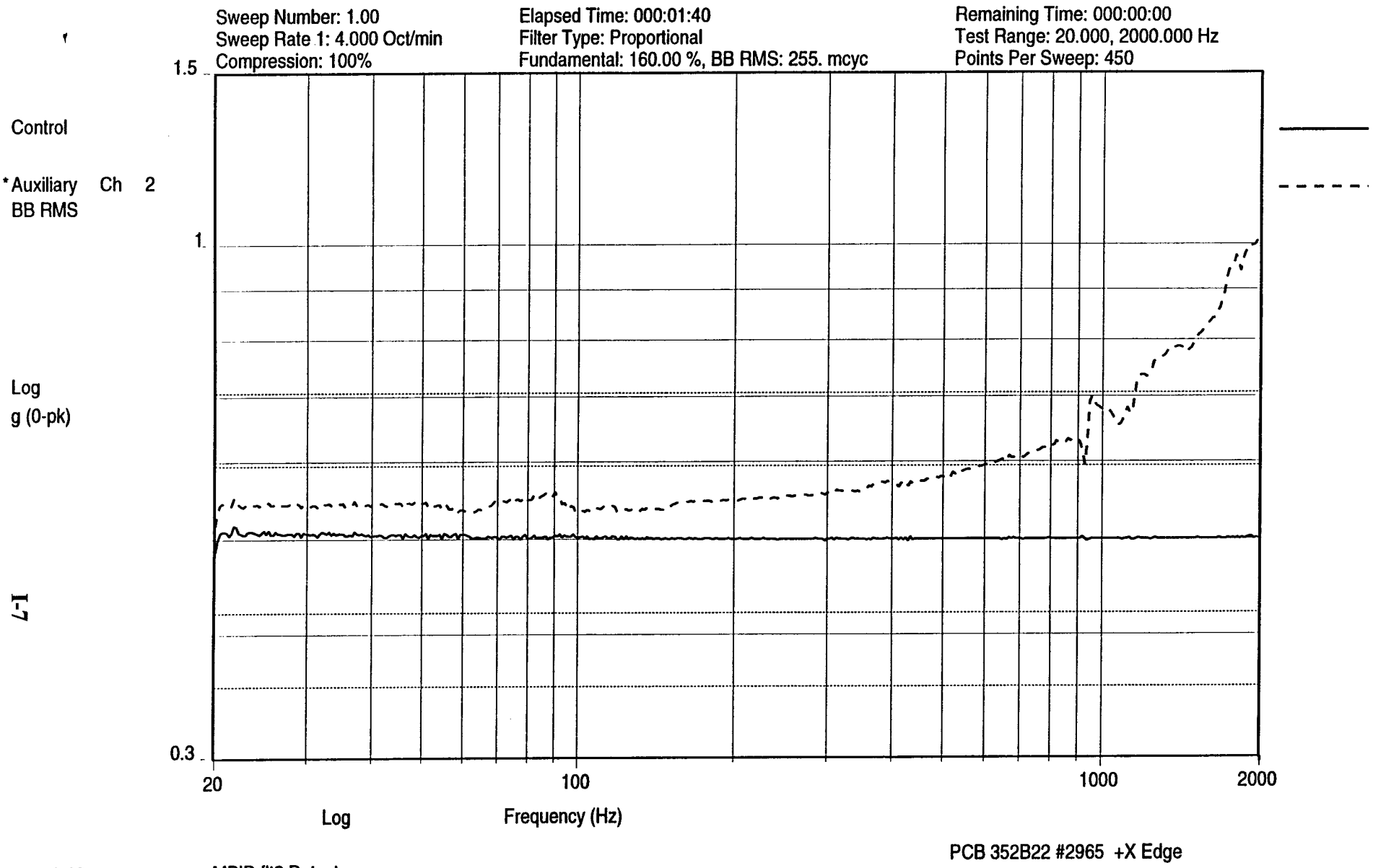


**Figure I-5. Post-Sine Sweep, 1/2 G**

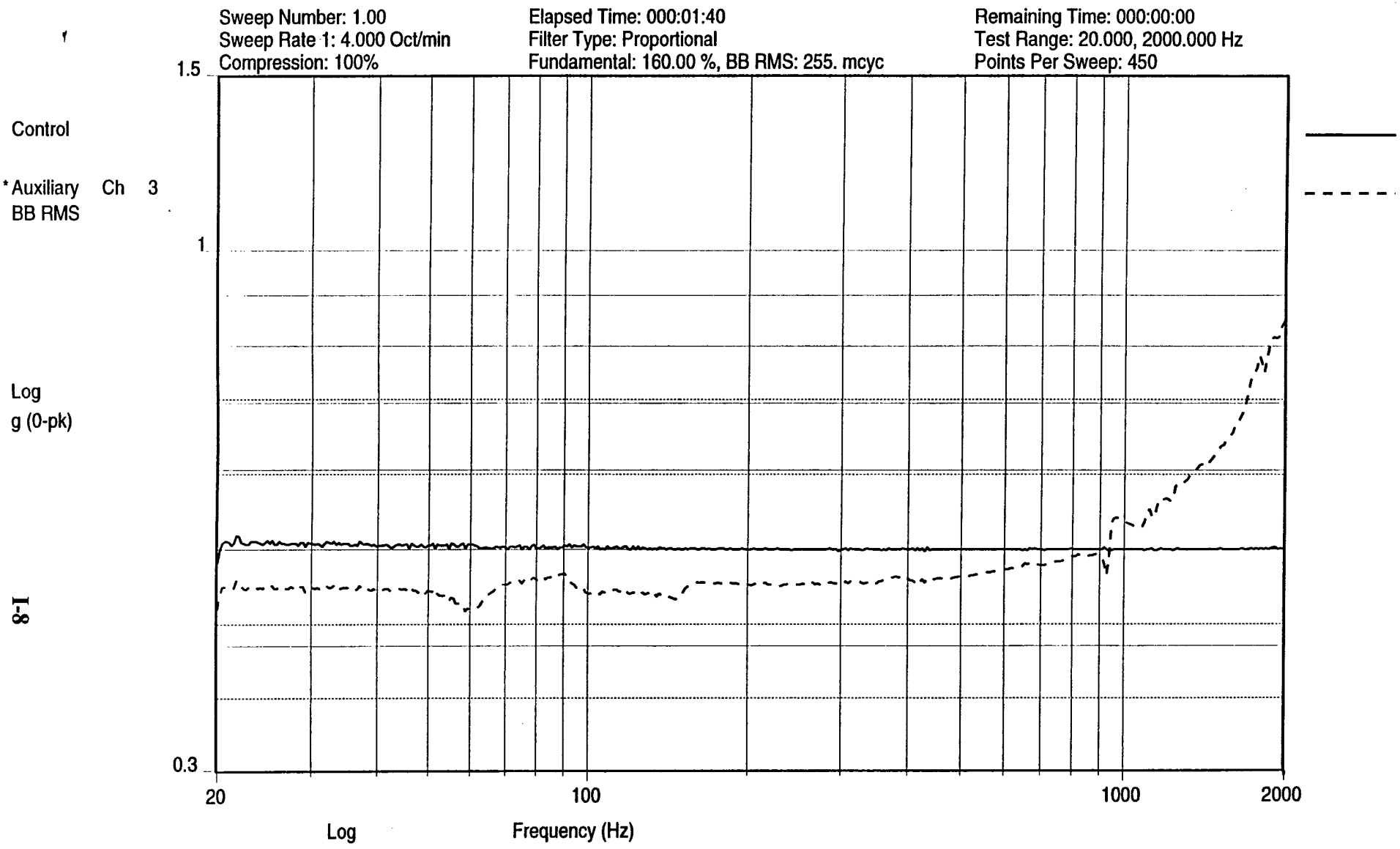


**Figure I-6. Post-Sine Sweep, 1/2 G**

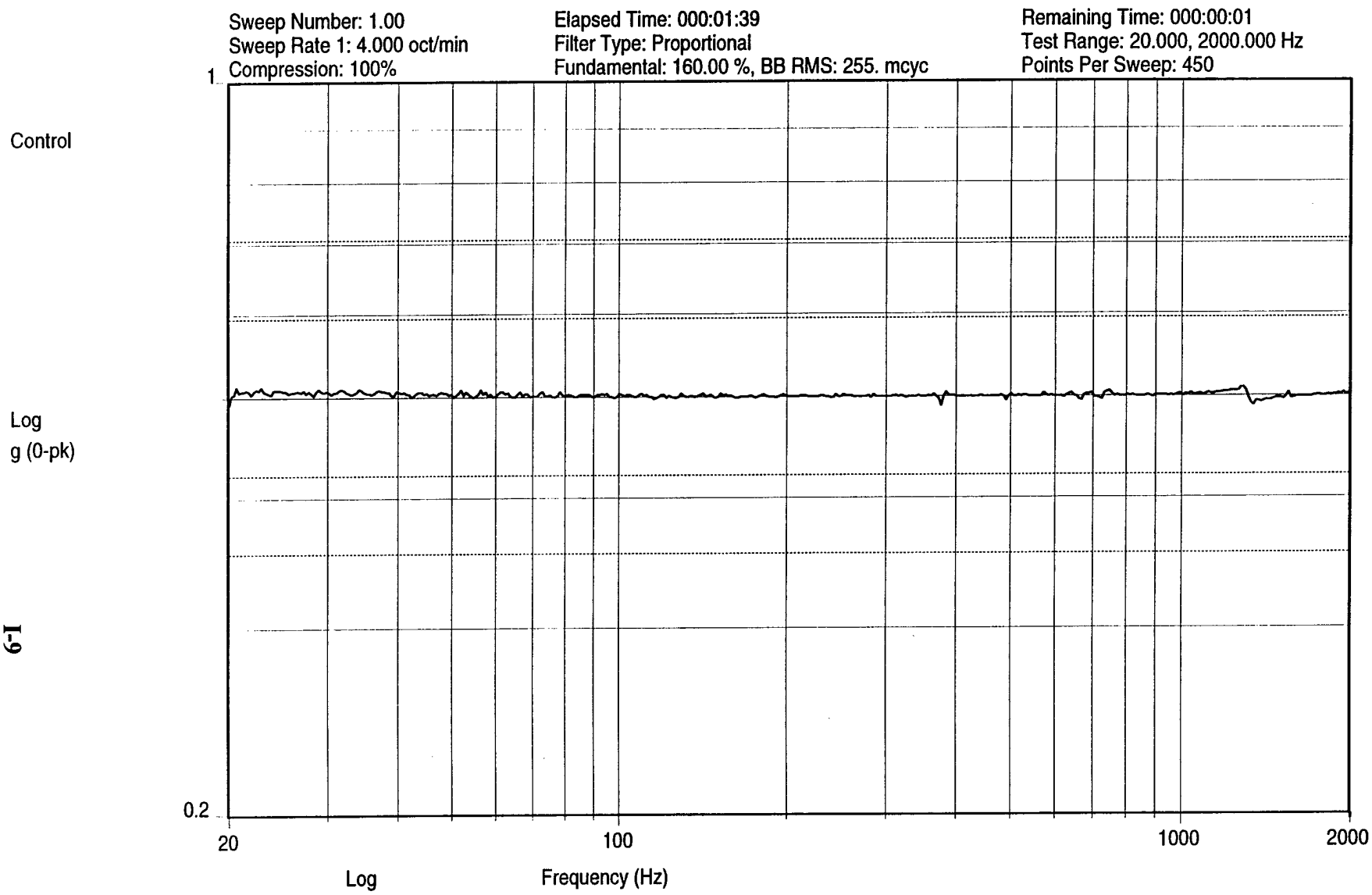


**Figure I-7. Pre-Sine Sweep, 1/2 G**

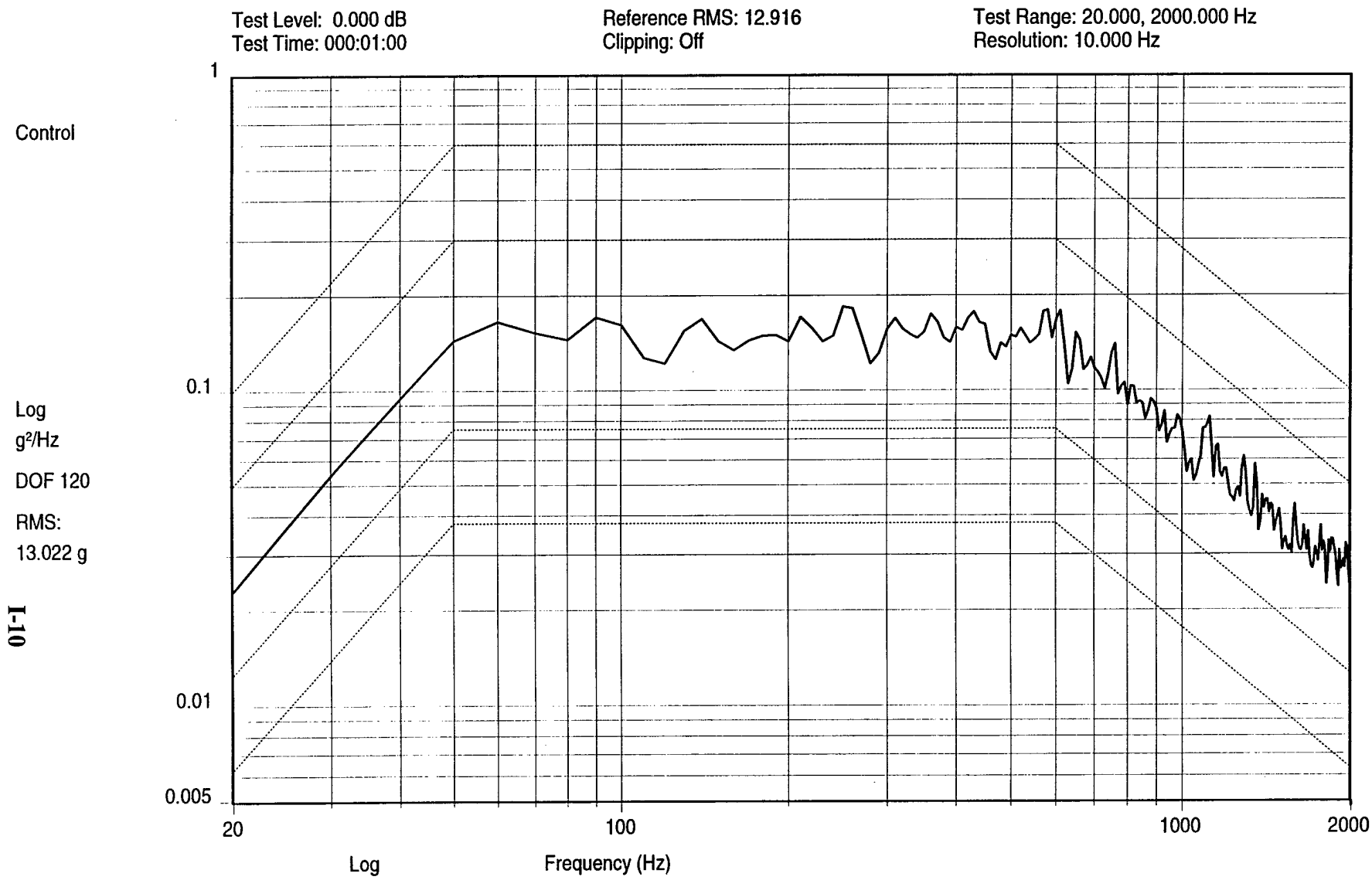


**Figure I-8. Random**

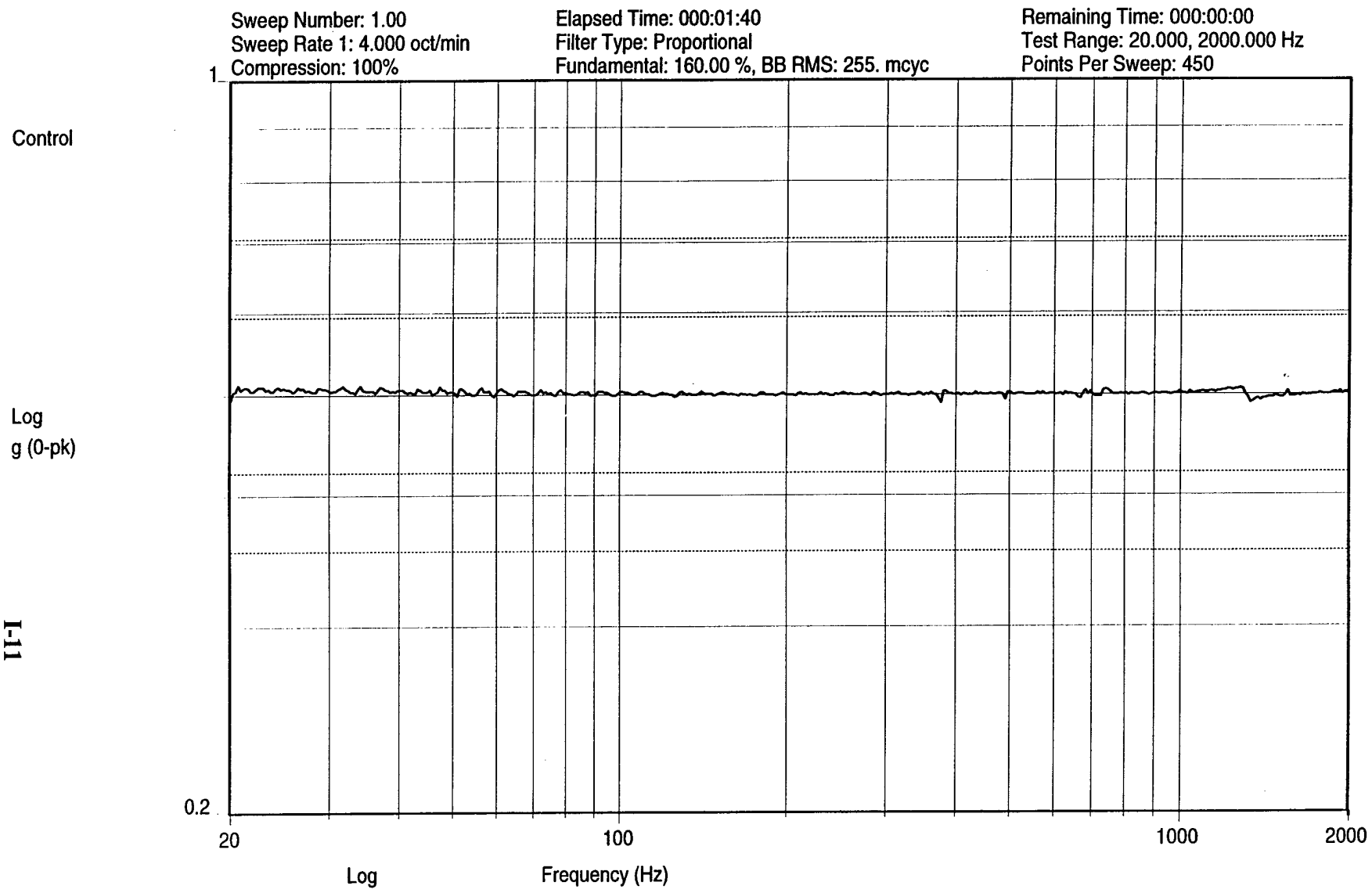


**Figure I-9. Post-Sine Sweep, 1/2 G**

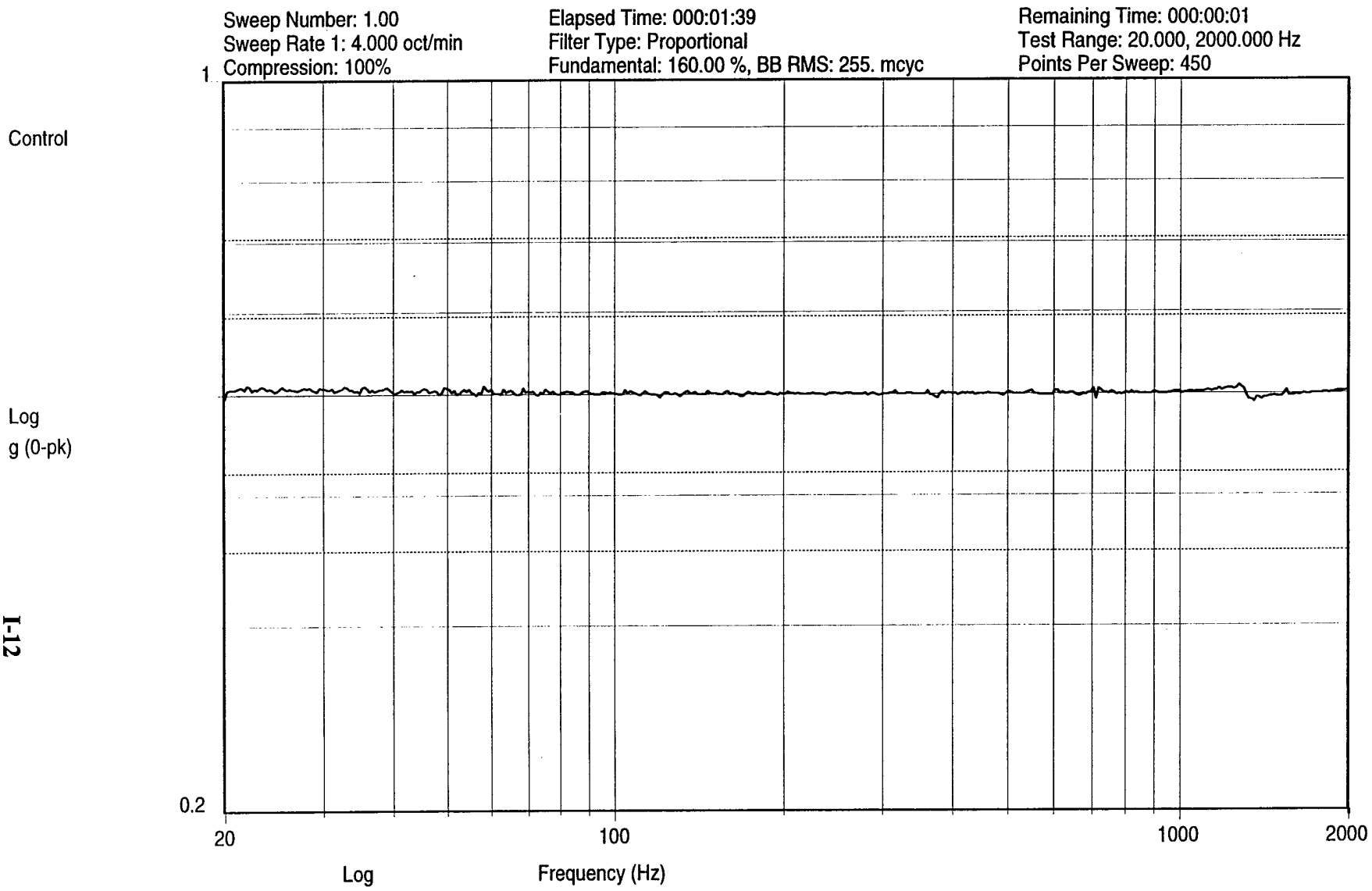


16:03:29
Wed Jan 08 1997

MPID flt3 Detector
1/2 g Sine Sweep y pre

Sine Data Review Name: mpid_1_8_97.010

**Figure I-10. Pre-Sine Sweep, 1/2 G**

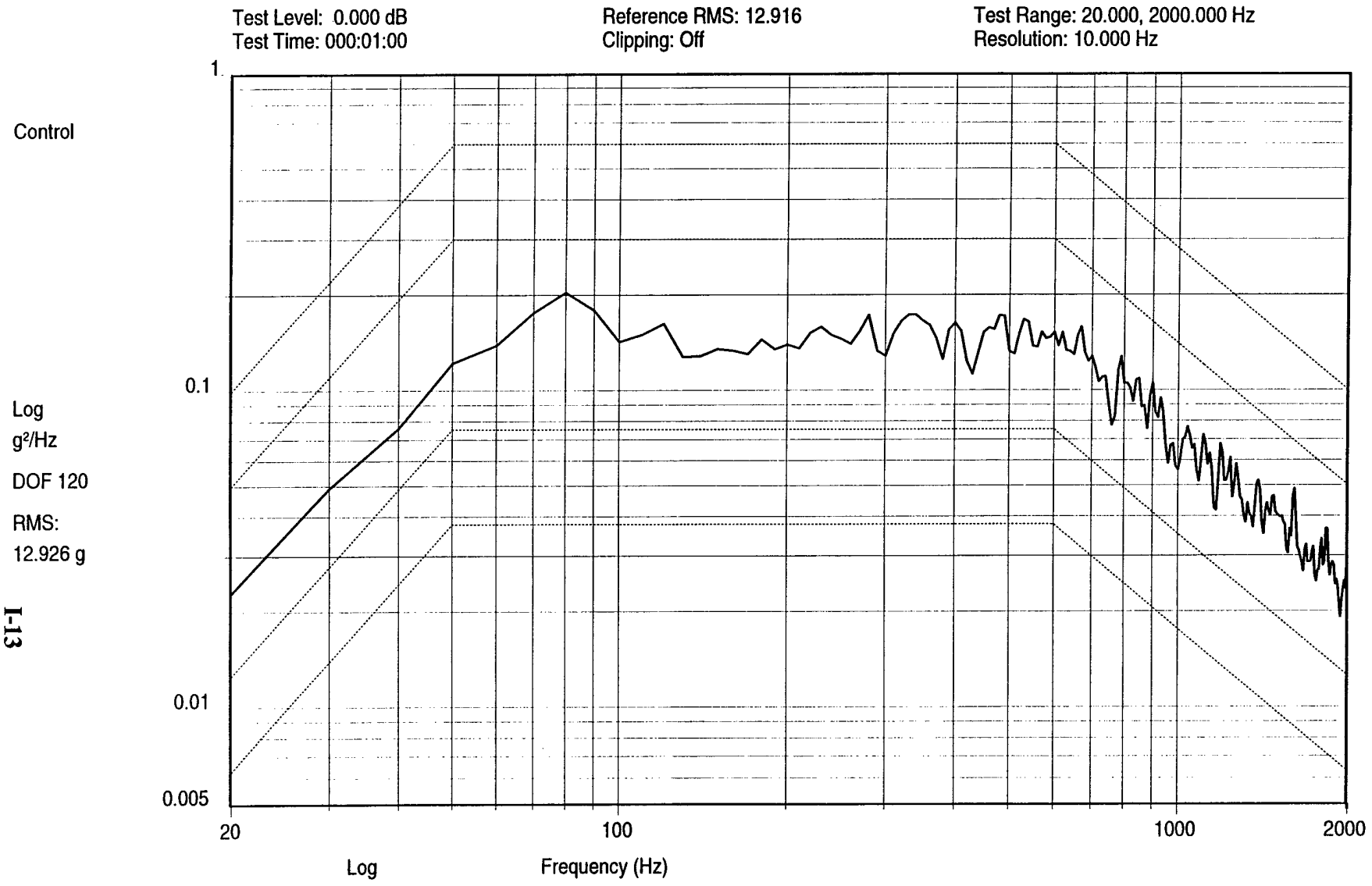


**Figure I-11. Random**

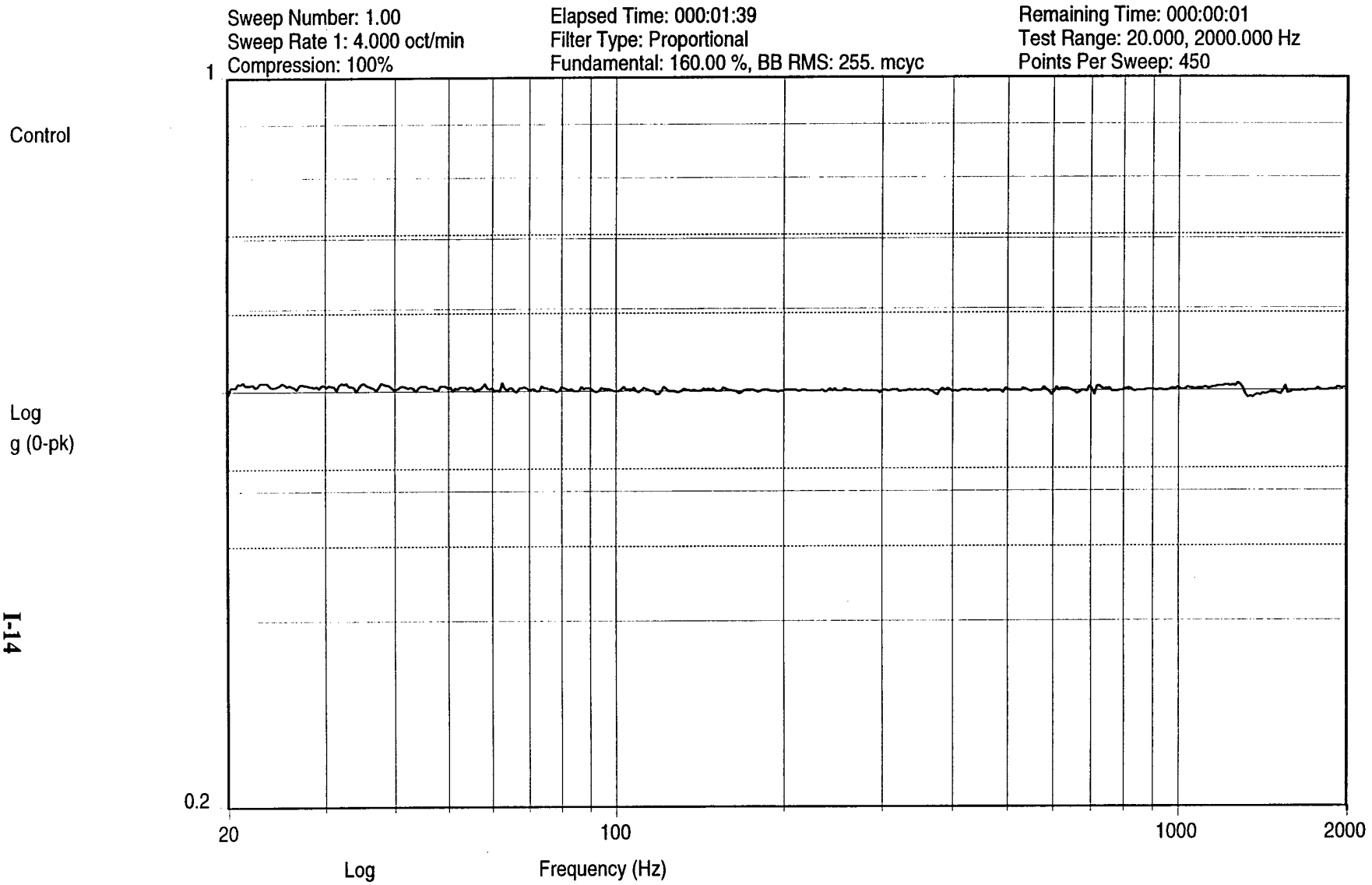


**Figure I-12. Post-Sine Sweep, 1/2 G**

# APPENDIX J

## Vibration Accelerometer Data, Detector #3

Vibration Acceleromenter Data, Detector #3

| Appendix Page Number | Figure Number | Time of Test | Vibration Axis | Accelerometer Location | Vibration Type |
|---|---|---|---|---|---|
| J-3 | J-1 | 11:32 | Z | A | Pre-Sine Sweep, 1/2 g |
| J-4 | J-2 | 11:32 | Z | B | Pre-Sine Sweep, 1/2 g |
| J-5 | J-3 | 11:38 | Z | A | Random |
| J-6 | J-4 | 11:38 | Z | B | Random |
| J-7 | J-5 | 11:44 | Z | A | Post-Sine Sweep, 1/2 g |
| J-8 | J-6 | 11:44 | Z | B | Post-Sine Sweep, 1/2 g |
| J-9 | J-7 | 13:25 | X | Control | Pre-Sine Sweep, 1/2 G |
| J-10 | J-8 | 13:28 | X | Control | Random |
| J-11 | J-9 | 13:32 | X | Control | Post-Sine Sweep, 1/2 G |
| J-12 | J-10 | 16:33 | Y | Control | Pre-Sine Sweep, 1/2 G |
| J-13 | J-11 | 16:36 | Y | Control | Random |
| J-14 | J-12 | 16:40 | Y | Control | Post-Sine Sweep, 1/2 G |

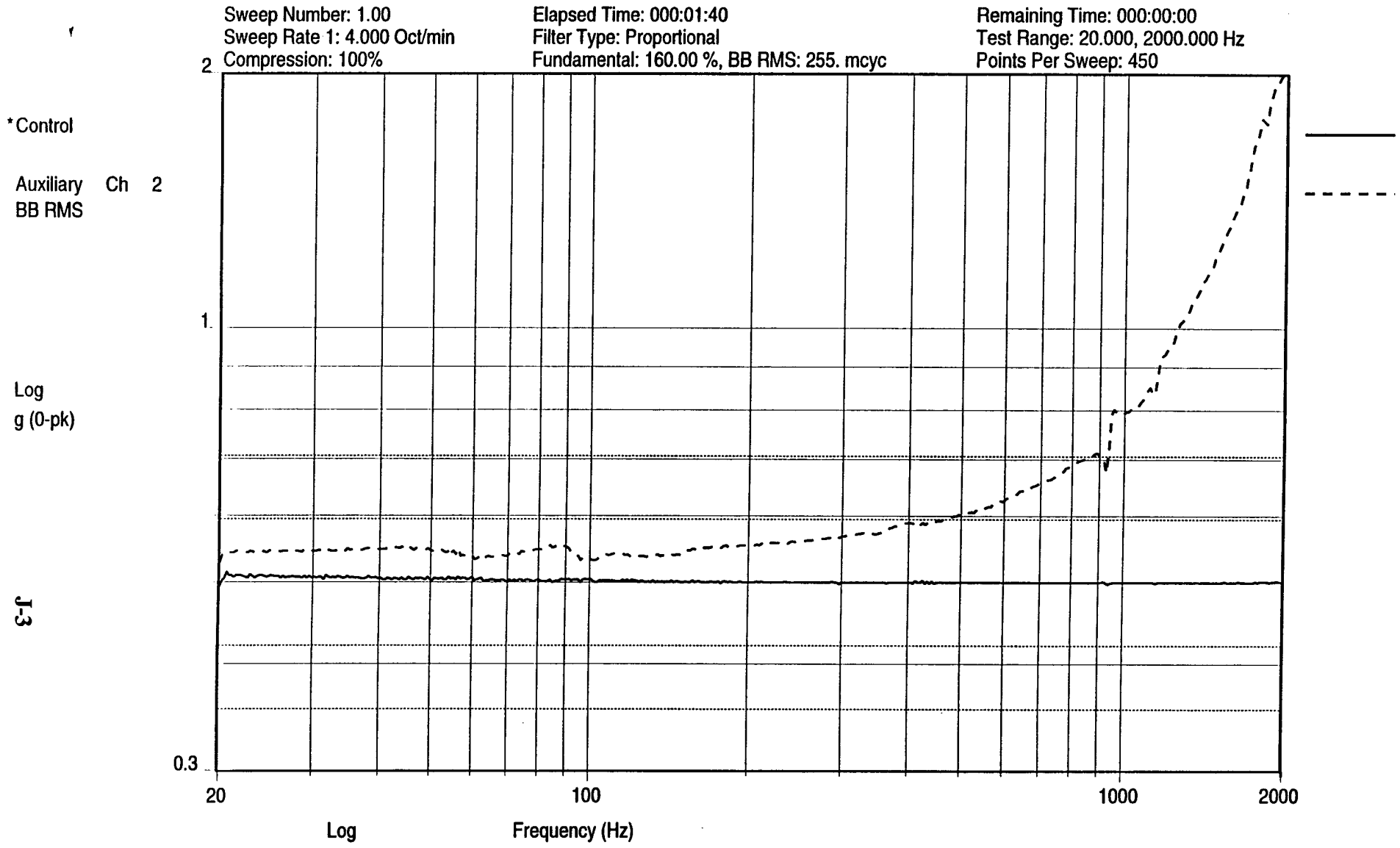


**Figure J-1. Pre-Sine Sweep, 1/2 g**

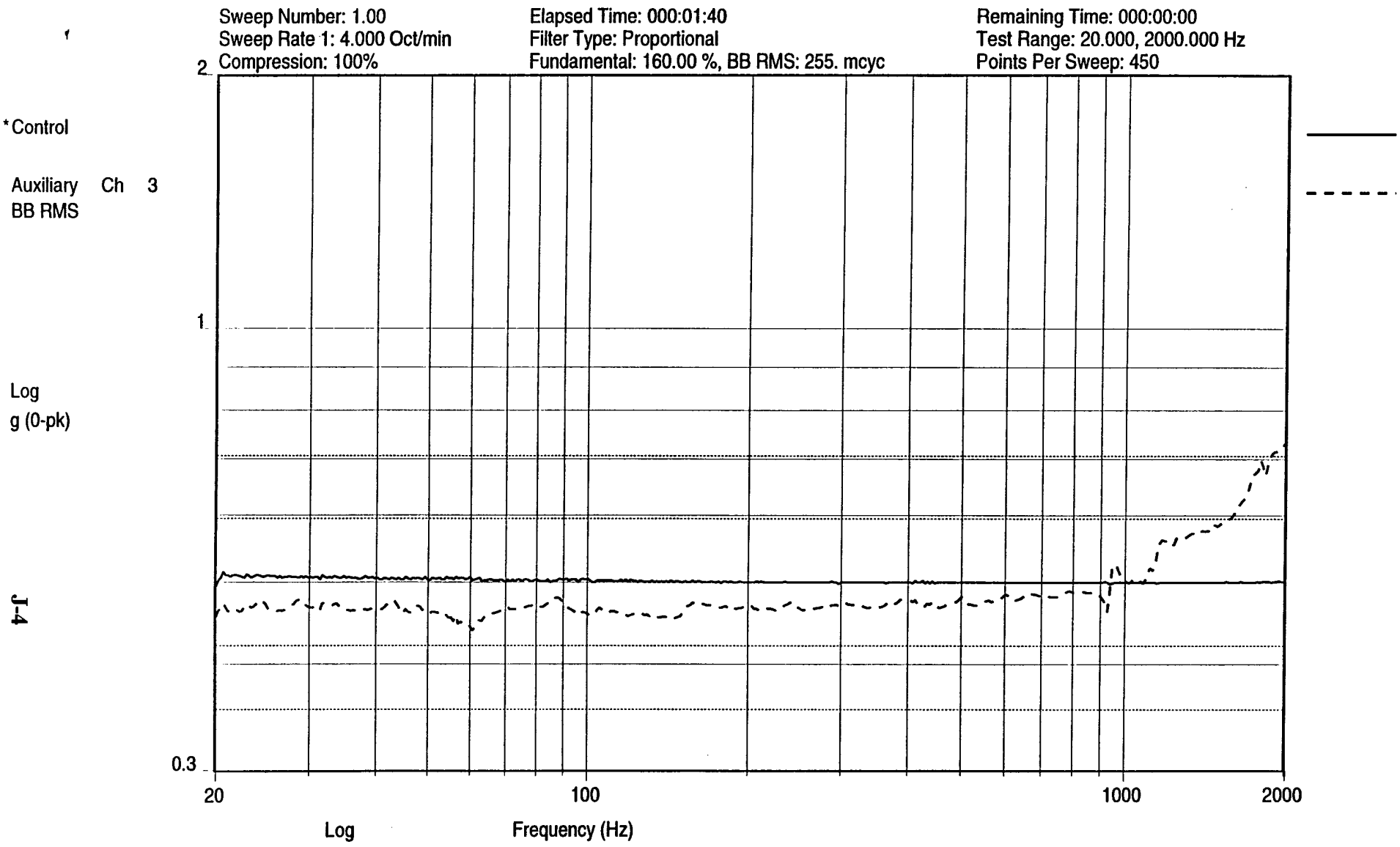




**Figure J-2. Pre-Sine Sweep, 1/2 g**

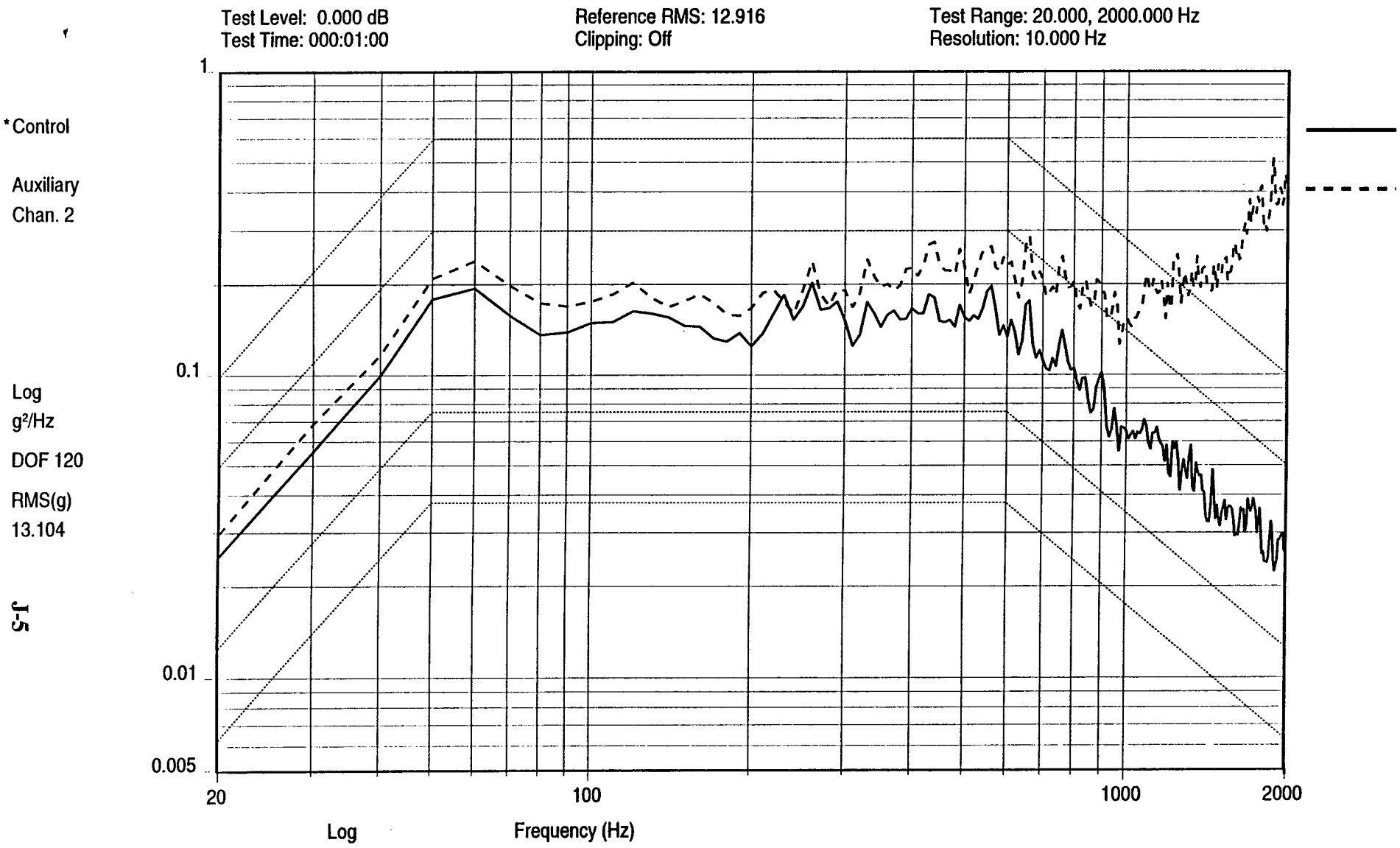


**Figure J-3. Random**

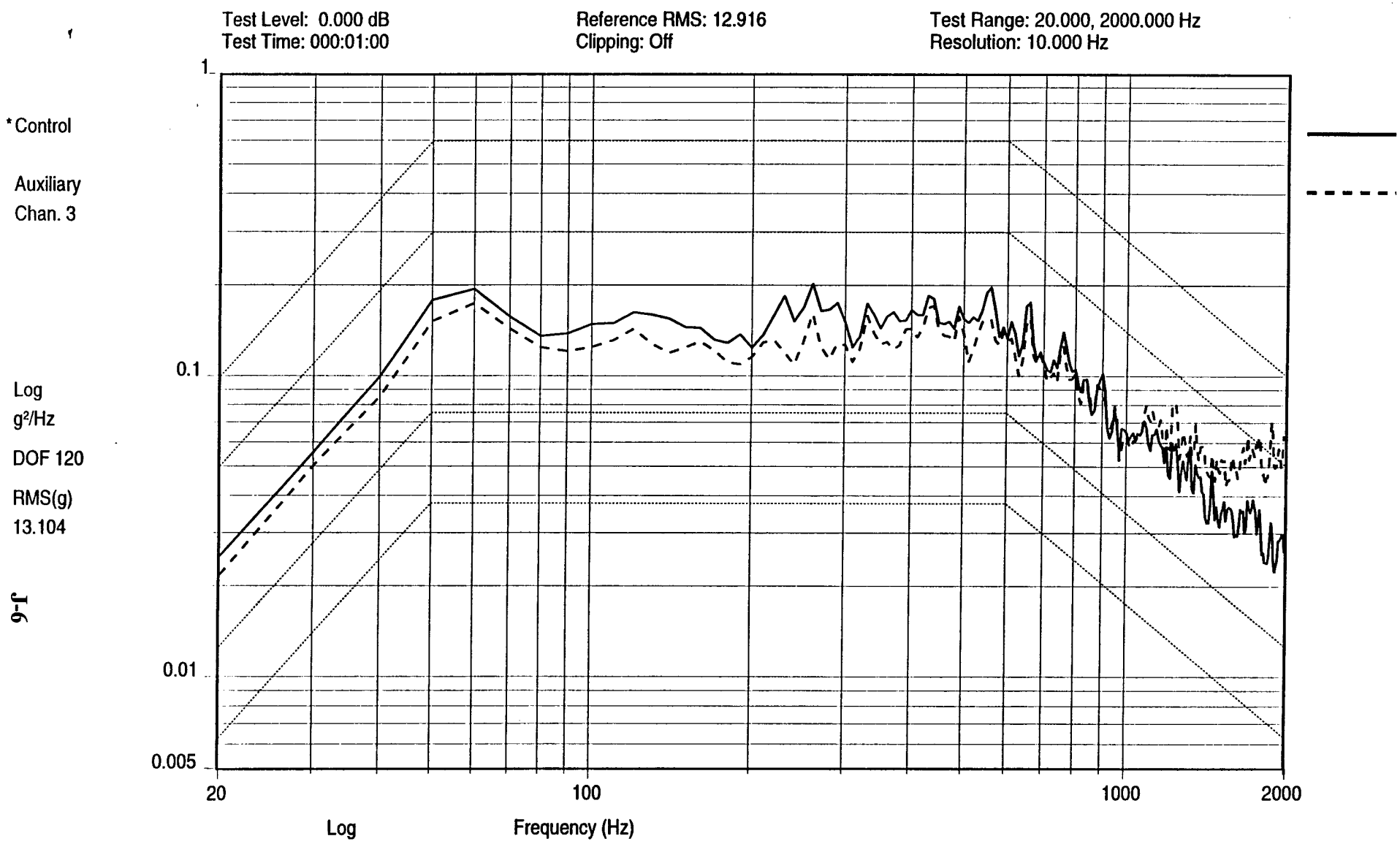


**Figure J-4. Random**

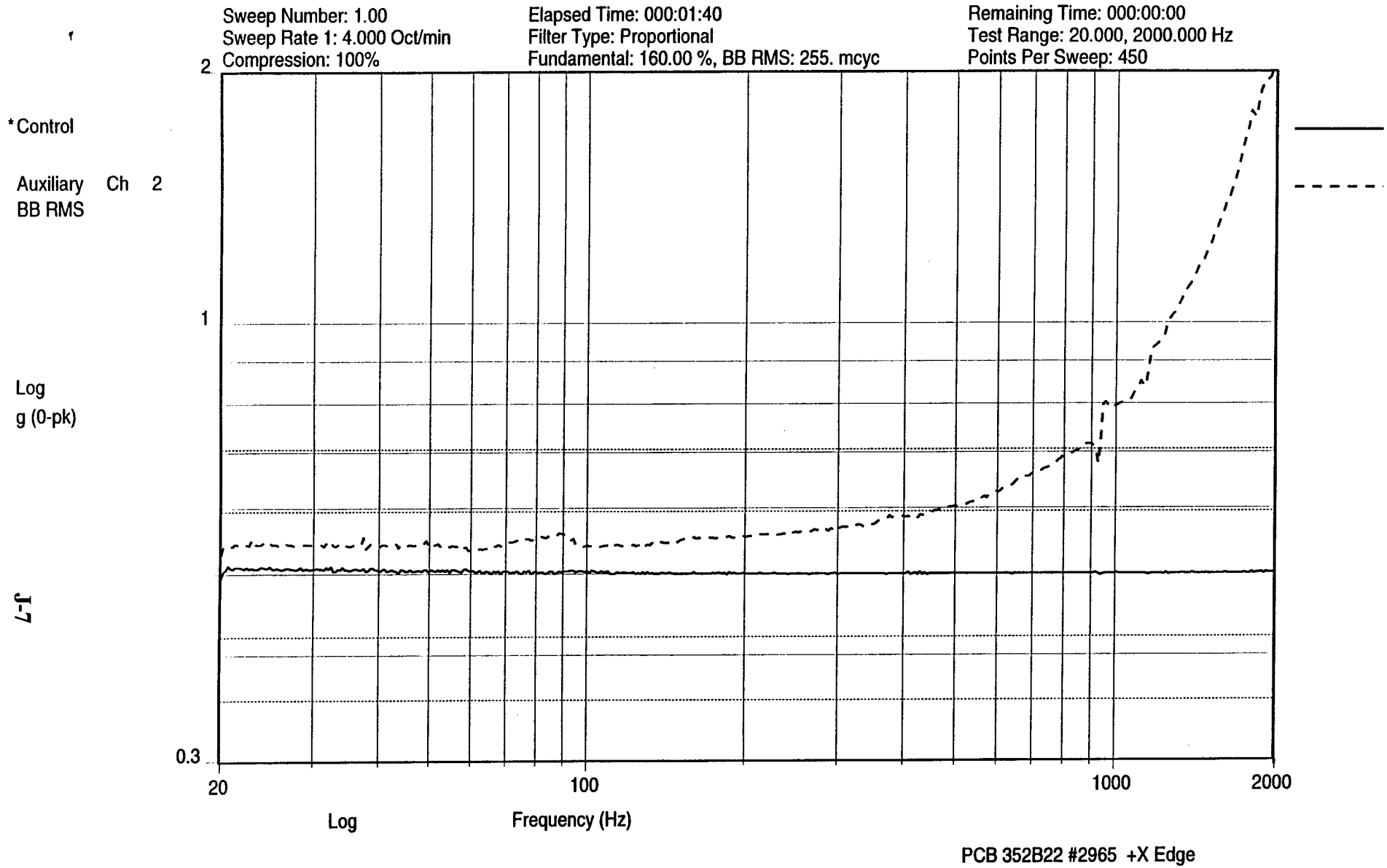


**Figure J-5. Post-Sine Sweep, 1/2 G**

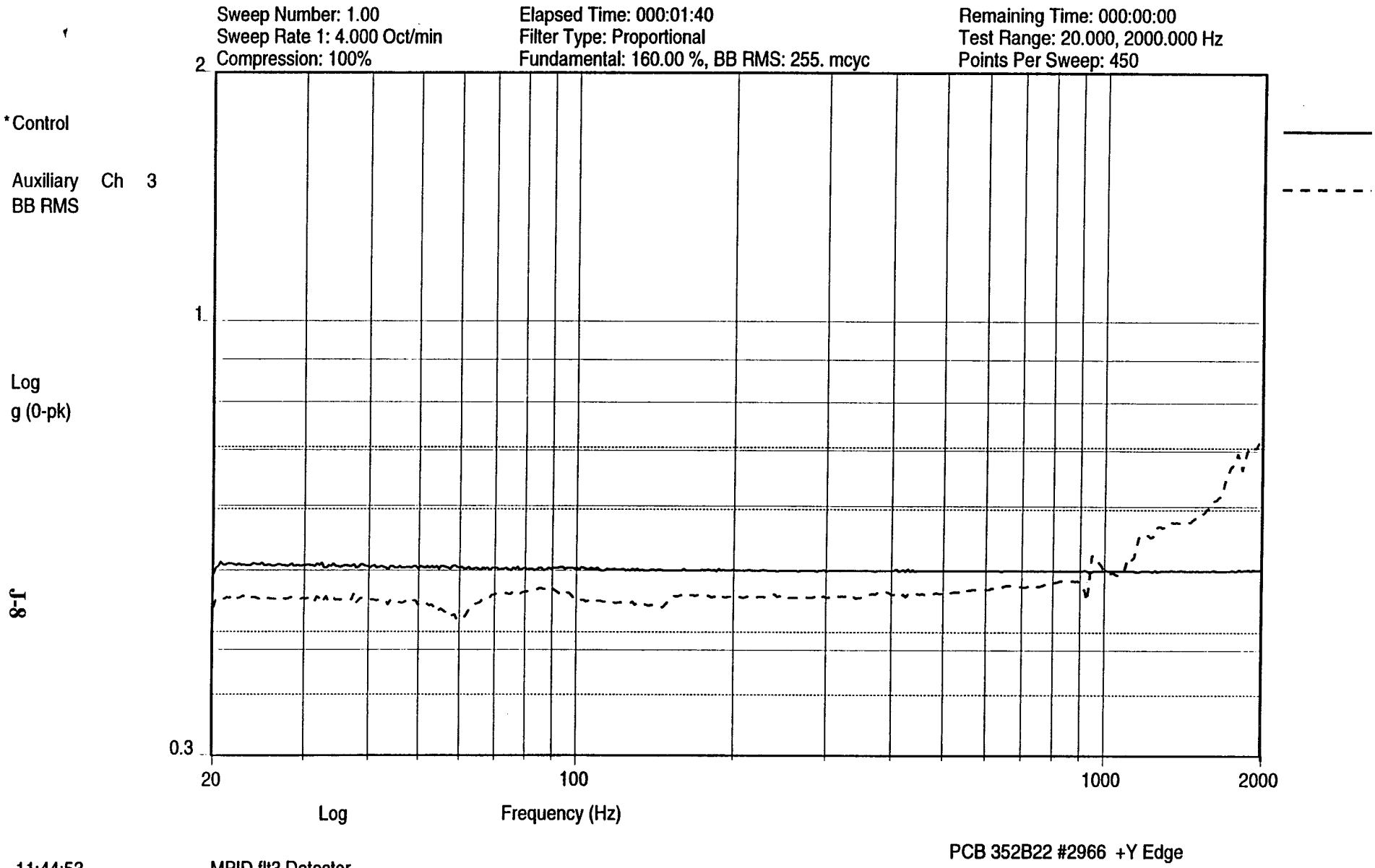


**Figure J-6. Post-Sine Sweep, 1/2 G**

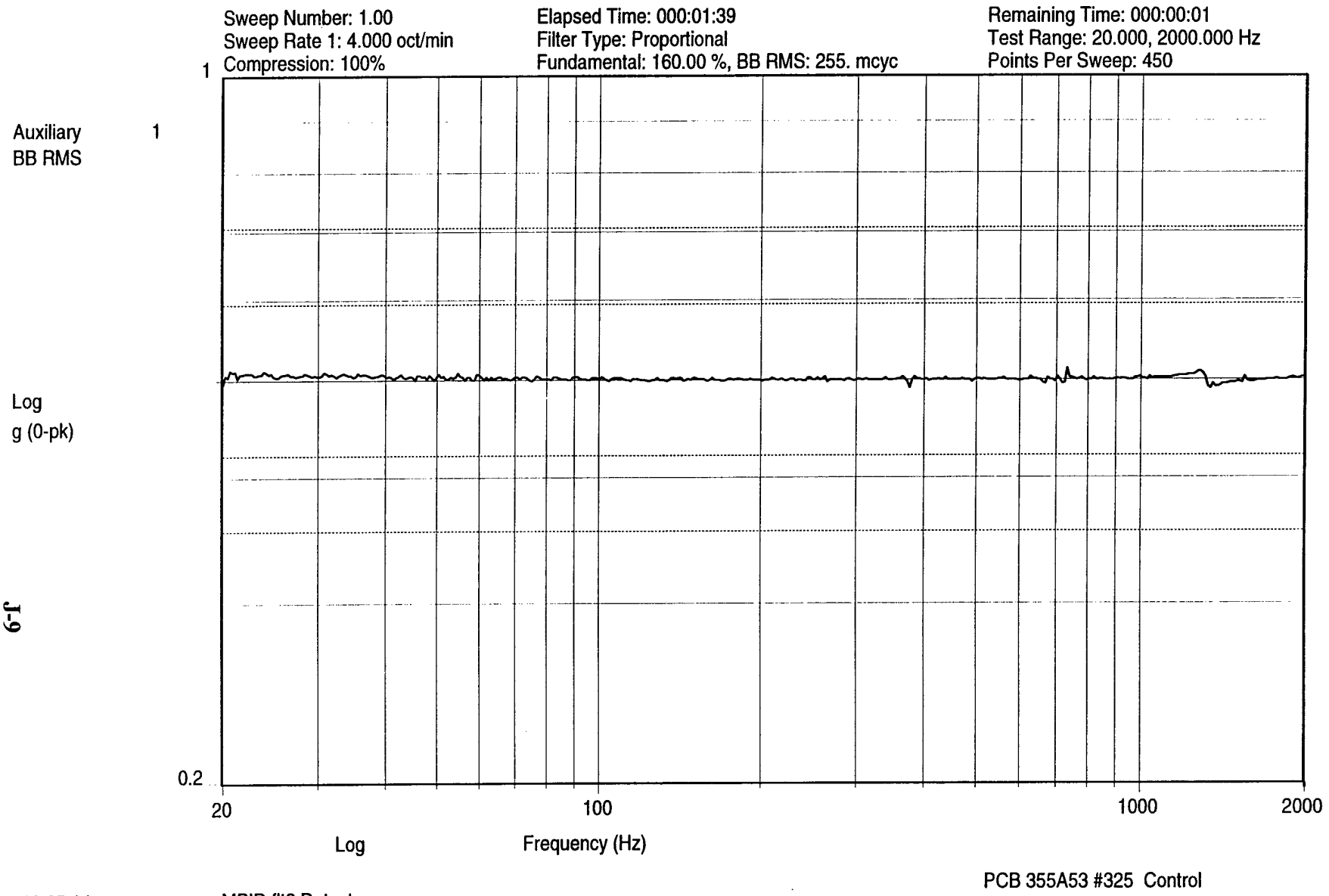


**Figure J-7. Pre-Sine Sweep, 1/2 G**

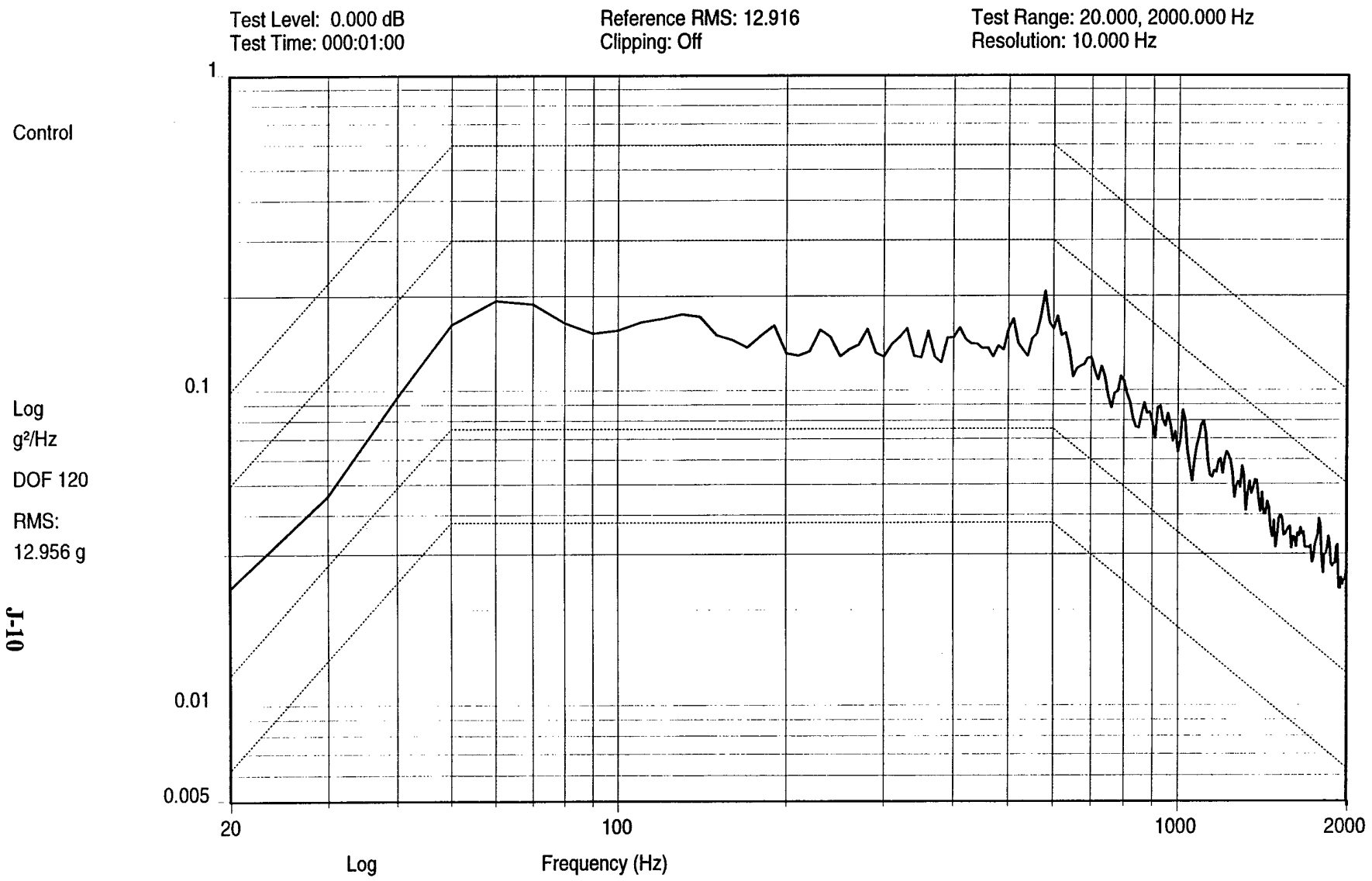


**Figure J-8. Random**

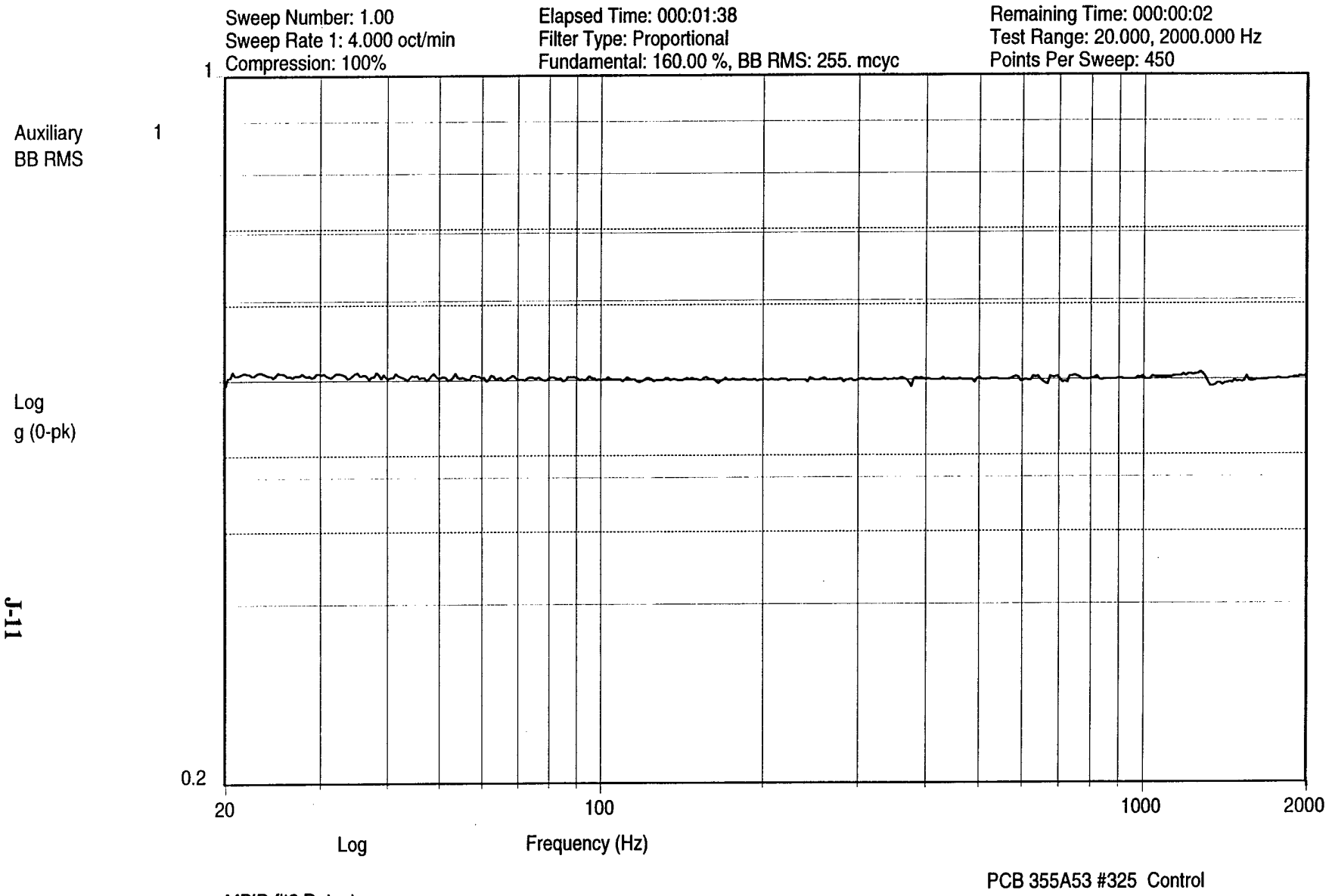


**Figure J-9. Post-Sine Sweep, 1/2 G**

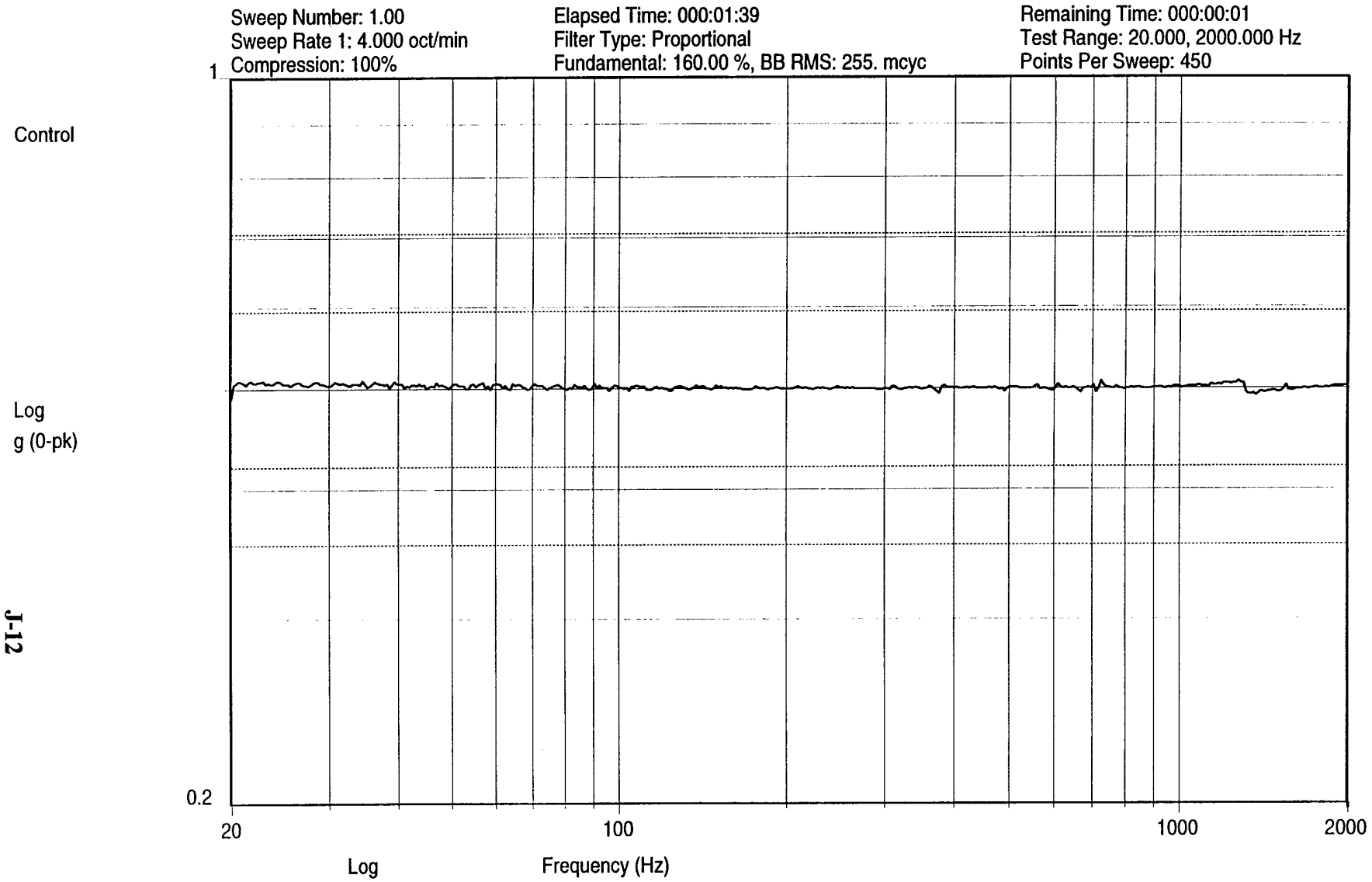


16:33:34
Wed Jan 08 1997

MPID flt2 Detector
1/2 g Sine Sweep y pre

Sine Data Review Name: mpid_1_8_97.012

**Figure J-10. Pre-Sine Sweep, 1/2 G**

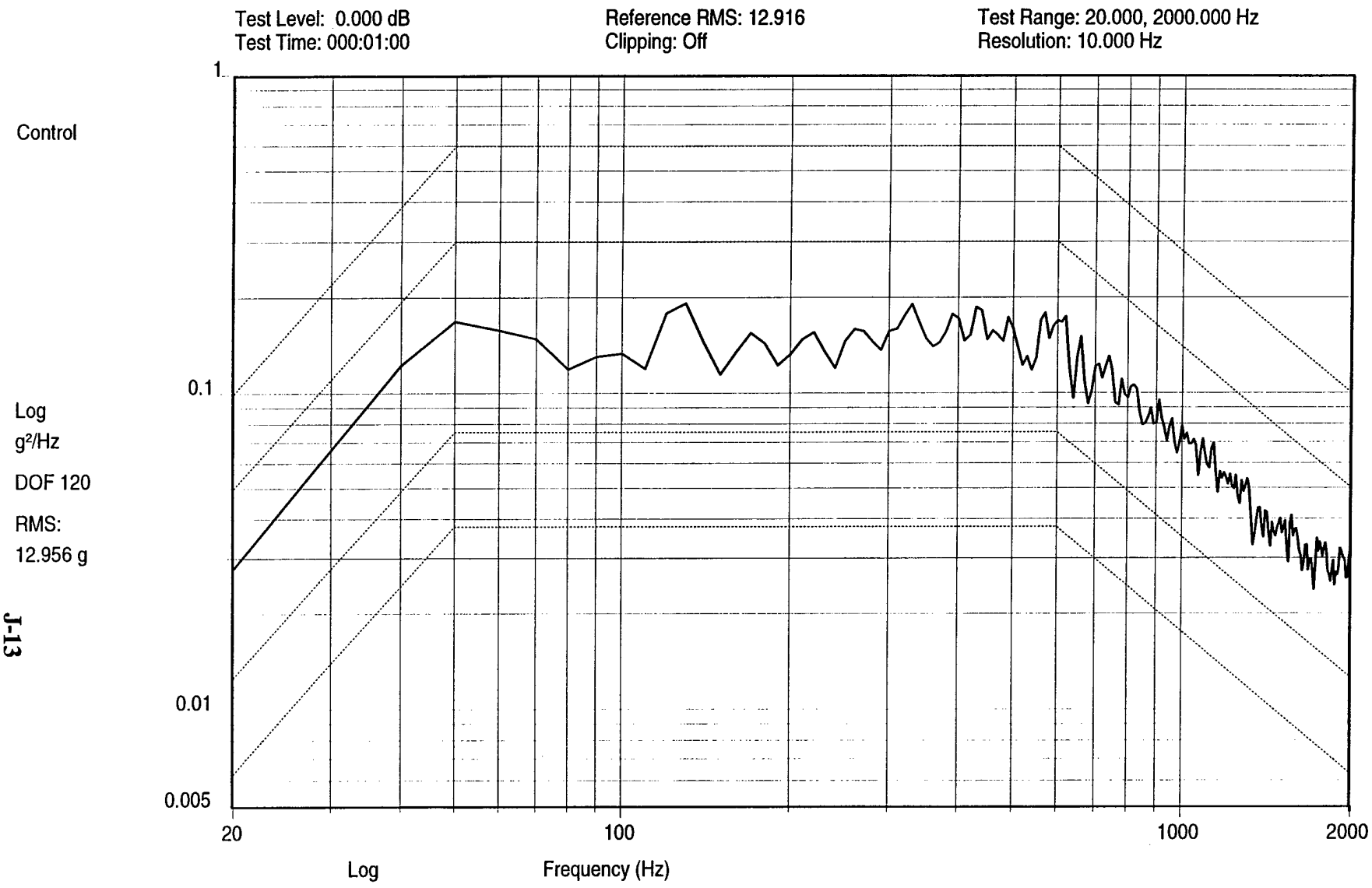


**Figure J-11. Random**

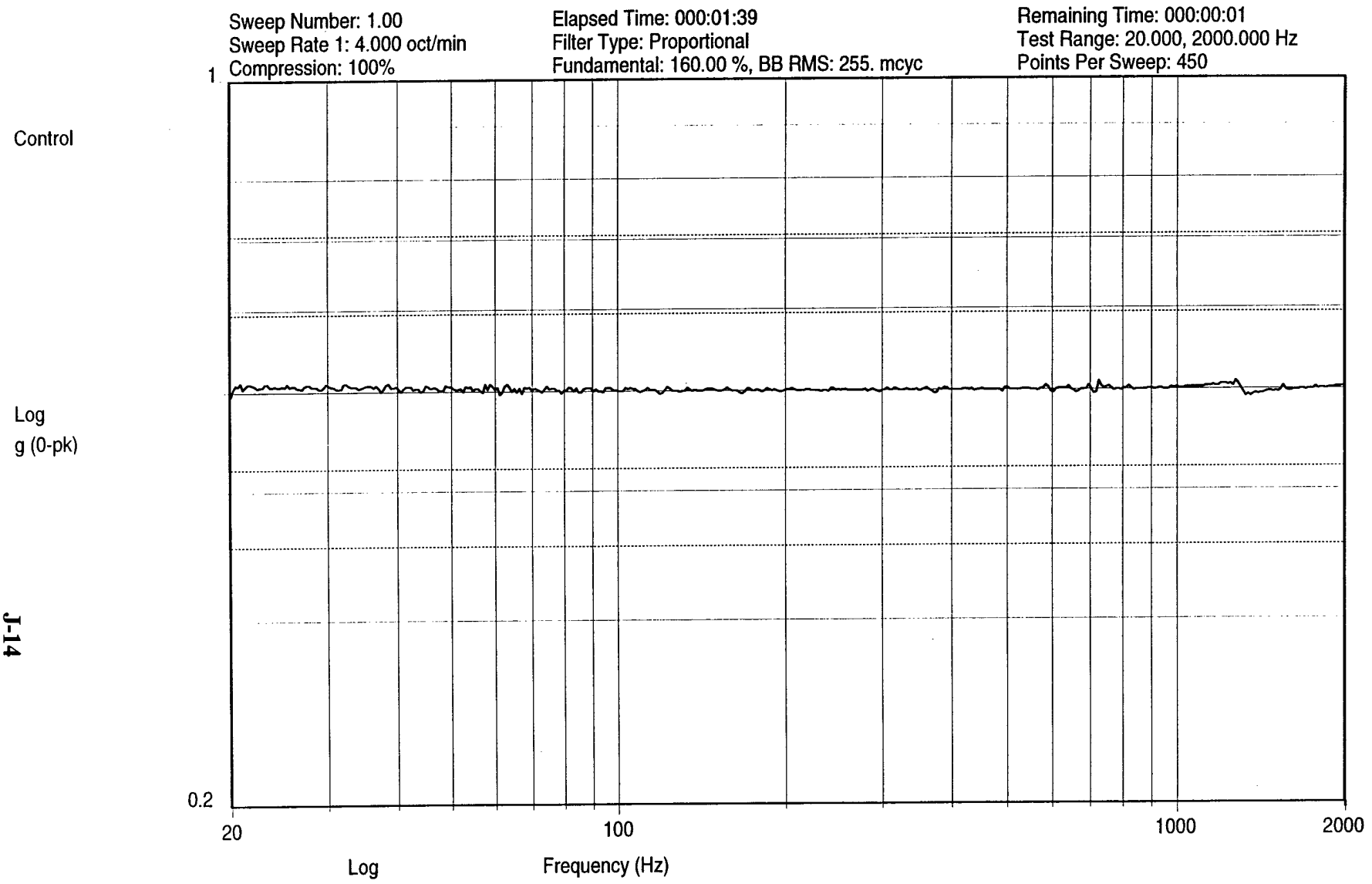


16:40:42
Wed Jan 08 1997

MPID flt2 Detector
1/2 g Sine Sweep y post

Sine Data Review Name: mpid_1_8_97.013

**Figure J-12. Post-Sine Sweep, 1/2 G**

DISTRIBUTION LIST

AUL/LSE
Bldg 1405 - 600 Chennault Circle
Maxwell AFB, AL 36112-6424 1 cy

DTIC/OCP
8725 John J. Kingman Rd, Suite 0944
Ft Belvoir, VA 22060-6218 2 cys

AFSAA/SAI
1580 Air Force Pentagon
Washington, DC 20330-1580 1 cy

AFRL/PSOTL
Kirtland AFB, NM 87117-5776 2 cys

AFRL/PSOTH
Kirtland AFB, NM 87117-5776 1 cy

AFRL/VSDI (C. Neslen)
Kirtland AFB, NM 87117-5776 2 cys

Science Applications International Corp.
Attn: Renzo Del Frate
2109 Air Park Road, SE
Albuquerque, NM 87106 2 cys

NASA
Langley Research Center
MS 118B (J. Jones, W. Kinard)
Hampton, VA 23681-0001 2 cys

North Carolina State University
EECE Department
Attn: Prof. J. Wortman
P.O. Box 7911
Raleigh, NC 27695 2 cy

Official Record Copy
AFRL/VSSE (P. Serna)
Kirtland AFB, NM 87117-5776 10 cys